UNIVERSITAT DE BARCELONA

RTP801: a novel regulator of the tRNA ligase complex in Alzheimer's disease

Genís Campoy Campos

UNIVERSITAT DE BARCELONA

RTP801: a novel regulator of the tRNA ligase complex in Alzheimer's disease

Dissertation submitted by

Genís Campoy Campos

This work was performed at the Department of Biomedical Sciences of the Faculty of Medicine and Health Sciences of the University of Barcelona, under the supervision of Dr. Cristina Malagelada Grau and Dr. Esther Pérez Navarro.

Dr. Cristina Malagelada Grau Genís Campoy Campos Dr. Esther Pérez Navarro

Doctoral program in Biomedicine

May 2024

A la gent que estimo

What I love about science is that as you learn, you don't really get answers.
You just get better questions.

John Green

Nothing in life is to be feared, it is only to be understood

Marie Curie

Qui fa el que pot, no està obligat a més

Refrany català

PUBLICATIONS AND FUNDING

This work herein presented is based on the following *submitted* publication:

RTP801 interacts with the tRNA ligase complex and dysregulates its RNA ligase activity in Alzheimer's disease. Campoy-Campos G, Solana-Balaguer J, Guisado-Corcoll A, Chicote-González A, Garcia-Segura P, Pérez-Sisqués L, Torres AG, Canal M, Molina-Porcel L, Fernández-Irigoyen J, Santamaria E, Ribas de Pouplana L, Alberch J, Martí E, Giralt A, Pérez-Navarro E, and Malagelada C. *Submitted* in Nucleic Acids Research.

And has been supported by:

1. Grant from the Agència de Gestió d'Ajuts Universitaris i de Recerca (AGAUR, Catalonia) under number #FI-B-00378

2. Grants from the Ministerio de Ciencia, Innovación y Universidades (MICIU)/Agencia Estatal de Investigación (AEI)/10.13039/501100011033 and by "ERDF A way of making Europe" under project number SAF2017-88812-R, PID2020-119236RB-I00, and PID2019-106447RB-I00.

3. María de Maetzu Unit of Excellence, Institute of Neurosciences, University of Barcelona, MDM-2017-0729 from the Ministerio de Ciencia, Innovación y Universidades (MICIU).

The funders were not involved and had no role in the study design, data collection, analysis and interpretation of the data, the writing of manuscripts or the decision to publish the manuscripts (including this PhD thesis).

ABSTRACT

RTP801/REDD1 is a stress-responsive protein overexpressed in neurodegenerative diseases such as Alzheimer's disease (AD) that contributes to cognitive deficits and neuroinflammation. Here we found that RTP801 interacts with HSPC117, DDX1, and CGI-99, three members of the tRNA ligase complex (tRNA-LC), which ligates the excised exons of intron-containing tRNAs and the mRNA exons of the transcription factor XBP1 during the unfolded protein response (UPR). We also found that RTP801 modulates the mRNA ligase activity of the complex *in vitro*, since RTP801 knockdown promoted *XBP1* splicing and the expression of its transcriptional target, *SEC24D*. On the contrary, RTP801 overexpression inhibited the splicing of *XBP1*. In this line, in human AD postmortem hippocampal samples, where RTP801 protein levels are upregulated, we found that XBP1 splicing dramatically decreased. In the 5xFAD mouse model of AD, silencing RTP801 expression in hippocampal neurons promoted *Xbp1* splicing and prevented the accumulation of intron-containing pre-tRNAs. Finally, the tRNA-enriched fraction obtained from 5xFAD mice promoted abnormal dendritic arborization in cultured hippocampal neurons, and RTP801 silencing in the source neurons prevented this phenotype. Altogether, these results show that elevated RTP801 impairs RNA processing *in vitro* and *in vivo*, in the context of AD and suggest that RTP801 inhibition could be a promising therapeutic approach.

RESUMEN

Las enfermedades neurodegenerativas son un conjunto de enfermedades devastadoras principalmente caracterizadas por la pérdida de poblaciones neuronales específicas. Entre las más destacadas se incluyen la enfermedad de Alzheimer (EA), la enfermedad de Huntington (EH) o la enfermedad de Parkinson (EP). En los últimos años se ha propuesto que un mecanismo patogénico común en las distintas enfermedades neurodegenerativas es una síntesis proteica alterada. Precisamente, los ARN mensajeros (ARNm) y de transferencia (ARNt) son elementos esenciales para una correcta traducción.

El complejo ARNt ligasa es un complejo multiproteico descubierto en 2011 compuesto por las proteínas HSPC117, DDX1, CGI-99, FAM98B y ASW. Este complejo participa en el procesamiento de los ARNt con intrón y de ARNm específicos, como por ejemplo el ARNm del factor de transcripción XBP1. Concretamente, el complejo ARNt ligasa se encarga de ligar los exones después del corte endonucleolítico. Por lo tanto, un correcto funcionamiento de este complejo es clave para regular el reservorio de ARNt y ARNm de las células.

RTP801 es una proteína de respuesta al estrés cuyos niveles están incrementados en los cerebros de pacientes con enfermedades neurodegenerativas como la EA, la EH o la EP. Resultados previos del grupo demostraron que el silenciamiento de RTP801 en el hipocampo de ratones modelo de la EA y de la EH mejoraba su cognición y reducía su neuroinflamación. Así pues, niveles aumentados de RTP801 parecen ser patológicos para el cerebro. Curiosamente, en resultados preliminares del grupo se observó que RTP801 interaccionaba físicamente con HSPC117 y DDX1, dos de los miembros del complejo ARNt ligasa.

Por este motivo, nuestra hipótesis de trabajo en esta tesis era que los altos niveles de RTP801 en la EA podrían estar afectando el funcionamiento del complejo ARNt ligasa y, por ende, el reservorio de ARNt y ARNm celulares, lo que contribuiría a la exacerbación de la patología.

Así pues, en el primer objetivo de esta tesis hemos estudiado la naturaleza de la interacción entre RTP801 y los miembros del complejo ARNt ligasa.

Mediante la técnica de la inmunoprecipitación, confirmamos la interacción de RTP801 con HSPC117 y DDX1, y, además, observamos que RTP801 también interaccionaba con CGI-99, otro miembro del complejo. A continuación, analizamos si la interacción de RTP801 con el complejo podría estar estabilizando o desestabilizando dicho complejo. Observamos que los niveles proteicos de RTP801 no influían en los niveles proteicos de los miembros del complejo, ni en

neuronas corticales de rata en cultivo ni en células HEK293 humanas. De forma similar, los niveles de RTP801 tampoco afectaban a la expresión genética de DDX1 ni de HSPC117. Estos resultados sugieren que RTP801 no estabiliza los miembros del complejo ARNt ligasa ni tampoco promueve su degradación.

Por el contrario, observamos que los niveles proteicos de DDX1 y de HSPC117 sí que afectaban a los niveles proteicos de RTP801. Concretamente, DDX1 y HSPC117 parecían estabilizar a la proteína RTP801. Por el contrario, los niveles de DDX1 y HSPC117 no regulan la expresión genética de RTP801. Esto indica que la interacción de RTP801 con el complejo puede estar evitando su propia degradación por parte del proteasoma.

Teniendo en cuenta que la interacción de RTP801 con el complejo no parecía estabilizadora ni de carácter estructural, nos planteamos que RTP801 podría estar modulando su actividad ARNm ligasa. Por ello, en el segundo objetivo de esta tesis investigamos el rol de RTP801 en la actividad ARNm ligasa del complejo sobre *XBP1*, tanto a nivel fisiológico como en el contexto de la EA.

En primer lugar, observamos que el silenciamiento de RTP801 en células HEK293 promovía el empalme de *XBP1* y la transcripción de una de sus dianas transcripcionales, llamada *SEC24D*. Por el contrario, la sobreexpresión de RTP801 en el mismo modelo celular inhibía el empalme de *XBP1*. Estos resultados indican que RTP801 inhibe el empalme de *XBP1 in vitro,* puesto que sus niveles están inversamente correlacionados.

En segundo lugar, estudiamos el estado de RTP801, de los miembros del complejo y del empalme de XBP1 en muestras de hipocampo de pacientes de la EA. Confirmamos, como ya habíamos descrito anteriormente, que los niveles de RTP801 están aumentados en pacientes de la EA en comparación con individuos sanos. Sin embargo, los niveles de los miembros del complejo ARNt ligasa permanecían invariables entre condiciones. Sorprendentemente, el empalme de XBP1 estaba drásticamente alterado en el hipocampo de pacientes de la EA. Estos resultados indican que, a pesar de que los miembros del complejo no están alterados en la EA, su actividad parece estarlo. Además, descubrimos que los niveles proteicos de RTP801, de la forma ligada de XBP1 y de la forma fosforilada de una proteína marcadora de estrés reticular (eIF2α) eran muy buenos clasificadores de la presencia o ausencia de la EA.

Por último, usamos ratones modelo de la EA (5xFAD) para estudiar el empalme de XBP1 *in vivo*, y el papel que RTP801 jugaba en él. Como en trabajos anteriores, inyectamos virus

adenoasociados en el hipocampo de ratones control y de ratones 5xFAD con el objetivo de disminuir la expresión de RTP801 específicamente en las neuronas. Un mes después, aislamos el ARN del hipocampo para analizar el estado del empalme de *Xbp1*. Observamos que la disminución de la expresión de RTP801 promovía significativamente su empalme, de forma similar a los resultados obtenidos *in vitro*. Interesantemente, la disminución de la expresión de RTP801 en el hipocampo de ratones 5xFAD también promovía la expresión de una diana transcripcional de XBP1 llamada *Bdnf*, que resulta ser una neurotrofina muy importante para la plasticidad neuronal, el aprendizaje y la memoria.

Así pues, los resultados del segundo objetivo de la tesis sugieren que RTP801, la cual está incrementanda en el contexto de la EA, inhibe el empalme de XBP1, y muy probablemente lo hace a través de su interacción con los miembros del complejo ARNt ligasa.

Finalmente, en el tercer objetivo de esta tesis exploramos si RTP801 también inhibía la actividad ARNt ligasa del complejo, es decir, si RTP801 podía modular el empalme de los ARNt con intrón. Para ello, aprovechamos el modelo animal descrito en el segundo objetivo y a partir del RNA obtenido aislamos la fracción de ARN que contiene mayormente los ARNt. Una parte de este ARNt lo usamos para experimentos de secuenciación y la otra parte para analizar su posible toxicidad y su funcionalidad.

Con respecto a los experimentos de secuenciación, observamos que los ratones 5xFAD presentaban una acumulación de ARNt inmaduro (pre-ARNt) en el hipocampo, pero solo de aquellas familias de ARNt que presentan intrón. Estos resultados sugieren que en los ratones 5xFAD hay un problema en el procesamiento de ARNt, y específicamente en su empalme.

Para dilucidar si RTP801 podía estar jugando un papel en este empalme aberrante, estudiamos los niveles de pre-ARNt exclusivamente para aquellas familias de ARNt con intrón en el hipocampo de las siguientes condiciones: ratones control y ratones 5xFAD, con o sin disminución de la expresión de RTP801. Sorprendentemente, observamos que casi todos los pre-ARNt se acumulaban en los ratones 5xFAD y que el silenciamiento de RTP801 prevenía este fenómeno. En otras palabras, RTP801 realmente estaba contribuyendo a la acumulación de pre-ARNt con intrón en los ratones 5xFAD, probablemente mediante la inhibición del complejo ARNt ligasa.

En último lugar, analizamos si los ARNt procedentes de los ratones 5xFAD eran tóxicos para neuronas en cultivo, o si afectaban a su arborización. Para ello, transfectamos neuronas

hipocampales en cultivo con ARNt procedente de las condiciones experimentales indicadas anteriormente, y realizamos una inmunofluorescencia. Para ello se utilizó un anticuerpo contra MAP2 para marcar las neuronas y un anticuerpo contra la proteína caspasa 3 activa como marcador de apoptosis incipiente. Observamos que el ARNt transfectado no era tóxico en ninguna de las condiciones, a juzgar por el grado de condensación de la cromatina y por la intensidad y la distribución del marcaje para la caspasa 3 activa. Sin embargo, en referencia al efecto de los ARNt sobre la arborización neuronal, observamos que los ARNt provenientes del hipocampo de ratones 5xFAD inyectados con los virus control inducían un aumento de la ramificación neuronal, el cual era prevenido por el noqueo de RTP801. Estos resultados sugieren que el reservorio de pre-ARNt diferencial de los ratones 5xFAD sin noqueo de RTP801 puede influir en la ramificación de las neuronas, sin llegar a afectar su viabilidad.

En conjunto, en esta tesis demostramos el rol inhibitorio de RTP801 en la actividad ARNm ligasa y ARNt ligasa del complejo ARNt ligasa. Además, presentamos este rol como un nuevo mecanismo patológico en la EA, que puede contribuir a su exacerbación. Por tanto, esta tesis describe una nueva función de la proteína RTP801 la cual tendrá que ser estudiada en mayor profundidad, ya que supone una potencial diana terapéutica para la EA.

TABLE OF CONTENTS

ABBREVIATIONS

β-TrCP	Beta-transducin repeat containing
2D	Two-dimensional
3D	Three-dimensional
4EBP1	Eukaryotic translation initiation factor 4E-binding protein 1
6-OHDA	6-hydoxydopamine
Aβ	Amyloid beta
aaRS	Aminoacyl-tRNA synthetase
AAV	Adeno-associated virus
AD	Alzheimer's disease
AICD	Amyloid precursor protein intracellular domain
ANOVA	Analysis of variance
ANG	Angiogenin
APOE	Apolipoprotein E
APP	Amyloid precursor protein
ASW	Ashwin
ATF4	Activating transcription factor 4
ATF6	Activating transcription factor 6
ATP	Adenosine triphosphate
AUC	Area under the curve
BDNF	Brain-derived neurotrophic factor
BLAST	Basic local alignment search tool
BSA	Bovine serum albumin
CA1	Cornu Ammonis 1
cAMP	Cyclic adenosine monophosphate
CDR	Clinical dementia rating
C/EBP	CCAAT/enhancer-binding protein
CHAPS	3-((3-cholamidopropyl) dimethylammonium)-1-propanesulfonate
Clp1	Cleavage factor polyribonucleotide kinase subunit 1
ClvCas3	Cleaved caspase 3
CMV	Cytomegalovirus
CNP	2',3' cyclic nucleotide phosphodiesterase
CREB	Cyclic adenosine monophosphate response element-binding protein
CRG	Centre de regulació genòmica
CT	Control
CTF	C-terminal fragment

CUL4	Cullin 4
DDB1	Damage-specific DNA binding protein 1
DDIT4	DNA damage inducible transcript 4
DDIT4L	DNA damage inducible transcript like
DDX1	DEAD-box helicase1
DEPC	Diethyl pyrocarbonate
DG	Dentate gyrus
Dig2	Dexamethasone-induced gene 2
DIV	Days *in vitro*
DMEM	Dulbecco's modified Eagle's medium
DNA	Deoxyribonucleic acid
DSP	Dithiobis(succinimidyl propionate)
E18	Embryonic day 18
EDTA	Ethylenediaminetetraacetic acid
eEF1A	Eukaryotic elongation factor 1A
eGFP	Enhanced green fluorescent protein
eIF2α	Eukaryotic translation initiation factor 2α
EOAD	Early-onset Alzheimer's disease
ER	Endoplasmic reticulum
eRF1	Eukaryotic release factor 1
EVs	Extracellular vesicles
FAM98B	Family with sequence similarity 98 member B
FBS	Fetal bovine serum
FDA	Food and Drug Administration
GC	Genome copies
GFP	Green fluorescent protein
GO	Gene Ontology
GSK3β	Glycogen synthase kinase 3 beta
GTP	Guanosine triphosphate
GtRNAdb	Genomic transfer ribonucleic acid database
HD	Huntington's disease
HEK293	Human embryonic kidney 293
HIF-1	Hypoxia-inducible factor 1
hPGK	Human phosphoglycerate kinase

HPRT	Hypoxanthine phophoribosyltransferase 1
HRP	Horseradish peroxidase
Hsp70	70-kDa heat shock protein
Hydro-tRNA-seq	Hydrolysis-based tRNA sequencing
IκBα	NF-κB inhibitor alpha
IgG	Immunoglobulin G
IP	Immunoprecipitation
IRE1	Inositol-requiring enzyme 1
ISR	Integrated stress response
KO	Knockout
LAS X	Leica Application Suite X
LB	Lysogeny broth
LDL	Low-density lipoprotein
lncRNA	Long non-coding ribonucleic acid
LOAD	Late-onset Alzheimer's disease
lRNA	Long ribonucleic acid
LTP	Long-term potentiation
MAP2	Microtubule-associated protein 2
MCI	Mild cognitive impairment
mhtt	Mutant huntingtin
miRNA	Micro ribonucleic acid
MOI	Multiplicity of infection
MOPS	3-(N-morpholino)propane sulfonic acid
MPTP	N-methyl-4-phenyl-1,2,3,6-tetrahydropyridine
mRNA	Messenger ribonucleic acid
MS	Mass spectrometry
mt-tRNA	Mitochondrial transfer ribonucleic acid
mTOR	Mechanistic target of rapamycin
mTORC1/2	Mechanistic target of rapamycin complex 1/2
M.W.	Molecular weight
MWM	Morris water maze
NAD(P)$^+$	Nicotinamide adenine dinucleotide (phosphate)
NCBI	National Center for Biotechnology Information
ncRNA	Non-coding ribonucleic acid
NEDD4	Neural precursor cell expressed, developmentally down-regulated 4

NLRP1/3	NLR family pyrin domain containing 1/3
NMDAR	N-methyl-D-aspartate receptor
Nsun2	NOP2/Sun RNA methyltransferase 2
NF-κB	Nuclear factor kappa B
nt	Nucleotide
OH	Hydroxyl
O/N	Overnight
PBS	Phosphate buffered saline
PCH	Pontocerebellar hypoplasia
PD	Parkinson's disease
PEI	Polyethyleneimine
PERK	Protein kinase R-like endoplasmic reticulum kinase
PET	Positron emission tomography
PFA	Paraformaldehyde
PI3K	Phosphoinositide 3-kinase
PKC	Protein kinase C
PKR	Protein kinase R
PMD	Postmortem delay
PMSF	Phenylmethylsulphonyl fluoride
PNK	Polynucleotide Kinase
PP2A	Protein phosphatase 2A
PPARγ	Peroxisome proliferator-activated receptor γ
Pre-tRNA	Precursor transfer ribonucleic acid
PSEN1/2	Presenilin 1/2
PTP1B	Protein tyrosine phosphatase 1B
PYROXD1	Pyridine nucleotide-disulfide oxidoreductase domain 1
qPCR	Quantitative polymerase chain reaction
rAAV	Recombinant adeno-associated virus
Ran	Ras-related nuclear protein
REDD1	Regulated in development and DNA damage responses 1
Rheb	Ras homologue enriched in brain
RIN	Ribonucleic acid integrity number
RNA	Ribonucleic acid
RNAi	Ribonucleic acid interference

RNAse MRP	Ribonuclease for mitochondrial ribonucleic acid processing
RNAse P	Ribonuclease P
RNAse Z	Ribonuclease Z
ROC	Receiver operating characteristic
ROC1	Regulator of cullin 1
ROS	Reactive oxygen species
rRNA	Ribosomal ribonucleic acid
RSV	Rous sarcoma virus
RT	Room temperature
RT-qPCR	Reverse transcription – quantitative polymerase chain reaction
RTD	Rapid tRNA decay
SDS	Sodium dodecyl sulfate
SEM	Standard error of the mean
SGK1	Serum and glucocorticoid regulated protein kinase 1
shRNA	Short hairpin ribonucleic acid
sncRNA	Small non-coding ribonucleic acid
snoRNA	Small nucleolar ribonucleic acid
SNP	Single-nucleotide polymorphism
S.O.C.	Super optimal broth with catabolite repression
SORL1	Sortilin-related receptor 1
SREBP1	Sterol regulatory element-binding protein 1
TBE	Tris-borate-ethylenediaminetetraacetic acid
TBS-T	Tris buffered saline – Tween
tiRNA	Stress-induced transfer ribonucleic acid
TLC	Thin-layer chromatography
tRAX	Transfer ribonucleic acid analysis of expression
TRDMT1	Transfer ribonucleic acid aspartic acid methyltransferase 1
tRF	Transfer ribonucleic acid-derived fragments
(tric)RNA	Transfer ribonucleic acid intronic circular ribonucleic acid
TRMT61B	Transfer ribonucleic acid methyltransferase 61B
tRNA	Transfer ribonucleic acid
tRNA-LC	Transfer ribonucleic acid splicing ligase complex
TRNT1	Transfer ribonucleic acid nucleotidyl transferase 1
TSC1/2	Tuberous sclerosis proteins 1/2
TSEN	Transfer ribonucleic acid splicing endonuclease

tsRNA	Transfer ribonucleic acid-derived small RNAs
UbC	Ubiquitin C
ULK-1	Unc-51 like autophagy activating kinase 1
UPR	Unfolded protein response
UV	Ultraviolet
WB	Western blot
WT	Wild type
XBP1	X-box binding protein 1

INTRODUCTION

1. Alzheimer's disease

Neurodegenerative diseases are a heterogeneous group of progressive disorders that affect the nervous system and are characterized by the loss of specific populations of neurons. One specific hallmark of neurodegenerative diseases is the pathological aggregation of proteins, which eventually leads to chronic neuroinflammation. This is usually accompanied by an altered energy homeostasis and an aberrant proteostasis. These abnormalities cause synaptic deficits and deteriorate communication between neurons. Therefore, patients present a range of symptoms including impaired memory, cognitive decline, mood changes, and loss of motor functions, among others. Neurodegenerative diseases mainly affect elder people, although those ones with a genetic cause might develop on younger adults. Most neurodegenerative diseases have no cure, and the treatments are restricted to the relief of symptoms [1], [2]. Thus, extensive research is required to fully comprehend the mechanisms of these diseases and to be able to eradicate them.

The most common neurodegenerative diseases include Alzheimer's disease (AD), Parkinson's disease (PD), amyotrophic lateral sclerosis, Huntington's disease (HD), and spinal muscular atrophy.

In this work we will focus on AD, the most common type of dementia, affecting millions of people worldwide [3]. Memory loss is the most paradigmatic symptom, and one of the first to appear. However, as the disease progresses, deficits in cognition and attention appear, as well as changes in personality and behavior. The main risk factor is age, and since the world life expectancy is continually rising, it is estimated that its prevalence could double in the next decades [4].

1.1. History

Alzheimer's disease is named after the German psychiatrist and neuroanatomist, Alois Alzheimer. In 1906, he reported "a peculiar severe disease process of the cerebral cortex" to a Psychiatry conference [5]. He described the case of Auguste Deter, a 51-year-old woman suffering from memory problems, paranoia, confusion, and aggression. In the brain histology, he found plaques and neurofibrillary tangles. Nonetheless, his discovery did not elicit much interest until several decades later [6].

AD is characterized by the accumulation in the brain of extracellular amyloid β (Aβ) plaques and intracellular neurofibrillary tangles of hyperphosphorylated tau. Although these plaques were already described by Alois Alzheimer in 1906, the responsible protein was not identified until

1984, when Glenner *et al*. [7] purified "an amyloid protein", which was initially named "β-peptide" or "amyloid A4 protein". Two years later, different groups simultaneously identified tau as the main component of the neurofibrillary tangles [8], [9], [10].

In 1987, the first drug trials specifically targeting the symptoms of AD were launched, trying to assess the effectivity of tacrine. That same year, the first gene linked to hereditary types of AD was discovered [11]. The gene, found on chromosome 21, coded for the amyloid precursor protein (APP), the precursor of Aβ. Since Down syndrome patients present a trisomy of chromosome 21 and develop premature deposition of amyloid in the brain, the authors speculated that AD might be consequence of an aberrant processing of APP.

In the 1990s, treatments for AD started to appear. Indeed, the drug tacrine was approved by the Food and Drug Administration (FDA) for the treatment of memory and thinking symptoms. In 1993, APOE (apolipoprotein E) ε4 allele was identified as the first risk factor gene for AD [12], [13]. Also in this decade, the first transgenic mouse models of AD were developed, which expressed one or more isoforms of the human APP gene. Interestingly, most of them presented behavioral or/and biochemical deficits observed in AD (reviewed in [14]).

With the arrival of the new millennium, major advances were achieved in the field of AD, leading to a better understanding, diagnosis, and treatment of the disease. For instance, in 2004, a novel imaging technique based on the detection of a tracer called Pittsburgh Compound-B was announced [15]. This compound is bound to amyloid deposits and thus, can be detected by positron emission tomography (PET). In the last years, the number of articles focusing on AD has grown exponentially, which highlights the huge impact of this disease and the efforts done to eradicate it [16].

1.2. Epidemiology

In 2006, it was estimated that 26.6 million people lived with AD worldwide. Moreover, this number was expected to quadruple by 2050 [17]. As aforementioned, the main risk factor for AD is age, and thus, its prevalence rises exponentially after 65 years. Indeed, an estimated 6.7 million Americans over 65 were living with AD in 2023. Of those, two-thirds were women, which could be explained because of women's longer life expectancy [4]. Regarding Europe, a meta-analysis reported that the prevalence of AD was 5.05%, and again, it was higher in women than in men [18]. Strikingly, in the United States, Black and Hispanic adults over 65 were much more likely than White older adults to develop AD (19%, 14% and 10%, respectively). However, these huge differences cannot be attributed to genetic factors, but rather, to socioeconomic differences and structural racism [4].

1.3. Symptoms

AD can be classified into two categories: early-onset AD (EOAD) and late-onset AD (LOAD). EOAD refers to those AD cases that develop in patients younger than 65, generally in their 40s and 50s. It represents approximately 5% of all cases and it usually has a rapid progression and an aggressive course [19]. Indeed, the first case described by Alois Alzheimer corresponded to an EOAD. On the other hand, the vast majority of AD cases are LOAD. LOAD is characterized by progressive memory loss, including both the inability to acquire new memories and the struggle to recall recent facts. This is followed by alterations in complex attention, executive function, language, visuospatial function, and behavior [20]. EOAD patients differ from LOAD patients on several clinical, neuroimaging and neuropathological features. For instance, EOAD patients tend to have better memory but worse attention and visuospatial skills than LOAD patients. In addition, EOAD patients present greater atrophy in the neocortex [19].

In most cases, AD is not diagnosed until there are clinical symptoms. However, longitudinal studies show that pathological features of the disease start 10 to 20 years before that (preclinical AD). Indeed, the 42 amino acid form of Aβ ($A\beta_{42}$), and Aβ plaques are respectively found in the cerebrospinal fluid (CSF) and in the brain years before the onset of AD [20]. The Aβ pathology leads to neuroinflammation, which becomes chronic. The tau pathology tends to occur later than the amyloidosis. All these pathological changes impair synaptic function and neuron viability and eventually affect the patient's cognition.

Mild cognitive impairment (MCI) is an early stage of memory loss or thinking problems that develops between preclinical and symptomatic AD. However, people can also suffer MCI not related to AD, and thus the diagnosis of AD in this stage must be performed using neuropsychologic tests, but also studying the patient's and relatives' medical history, neuroimaging, and biomarkers [21]. From this moment (symptomatic AD), the tau pathology, the synaptic dysfunction, the brain atrophy, and the cognitive deficits progressively increase until the appearance of dementia. The mean life expectancy after AD diagnosis is 7 years [21]. A thorough neuropathologic analysis of the postmortem brain is necessary for a definitive diagnosis of AD. Nonetheless, it is estimated that nowadays AD is correctly diagnosed in living patients with more than 95% accuracy [21]. The course of preclinical and symptomatic AD is illustrated in **Figure 1**.

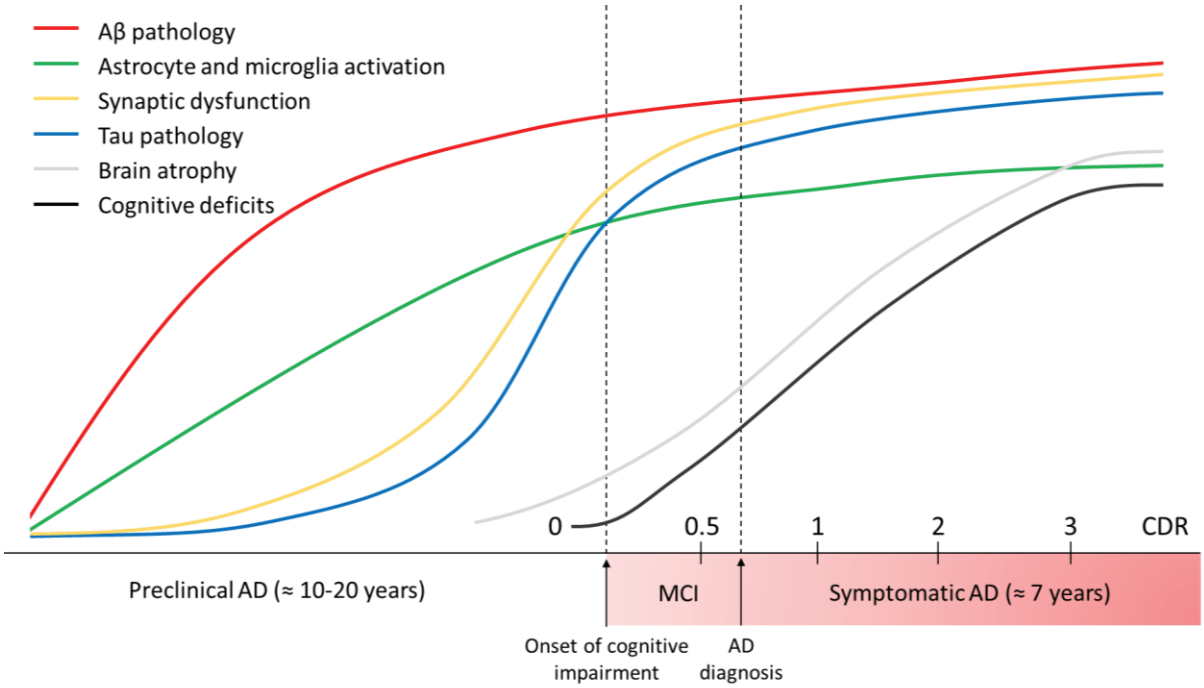

Figure 1. Time progression of major AD pathophysiological events. In the preclinical stage of AD, pathological features such as accumulation of Aβ and neurofibrillary tangles, glial activation, and synaptic deficits are already observed. With the onset of the cognitive impairment, the MCI phase starts. In this stage, patients can be diagnosed with AD by neuroimaging and analysis of biomarkers. All these features, as well as brain atrophy, continue to progress until the patient develops dementia. Death generally occurs approximately 7 years after diagnosis. Severity of clinical symptoms in AD are represented with the Clinical Dementia Rating (CDR) scale, ranging from 0 (normal cognition) to 3 (severe dementia). Image adapted from Long *et al.* [20] and Counts *et al.* [22].

1.4. Risk factors

As aforementioned, age is the main risk factor for the development of AD [23]. Indeed, it is estimated that the prevalence of AD practically doubles every 5 years after aged 65 [24]. Thus, one third of the people age 85 or older have AD dementia [4].

In 1983, Heyman *et al.* [25] reported that EOAD was associated to a genetic factor. Later, Ballard *et al.* [26] affirmed that genetics could explain 70% of the risk of developing AD. However, only 5-10% of EOAD cases (which in turn represent 5% of all AD cases) are directly caused by pathological genetic mutations [27]. Thus, many genetic variants modulate the susceptibility to AD, but they are rarely the direct cause of the pathology. The 3 genes sufficient to cause EOAD are: *APP*, *PSEN1* and *PSEN2* (amyloid precursor protein, presenilin 1 and presenilin 2, respectively). Of them, *PSEN1* mutations are the most common and are characterized by the earliest onset ages. Conversely, *APP* and *PSEN2* mutations are rarer [27]. Interestingly, the

proteins encoded by all these genes participate in the pathway involved in the production of Aβ. Other mutated genes have been linked to EOAD, but not as disease-causing, but rather, as risk variants. For instance, rare variants of sortilin-related receptor 1 gene (*SORL1*) are enriched in EOAD patients compared to controls [27], [28], [29]

A well-known risk factor for LOAD is the isoform ε4 of apolipoprotein E. *APOE* gene has 3 common isoforms: *APOE* ε2, ε3, and ε4, with a frequency of 8.4%, 77.9%, and 13.7%, respectively [30]. The ε3 allele is neutral regarding AD risk, whereas ε2 allele is protective. On the other hand, the ε4 allele is highly present among AD patients and it is associated with earlier disease onset ages [27]. Although *APOE* ε4 variant is not necessary nor sufficient to cause AD, the risk of having the disease at age 85 for ε4/ ε4 homozygotes is 51-60% [27], [31].

Besides genetic factors, there are some acquired risk factors that increase the risk of developing AD (reviewed in Silva *et al.* [32]). For instance, people with cerebrovascular diseases, hypertension, type 2 diabetes, and traumatic brain injuries [33] are in more risk to develop AD. It is unclear whether obesity is a risk factor for AD, since different meta-analysis have obtained contradictory results. On the other hand, there are some factors that have been associated with reduced risk of developing AD. These protective factors are the cognitive reserve, a healthy diet or physical activity, among others. Indeed, a significant positive correlation was observed between physical exercise and plasma levels of brain-derived neurotrophic factor (BDNF) in patients with AD [34].

1.5. Etiology

As previously mentioned, AD is characterized by the accumulation of extracellular Aβ plaques and the presence of intracellular tangles of hyperphosphorylated tau.

The physiological function of Aβ has remained unclear for decades. However, the fact that it is expressed throughout the lifespan, it is found in all vertebrates, and it is highly conserved among species, suggests that it must have a crucial function [35]. In addition, Aβ depletion has adverse consequences in multiple animal models (reviewed in Brothers *et al.* [36]). Nowadays, Aβ is known to have antimicrobial activity, to promote recovery from brain injury, and to regulate synaptic function, among others [36].

Aβ derives from APP, which is a single transmembrane glycoprotein with a large extracellular N-terminus and a shorter cytoplasmic C-terminus. APP is expressed in many tissues, especially in neuron synapses [37], where it regulates synaptic formation [38], neurite outgrowth [39], and cell adhesion [40]. APP can be processed by two different pathways. In the amyloidogenic

pathway (termed like this because it promotes Aβ production), APP is initially cleaved by β-secretase (also known as β-APP-cleaving enzyme-1 or BACE1), generating a membrane-bound C-terminal fragment (CTFβ) and releasing N-terminal sAPPβ. CTFβ is then cleaved by the γ-secretase complex (composed of presenilin 1 or 2 and other proteins), which results in the release of Aβ into the extracellular space and of APP intracellular domain (AICD) into the cytoplasm. In the non-amyloidogenic pathway, APP is first cleaved by α-secretase, releasing sAPPα and generating a membrane-tethered CTFα. Later, CTFα is cleaved by the γ-secretase complex producing AICD and releasing the P3 peptide [37], [41]. The processing of APP is depicted in **Figure 2A**.

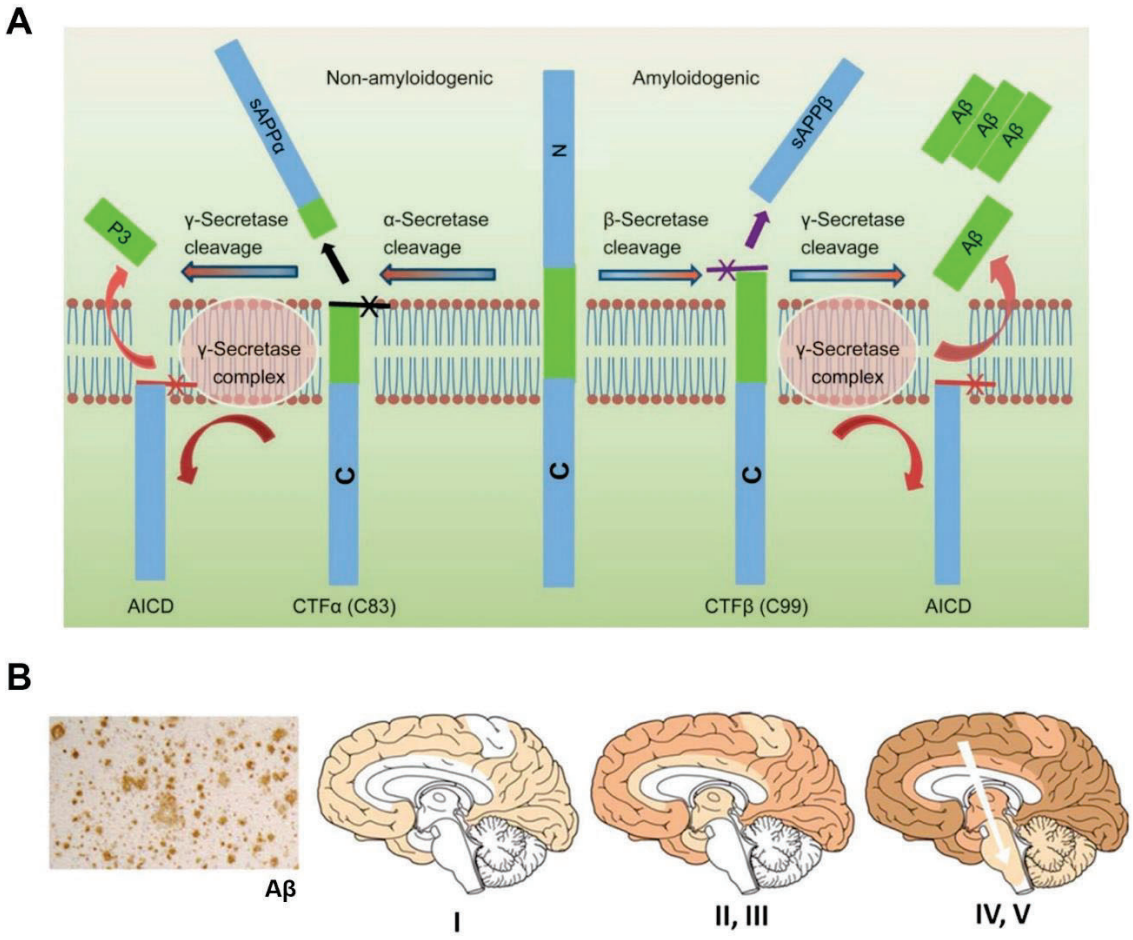

Figure 2. Formation of Aβ peptides and brain spreading of Aβ plaques. (A) Generation of Aβ peptides. APP can be sequentially cleaved by α- and γ-secretase, releasing sAPPα and P3 into the extracellular space, and AICD into the cytosol. However, if APP is first cleaved by β-secretase, the action of γ-secretase will result in the production of an Aβ monomer and AICD. Image obtained from Chen *et al.* [42] **(B)** Immunohistochemistry and spatiotemporal evolution of Aβ pathology according to Thal staging. Increasing color intensity indicates increased pathology. Image obtained from Jouanne *et al*. [43].

In 2002, Thal *et al.* [44] proposed that the Aβ pathology followed a descendent progression from the neocortex (stage I) to the limbic system including the hippocampus, amygdala, and thalamus (stages II-III), and finally, to the brainstem, pons and cerebellum (stages IV-V) (**Figure 2B).** Nonetheless, this spatiotemporal pattern of Aβ progression is less predictable than that of neurofibrillary tangles [45].

Tau is a microtubule-associated protein that stabilizes the microtubules and therefore is essential for cytoskeletal organization, trafficking, and neurite outgrowth [46]. Tau has multiple phosphorylation sites, and several kinases and phosphatases can regulate its phosphorylation status and function [47]. In physiological conditions, tau surrounds the microtubules and ensures they stay in a compact form. Nonetheless, when there is an imbalance between phosphorylation and dephosphorylation that results in tau hyperphosphorylation, tau self-assembles and aggregates, generating insoluble neurofibrillary tangles [47] (**Figure 3A**). As a result, the microtubules dissociate, and neuron viability is compromised. The aberrant deposition of tau is not exclusive of AD, but rather, it is the hallmark of all tauopathies [48].

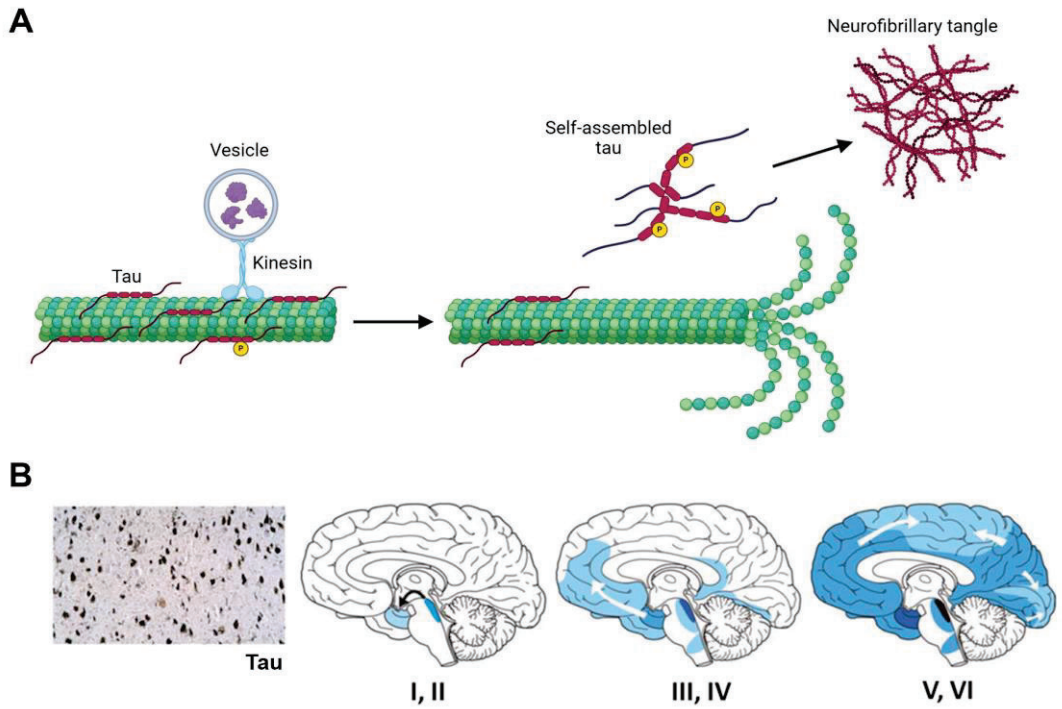

Figure 3. Formation and brain spreading of neurofibrillary tangles. (A) Generation of pathological neurofibrillary tangles. In physiological conditions tau stabilizes microtubules allowing a correct cytoskeletal organization and kinesin-mediated vesicle trafficking. In AD, tau is hyperphosphorylated, causing its dissociation from microtubules and its aggregation, which eventually generates neurofibrillary tangles. As a result, microtubules are disrupted, affecting their function, and leading to neuron death. **(B)**

Immunohistochemistry and spatiotemporal evolution of neurofibrillary tangles according to Braak staging. Increasing color intensity indicates increased pathology. Image obtained from Jouanne *et al*. [43].

The Braak stages, which were introduced by Braak *et al*. [49], are a measure of the severity and the distribution of the neurofibrillary tangles' pathology across the brain. Tau pathology starts in the entorhinal region (stages I-II), then moves to the limbic regions (III-IV) and finally spreads to the neocortex (V-VI) (**Figure 3B**). The fact that the spreading of neurofibrillary tangles follows a clear pattern has led to the hypothesis that they might propagate like prions [50]. However, the mechanism of propagation remains largely unknown. Interestingly, phosphorylation of tau at serine-202 and threonine-205 appear to be crucial for tau aggregation and AD pathogenesis since the phosphorylation status of these sites positively correlates with Braak staging [51].

1.6. Treatment

Unfortunately, there is no cure for AD or any drug that can arrest the progression of the disease. Thus, all available treatments are intended to palliate the symptoms.

Acetylcholine is an important neurotransmitter for memory and learning, whose levels decrease as AD advances [52]. The cholinergic hypothesis suggests that the cognitive decline observed in AD is due to the dysfunction of cholinergic neurons [53]. Currently, patients at any stage of the disease are treated with cholinesterase inhibitors, including donepezil, galantamine, tacrine or rivastigmine, among others [54]. Different meta-analyses have shown that the treatment with cholinesterase inhibitors has mild but significant therapeutic effect [55], [56].

N-methyl-D-aspartate receptors (NMDARs) are glutamate receptors also involved in memory and learning. NMDARs are present in the synapses but also in extrasynaptic locations. It is thought that extrasynaptic receptors might be activated by glutamate spillover from synapses or by ectopic release of glutamate [57]. Therefore, activation of extrasynaptic NMDARs is linked to a hyperactivity of glutamatergic neurons and might lead to excitotoxicity. Indeed, chronic activation of extrasynaptic NMDARs triggers cell death pathways [58]. Since glutamate excitotoxicity has been described in AD, different NMDAR antagonists have been tested. For instance, memantine, an antagonist of extrasynaptic NMDARs is currently used for the treatment of AD patients with dementia [59]. Clinical trials have demonstrated that memantine is effective in patients with moderate to severe AD, either as monotherapy or in combination with a cholinesterase inhibitor. However, its effect in patients at earlier stages remains unclear [60].

In recent years, immunotherapy against Aβ has appeared as a promising option for the treatment of AD. Currently, there are 4 monoclonal antibodies targeting Aβ aggregates in the late phase of clinical trials: lecanemab, aducanumab, gantenerumab, and donanemab [61]. Indeed, aducanumab and lecanemab were approved by the FDA in 2021 and 2023, respectively, for the treatment of early stages of AD. Both reduced brain Aβ plaques and slowed down the cognitive decline [62], [63]. These immunotherapies are expected to be successfully implemented in a near future, giving hope for many patients.

2. RTP801/REDD1

2.1. DDIT4 gene

RTP801, otherwise known as REDD1 (regulated in development and DNA damage responses 1) or Dig2 (dexamethasone-induced gene 2), is a stress-responsive protein encoded by the gene *DDIT4* (DNA damage inducible transcript 4). In 2002, two different groups concurrently cloned this gene and observed that its expression strongly increased under stress conditions. Shoshani *et al*. [64] found that the expression of this gene, which they called *RTP801*, increased by hypoxia via the transcription factor hypoxia-inducible factor 1 (HIF-1). Simultaneously, Ellisen *et al.* [65] identified it as a transcriptional target of p53 in response to DNA damage and designated it as *REDD1*. Soon afterwards, Wang *et al.* [66] described a novel dexamethasone-induced gene, called *dig2.* Eventually, *DDIT4* was the gene's official name.

In humans, *DDIT4* is located in the long arm of chromosome 10 (10q22.1) and it has a length of 2.1 kb. It presents 3 exons and 2 introns, and it has 3 splice variants [67]. *DDIT4* is ubiquitously expressed at low levels in human and mouse adult tissues, with lower expression in the brain. *DDIT4L* (DNA damage inducible transcript like) is a paralog of *DDIT4* and encodes for a protein with 50% homology with RTP801, known as RTP801L or REDD2 [65], which has similar functions [68].

Since the cloning of *DDIT4*, multiple stressors have been described to rapidly induce its expression, such as reactive oxygen species (ROS) [69], heat shock or endoplasmic reticulum (ER) stressors tunicamycin and thapsigargin [66], among others (reviewed in Kim *et al.* [70]). With respect to the nervous system, *DDIT4* is upregulated by dopaminergic neurotoxins like 6-hydroxydopamine (6-OHDA), N-methyl-4-phenyl-1,2,3,6-tetrahydropyridine (MPTP) and rotenone [71], and by toxic proteins such as Aβ [72] and mutant huntingtin (mhtt) [73]. These stressors act through many different transcription factors such as CCAAT/enhancer-binding protein (C/EBP) [74], [75], [76], activating transcription factor 4 (ATF4) [76], or cyclic adenosine monophosphate (cAMP) response element-binding protein (CREB) [77], among others (reviewed in Kim *et al.* [70]). On the other hand, *DDIT4* expression decreases by testosterone [78], acute resistance exercise [79] or suppressed mTORC1 activity [67].

Moreover, *DDIT4* expression can be regulated by multiple micro RNAs (miRNAs). For instance, miR-221, miR-495 and miR-630 downregulate *DDIT4* (reviewed in Tirado-Hurtado *et al*. [67]).

2.2. RTP801 protein

While human RTP801 is composed by 232 amino acids, the protein found in rat and mouse is formed by 229 amino acids and has an 85% homology with humans. Like *DDIT4* gene, RTP801 protein is ubiquitously expressed at low levels [64]. RTP801 is mainly localized in the cytoplasm [65], although it is also present in the nucleus [74], [80], mitochondria [81], [82], [83], and membranes [80], [84]. Interestingly, it is also found in dendrites, dendritic spines [85], and inside extracellular vesicles (EVs) [86].

To date, any functional motif or structural domain has been identified from RTP801 amino acid sequence. Indeed, RTP801 has not been associated to any enzymatic activity yet. Furthermore, the entire crystal structure of RTP801 remains elusive. However, Vega-Rubin-de-Celis *et al.* [87] were able to crystallize a portion of the human protein encompassing amino acids 89 to 226 when the non-conserved hydrophobic segment ^{200}FLPGF^{204} was deleted. They reported that RTP801 contains two α-helices and four β-sheets, and they found that two non-contiguous segments in the primary sequence clustered together in the three-dimensional (3D) structure to form a surface patch with highly conserved residues. These segments are ^{138}EPCG^{141} and a lysine-rich sequence in the C-terminus (^{218}KKKLYSSE^{225}), and the surface patch they form is essential for the inhibitory role of RTP801 upon mTORC1 [87], probably because it is the region of interaction with binding partners (**Figure 4A-E**). The importance of this region is manifested by two more findings. First, ^{219}KK^{220} promote an atypical activation of NF-κB (nuclear factor kappa B) through the sequestration of IκBα (NF-κB inhibitor alpha) [88], [89]. Second, ^{218}KKK^{220} are thought to be essential for the subcellular localization of RTP801 [80], and for its ubiquitination and subsequent degradation [70], [90].

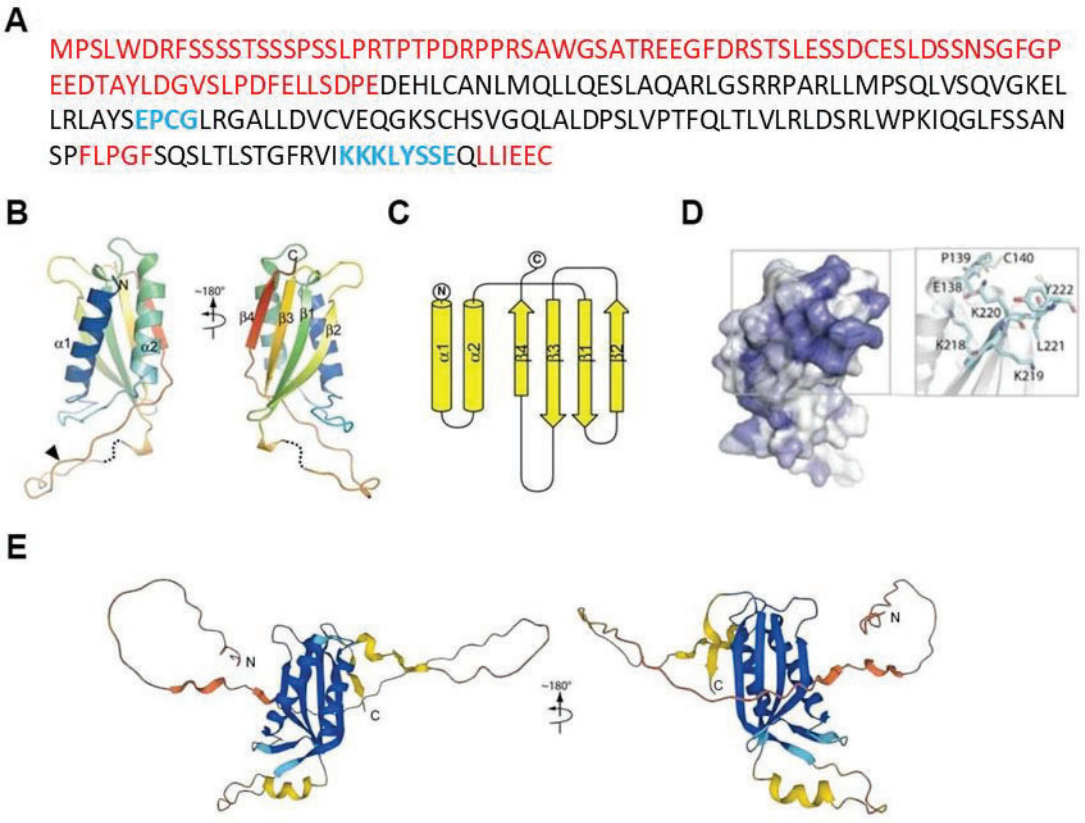

Figure 4. RTP801 protein structure. (A) Amino acid sequence of human RTP801 protein. Amino acids in red represent the non-crystalized regions. Amino acids in blue are highly conserved and form a surface patch necessary for RTP801-mediated inhibition of mTORC1. **(B)** Representation of RTP801 structure (the crystalized regions) colored in rainbow mode from the N- to the C-terminus. The dotted line depicts a disordered region, and the arrowhead indicates the location of the hydrophobic ^{200}FLPGF^{204} deletion. **(C)** Diagram of RTP801 topology. **(D)** Surface and stick representation of RTP801 conserved patch. The blue gradient is proportional to the degree of conservation of the residues. **(E)** Prediction of RTP801 structure according to AlphaFold Protein Structure Database. The color code indicates the model's confidence, which ranges from dark blue (very high confidence) to orange (very low confidence). Figure adapted from Vega-Rubin-de-Celis *et al.* [87].

Both *DDIT4* messenger RNA (mRNA) [66] and RTP801 protein [91], [92], [93] have very short half-lives, with the latter ranging from 2 to 8 minutes, and thus they are accurately regulated. RTP801 is mainly degraded via the ubiquitin-proteasomal system [65], [94], although it can also be degraded in the lysosomes [90]. Thus far, three E3 ligases are known to polyubiquitinate RTP801, targeting it for degradation: the CUL4-DDB1-ROC1-β-TrCP (cullin 4 – damage-specific DNA binding protein 1 – regulator of cullin 1 – β-transducin repeat containing) E3 ligase complex, which previously requires RTP801 phosphorylation by GSK3β (glycogen synthase kinase 3 beta)

[93], Parkin [95] and NEDD4 (neural precursor cell expressed, developmentally down-regulated 4) [90].

2.3. RTP801 physiological functions

The main described function of RTP801 is to negatively regulate the mTOR/Akt pathway (mTOR stands for mechanistic target of rapamycin) [71], [96], [97] although the exact mechanism is not completely clear. mTOR is a serine/threonine kinase that can associate with different proteins to form two complexes, mTORC1 (mTOR complex 1) and mTORC2 (mTOR complex 2). Briefly, mTORC1 is mainly activated by nutrients such as amino acids, and it promotes translation and the synthesis of biomolecules (lipids, nucleotides…) required for cell growth and proliferation. Moreover, mTORC1 inhibits catabolism, by repressing autophagy and the biogenesis of lysosomes. On the other hand, mTORC2 is generally activated by growth factors and promotes actin cytoskeleton organization, proliferation, and survival [98] (**Figure 5**).

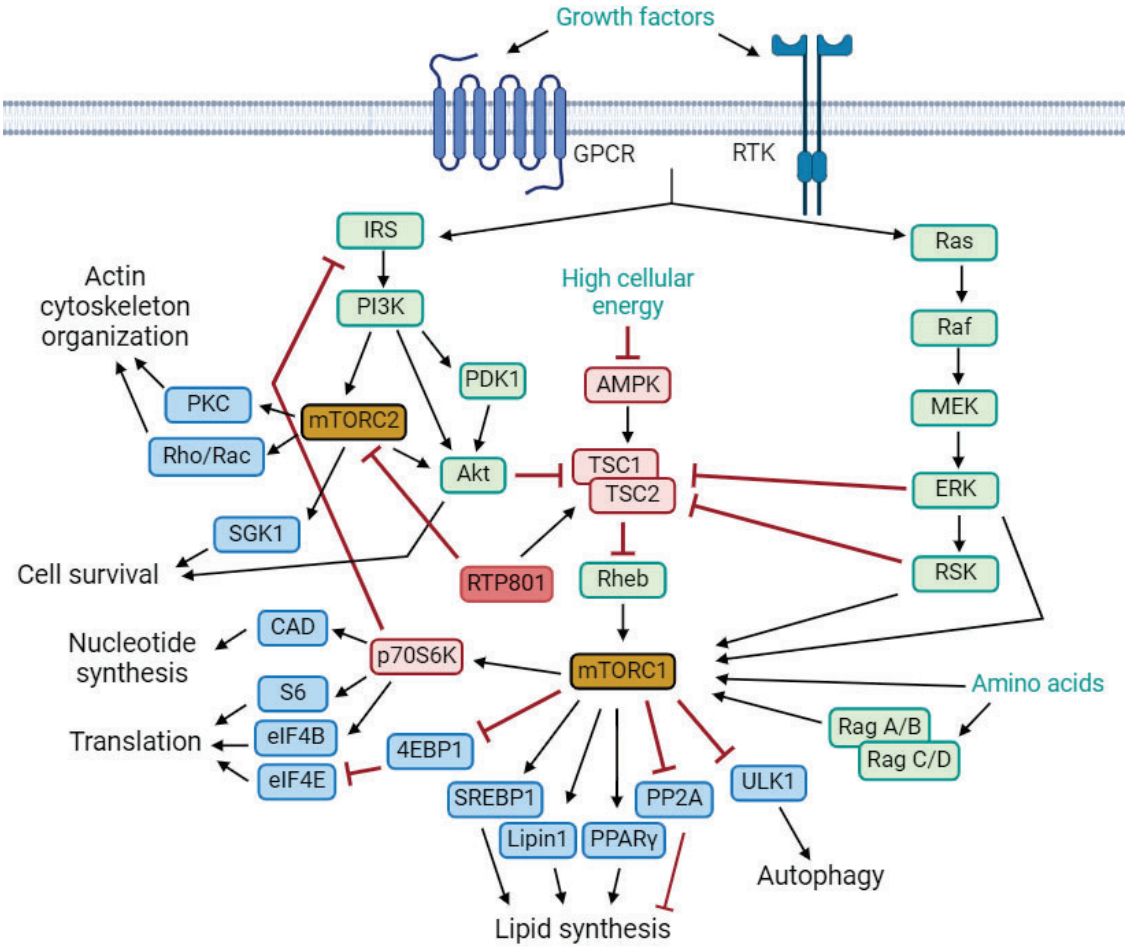

Figure 5. Schematic representation of the mTOR signaling pathway. The main cellular pathways that lead to the activation of mTORC1 and mTORC2 (in yellow) are illustrated. Direct or indirect activators of mTORC1 and mTORC2 are shown in green, while indirect inhibitors of the complexes are in red (RTP801

is depicted in darker red). Downstream mTORC1/2 effectors are shown in blue. mTORC1 promotes the biosynthesis of nucleotides through p70S6K; protein synthesis through p70S6K and inhibition of 4EBP1 (eukaryotic translation initiation factor 4E-binding protein 1); lipogenesis via Lipin1, SREBP1 (sterol regulatory element-binding protein 1), PPARγ (peroxisome proliferator-activated receptor γ), and PP2A (protein phosphatase 2A); and autophagy repression via ULK1 (Unc-51 like autophagy activating kinase 1) inhibition. mTORC2 mediates actin polymerization through PKC (protein kinase C), RhoA and Rac1, and cell survival via Akt and SGK1 (serum and glucocorticoid regulated protein kinase 1). Figure adapted from Kim *et al.* [99] and Laplante *et al.* [100] with *Biorender.com*.

In the nervous system, the mTOR pathway can also be activated by cytokines, neurotrophins like BDNF or neurotransmitters [101], [102], [103]. All these inputs eventually activate either the PI3K (phosphoinositide 3-kinase) pathway, the Ras pathway or both, which converge in the inhibition of the heterodimer formed by TSC1 and TSC2 (tuberous sclerosis proteins 1 and 2).

The TSC1/TSC2 dimer acts as a GTPase-activating protein for the small G-protein Rheb (Ras homologue enriched in brain), and thus catalyzes the transition from Rheb-GTP to Rheb-GDP, its inactive form [104]. Phosphorylated TSC2 translocates from endomembranes to the cytosol [105], which leads to the activation of Rheb and mTORC1 [70], [106]. Brugarolas *et al.* [96] demonstrated that mTOR inhibition in response to hypoxia required RTP801 and TSC1/2 but seemed independent of TSC2 phosphorylation. In the same year, Reiling *et al.* [107] reported that Scylla and Charybdis (the orthologues of RTP801 in *Drosophila*) inhibited mTOR-mediated growth by acting upstream of TSC1/2. Since RTP801 does not have any described enzymatic activity or functional domains, the mechanism by which it regulates the mTOR pathway remains a mystery. Different models have been proposed to answer how RTP801 activates TSC1/2, but none of them have been completely demonstrated [84], [108].

Besides regulating the mTOR pathway, RTP801 regulates the timing of cortical neurogenesis and neuron migration during brain development [109]. Indeed, RTP801 levels decrease as neuroprogenitors differentiate into neurons. Thus, RTP810 knockdown in neuroprogenitors accelerates their differentiation and alters their migration to the cortical plate resulting in an ectopic localization of mature neurons.

In adulthood, RTP801 modulates neuronal plasticity and learning, since RTP801 knockout (KO) mice present enhanced excitatory synaptic transmission and improved motor learning [110]. The improvement in motor learning, assessed by their performance in the accelerating rotarod, correlated with increased filopodia and mushroom spines in the basal dendrites of neurons in the motor cortex layer V [110].

Moreover, our group has recently described that RTP801 also regulates the content and the release of EVs [86]. Strikingly, endogenous RTP801 is present in EVs and its overexpression increases their release. Regarding the content of EVs, both the silencing and the overexpression of RTP801 affected their cargo. Thus, RTP801 overexpression promoted the loading of vesicles with pro-apoptotic proteins, whereas RTP801 silencing led to the loading with anti-apoptotic proteins.

Noticeably, RTP801 has a dual role depending on the cellular context. Thus, in proliferating cells it has an anti-apoptotic role [64] while in differentiated cells it is pro-apoptotic [64], [71]. In this context, RTP801 elevation has been associated both to cancer [111], [112], [113] and neurodegeneration [71], [73], [95], [114].

2.4. RTP801 in neurodegeneration

2.4.1. RTP801 in Parkinson's disease

In 2006, Malagelada *et al.* [71] reported that RTP801 was induced in cellular and animal models of PD. They found that both *DDIT4* mRNA and RTP801 protein levels were increased when differentiated PC12 cells were treated with 6-OHDA. In addition, treatment with MPTP and rotenone also increased RTP801 protein levels. RTP801 was also upregulated in the substantia nigra of mice treated with MPTP, as well as in substantia nigra neurons of PD patients. Interestingly, the authors described that RTP801 upregulation promoted cell death in cellular models of PD, whereas cell death was prevented when RTP801 was silenced. Thus, RTP801 was sufficient and necessary for neuronal death. Two years later, the same group described that RTP801 promotes cell death in cellular models of PD by inhibiting mTOR signaling and reducing the phosphorylation status of Akt at the serine 473 residue, which is essential for cell survival (see **Figure 5**) [115]. Later, rapamycin was reported to protect against neuron death in *in vitro* and *in vivo* models of PD, probably by blocking the translation of *DDIT4* [92].

In 2013, the transcription factor ATF4 was found to protect against neuronal death in cellular models of PD by maintaining the levels of the E3 ligase parkin, although the exact mechanism by which parkin promoted survival was not clear [116]. One year later, RTP801 was described as a parkin substrate [95]. Similarly, in 2016, the E3 ligase NEDD4 was also found to polyubiquitinate RTP801, targeting it for proteasomal degradation [90]. Indeed, both parkin and NEDD4 overexpression protected cells from 6-OHDA/RTP801-induced death.

Finally, in 2018, Zhang *et al.* [117] found that a mouse model of PD subjected to chronic stress showed increased RTP801 levels specifically in dopaminergic neurons of the substantia nigra.

Interestingly, they also described a reduced proteasomal degradation of RTP801, which contributed to its high content. However, when RTP801 was inhibited the symptoms of neurodegeneration were ameliorated. Altogether, these results show that RTP801 is induced by PD mimetics, which leads to mTOR suppression, Akt inactivation, and cell death. Moreover, RTP801 proteasomal degradation is impaired in PD. Thus, overexpression of RTP801-targeting E3 ligases prevents cell death and slows down neurodegeneration, as illustrated in **Figure 6.**

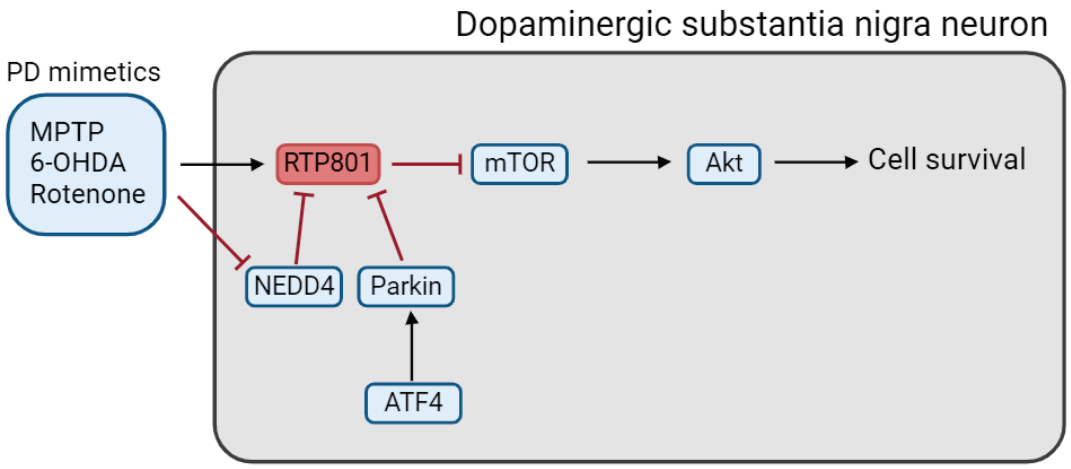

Figure 6. Schematic representation of RTP801 regulation in PD. PD mimetics promote the upregulation of RTP801 in substantia nigra neurons, which leads to the inhibition of mTOR and Akt, and suppressed pro-survival signaling. Moreover, 6-OHDA decreases NEDD4 protein expression [90]. NEDD4 and parkin, as E3 ligases, polyubiquitinate RTP801 targeting it for proteasomal degradation and preventing cell death. Figure created with *Biorender.com*.

2.4.2. RTP801 in Huntington's disease

In 2016, our group found that mhtt elevated RTP801 mRNA and protein levels *in vitro* by promoting its expression but also by inhibiting its proteasomal degradation [73]. RTP801 upregulation by mhtt induced cell death, and RTP801 silencing prevented it. Strikingly, while RTP801 expression seemed not to be altered in the striatum of two HD mouse models (HdHQ7/Q111 and R6/1), increased levels were observed in the striatum and cerebellum of human HD postmortem brains.

Four years later, we reported that mhtt overexpression in rat cortical cultures induced a significant reduction in the number of spines, which was accompanied by increased levels of RTP801 in the remaining spines [85]. Likewise, RTP801 was enriched in the striatal synaptosomes of HD patients, and of HdHQ7/Q111 and R6/1 mice. In addition, striatal RTP801 knockdown in

R6/1 mice improved their performance in the accelerating rotarod, reverted abnormally high levels of phosphorylated Akt, and increased the expression of synaptic proteins.

Recently, we described increased levels of RTP801 in the hippocampus of HD patients, which positively correlated with gliosis markers [118]. Interestingly, although RTP801 was not altered in the hippocampus of R6/1 mice, its silencing in neurons of the dorsal hippocampus prevented cognitive deficits, partially rescued synaptic markers, and reduced gliosis. Moreover, the NLR family pyrin domain containing 1/3 (NLRP1/3) inflammasomes were drastically activated in R6/1 mice, and RTP801 silencing corrected their levels.

Overall, these results suggest that mhtt induces RTP801 overexpression especially in the synapses, which ends up affecting synaptic function and leads to motor and cognitive deficits. The hallmarks of RTP801 in HD pathophysiology are illustrated in **Figure 7**.

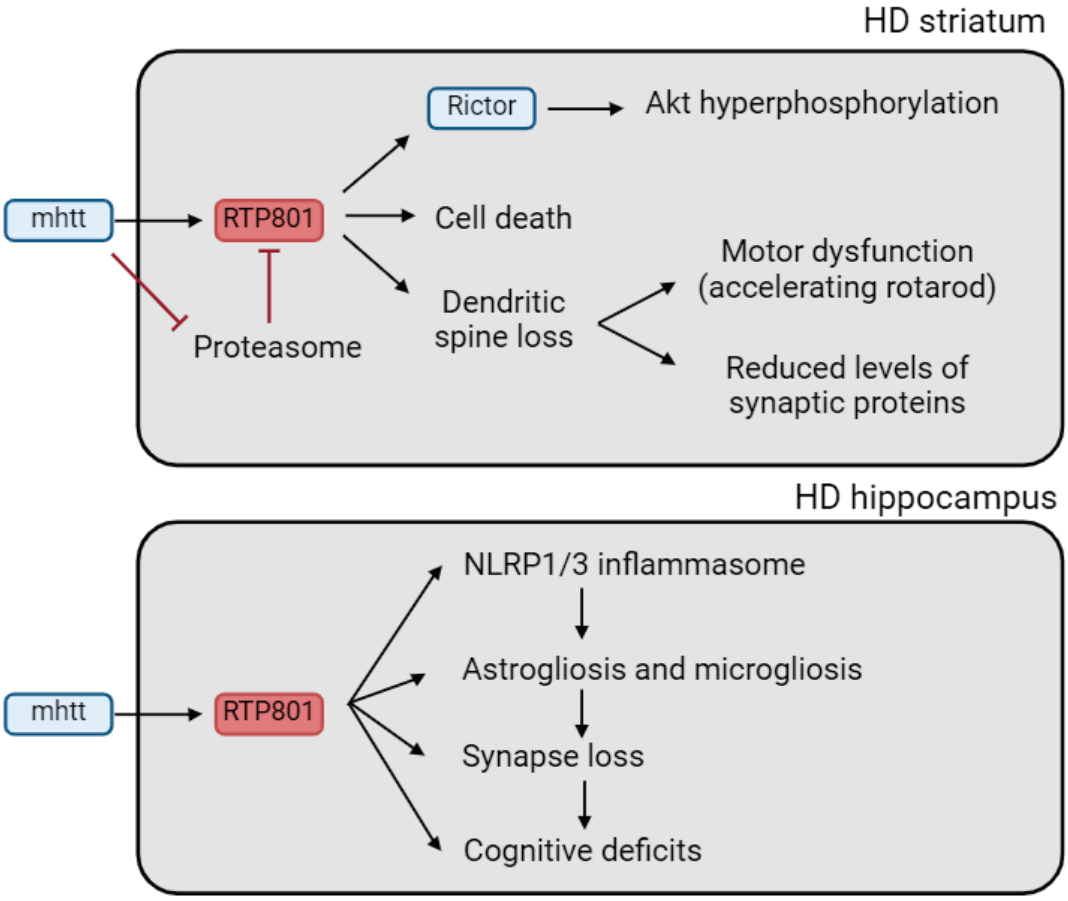

Figure 7. Proposed model of RTP801 effects in HD. Mhtt causes the upregulation of RTP801 in the striatum and the hippocampus of HD patients, as well as in the striatal synaptosomes of HD mouse models. The silencing of RTP801 in striatal neurons prevents aberrant Akt hyperphosphorylation, motor dysfunction and loss of synaptic proteins. Hippocampal silencing of RTP801 prevents the increase in

inflammasome components, gliosis, synapse loss, and cognitive deficits. Figure created with *Biorender.com*.

2.4.3. RTP801 in Alzheimer's disease

In 2003 Kim *et al.* [72] identified *DDIT4* as an Aβ-responsive gene in a human cell line. Interestingly, overexpression of RTP801 increased cell sensitivity to Aβ-toxicity while RTP801 downregulation had the opposite effect. Likewise, in 2020, Yi *et al.* [119] reported that Aβ exposure increased RTP801 levels in mouse hippocampal slices. Moreover, they found that both RTP801 overexpression and Aβ treatment suppressed hippocampal long-term potentiation (LTP). However, when Aβ treatment was accompanied by RTP801 downregulation, the impairment in LTP was abrogated. Furthermore, RTP801 downregulation reverted Aβ-induced memory impairments. These results indicate that RTP801 contributes to AD pathogenesis.

In AD, there is an upregulation of the PKR (protein kinase R) pathway (reviewed in Hugon *et al.* [120]), which senses many different stress signals. In 2009, Damjanac *et al.* [121] described increased levels of phosphorylated p53 and RTP801 in lymphocytes from AD patients. Moreover, the levels of phosphorylated PKR positively correlated with the levels of phosphorylated p53, which in turn, had a significant correlation with RTP801 levels. Indeed, the knockout of PKR in the 5xFAD mouse model of AD improved spatial memory, reduced brain amyloid accumulation and neuroinflammation markers [122].

Similarly, our group recently reported that RTP801 mediates neuroinflammation in mouse models of AD [114] and HD [118] (see Introduction section 2.4). Regarding AD, we described that RTP801 downregulation in hippocampal neurons of 5xFAD mice ameliorated cognitive deficits, reduced neuroinflammation, and corrected the levels of inflammasome markers [114]. Moreover, our work described increased levels of RTP801 in postmortem hippocampal samples, which positively correlated with both Braak and Thal stages of the disease. These results demonstrated that RTP801 accumulates as the disease advances and therefore, could be a biomarker of the progression of the pathology.

In line with this role in neuroinflammation, and as previously mentioned, RTP801 promotes an atypical activation of NF-κB through the sequestration of IκBα [88], [89]. Noteworthily, the expression of NLRP1 and NLRP3 inflammasomes is regulated by NF-κB [123], [124]. Indeed, treatment of macrophages with lipopolysaccharide (LPS) increased RTP801 expression, NF-κB activation, and inflammation, but these responses were suppressed by RTP801 knockdown. On the contrary, RTP801 overexpression promoted NF-κB-dependent inflammation [89].

Altogether, evidence shows that RTP801 regulates inflammation and neuroinflammation by modulating the NF-κB pathway and the inflammasome (**Figure 8**).

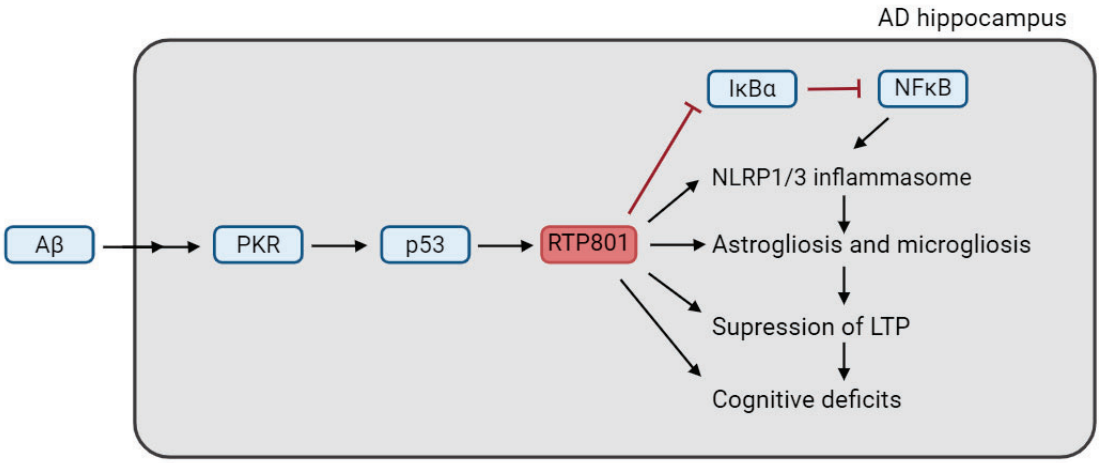

Figure 8. Graphical model of the pathological role of RTP801 in AD. The extracellular deposits of Aβ eventually activate the PKR pathway, which promotes the transcription of *DDIT4*. RTP801 protein sequesters IκBα, thus activating NFκB. RTP801 also modulates the NLRP1/3 inflammasome, gliosis, the LTP and cognitive deficits, as observed by silencing it in hippocampal neurons [114]. Figure created with *Biorender.com*.

Overall, RTP801 appears to be a master regulator of neurodegeneration, and its dysregulation contributes to the progression and severity of the pathology. The great importance of RTP801 might be due to its regulation upon the inflammasome, but also upon mTOR, and thus, upon cell growth, survival, and protein synthesis.

2.5. RTP801 potential novel functions

To date, any enzymatic activity has been linked to RTP801. Therefore, it is unclear how it regulates the multiple processes in which it participates. What is more, RTP801 might have functions not yet described. In order to assess this question, our group studied its physical interactors by mass spectrometry (MS) [125]. Briefly, RTP801 was immunoprecipitated from rat primary cortical neuronal cultures and the resulting immunocomplexes were resolved by electrophoresis. The bands were numbered, cut, and analyzed by MS. Interestingly, two of the identified proteins were DDX1 (DEAD-box helicase 1) and HSPC117, which are part of the tRNA splicing ligase complex (tRNA-LC), first described by Popow *et al.* in 2011 [126]. Thus, RTP801 might have an unknown role in RNA splicing.

3. RNA splicing

There are several different types of RNA, which can be classified by their function, structure, and length. The RNAs that encode proteins are called mRNAs (or coding RNAs) and represent less than 3% of our genome [127]. Indeed, the vast majority of our genome is transcribed to non-coding RNA, which can be divided by its length in small or long non-coding RNA (sncRNA and lncRNA, respectively). Generally, RNAs shorter than 200 nucleotides (nt) in length are considered sncRNAs. In this group, we can find ribosomal RNA (rRNA), transfer RNA (tRNA) or miRNA, among others. On the other hand, lncRNAs include transcripts from intergenic regions, introns, or antisense transcripts [128].

All these RNAs, independently of their size or function, need to be processed to be physiologically active. In this work, we will focus on the splicing of tRNAs and the unconventional splicing of X-box binding protein 1 (*XBP1)* mRNA, in which the tRNA-LC participates.

3.1. tRNA

tRNAs are a type of sncRNA with a major role in protein synthesis since they allow decoding the mRNA sequence into amino acids. Each tRNA molecule binds an amino acid and has a 3-nt sequence called anticodon. When the anticodon of the tRNA is complementary to the 3-nt sequence in the mRNA called codon, the respective amino acid is added to the nascent protein.

3.1.1. Structure

Nowadays, more than 150,000 tRNA molecules from different species spanning all domains of life have been sequenced [129]. Strikingly, the great majority of tRNAs share a common structure, which manifests the relevance of their unique architecture for proper function.

The length of canonical tRNAs ranges between 76 and 90 bases and their average mass is over 26,000 g/mol (=26 kDa), similarly to a 230 amino acid residue protein. Their secondary structure is represented by the cloverleaf model and depends on internal base pairing that forms a stem-loop or hairpin pattern when represented in two dimensions (2D). From 5' to 3', the hairpin structures are the acceptor stem, the D-arm, anticodon stem, variable loop, and T-arm. The D-arm, which stabilizes the tRNA tertiary structure, is named for the modified dihydrouridine base found in the loop. The variable loop has a variable length, as its name implies. The T-arm, often referred as the TΨC arm, is crucial for enabling interactions with the ribosome and is named after the presence of the universally conserved modified bases thymidine, pseudouridine and cytidine. The anticodon is a 3-nt single-stranded region that determines translation specificity

by base pairing with the mRNA's codon. The cytosine/cytosine/adenine (CCA) 3'-terminal group, found in the acceptor stem of tRNAs, is the region where the amino acid is covalently bound by an ester linkage. The addition of the amino acid to the tRNA is known as charging or aminoacylation and is performed by specific enzymes called aminoacyl-tRNA synthetases (aaRSs). The ribosome does not read the amino acid carried by the tRNA, hence the specificity of aminoacylation by aaRSs is essential. Therefore, if the tRNA is wrongly aminoacylated, the protein will incorporate an improper amino acid even though the codon-anticodon base pairing is correct, which was elegantly shown by Chapeville *et al.* in 1962 [130]. The base 5' to the terminal CCA is called the discriminator base because it is crucial for aminoacylation specificity. Neither the CCA trinucleotide nor the discriminator base are base paired. The cloverleaf model of the tRNA secondary structure is depicted in **Figure 9A**. Regarding the tertiary structure, tRNAs fold into an L-shaped conformation, mainly through intramolecular interactions of the D- and T-arms. Thus, 3D tRNAs present two branches: the acceptor branch and the anticodon branch. The region where the branches meet is known as the elbow (**Figure 9B**).

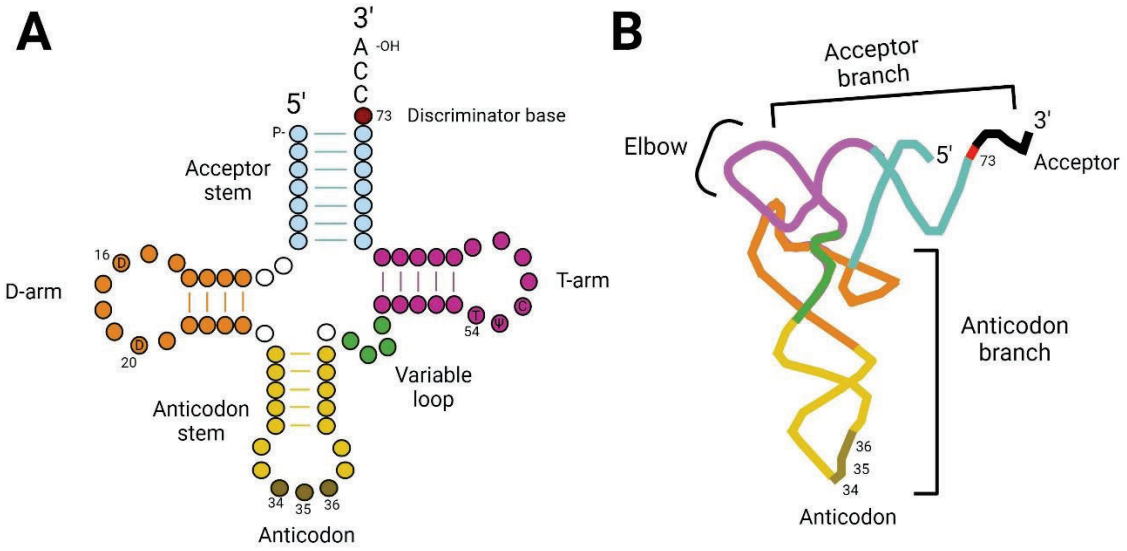

Figure 9. tRNA structure. (A) Cloverleaf representation of a tRNA in 2D. From 5' to 3' the regions are: acceptor stem (blue), D-arm (orange), anticodon stem (yellow) containing the anticodon (gold), variable arm (green) and T-arm (purple). The discriminator base is represented in red. The canonical positions of the anticodon (34-36) and the discriminator base (73) are indicated, as well as the positions of conserved modified bases such as dihydrouridine-16, and dihydrouridine-20 in the D-arm, and thymidine-54 in the T-arm. Thin lines between bases represent internal base pairing. **(B)** Representation of the L-shaped 3D tRNA structure. The different regions of the tRNA are depicted with the same color pattern as in **(A)**. Intramolecular interactions between the D- and T-arms (orange and purple respectively) in the elbow

region promote tRNA folding. Canonical positions of the anticodon and the discriminator base are shown. Figure adapted from Berg *et al.* [131].

3.1.2. Transcription

Codon degeneracy refers to the fact that different codons specify the same amino acid. For example, both GCC and GCG codons specify the amino acid alanine (Ala). For this reason, there are tRNAs with different anticodons that are charged with the same amino acid. These tRNAs are called isoacceptor tRNAs (e.g., tRNA-Ala). The reason of this degeneracy is that there are 61 codons (besides the 3 termination codons) but only 20 amino acids, or 21 if we consider selenocysteine. In addition, an isoacceptor set can be composed of multiple tRNA species that slightly differ in their nucleotide sequence. These tRNA species with the same anticodon are called isodecoder tRNAs (e.g., tRNA-Ala-CGC) and each of them is encoded by a different gene, as depicted in **Figure 10**. Indeed, there are 429 tRNA genes encoded by the human genome according to GtRNAdb (Genomic tRNA database) [132]. The reason of this genetic expansion remains elusive. However, a recent study suggests that the presence of isodecoders is required to ensure proper translation and cell viability. For instance, murine tRNA-Phe-GAA-1-1 is required for neuronal function and its loss is partially compensated by increased expression of other tRNAs [133]. Therefore, not all human tRNA genes are transcribed in all cells and tRNA expression is tissue-specific [134].

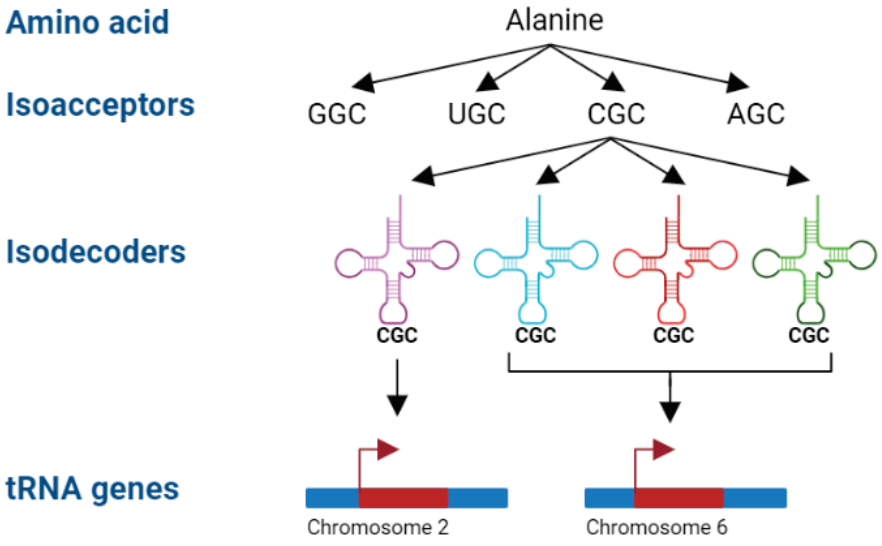

Figure 10. Scheme of alanine isoacceptors and isodecoders. The amino acid alanine has 4 different isoacceptor tRNAs (tRNA-Ala-GGC, tRNA-Ala-UGC, tRNA-Ala-CGC and tRNA-Ala-AGC). tRNA-Ala-CGC presents 4 isodecoders (tRNA-Ala-CGC-1-1, tRNA-Ala-CGC-2-1, tRNA-Ala-CGC-3-1 and tRNA-Ala-CGC-4-1).

tRNA-Ala-CGC-1-1, tRNA-Ala-CGC-2-1 and *tRNA-Ala-CGC-4-1* genes are found on chromosome 6 while *tRNA-Ala-CGC-3-1* localizes on chromosome 2. Figure adapted from Loher *et al.* [135] with *Biorender.com*.

In eukaryotes, tRNA genes are transcribed by RNA polymerase III (RNA Pol III) and are highly expressed at approximately 300,000 copies per cell. Transcription generates precursor tRNA molecules (pre-tRNAs), which must be processed in order to obtain the mature tRNAs.

Besides nuclear tRNA genes, there are also mitochondrial tRNA (mt-tRNA) genes. In fact, 22 of the 37 genes found in human mitochondrial DNA encode for tRNA genes. In humans, mitochondrial transcription is driven by an RNA polymerase called POLRMT [136] and generates long polycistronic transcripts from both chains of mitochondrial DNA. These long transcripts are cleaved by endonucleases in order to separate mt-tRNAs from rRNAs and mRNAs. Processing of mt-pre-tRNAs takes places in the mitochondria and requires the transport into this organelle of nuclear-encoded aaRSs. Mature mt-tRNAs will participate in local protein synthesis within mitoribosomes [137], [138].

3.1.3. Processing

In vertebrates, early tRNA processing occurs in the nucleus and includes intron splicing and removal of the 5’ leader and 3’ trailer. However, it remains unclear which step occurs before, or whether they happen simultaneously. Late tRNA processing includes addition of a CCA trinucleotide on the 3’ end, nuclear export and aminoacylation. Throughout the processing, many posttranscriptional modifications are introduced to the pre-tRNAs, which are essential for their proper function [139].

3.1.3.1. Leader and trailer removal

The 5’ leader and the 3’ trailer are short sequences of nucleotides found in the 5’ and the 3’ ends of all pre-tRNAs, respectively. They have a variable length, with the average length of 6 nt at the 5’ leader and 10 nt at 3’ trailer of human pre-tRNAs [140]. 5’ leader removal is enzymatically performed by ribonuclease P (RNase P) whereas 3’ trailer removal is performed by ribonuclease Z (RNase Z, also known as ELAC2 in human). ELAC2 precisely cleaves the pre-tRNA after the discriminator base to generate a new 3’ end site to which the CCA trinucleotide will be added.

3.1.3.2 Intron splicing

All human pre-tRNAs have a 5’ leader and a 3’ trailer but only 28 of them present an intron, which is between 12 and 26 nt long and must be spliced out for tRNA maturation. The proportion of tRNA genes with intron varies considerably between species. While this fraction is relatively

similar within mammals and invertebrates (~7% in human, ~ 5% in mice, ~ 6% in both *Drosophila* and *Caenorhabditis*), yeast genomes contain a higher proportion of intron-containing tRNA genes (~ 25%) [141]. Human introns are always positioned one nucleotide 3' to the anticodon, although noncanonical positioning is detected both in eukarya and specially in archaea [142]. tRNA splicing consists in two steps, first the cleavage, to remove the intron, and then the ligation of the intron-free halves.

In mammals, the cleavage is performed by the tRNA splicing endonuclease (TSEN) complex, which consists of two structural proteins (Tsen15 and Tsen54), two catalytic proteins (Tsen2 and Tsen34), and cleavage factor polyribonucleotide kinase subunit 1 (Clp1), an essential kinase whose exact function in tRNA splicing remains unclear but might play a regulatory role in tRNA splicing *in vivo* [143]. Endonucleolytic cleavage generates two exons and one intron. 5' exon has a 2',3'-cyclic phosphate terminus while 3' exon has a 5'-hydroxyl (OH) terminus.

The excised tRNA exons are joined by tRNA ligases. There are two different chemical ligation pathways classified from the origin of the phosphate group that bridges the exons: the 5'-phosphate ligation pathway, found in plants and fungi, which takes a phosphate from the 5' end in the 3' exon, and the 3'-phosphate ligation pathway, predominant in animals, which uses the phosphate group in the 3' end of the 5' exon. Both pathways first need to open the 2',3'-cyclic phosphodiester on the 5' exon.

In plants and fungi, the modification of the pre-tRNA ends and the ligation in the 5'-phosphate ligation pathway is performed by an enzyme called Trl1. It is unclear whether this pathway is present in animals since a metazoan 5'-phosphate ligase has not yet been identified. However, Clp1 associated to the TSEN complex was described to phosphorylate the 5' terminus of the 3' exon *in vitro*, suggesting the occurrence of coupled endonuclease and kinase reactions in humans [144]. Therefore, even if vertebrates have the complete set of enzymes required for this pathway, it might contribute to only a small, if any, fraction of tRNA splicing [142], [145].

In the 3'-phosphate ligation pathway, also known as animal pathway, the pre-tRNA halves are directly ligated using the phosphate left on the 3' end of the 5' exon [142], [146]. In mammals, the ligation is performed by the tRNA-LC, and specifically, by HSPC117, a ligase discovered by Popow *et al.* in 2011 [126]. They found that HSPC117, also known as RtcB, is the essential subunit of the complex since depletion of HSPC117 mediated by RNA interference (RNAi) inhibited maturation of intron-containing pre-tRNAs both *in vitro* and in living cells. Additionally, a mutation in a conserved cysteine residue abolished its ligase activity. However, RNAi-mediated depletion of the other members of the complex did not compromise ligation as severely.

HSPC117 joins the tRNA exon halves by incorporating the phosphate in the 3' end of the 5' exon into the mature tRNA as a canonical 3',5'-phosphodiester (**Figure 11**).

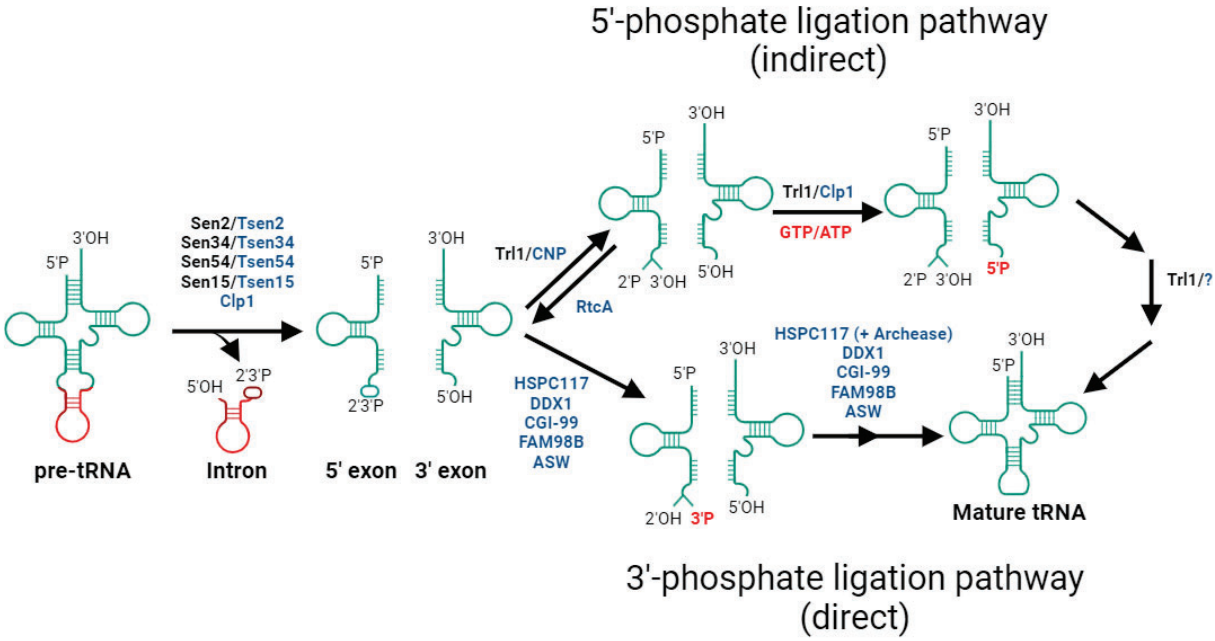

Figure 11. The 5'- and the 3'-phosphate ligation pathways for tRNA intron splicing. The chemical reactions illustrating the cleavage of pre-tRNA (left), the 5'-phosphate ligation pathway (upper), and the 3'-phosphate ligation pathway (lower) are shown. Proteins and enzymes involved in individual reactions are also shown and unidentified factors are indicated by question marks. Proteins of plants and yeast are shown in black while proteins of mammal are written in blue. The origin of the phosphate group used to bridge the 2 exons is marked in red. In the 5'-phosphate ligation pathway, yeast Trl1 uses guanosine triphosphate (GTP) as a phosphate donor for 5'-phosphorlyation while mammalian Clp1 uses adenosine triphosphate (ATP). In the 3'-phosphate ligation pathway all the steps are performed by the tRNA-LC, but HSPC117 is the 5' ligase and the essential subunit, which requires cofactors like archease for full activity. Figure adapted from Yoshihisa *et al.* [142] with *Biorender.com*.

Thus, phosphorylation of the 5' terminus of the 3' exon by Clp1 interferes with HSPC117-mediated ligation [126], [146]. The other components of the tRNA-LC are DDX1, CGI-99, Ashwin (ASW) and FAM98B (family with sequence similarity 98 member B). Moreover, this complex also has some cofactors and some competitors. The name and function in tRNA processing of the complex members and their regulators are summarized in **Table 1**.

	Name	Function in tRNA processing
tRNA-LC	**HSPC117**/RtcB	tRNA halves ligation [126]
	DDX1	Promotes ligation by enabling the formation of an HSPC117-guanylate intermediate [147]
	CGI-99/CLE/RTRAF	Unknown
	ASW	Unknown
	FAM98B	Unknown
Coenzymes	**Archease**	Promotes ligation by enabling the formation of an HSPC117-guanylate intermediate [147], [148]
	Pyridine nucleotide-disulfide oxidoreductase domain 1 (**PYROXD1**)	Protects HSPC117 from oxidation with the help of nicotinamide adenine dinucleotide (phosphate) ($NAD(P)^+$) [149]
	RNA 3'-terminal phosphate cyclase (**RtcA)**	Circularizes the 2',3'-phosphate in the 3' end to a 2',3'-cyclic phosphate (antagonist of CNP) [150], [151]
Competitors	**Clp1**	Phosphorylates the 5' end of the 3' exon, impeding HSPC117 ligation [144]
	ANGEL2	Dephosphorylates the 2',3'-cyclic phosphate in the 3' end of the 5' exon [152]
	2',3' cyclic nucleotide phosphodiesterase (**CNP**)	Hydrolyses the 2',3'-cyclic phosphate in the 3' end of the 5' exon to a 2'-phosphate and a 3'-hydroxyl (antagonist of RtcA) [150], [153]

Table 1. Function in tRNA processing of the members of the tRNA-LC, their coenzymes, and competitors. Names and protein symbols are shown. Bold symbols indicate the form preferentially used in this work. Table adapted from Gerber *et al.* [146].

Recently, Kroupova *et al.* [154] presented an elegant work identifying the regions of physical interaction between the components of the human tRNA-LC, along with the crystal structures of HSPC117 and the N-terminal domain of CGI-99. They also showed that the core of the complex is formed by HSPC117 and the C-terminal alpha-helical regions of DDX1, CGI-99 and FAM98B, all of which are necessary for complex integrity (**Figure 12**). These results suggest that these three noncatalytic subunits (DDX1, CGI-99 and FAM98B) might function synergistically to generate an interaction platform for HSPC117. On the contrary, the absence of ASW did not affect the formation of the core of the complex.

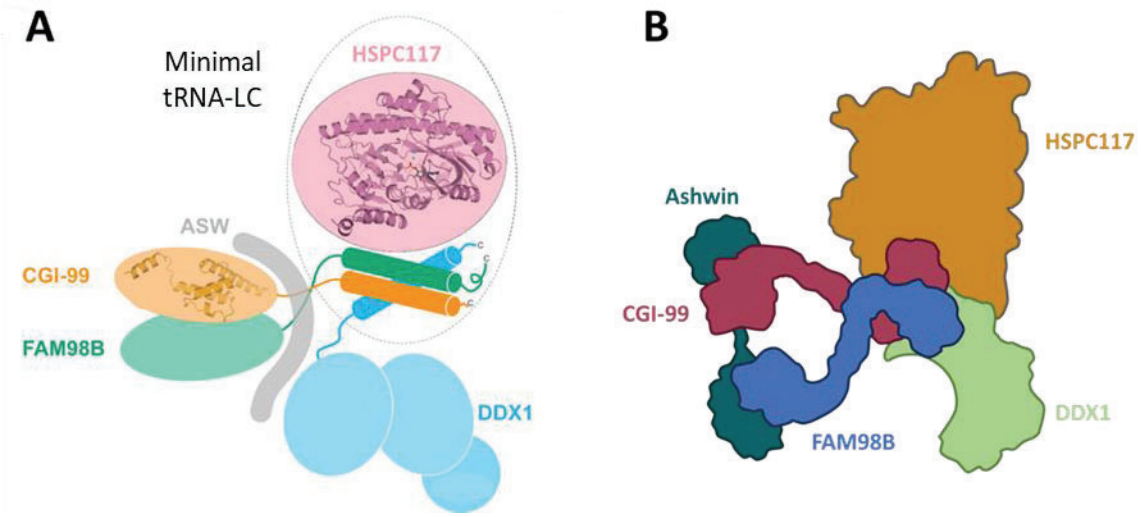

Figure 12. Architecture of the tRNA-LC. (A) HSPC117, along with the C-terminal alpha-helical regions of DDX1, CGI-99, and FAM98B, constitutes the core of the tRNA-LC. ASW is not essential for the formation of the complex. Figure adapted from Kroupova *et al.* [154]. **(B)** Schematic representation of the tRNA-LC.

3.1.3.3. CCA addition

Once removed the 5' leader, the 3' trailer, and the intron (if present), the next step in tRNA processing is the addition of CCA nucleotides to the 3' terminus by tRNA nucleotidyl transferase 1 (TRNT1). TRNT1 is a template-independent RNA polymerase that also catalyzes the addition of CCA in mitochondrial tRNAs. The presence of 3' CCA prevents the action of 3' endoribonucleases, is necessary for nuclear export, and serves as a substrate for aaRSs in the cytoplasm [139], [155].

3.1.3.4. Nucleus-cytoplasm transport

In mammalian cells, nuclear primary export of mature tRNAs is mainly performed by exportin-t but also by exportin 5 [156], [157]. Both exportins require the cooperation of a small G-protein called Ras-related nuclear protein (Ran) loaded with GTP in order to export the tRNA. Experiments performed in *Xenopus* oocytes show that removal of the 5' leader, the 3' trailer, and the intron, as well as 3' CCA addition, nucleoside modification, and correct folding are important for nuclear export [158].

Retrograde transport refers to the transport of tRNAs back into the nucleus and it is found in animals, but is associated to stress conditions, such as amino acid deprivation [159] or viral infections [160]. Indeed, Schwenzer *et al.* [161] described that, in human cells, oxidative stress activates tRNA retrograde transport, which is rapid, reversible, and selective for certain tRNA species. They also showed that tRNA retrograde transport is regulated by the integrated stress response (ISR) pathway via the PERK-RTP801-mTOR axis (PERK stands for PKR-like ER kinase).

Overall, tRNA retrograde transport is thought to represent a universal mechanism for posttranscriptional regulation of global gene expression in response to energy availability [159].

3.1.3.5. Aminoacylation

Chemical binding of the amino acid to its cognate tRNA is known as aminoacylation and it is performed by aaRSs. Aminoacylation happens mainly in the cytoplasm and the mitochondria although it can also occur in the nucleus to a much lower extent. Indeed, it is unclear whether tRNAs aminoacylated in the nucleus participate in cytoplasmic translation [162]. Aminoacylation of the 22 human mt-tRNAs is performed by 20 nuclear-encoded mitochondrial aaRSs, homologous to their cytosolic counterparts [139]. The GTPase named eukaryotic elongation factor 1A (eEF1A) binds the aminoacylated tRNA and delivers it to the A site of the ribosome, where it will do its canonical function in translation [163]. There is a specific aaRS for each isoacceptor family (e.g., alanyl-tRNA synthetase charges the amino acid alanine to the alanine isoacceptor family). In other words, there are 20 aaRSs, one for each of the 20 standard amino acids. In mammals, the only exception is selenocysteine tRNA (tRNA-Sec), which is aminoacylated by seryl-tRNA synthetase with a serine that is enzymatically modified. For many tRNAs, the anticodon is the region that makes direct contact with the aaRS, thus ensuring a correct charging. In addition, other specific nucleotides in the acceptor stem might be also critical for recognition. Concretely, base 73, known as the discriminator base, is a common point of recognition [131]. Besides the catalytic domain, some aaRSs have an editing domain that can survey and correct misincorporation of amino acids to their cognate tRNA [164].

3.1.3.6. tRNA modifications

Nuclear-encoded mature tRNAs present the highest density of posttranscriptional modifications among all RNAs [165], with an average of 13 modified bases per tRNA molecule. However, this number can range from a few modifications to over 20, indicating that individual tRNAs are modified unevenly. Mt-tRNAs are generally modified to a lesser extent, presenting 5 modifications per molecule on average [134]. The high density of modified nucleotides interferes with standard quantitative polymerase chain reaction (qPCR), complicating the study of tRNAs and forcing the use of recently developed techniques such as hydrolysis-based tRNA sequencing (Hydro-tRNA-seq) [140]. In general, modifications occurring within the structural core of tRNAs (in the D- or T-arm) are important for tRNA stability and proper folding, and their absence can lead to tRNA degradation [165], [166]. On the other hand, modifications occurring at or near the anticodon regulate codon-anticodon interactions, ensuring translational efficiency and fidelity [131].

Many neurological and metabolic diseases have been associated with tRNA hypomodification and deregulation of tRNA-modifying enzymes, as discussed in [166]. For instance, TRMT61B (tRNA methyltransferase 61B), an enzyme that methylates adenosine at position 58 of human mt-tRNAs, is significantly downregulated in AD astrocytes [167]. All these human diseases caused by abnormal RNA modification are named RNA modopathies.

As aforementioned, tRNA modifications are introduced throughout tRNA processing, and result in the generation of mature tRNAs ready to function. A summary of the processing of human nuclear and mitochondrial tRNAs is illustrated in **Figure 13**.

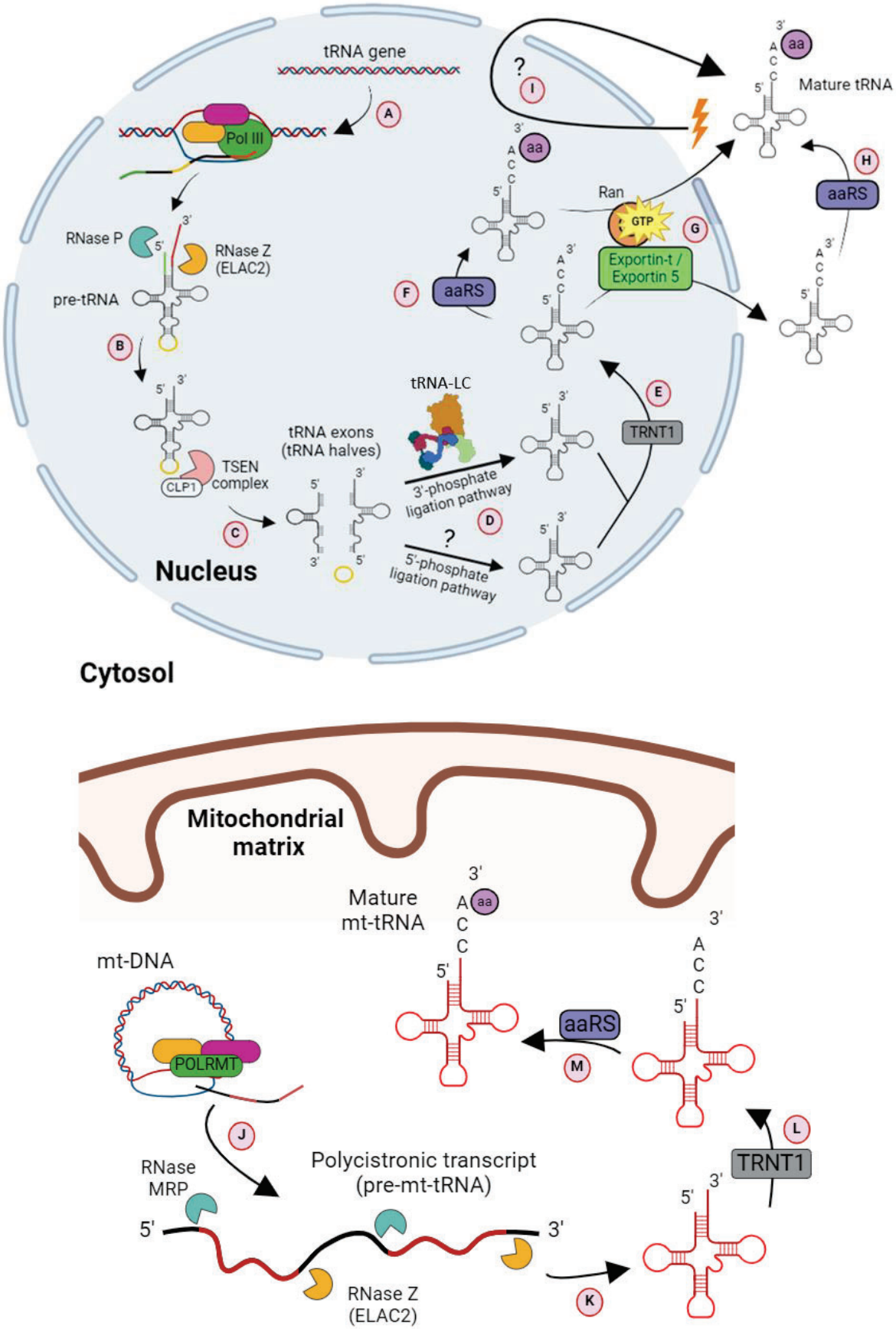
tRNA gene
Pol III
A
RNase P
RNase Z
(ELAC2)
pre-tRNA
B
TSEN
complex
CLP1
C
tRNA exons
(tRNA halves)
tRNA-LC
3'-phosphate
ligation pathway
D
5'-phosphate
ligation pathway
E
TRNT1
F
aaRS
Ran
GTP
G
Exportin-t /
Exportin 5
H
aaRS
I
Mature tRNA
Nucleus
Cytosol
Mitochondrial
matrix
mt-DNA
POLRMT
J
RNase
MRP
Polycistronic transcript
(pre-mt-tRNA)
RNase Z
(ELAC2)
K
Mature
mt-tRNA
M
aaRS
L
TRNT1

Figure 13. Human nuclear and mitochondrial tRNA processing. (A) Binding of transcription factors to tRNA genes recruits RNA Pol III, whose action generates pre-tRNAs. (B) 5' leader is removed by RNAse P whereas 3' trailer is removed by RNAse Z (ELAC2). (C) Introns, if present are spliced out by the TSEN complex. (D) tRNA exons are predominantly ligated by the 3'-phosphate ligation pathway via the tRNA-LC, although the 5'-phosphate ligation pathway might also exist in humans. It is unclear whether splicing occurs before or after leader and trailer removal. (E) 3' end CCA addition is performed by TRNT1. (F) nuclear aminoacylation is performed by aaRSs, although it is much less common than cytoplasmic aminoacylation (H). (G) Nuclear export is mediated by exportin-t or exportin 5 in collaboration with Ran-GTP. (I) Under stressful conditions, tRNAs can be retrogradely imported to the nucleus in a rapid and reversible process. (J) Mt-DNA is transcribed by POLRMT with the aid of transcription factors, generating long polycistronic transcripts that contain different pre-mt-tRNAs as well as mRNAs and other RNAs. (K) RNase MRP (RNase for mitochondrial RNA processing) acts first, cleaving and processing the 5' end of these pre-mt-tRNAs, and then ELAC2 acts on 3' termini. (L) As in the nucleus, TRNT1 performs the addition of a CCA trinucleotide. (M) Finally, aaRSs aminoacylate the mt-tRNAs. All depicted mitochondrial enzymes are nuclear-encoded and transported to the mitochondria. Mature tRNAs are ready to act on ribosomes or mitoribosomes. Question marks indicate that the human enzyme responsible for that step is unknown. tRNA posttranscriptional modifications occur throughout its processing but have not been illustrated for simplicity. Figure adapted from Schaffer *et al.* [139] with *Biorender.com*.

3.1.4. Function

3.1.4.1. Canonical functions

The primary function of tRNAs is to act as a bridge in the central dogma of molecular biology, deciphering mRNA into amino acids. Mature tRNAs are bound by eEF1A and transported to the A site of the ribosome. When the anticodon of the tRNA is complementary to the mRNA's codon (either by strict Watson-Crick base pairing or wobbling) the amino acid charged into the tRNA is transferred to the nascent polypeptide. Translation can be divided into 3 phases: initiation, elongation, and termination.

Translation begins with the assembly of an initiation complex on mRNA and the identification of the start codon, which is usually the first AUG codon downstream of the mRNA's 5' cap structure. The AUG codon specifies the amino acid methionine (Met), and therefore, virtually all proteins specified by the genetic code begin with methionine. In the next phase, elongation factors promote the transference of the growing peptide to the incoming aminoacyl-tRNA, and the empty tRNA then leaves the ribosome. Termination happens when eukaryotic release factor 1 (eRF1), which is structurally analogous to tRNA, recognizes 1 of the 3 termination codons in

mRNA and recruits another release factor to hydrolyze the polypeptide chain from the tRNA. In addition, ribosomal subunits are dissociated, allowing for another round of translation. Interestingly, multiple ribosomes can translate a single mRNA at the same time forming complexes known as polysomes [168], [169].

Mistranslation refers to the addition into the nascent polypeptide of an amino acid that differs from what is specified by the codon. Mistranslation occurs naturally in all cells at frequencies ranging from 1 in 3,000 to 1 in 1,000,000 depending on the amino acid. Mistranslation can be due to different factors such as tRNA misacylation, defective tRNA modification that leads to wrong base pairing, or an altered pool of aminoacylated-tRNAs [131]. For instance, low cellular levels of asparagine might lead to the misincorporation of serine in mammalian cells [170]. Interestingly, the composition and abundance of the cellular tRNA pool is coordinated to match the codon demand of the transcriptome, enabling translation optimization [171]. In fact, it is known that proliferating and differentiated cells express different sets of tRNAs in a codon usage-dependent manner [172].

3.1.4.2. Noncanonical functions

Besides their well-described role in translation, tRNAs (and pre-tRNAs) can be enzymatically cleaved to generate tRNA-derived small RNAs (tsRNAs), which are 14 to 50 nt long and participate in different biological processes such as gene expression regulation [173], [174], [175]. Based on their length and original location in the parental tRNA, tsRNAs can be classified into tRNA-derived fragments (tRFs) and stress-induced tRNAs (tiRNAs).

tiRNAs are usually 29 to 50 nt long and are generated by specific cleavage of angiogenin (ANG) at the middle of the anticodon loop of mature tRNAs. 5’ tiRNAs contain the 5’ end of the tRNA, whereas 3’ tiRNAs contain the 3’ end. They must not be confounded with the tRNA exon halves generated from pre-tRNAs during intron splicing. tiRNAs are generally produced under stress conditions such as hypoxia, heat shock, and oxidative stress [176]. Nonetheless, tiRNAs are also produced in a lesser extent in physiological conditions [174].

tRFs are shorter than tiRNAs (14-30 nt) and can be originated from either mature tRNA or pre-tRNA. They are generated by the specific cleavage of ELAC2, ANG or Dicer, among other nucleases. The classification and the generation of tsRNAs is summarized in **Figure 14A-B**.

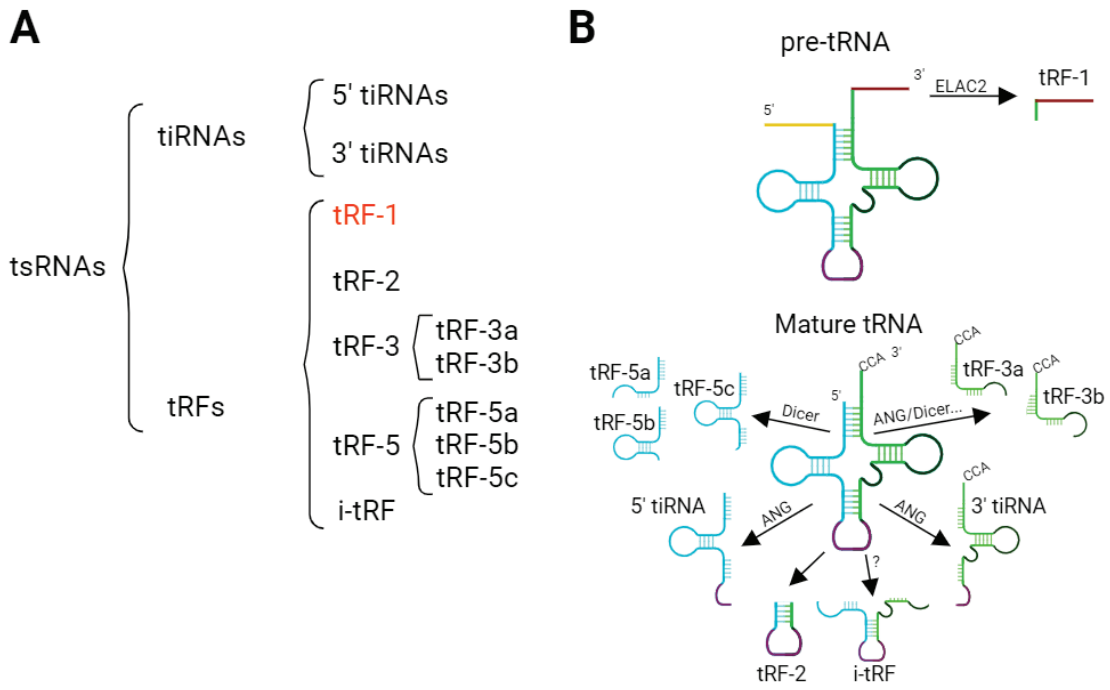

Figure 14. Classification and biogenesis of tiRNAs and tRFs. (A) Categorization of tsRNAs. Molecules in red derive from pre-tRNA whereas molecules in black originate from mature tRNA. **(B)** Graphical representation of tsRNA synthesis from precursor and mature tRNA. The question mark indicates that the enzyme responsible for i-tRF generation is unknown. Figure adapted from Xie *et al.* [177] with *Biorender.com*.

tsRNAs have diverse functions as reviewed in Su *et al.*, [178]. For instance, they regulate apoptosis, protein translation (either promotion or inhibition), and gene expression by base-pairing with target mRNAs and silencing them. Moreover, tsRNAs have been described to sequester RNA-binding proteins, and they also participate in the defense against viral infections. All these functions reflect the importance of a well-regulated biosynthesis of tsRNAs in the cell. Indeed, certain types of tsRNAs are dysregulated in cancer tissues [175], [179].

3.1.5. Degradation

Mature tRNA, thanks to its highly folded structure and the presence of numerous modifications, is one of the most stable species of RNA. In fact, mature mammalian tRNAs have a half-life on the order of 100 hours [180]. However, changes in the tRNA primary sequence or in the modifications lead to a rapid decay of the aberrant transcript, ensuring the existence of functional tRNA pools [181]. On the contrary, the half-life of pre-tRNA is between 15 and 30 minutes [180]. The short half-life of pre-tRNAs might be explained by their fast processing [182] and their reduced stability in comparison to mature molecules.

In yeast, there are two pathways for removing malformed or/and hypomodified tRNAs: the nuclear surveillance pathway, which acts primarily on pre-tRNAs, and the rapid tRNA decay (RTD) pathway, predominant in mature tRNAs [183]. Not much is known about tRNA quality control pathways in mammals. However, many of the enzymes involved in the nuclear surveillance pathway and the RTD pathway exist in mammals [184], which suggests that these tRNA degradation pathways might be shared from yeast to vertebrates.

3.1.6. tRNA-associated diseases

There are hundreds of tRNA-associated diseases, which can be due to pathological mutations in tRNA genes or in tRNA processing enzymes. Interestingly, the vast majority of the disease-causing mutations in tRNA genes are found in mt-tRNA genes. Indeed, over 370 mutations in all 22 mt-tRNA genes have been reported in recent years [185], [186]. These mutations affect the folding, aminoacylation and function of mt-tRNAs, which leads to an impaired mitochondrial translation of oxidative phosphorylation enzymes. Thus, mt-tRNA mutations are more relevant in high-energy consuming tissues like the muscular and nervous systems [187]. On the contrary, little is known about mutations in nuclear-encoded tRNA genes. This could be explained by the expansion of nuclear tRNA genes, which might compensate for a pathological mutation in one of the copies. However, a single-nucleotide polymorphism (SNP) in the nuclear-encoded *tRNA-Arg-TCT-4-1* causes neurodegeneration in mice [188]. Interestingly, this tRNA is uniquely expressed in neurons, which could explain its relevance and why a SNP is so deleterious.

As for the mutations in tRNA processing enzymes, they can affect almost every step in tRNA processing, which impacts on tRNA abundance, folding, and splicing, among others [187]. Indeed, mutations in tRNA-modifying enzymes are so important that the diseases caused by them are known as tRNA modopathies [189]. Most of the tRNA-associated diseases cause selective vulnerability, which means that while certain brain areas are highly affected, other tissues appear to be unaffected [190]. The neurological diseases caused by mutations in tRNA genes or tRNA-modifying enzymes are reviewed in Schaffer *et al.* [139].

3.2. XBP1 mRNA

Besides its role in tRNA ligation, the tRNA-LC also participates in the unconventional splicing of *XBP1* mRNA during the unfolded protein response (UPR) [191].

The UPR is a cellular stress response activated when unfolded or misfolded proteins accumulate in the ER. There are three ER-resident transmembrane proteins orchestrating the UPR: activating transcription factor 6 (ATF6), PERK, and inositol-requiring enzyme 1 (IRE1). These

proteins are inactive under physiological conditions because their luminal domains are bound to the chaperone BiP. Accumulation of unfolded or misfolded proteins inside the ER competes for BiP binding, therefore releasing PERK, ATF6, and IRE1, and triggering downstream signaling.

XBP1 is an effector of the UPR whose mRNA experiments canonical splicing in the nucleus, but retains a short, 26-nucleotide intron. Translation of this intron-containing mRNA generates the protein XBP1u (unspliced), which has a molecular weight of 33 kDa. During the UPR, the activation of the cytosolic endonuclease domain of IRE1 results in the cleavage of *XBP1* mRNA at the splice sites, releasing the 26-nucleotide intron [192]. Subsequent ligation of *XBP1* mRNA exons is performed by the tRNA-LC [191]. Intron removal causes a shift in the open reading frame, therefore skipping a stop codon and generating the 55-kDa XBP1s (spliced) protein. XBP1s, but not XBP1u, acts as a transcription factor that promotes the expression of genes necessary to restore ER homeostasis such as chaperones and proteins involved in ER-associated protein degradation.

Besides alleviating ER stress, XBP1s regulates the transcription of genes involved in lipid and glucose metabolism, secretory functions, and immune responses. Therefore, XBP1s has a key role in secretory cells such as plasma cells, hepatocytes, or pancreatic β-cells [192]. Indeed, HSPC117 (the ligase of the tRNA-LC) was first described to mediate *XBP1* ligation in plasma cells, which eventually results in the production of immunoglobulins [191]. Interestingly, depletion of HSPC117 alone did not impair *XBP1* ligation, but simultaneous knockdown of HSPC117 and its cofactor archease did.

On the other hand, the physiological role of XBP1u is not fully understood. According to recent studies, XBP1u appears to be a negative regulator of XBP1s. First, XBP1u is thought to physically interact with XBP1s and suppress its transcriptional function [193], [194]. Second, XBP1u inhibits XBP1s by targeting it for proteasomal degradation [195].

Interestingly, a polymorphism in the promoter of XBP1 was identified as a risk factor for AD [196]. In line with this, XBP1s has been recently described to regulate synaptic plasticity and memory in different mouse models of AD [197], [198]. Indeed, Cissé *et al.* [198] showed that delivery of XBP1s in the hippocampus of 3xTg-AD mice rescued spine density, synaptic plasticity, and memory function assessed by the Morris water maze (MWM). They also demonstrated that this attenuation of AD phenotype was due to the expression of *Kalirin-7*, a transcriptional target of XBP1s. Likewise, Duran-Aniotz *et al.* [197] reported that overexpression of XBP1s in the brain of 5xFAD mice reduced Aβ load and astrogliosis, and attenuated cognitive deficits. Moreover, overexpression of XBP1s specifically in the hippocampus of 5xFAD mice caused a significant

improvement in the performance of the MWM and the Barnes maze, as well as a restoration of the synaptic plasticity and a correction of proteomic alterations.

The role of XBP1s in contextual memory formation and synaptic plasticity was also studied by Martínez *et al.* [199]. They found that mice lacking XBP1 in the nervous system exhibited altered memory and long-term potentiation (LTP), whereas neuronal XBP1s overexpression enhanced performance in memory tasks. Interestingly, they reported that XBP1s controls the expression of several memory-related genes, including *Bdnf*. Indeed, overexpression of BDNF in the hippocampus of XBP1-deficient reverted the phenotype. The processing and function of XBP1 is illustrated in **Figure 15**.

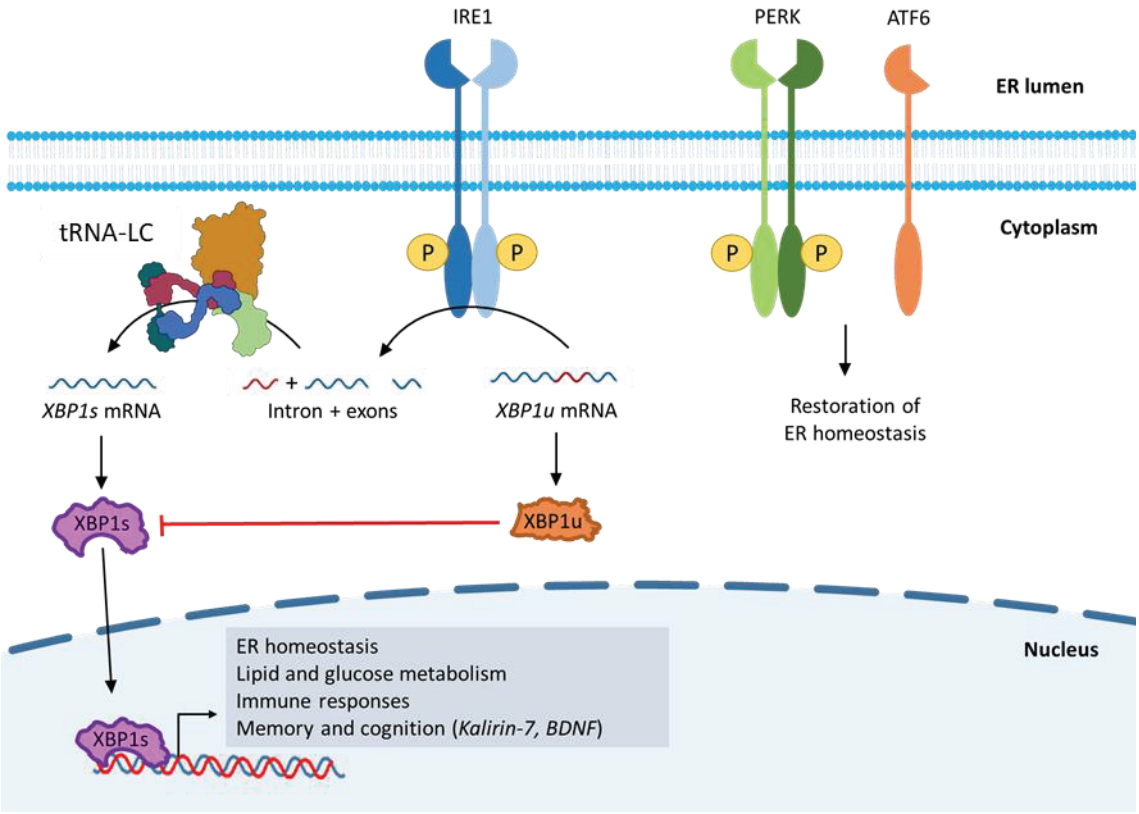

Figure 15. The IRE1 branch of the UPR. When unfolded or misfolded proteins accumulate in the ER lumen, the transmembrane enzymes IRE1, PERK, and ATF6 become active to promote the restoration of ER homeostasis. IRE1 cleaves *XBP1u* mRNA, which is then ligated by the tRNA-LC. *XBP1s* is translated generating a transcription factor that promotes the transcription of genes that help restore ER homeostasis, as well as genes involved in lipid and glucose metabolism, immune responses, *Kalirin-7* and *BDNF*, among others. XBP1u does not act as a transcription factor, but rather, as an inhibitor of XBP1s.

Altogether, these studies reveal XBP1s as a pivotal factor in cognitive processes, particularly in memory formation and maintenance, suggesting its dysfunction as a contributing factor to the cognitive deficits observed in neurodegenerative diseases.

AIMS

AD is the most prevalent form of dementia, marked by a progressive decline in cognitive abilities, executive function, and memory. It also affects language, and patients might present emotional and psychiatric symptoms. AD is characterized by the presence of extracellular Aβ plaques and intracellular tangles of hyperphosphorylated tau, which eventually disrupts synaptic functioning, triggers neuroinflammation, and leads to neuronal death, resulting in brain atrophy and gliosis. The exact mechanisms by which these events take place are not yet elucidated, but RNA translation impairment could contribute to the pathogenesis of the disease.

RTP801 is a negative regulator of mTOR and Akt, kinases that are essential for translation and survival, respectively. In this line, RTP801 is an active trigger of the inflammasome cascade, and it is also found in EVs mediating transneuronal toxicity. These pro-apoptotic and pro-inflammatory events are the result of an impaired integrative response of the mTOR/Akt axis, which also impacts the availability of mRNA and tRNA pools. Increased levels of RTP801 have been found in the brains of patients with neurodegenerative diseases such as AD, HD, and PD. In animal models of these diseases, silencing RTP801 in neurons of the compromised regions has been proved beneficial for cognitive and motor deficits, and neuroinflammation, events that deeply depend on translation. On the other hand, RTP801 KO mice are more resilient to stress-induced synaptic and behavioral deficits.

The tRNA-LC is a pentameric complex that catalyzes the ligation of tRNA and specific mRNA exons during splicing. Indeed, it participates in the unconventional splicing of *XBP1* mRNA during the UPR. The essential subunit of the complex is HSPC117, which constitutes its core and presents the ligase activity. The other components are the RNA helicase DDX1, and the adaptor proteins CGI-99, ASW, and FAM98B. Interestingly, preliminary MS results from our group indicated that RTP801 interacts with DDX1 and HSPC117, and thus, it might have an unknown role in tRNA and mRNA splicing.

Taking all this into consideration, the objective of this thesis is **to explore the effect of RTP801 on the activity of the tRNA-LC, in health and disease** (**Figure 16**).

Hence, the specific aims of this thesis are the following:

AIM 1. To study the nature of the interaction between RTP801 and the members of the tRNA-LC.

1.1. To confirm the interaction of RTP801 with DDX1 and HSPC117.

1.2. To evaluate the role of RTP801 in the protein stability of the members of the complex and vice versa.

AIM 2. To investigate the role of RTP801 in the mRNA ligase activity of the complex, in health and AD.

2.1. To assess whether RTP801 affects the mRNA ligase activity of the complex over *XBP1*.

2.2. To determine whether this activity is altered in the context of AD.

2.3. To study the effect of RTP801 on the mRNA ligase activity of the complex in an *in vivo* model.

AIM 3. To explore the contribution of RTP801 in the tRNA ligase activity of the tRNA-LC, in health and AD.

3.1. To check whether the pre-tRNA and tRNA pools are altered in a mouse model of AD.

3.2. To analyze whether RTP801 downregulation influences the composition and toxicity of these pools.

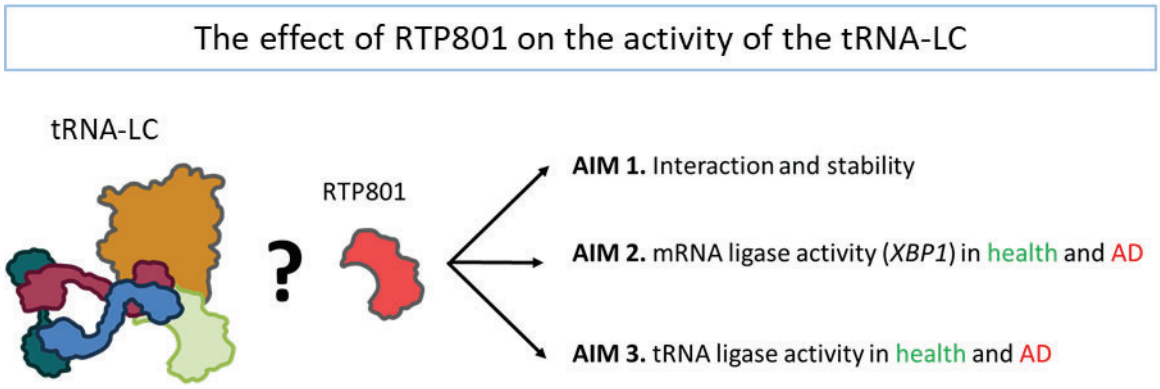

Figure 16. Overview of the aims of this thesis. The main objective of this work was to study the effect of RTP801 on the activity of the tRNA-LC. We studied the interaction of RTP801 with the members of the complex and its effect on their protein stability (Aim 1), and the effect of RTP801 on the mRNA (Aim 2) and tRNA ligase (Aim 3) activity of the complex, in health and in AD.

METHODOLOGY

1. Cell cultures

1.1. HEK293 culture

Human Embryonic Kidney 293 (HEK293) is a cell line originally derived from human embryonic kidney cells. In this study, HEK293 cells were cultured in plastic plates with Dulbecco's modified Eagle's medium (DMEM) supplemented with 10% fetal bovine serum (FBS) and 1% penicillin/streptomycin (all from Thermo Fisher Scientific). Cells were kept in a 5% CO_2 atmosphere at 37°C and were reseeded when confluent.

1.2. Rat primary cortical cultures

Rat primary cortical cultures were prepared by dissecting out the cortex from embryonic day 18 (E18) Sprague-Dawley rats (from Envigo) as previously described [73]. Briefly, the tissue was dissociated with 0.05% trypsin (from Thermo Fisher Scientific) for 30 min, followed by a mechanical dissociation with rounded-end glass Pasteur pipettes. Cells were seeded at a density of 750 cells/mm^2 on plastic plates coated with 0.25 mg/mL poly-L-lysine (from Merck). Neurons were maintained in Neurobasal medium supplemented with serum-free B27 (1:50), 2 mM GlutaMAX, and 1% penicillin/streptomycin (all from Thermo Fisher Scientific). Cell cultures were kept in a 5% CO_2 atmosphere at 37°C. One week after the culture, a third of the medium was replaced by fresh medium. All experiments were performed at 13-14 Days *in vitro* (DIV).

1.3. Mouse primary hippocampal cultures

Mouse primary hippocampal cultures were prepared by dissecting out the hippocampus from E18 B6CBA wild-type (WT) mice. The tissue was dissociated with 0.25% trypsin (from Thermo Fisher Scientific) for 15 min, followed by a mechanical dissociation with rounded-end glass Pasteur pipettes. Cells were seeded at a density of 400 cells/mm^2 onto autoclaved 12 mm glass coverslips pre-coated with 0.1 mg/mL poly-D-lysine (from Merck). As in Methodology section 1.2, neurons were maintained in supplemented Neurobasal medium and kept in a 5% CO_2 atmosphere at 37°C. Experiments were performed at 13-14 DIV.

2. Animal and human tissue

2.1. Human postmortem samples

Postmortem hippocampal samples from AD patients and age-matched control (CT) individuals were acquired from the Neurological Tissue Bank, (Biobank-Hospital Clínic-FRCB-IDIBAPS, Barcelona). All brain tissue samples were obtained from patients after they or their legal representatives gave written informed consent for the use of their brain tissue and medical

records for research purposes, as approved by the Ethics Committee of the Brain Bank institution, in accordance with the 1964 Declaration of Helsinki. The neuropathological examination was performed according to standardized protocols at the Neurological Tissue Bank of the IDIBAPS Biobank. Briefly, half of the brain was dissected in the fresh state, then frozen and stored at -80°C, while the remaining half was fixed in formaldehyde solution for three weeks. For histological evaluation, 5-µm-thick paraffin-embedded sections from at least 25 representative brain regions were stained, and immunohistochemistry was performed (see [200] for more information). **Table 2** contains case information.

Clinical diagnosis	Patient	Braak stage	Thal stage	Sex	Age (years)	PMD (hh:mm)
CT	1	II	5	F	97	7:20
	2	II	4	F	93	5:30
	3	II	3	M	86	7:35
	4	II	2	F	88	24:00
	5	II	3	M	64	10:00
	6	0	1	M	83	13:00
	7	III	0	M	86	7:25
	8	I-II	1	M	78	6:00
	9	0	0	M	76	11:30
	10	III	3	F	90	13:40
	11	II	0	F	83	7:30
	12	II	5	F	83	7:33
AD	13	VI	5	F	84	11:00
	14	VI	5	M	78	7:20
	15	VI	5	F	90	5:30
	16	V	4	F	83	10:45
	17	VI	5	F	78	11:30
	18	VI	5	F	88	13:30
	19	VI	5	F	82	16:45
	20	V-VI	5	M	77	7:30
	21	VI	5	M	82	4:30
	22	VI	5	F	64	5:30
	23	VI	5	F	74	6:30
	24	V	4	M	76	6:00
	25	VI	5	F	85	12:00
	26	VI	4	F	80	15:00
	27	V	3	M	86	17:30
	28	V	5	F	85	16:00

Table 2. Human postmortem hippocampal samples. PMD = postmortem delay; M = male; F = female.

2.2. 5xFAD mice

The transgenic mouse line 5xFAD maintained in B6SJL background (MMRRC catalog #034840-JAX, RRID:MMRRC_034840-JAX) was utilized for this investigation. Specifically, heterozygous 5xFAD mice were used, which overexpress the 695-amino acid isoform of the human amyloid precursor protein (APP695) carrying the Swedish (K670N/M671L), London (V717I), and Florida (I716V) mutations under the control of the murine Thy-1 promoter. Additionally, 5xFAD mice express human presenilin-1 (PSEN-1) with the M146L and L286V mutations, also under the control of the Thy-1 promoter. Thus, 5xFAD mice overexpress two human transgenes with a total of 5 AD-linked mutations, which results in a high production of $A\beta_{42}$ [201].

The 5xFAD model rapidly develops critical amyloid pathology. Indeed, extracellular accumulation of Aβ can be detected around 2 months of age in the hippocampal subiculum. At 6 months, Aβ deposits are found throughout the hippocampus and cortex. Astrogliosis and microgliosis are also early pathological events, which begin at 2 months of age, developing in parallel with plaque deposition [201]. Tau hyperphosphorylation has also been reported at early stages [202]. Synaptic degeneration, assessed by the levels of synaptophysin, usually starts at 4 months of age [201]. Cognitive impairment has been observed from 5 months of age, including problems with spatial memory [201], [203], and long-term memory [114]. However, motor impairments occur later, beginning at 9 months of age [204], simultaneously with neuron loss [205]. The life expectancy of 5xFAD mice is around 15 months [206]. The alterations found in 5xFAD mice are illustrated in **Figure 16**.

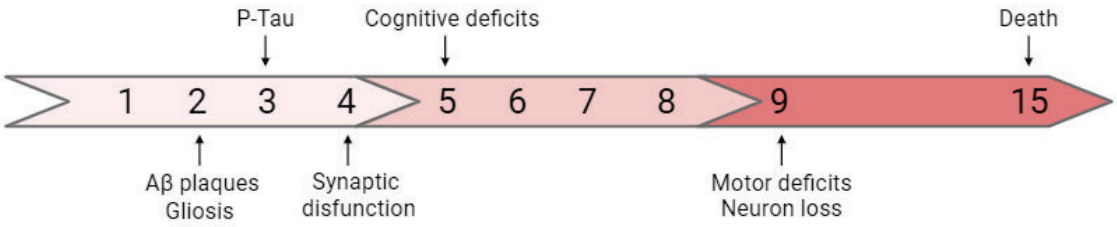

Figure 16. Time course of alterations found in 5xFAD mice. As in human AD pathology, Aβ accumulation, astro- and microgliosis, accumulation of hyperphosphorylated tau, and synaptic deficits are early events that lead to cognitive impairment. At later stages, neuron loss and motor deficits appear. The mean lifespan is around 15 months. Figure created with *Biorender.com*.

In this work, all animals were housed in colony rooms with a 12:12-h light/dark cycle, maintained at 19–22 °C and 40–60% humidity, with unlimited access to food and water. All the experimental animals were male, and they were used from 6 months of age onwards. All procedures were in accordance with the Guide for the Care and Use of Laboratory Animals (NIH Publication No. 85-

23, 1985 Revision), the European Community Guidelines, and Spanish guidelines (RD53/2013) and they were approved by the local ethical committee (University of Barcelona, 55/21 and Generalitat de Catalunya, 11559).

3. Molecular biology

3.1. Plasmid description

The plasmid constructs used in this work and their features are summarized in **Table 3**.

Empty vector and characteristics	Construct	Characteristics
pLL3.7 Purchased from Addgene. Empty backbone for expression of shRNA under the U6 promoter. Confers ampicillin resistance and expresses a CMV-eGFP reporter to monitor expression.	**pLL3.7-shCT**	Validated scrambled control sequence 5'-GTGCGTTGCTAGTACCAAC-3' for human, rat, and mouse [71]. Flanked by HpaI and XhoI.
	pLL3.7-shRTP801	Validated sequence 5'-AAGACTCCTCATACCTGGATG-3' targeting human, rat, and mouse RTP801 [71]. Flanked by HpaI and XhoI.
rAAV2/8 Provided by the Viral Vector Production Unit (Universitat Autònoma de Barcelona). Expresses the shRNA under the H1 promoter and eGFP under the control of RSV promoter.	**rAAV2/8-shCT**	Validated scrambled control sequence 5'- GTGCGTTGCTAGTACCAAC-3' for mouse [114], [118].
	rAAV2/8-shRTP801	Validated sequence 5'-AAGACTCCTCATACCTGGATG-3' for mouse RTP801 [114], [118].
pRP Purchased from VectorBuilder. Empty backbone for expression of shRNA under the U6 promoter. Confers ampicillin resistance and expresses an hPGK-mCherry reporter to monitor expression.	**pRP-shCT**	Scrambled control sequence 5'-CCTAAGGTTAAGTCGCCCTCG-3' for human and mouse.
	pRP-shHSPC117	Sequence 5'-CAATGAATGCCAAAGACTTGG-3' for human, rat, and mouse HSPC117.
	pRP-shDDX1	Sequence 5'-GATGTGGTCTGAAGCTATTAA-3' for human, rat, and mouse DDX1.
FUGWm Purchased from Addgene. Empty backbone for gene overexpression under the CMV promoter. Confers ampicillin resistance and expresses an UbC-eGFP reporter to monitor expression.	**FUGWm-eGFP**	The original construct (pCMS-eGFP) was designed and validated in [71]. It was then subcloned to obtain FUGWm-eGFP, which was validated in [86].
	FUGWm-eGFP-RTP801	The original construct (pCMS-eGFP-RTP801) was designed and validated in [71]. It was then subcloned to obtain FUGWm-eGFP-RTP801, which was validated in [86].

Table 3. List of plasmids used. shRNA = short hairpin RNA; CMV = cytomegalovirus; eGFP = enhanced green fluorescent protein; AAV2/8 = recombinant adeno-associated virus serotypes 2/8; RSV = Rous sarcoma virus; hPGK = human phosphoglycerate kinase; UbC = ubiquitin C.

3.2. Bacterial transformation

To amplify DNA plasmids, *Escherichia coli* DH5α competent cells (from Thermo Fisher Scientific) were used. The DNA plasmids were mixed with the cells and incubated at 40°C for 30 seconds. The mixture was then kept on ice for 5 min. Next, S.O.C. medium (super optimal broth with catabolite repression medium, from Thermo Fisher Scientific) was added to the mixture, which was incubated at 37°C for 1 h. After that, transformed bacteria were seeded on lysogeny broth (LB) agar (from Merck) plates with 100 ug/mL ampicillin (from Thermo Fisher Scientific). LB agar plates were incubated overnight (O/N) at 37°C.

3.3. Bacterial amplification and plasmid purification

A single colony of ampicillin-resistant bacteria was picked from the LB agar plate and grown in Terrific Broth medium supplemented with 100 ug/mL ampicillin (all from Thermo Fisher Scientific), for 8 h at 37°C and 200 rpm (revolutions per minute). To isolate the DNA plasmids, the HiPure Plasmid Filter Midiprep Kit (from Thermo Fisher Scientific) was used, following manufacturer's instructions. Then, the concentration of the DNA plasmids was assessed with the Nanodrop™ One Spectrophotometer (from Thermo Fisher Scientific).

3.4. Plasmid transfection

To modulate the mRNA and protein levels of RTP801, HEK293 cells were transfected with shRNA or RTP801-overexpressing vectors, using the polymer polyethyleneimine (PEI, from CliniSciences) and following manufacturer's instructions. DDX1 and HSPC117 were knocked down in HEK293 cells using the same procedure. In brief, PEI was diluted in Milli-Q water to 1 mg/mL, and it was filtered through a 0.22 µm filter. It was then mixed with the respective DNA vector (4 µg of PEI per each µg of DNA) and non-supplemented DMEM medium, for 20 min at room temperature (RT). After that, the medium of HEK293 cells was replaced by the mixture and cells were incubated 4 h in a 5% CO_2 atmosphere at 37°C. Then, the mixture was replaced by supplemented DMEM medium. Experiments were performed 48 h post-transfection (in the case of overexpression vectors) or 72 h post-transfection (in the case of shRNA vectors). For 6-well plates, 1.2 µg of DNA were used per well, whereas for 12-well plates, 0.4 µg of DNA were utilized per well.

3.5. Lentiviral production and transduction

Lentiviruses to knockdown neuronal RTP801 were produced in HEK293 cells transfected with a pLL3.7 vector expressing shRNA against RTP801 (shRTP801). Transfections were performed as in Methodology section 3.4 but using 100 mm plates and adding envelope and packaging plasmids (from Addgene). DNA vectors and quantities (µg/100 mm plate) necessary for lentiviral production are the following: pMD2.G (3.5), pCMV-Δr8.91 (2.5), pLL3.7-shCT (10), and pLL3.7-shRTP801 (10).

Cell medium was collected 72 h post-transfection and it was centrifuged for 5 min at 1500 rpm to remove cell debris. Virus-containing medium was filtered through a 0.45 µm filter and incubated with 8.5% polyethylene glycol 6000 (Panreac AppliChem) and 0.35 M NaCl for 90 min at 4°C. The mixtures were then centrifuged at 7500 × g for 15 min in a Sorvall R5-5C centrifuge with a SS-34 fixed-angle rotor, and the pellets were resuspended in sterile 1X phosphate buffered saline (PBS) with calcium and magnesium. Lentiviruses were stored at -80°C until transduction of neurons. Viral titer was assessed by transduction of rat primary cortical cultures with several viral dilutions. Lentiviral transductions were performed with a MOI (multiplicity of infection) of 2. Neurons were transduced at 11 DIV and were harvested 72 h post-transduction (at 14 DIV).

3.6. Stereotactic injection of adeno-associated viral vectors

6-month-old wild type (WT) and 5xFAD mice received bilateral hippocampal injections of adeno-associated viruses (AAVs) to genetically silence RTP801, as described in [114]. Summarizing, mice were injected in the CA1 (Cornu Ammonis 1) and in the dentate gyrus (DG) with neuron-targeted rAAV2/8-H1-shControl-RSV-GFP (1.2×10^{13} genome copies (GCs)) or rAAV2/8-H1-shRTP801-RSV-GFP (1.07×10^{13} GCs) (see **Table 3**). The cloning of shRNAs and the production of AAV viral particles were performed by the Unitat de Producció de Vectors from the Center of Animal Biotechnology and Gene Therapy at the Universitat Autònoma de Barcelona.

For the surgery, mice were deeply anesthetized with a mixture of isoflurane and 2% oxygen. For anesthesia induction, 2.5-3% isoflurane was used, whereas 1.5% isoflurane was used for maintenance. Mice were placed in a stereotactic apparatus and two injections were performed bilaterally (**Figure 17**). The following coordinates relative to Bregma were used: anteroposterior, -2; mediolateral, ±1.5; and dorsoventral, -2.1 (for DG) and -1.3 (for CA1). 1 µL of viral vector was injected every time, using a Hamilton™ syringe (syringe volume, 5 µL; needle length, 51 mm; needle gauge, 26s) at an infusion rate of 250 nL/min. Thus, each injection lasted 4 min. However, the needle was left in place for 2 additional min to ensure complete diffusion of the AAVs. After

1 h of careful monitoring, mice were returned to their cage for 4 weeks and were then euthanized via cervical dislocation for biochemical analysis. Tissue was kept at -80°C until use.

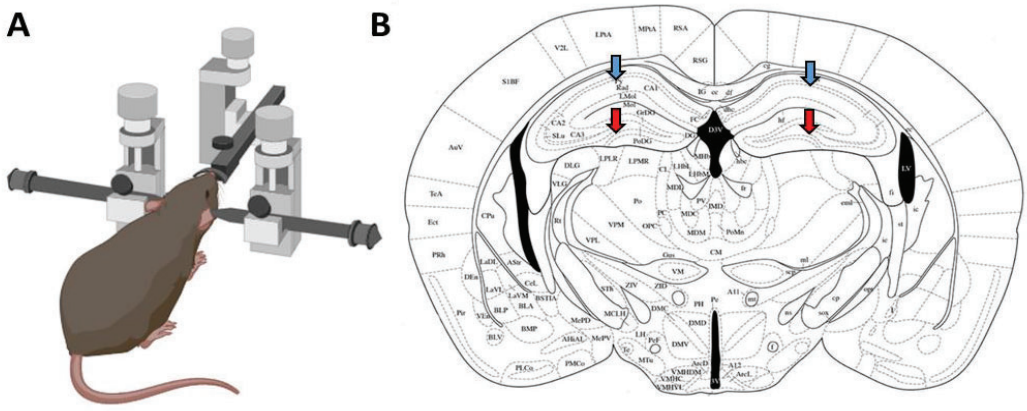

Figure 17. Stereotactic hippocampal surgery. (A) Graphic representation of a mouse placed in a stereotactic apparatus. **(B)** Brain coordinates used for intrahippocampal RTP801 silencing. The CA1 injection coordinates are represented in blue, whereas the injections in the DG are illustrated in red. Brain image obtained from the Allen Brain Atlas website. Figure created with *Biorender.com*.

4. Protein isolation, detection, and quantification

4.1. Immunoprecipitation (IP)

In order to detect weak or transient protein interactions, HEK293 cells were treated for 2 h with dithiobis(succinimidyl propionate) (DSP, from Thermo Fisher Scientific), a protein cross-linker that forms stable amide bonds between molecules, and following manufacturer's instructions. Cells were then lysed with Cell Lysis Buffer (from Cell Signaling Technology) supplemented with 1% phenylmethylsulphonyl (PMSF, from Merck) and centrifuged at 14,000 x g for 10 min to remove debris. The total protein concentration of the supernatant was quantified using the Bio-Rad Protein Assay and following manufacturer's instructions. Protein A-agarose beads (from Santa Cruz Biotechnology) were thoroughly washed with 3-((3-cholamidopropyl) dimethylammonium)-1-propanesulfonate (CHAPS) buffer (50 mM Tris pH = 7.4, 150 mM NaCl, 10 mM $MgCl_2$, 0.4% CHAPS) (all from Merck). Then, samples, beads, and antibody against RTP801 (Proteintech, #10638-1-AP) were mixed and incubated O/N on rotation at 4°C.

Numerous negative controls were included to ensure IP specificity: first, beads and samples were incubated without antibodies; second, rabbit normal immunoglobulins (IgG) (Merck #12-370) were added instead of the appropriate antibody; and third, lysis buffer was incubated instead of samples. The next day, the mixtures were washed 4 times with CHAPS buffer supplemented with protease inhibitor (cOmplete™ Mini Protease Inhibitor Cocktail), phosphatase inhibitor (PhosSTOP™) and 1% PMSF (all from Merck). Pierce™ Lane Marker

Reducing Sample Buffer (from Thermo Fisher Scientific) was added to the mixtures, which were heated at 96°C for 5 min for protein denaturation. Mixtures were then centrifuged 30 seconds at 14,000 x g and supernatant was stored at -20ºC until western blot was performed.

4.2. Western blot (WB)

WB was performed to detect the presence and abundance of specific proteins in cellular lysates and tissue homogenates, as previously described [114]. As in Methodology section 4.1, cellular extracts or tissue fragments were collected in Cell Lysis Buffer supplemented with 1% PMSF, centrifuged to remove debris, and protein concentration of the supernatant was determined with the Bio-Rad Protein Assay. Samples (20 µg per lane) were prepared with reducing buffer, denaturized, and resolved in 4-12% NuPAGE™ Novex™ polyacrylamide gels with MOPS SDS (3-(N-morpholino)propane sulfonic acid sodium dodecyl sulfate) running buffer. Gels were run in the XCell SureLock™ Mini-Cell system, and the molecular weight marker used was the PageRuler™ Prestained Protein Ladder. Proteins were transferred to nitrocellulose membranes with the iBlot™ 2 Dry Blotting System and using iBlot™ 2 Transfer Stacks. All reagents and machinery were obtained from Thermo Fisher Scientific. Membranes were washed thrice with TBS-T (Tris buffered saline (from Thermo Fisher Scientific) with 0.1% Tween® 20 (from Merck)) and blocked with 5% milk (from Bio-Rad) in TBS-T for 1 h at RT. Membranes were then incubated O/N at 4°C, in agitation, with the corresponding primary antibody (listed in **Table 4**) diluted in 5% BSA (bovine serum albumin, from Merck).

Antibody	Host	Dilution	Source
DDX1 (for IP)	Rabbit	1:1000	Bethyl, #A300-512A
DDX1	Mouse	1:500	Santa Cruz Biotechnology, #sc-271438
RTP801	Rabbit	1:500	Proteintech, #10638-1-AP
HSPC117	Mouse	1:1000	Santa Cruz Biotechnology, #sc-393966
CGI-99	Rabbit	1:500	Proteintech, #19848-1-AP
XBP1	Rabbit	1:500	Abcam, #ab37152
P-eIF2α Ser51	Rabbit	1:500	Cell Signaling Technologies, #9721
eIF2α	Rabbit	1:500	Cell Signaling Technologies, #9722
ATF4	Rabbit	1:500	Proteintech, #10835-1-AP
GFP	Rabbit	1:800	Cell Signaling Technologies, #2956

Table 4. List of primary antibodies used for WB. IP = immunoprecipitation; eIF2α = eukaryotic translation initiation factor 2α.

The antibody against β-actin (Merck #A3854), which was used as loading control, was already conjugated to horseradish peroxidase (HRP) and thus was directly incubated at RT for 30 min prior to chemiluminescence protein detection (diluted 1:100,000 in TBS-T). After primary antibody incubation, membranes were washed thrice with TBS-T and incubated for 1 h at RT with the corresponding secondary antibody (anti-mouse or anti-rabbit) diluted 1:10,000 in 5% milk in TBS-T. Both secondary antibodies were produced in goat, conjugated to HRP, and obtained from Thermo Fisher Scientific (anti-mouse #31430, anti-rabbit #31460).

Next, membranes were washed thrice with TBS-T and proteins were detected using either SuperSignal™ West Pico PLUS Chemiluminescent Substrate or SuperSignal™ West FEMTO Maximum Sensitivity Substrate (all from Thermo Fisher Scientific). Chemiluminescent images were acquired using a Chemidoc™ Imaging System (from Bio-Rad) and quantified by densitometric analysis with ImageJ software (Fiji).

To remove bound primary and secondary antibodies, membranes were incubated with Restore™ PLUS Western Blot Stripping Buffer (from Thermo Fisher Scientific) for 10-15 min at RT. Complete removal of the previous chemiluminescent signal was checked before continuing. Membranes were then washed with TBS-T, blocked, and incubated with new primary antibodies.

5. RNA isolation, detection, and quantification

5.1. Total RNA, sncRNA, lRNA, and tRNA isolation

WT and 5xFAD mice were euthanized by cervical dislocation and both hippocampi were dissected out and stored at -80°C until use. Total RNA was isolated using TRIzol™ Reagent (from Thermo Fisher Scientific) and following manufacturer's instructions. Briefly, frozen tissue was placed in 1 mL of TRIzol™ Reagent and mechanically homogenized. Chloroform (200 µL) was added to each sample, which was vortexed, incubated 3 min at RT and centrifuged for 15 min at 12,000 x g and 4°C. The obtained aqueous phase was mixed with an equal volume of isopropanol, vortexed, incubated 10 min at RT and centrifuged for 10 min at 12,000 x g and 4°C. Supernatant was then discarded and the pellet was washed with 75% ethanol. After that, the pellet was air-dried, resuspended in diethyl pyrocarbonate (DEPC)-treated water (from Thermo Fisher Scientific), and heated at 55°C for 5 minutes.

To remove salts, phenol, and other contaminants, samples were then incubated with a high salt solution. Thus, 4M NaCl and absolute ethanol were added to each sample (10% and 250% of the sample volume, respectively), which were vortexed and incubated at -80°C for at least 30 min. After that, samples were centrifuged for 30 min at 16,000 x g and 4°C. Again, the pellet was

washed with 75% ethanol, air-dried, resuspended in DEPC-water and heated. Determinations of RNA quantity and quality were made with a NanoDrop™ One Spectrophotometer (from Thermo Fisher Scientific) and a 4200 TapeStation System (from Agilent Technologies), respectively. Total RNA was kept in -80°C until use.

sncRNAs (17-200 nucleotides) and lRNAs (long RNAs, >200 nucleotides) were isolated from total RNA with the RNA Clean & Concentrator™-5 kit (from Zymo Research), according to manufacturer's instructions. sncRNAs and lRNA were stored at -80°C until use.

For the isolation of pre-tRNAs and mature tRNAs, which are generally between 76 and 90 nucleotides long, sncRNA samples were resolved in a 15% urea-polyacrylamide gel. Samples were mixed with a loading dye (from Thermo Fisher Scientific), heated for 5 min at 96°C, and run in 0.5x TBE (Tris-Borate-Ethylenediaminetetraacetic acid (EDTA)) buffer at 120 V for 45 min. Using ultraviolet (UV) shadowing with a fluor-coated thin-layer chromatography (TLC) plate, a band containing 60-100 nt sncRNAs was observed and excised. Then, gel bands were introduced in 0.5 mL microtubes whose bottom had been previously pierced with a 21G needle, which were, in turn, introduced in 2 mL microcentrifuge tubes. Bands were then centrifuged twice at maximum speed for 1 min, to ensure that the gel moved through the hole into the large microtube. After that, gel bands were incubated with DEPC-treated water for 3 h at 1100 rpm at RT. Then, samples were incubated with 4M NaCl and absolute ethanol (10% and 200% of the sample volume, respectively) O/N at -80°C. The next day, samples were centrifuged for 30 min at 16,000 x g and 4°C and the pellet was washed with 85% ethanol. Finally, the pellet was air-dried and resuspended with 16 µL of DEPC-treated water. tRNAs were stored at -80°C until use.

5.2. Hydrolysis-based tRNA sequencing (Hydro-tRNA-seq)

To determine the expression levels of pre-tRNAs and mature tRNAs, a recently developed sequencing protocol called Hydro-tRNA-seq [140], specifically designed for tRNA detection and quantification, was performed at the Centre de Regulació Genòmica (CRG, Barcelona). Briefly, Hydro-tRNA-seq is based on the hydrolysis of the tRNAs, which generates fragments with less structure and fewer modifications that are more amenable for sequencing.

tRNA factions were subjected to alkaline hydrolysis, dephosphorylation and rephosphorylation with T4 Polynucleotide Kinase (PNK), to finally prepare the small RNA cDNA library as described in [207] (**Figure 18**). Sequencing was performed on an Illumina HiSeq 2500 platform in a 50 base pair paired-end format (40 M reads).

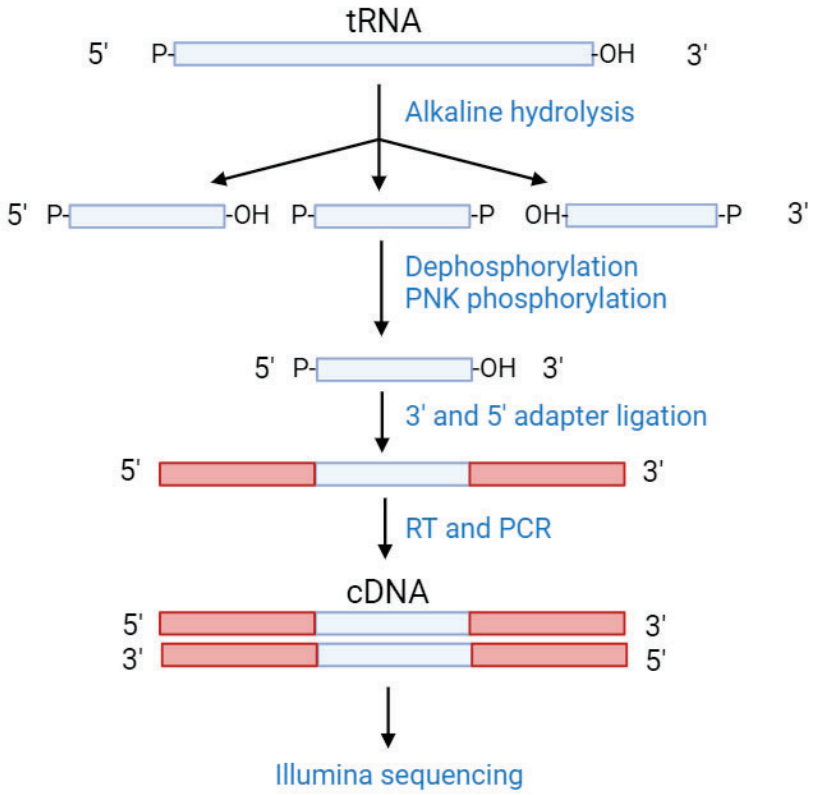

Figure 18. Hydro-tRNA-seq experimental pipeline. Pre-tRNAs, and especially mature tRNAs, are heavily modified and have thermodynamically stable secondary and tertiary structures. The first step in Hydro-tRNA-seq is the alkaline hydrolysis of tRNAs, which generates shorter RNA fragments that can be more easily sequenced. These fragments might present phosphate groups in their 5' and/or 3' termini, which are removed by Antarctic Phosphatase. PNK then phosphorylates all the RNAs at their 5' end (as well as removing 3' phosphates, if still present), generating 5'-P and 3'-OH ends, to which the adapters for RT (reverse transcription) and PCR (polymerase chain reaction) are ligated. Thus, the cDNA library is generated and is ready for Illumina sequencing. Figure created with *Biorender.com*.

Analysis of the sequencing data was performed by the Bioinformatics Unit of the CRG, using the tRNA Analysis of eXpression (tRAX) software (trna.ucsc.edu/tRAX/) (UC Santa Cruz), as described in [208].

5.3. Reverse transcription quantitative polymerase chain reaction (RT-qPCR)

The mRNA levels of the target genes were quantified by RT-qPCR. The NZY First-Strand cDNA Synthesis Kit (from NZYTech) was used to reverse transcribe cDNA from 1 ug of total RNA (in the case of HEK293 cells) or lRNA (in the case of WT and 5xFAD mice), according to manufacturer's instructions. qPCR was performed with the Fast SYBR™ Green Master Mix (from Thermo Fisher Scientific) in a 7500 Real Time PCR System (from Applied Biosystems). Expression results were

normalized by β-actin expression in human samples, and by *HPRT* (hypoxanthine phophoribosyltransferase 1) in murine samples. The specific primers for qPCR are summarized in **Table 5**.

Target gene	Target specie	Primer	Sequence (5'- 3')	Amplicon size (nt)	Source
DDIT4 (RTP801)	*Hs*	Fw	TTTGGGACCGCTTCTCGTC	388	Own design
		Rv	CGCAGTAGTTCTTTGCCCAC		
	Mm	Fw	GCCTAGCCTTTGGGATCGTT	520	
		Rv	CAGGGTCAACTGAAAGGTGG		
XBP1 (spliced)	*Hs, Mm*	Fw	GAGTCCGCAGCAGGTG	150	[191]
		Rv	GGAAGGGCATTTGAAGAACA		
XBP1 (unspliced)	*Hs, Mm*	Fw	ACTACGTGCACCTCTGCAG	159	
		Rv	GGAAGGGCATTTGAAGAACA		
BDNF	*Hs, Mm*	Fw	GGCGGCAGATAAAAAGACTG	202	Own design
		Rv	TACCCAGTCGTATGTTCGG		
SEC24D	*Hs*	Fw	TGGACCAGTCAGATGCAACAGG	155	Origene (#HP211178)
		Rv	GGACCACATTGGAAGAAGACTGG		
KALRN (Kalirin isoform 7)	*Mm*	Fw	GATACCATATCCATTGCCTCCAGGACC	127	[209]
		Rv	CCAGGCTGCGCGCTAAACGTAAG		
RTCB (HSPC117)	*Hs*	Fw	GAAGGAGCAACTTGCCCAAGCT	161	Own design
		Rv	AGTGCTCCTTGTCTTCAGCCCA		
ACTB (Actin)	*Hs*	Fw	TTGCCGACAGGATGCAGAAGGA	129	[210]
		Rv	AGGTGGACAGCGAGGCCAGGAT		
HPRT1	*Mm*	Fw	TGTTGTTGGATATGCCCTTG	259	[211]
		Rv	AATGTCAGTTGCTGCGTCC		

Table 5. Primers used for RT-qPCR. Hs = *Homo sapiens*; Mm = *Mus musculus*; Fw = Forward; Rv = Reverse.

For primer design, the human, mouse (and rat) gene sequences were obtained from the Gene database of NCBI (National Center for Biotechnology Information) and were aligned using the Clustal Omega program. Then, the conserved regions of the sequences (if present) were entered in the Primer-BLAST (basic local alignment search tool) of the NCBI, with the following parameters: PCR product size, Min = 70, Max = 1000; Primer melting temperatures (T_m), Min = 57.0, Opt = 60.0, Max = 63.0, Max T_m difference = 3. If there was little gene sequence conservation between species, the Primer-BLAST was separately used for each specie. The output primer pairs with less self-complementarity and fewer non-intended targets were chosen and bought to Integrated DNA Technologies.

5.4. tRNA transfection

Mouse primary hippocampal neurons seeded in 12 mm coverslips were transfected at DIV 11 with the fraction of the tRNA samples not used for Hydro-tRNA-seq (see Methodology section 5.2). tRNAs were transfected using the lipid reagent Lipofectamine™ 2000 (from Thermo Fisher Scientific) according to manufacturer's instructions. Each coverslip received 100 ng of tRNAs, as in Koltun *et al.* [212]. Concisely, for each well, tRNAs were mixed with 2 µL of Lipofectamine™ 2000 and 600 µL of non-supplemented Neurobasal medium, and incubated for 20 min at RT. Then, the culture medium was replaced by the mixture for 4 h, and neurons were kept in a 5% CO_2 atmosphere at 37°C. The original culture medium was stored at 4°C and was used to replace the mixture after the 4 h (it was warmed before being added to the neurons). Paraformaldehyde (PFA) fixation (see Methodology section 6.1) was performed 30 h post-transfection.

6. Immunofluorescence and image analyses

6.1. Immunofluorescence of neuronal cultures

Mouse primary hippocampal neurons treated with tRNAs were fixed with 4% PFA (from Electron Microscopy Sciences) in PBS for 20 min at RT. Next, coverslips were permeabilized with 0.25% Triton X-100 (from Merck) in PBS for 5 min at RT and were blocked with Superblock™ Blocking Buffer for 20 min at 37°C. Primary antibodies were diluted in Superblock™ Blocking Buffer and incubated O/N at 4°C (**Table 6**). The next day, coverslips were incubated with the corresponding secondary antibodies diluted in Superblock™ Blocking Buffer for 2 h at RT (**Table 6**). Simultaneously, nuclei were labeled with 1:5000 bisbenzimide H-33342 trihydrochloride (Hoechst 33342, from Thermo Fisher Scientific). Between all steps coverslips were washed thrice in PBS. After secondary antibody incubation, coverslips were washed with Milli-Q water and

were mounted on glass microscope slides using ProLong™ Gold Antifade Mountant (from Thermo Fisher Scientific).

Antibody	Host	Dilution	Source
MAP2	Mouse	1:500	Abcam, #ab11268
ClvCas3	Rabbit	1:200	Cell Signaling Technologies, #9661
Alexa Fluor™ 488 anti-mouse IgG	Goat	1:500	Thermo Fisher Scientific, #A-11017
Alexa Fluor™ 555 anti-rabbit IgG	Goat	1:500	Thermo Fisher Scientific, #A-21430

Table 6. Primary and secondary antibodies used for immunofluorescence of cultured neurons. MAP2 = microtubule associated protein 2. ClvCas3 = cleaved caspase 3. IgG = immunoglobulin.

Samples were observed under an epifluorescent microscope (Leica AF6000, Leica Application Suite X (LAS X) software) at the Advanced optical microscopy unit (Centres Científics i Tecnològics de la UB (CCiTUB), Campus Clínic). Images were obtained with a 20x objective, and 5 images were obtained per coverslip.

6.2. Neuron viability analysis

For the neuron viability and neuron branching analyses, the Cell Profiler software (www.cellprofiler.org, Broad Institute) [213], [214] was used as previously described [215]. Briefly, global nuclei and neuronal somas ($MAP2^+$) were identified as independent objects, and a mask with neuronal soma was used to obtain only neuronal nuclei. $MAP2^+$ nuclei classification into viable, condensed, or fragmented was based on intensity, intensity distribution, size and shape, texture, and granularity parameters, using machine learning in Cell Profiler Analyst software [216], [217]. ClvCas3 positive cells were identified as independent objects and were related with neuronal somas, with the *RelateObjects* module, to distinguish neurons positive or negative for ClvCas3. Measures of ClvCas3 mean intensity per neuron were obtained.

6.3. Neuron branching analysis

The analysis of neuronal branching was performed in MAP2 images using Cell Profiler software as previously described [86]. In short, the neurites of all neurons were subtracted to keep only the neuronal somas, which were identified as independent objects. Neurites were then enhanced using the enhancement method “line structures” and were turned into a binary image. From this image, and using the neuronal soma as input, whole neurons were identified as independent objects. Objects at the border of the image were discarded. Neuron objects were used to mask the binary image of enhanced neurites. From the masked image, the morphological skeleton was created with the *Morph* module (**Figure 19A**). Measurements of

trunks (primary dendrites), non-trunk branches (intermediate dendrites), branch ends (terminal branches), and total tree length were obtained per neuron, using the *MeasureObjectSkeleton* module (**Figure 19B**). Neurons from 5 fields per coverslip were analyzed.

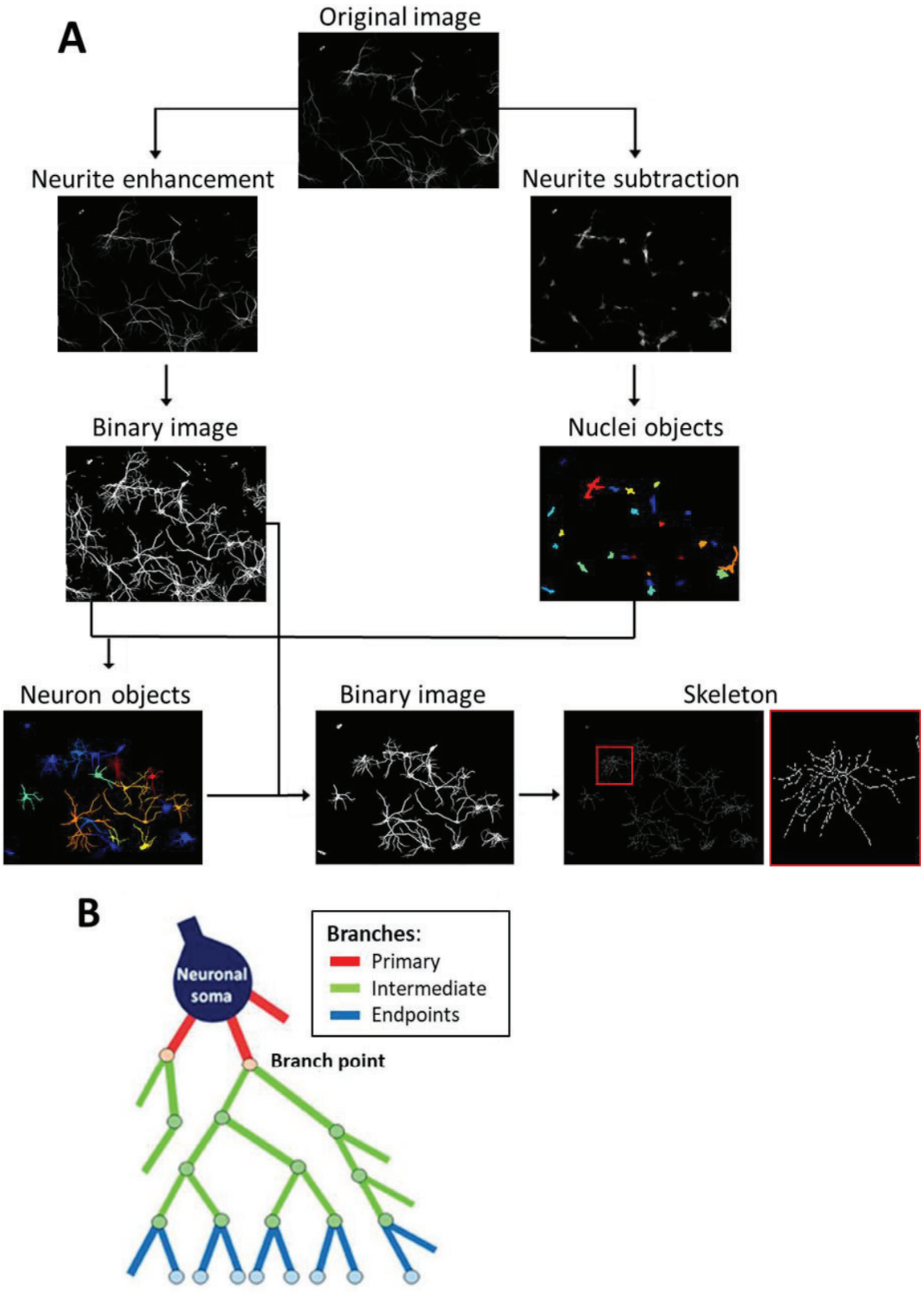

Figure 19. Analysis of neuron branching. (A) Schematic of the Cell Profiler pipeline used for the obtention of the neurons' skeleton. **(B)** Graphic representation of the types of neuronal branches analyzed. The length of all the branches combined is known as "total tree length". Panel obtained from [215].

7. Statistical and bioinformatics analyses

All *in vitro* experiments were performed with technical replicates and were repeated 3 times (n=3), unless otherwise stated in the figure legend. Normal distribution was assumed when all the data passed at least one of the following normality tests: D'Agostino & Pearson, Shapiro-Wilk, and/or Kolmogorov-Smirnov. When two normal conditions were compared, analyses were performed using the unpaired two-tailed Student's t-test (95% confidence). Welch's correction was applied when variances were significantly different between conditions according to F-test. When Gaussian distribution was not assumed, the Mann-Whitney U test was performed. For *in vivo* experiments, in which animals are classified into 4 groups based on 2 different variables (genotype and treatment), 2-way ANOVA (analysis of variance) with Bonferroni's or Tukey's post hoc test was performed. Correlation analyses were measured using Pearson correlation coefficient. To detect significant outlier values, Grubbs' and ROUT tests were used. All data are expressed as mean ± standard error of the mean (SEM). Values of $P < 0.05$ were considered statistically significant. All p-values are two-sided. All statistical tests were performed on GraphPad Prism 8.0, except for the receiver operating characteristic (ROC) curves and the Gene Ontology (GO) enrichment analyses, which were performed on R.

For the generation of ROC curves, protein expression values obtained from WB were used as predictor outcomes for the condition (CT or AD). R package pROC v.1.18.5 [218] was used for performance evaluation of the predictors, and ggplot2 v.3.4.4 [219] was used for graphical representation of the curves. Enrichment analysis of RTP801-interacting proteins was performed using enrichR R interface to the Enrichr database [220] and using the GO Molecular Function 2023 gene set library.

All mice bred for the experiments were used for pre-planned experiments and randomized to experimental groups. Data were collected, processed, and analyzed blindly.

RESULTS

1. Nature of the interaction between RTP801 and the members of the tRNA-LC

The cellular pools of tRNA and mRNA are crucial for the efficiency and accuracy of translation. Indeed, the translation time of a certain codon is positively correlated with the abundance of the tRNAs recognizing it [221]. Moreover, the tRNA and mRNA pools have been shown to change depending on the status of the cell. Thus, under physiological conditions, mRNAs tend to use common codons, whereas stress-responsive proteins use rare codons [222]. Thus, both the tRNA and mRNA pools are subject to a very tight, but dynamic regulation [223]. In this sense, the tRNA-LC has an important role, since it controls both the splicing of tRNAs and the unconventional splicing of specific mRNAs, such as *XBP1*, which encodes the transcription factor XBP1s. This complex is constituted by HSPC117, DDX1, CGI-99, FAM98B, and ASW.

Indeed, in preliminary results from our group in rat primary cortical neurons, endogenous RTP801 was immunoprecipitated to investigate its interactors by MS. We found 43 proteins, including DDX1 and HSPC117, two of the tRNA-LC effectors. However, to date, a role of RTP801 on tRNA or mRNA metabolism has not been described.

For this reason, in this work we decided to study the nature of the interaction between RTP801 and the members of the tRNA-LC, with the perspective of describing a novel function of this protein.

1.1. Confirmation of RTP801 interaction with DDX1 and HSPC117

As aforementioned, in preliminary results of our group endogenous RTP801 was immunoprecipitated in rat primary cortical neurons and 43 protein interactors were detected by MS. To unravel potential novel functions of RTP801, we started by checking whether these interactors were participating in similar physiological processes or had common functions. Thus, we first performed a Gene Ontology (GO) biological process enrichment analysis of the interactors (**Figure 20**). Interestingly, we found that 16 out of the 43 proteins were RNA binding proteins, suggesting that RTP801 might be involved in RNA metabolism. Interestingly, two of these RNA-binding proteins were DDX1 and HSPC117, two members of the tRNA-LC.

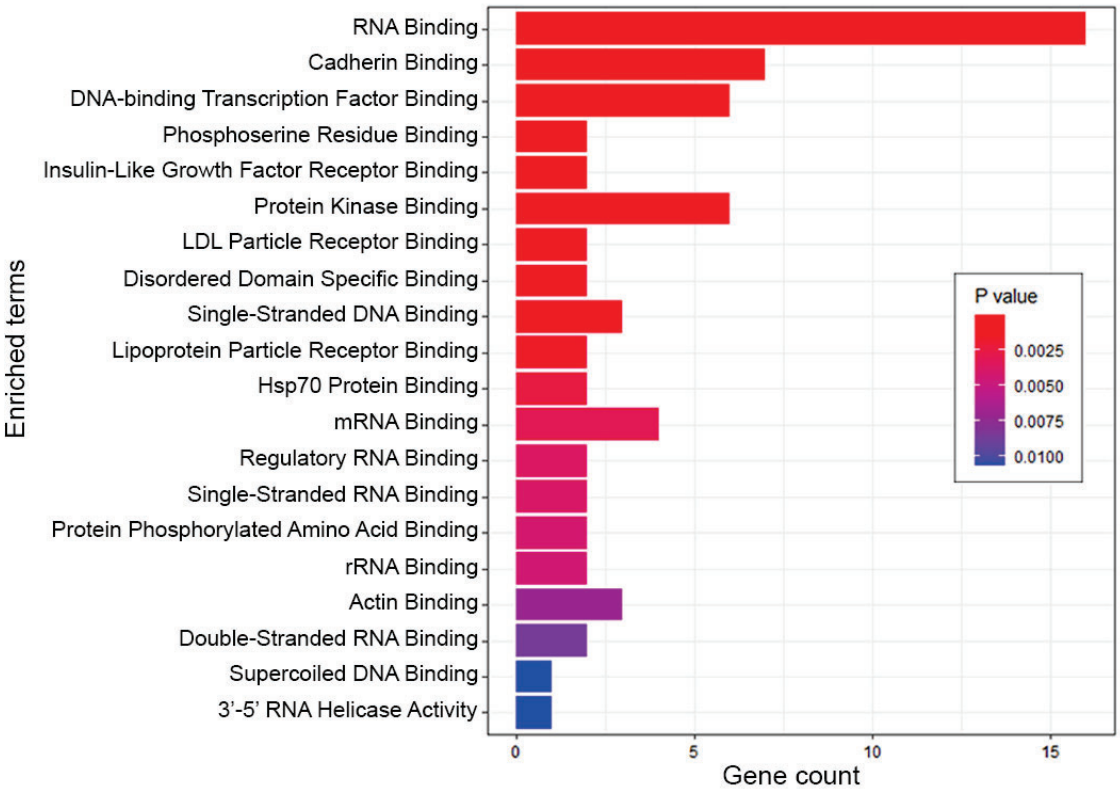

Figure 20. RTP801 mostly interacts with RNA binding proteins. GO biological process enrichment analysis of RTP801 interactors. For each enriched category, the Fisher's exact test p-value is calculated, and bars are colored according to it. The top 20 enriched GO molecular function terms are plotted. LDL = low-density lipoprotein. Hsp70 = 70-kDa heat shock protein.

To investigate whether these interactions were exclusive for rat embryonic neurons in culture, or they could be extended to other cell types and organisms, we turned to human proliferative cells. Hence, we treated HEK293 cells for 2 h with DSP, a chemical cross-linker, and we immunoprecipitated endogenous RTP801. As expected, we detected both DDX1 and HSPC117 by WB. Moreover, CGI-99, another member of the tRNA-LC, was also pulled down. On the contrary, actin, which was included as negative control, was not detected (**Figure 21**). Unfortunately, we were unable to detect FAM98B (which is also part of the complex) with the available antibody, even in the IP inputs. Thus, we confirmed the results obtained by MS, and, in addition, we could detect another tRNA-LC member, CGI-99, after pulling down RTP801.

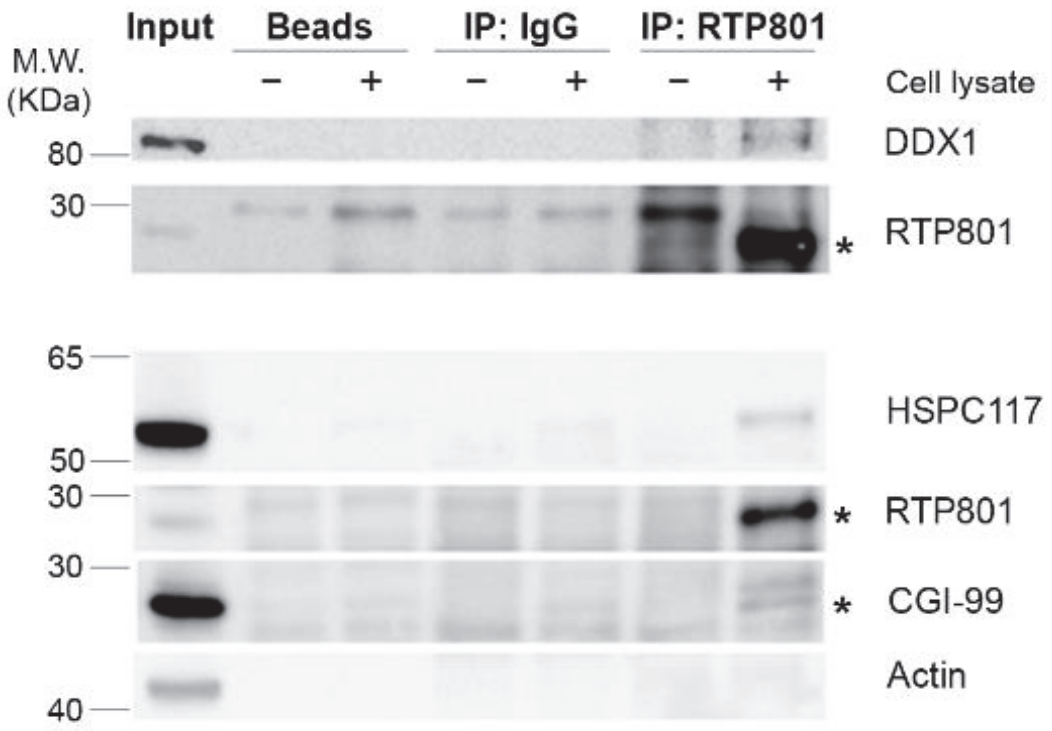

Figure 21. RTP801 co-immunoprecipitates with DDX1, HSPC117, and CGI-99 in HEK293 cells. After a 2-hour treatment with DSP, HEK293 cells were harvested and endogenous RTP801 was immunoprecipitated. Some lysates were incubated with beads or beads bound to normal IgGs as negative controls. Samples were then analyzed by WB. The asterisks indicate the bands corresponding to RTP801 (≈ 28 kDa) and CGI-99 (≈27 kDa). n = 2. M.W. = molecular weight.

1.2. RTP801 does not affect the protein stability of the complex members

Once confirmed the interaction of RTP801 with HSPC117, DDX1, and CGI-99, we investigated whether RTP801 could be mediating the stability, and therefore, the protein levels of the complex members. Hence, we used a shRNA to downregulate RTP801 in HEK293 cells (**Figure 22A-E**) and in rat primary cortical neurons (**Figure 22F-J**), the two cellular models where we had observed the interactions (**Figure 20, 21**). We downregulated RTP801 expression by a 30% in both cases, as previously reported [71], [114], [118], assessed by WB (**Figure 22B, G**). However, the levels of HSPC117, DDX1, and CGI-99 were unaffected by RTP801 silencing (**Figure 22C-E, H-J**). Thus, although the interaction of RTP801 with the tRNA-LC is conserved between species and cell types, it does not influence the protein levels of its members.

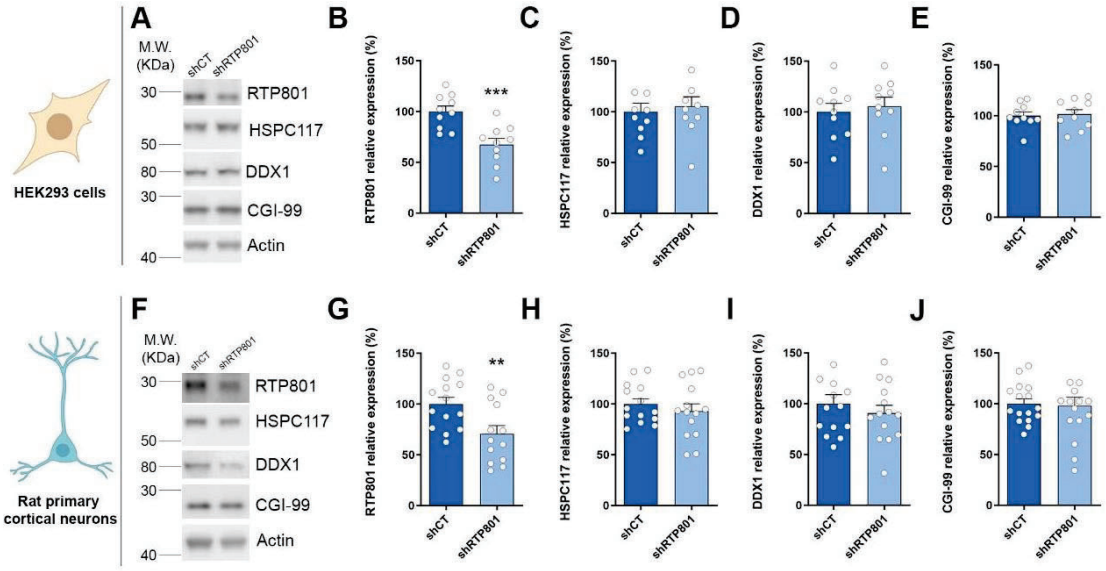

Figure 22. RTP801 does not affect the protein levels of the members of the tRNA-LC. **(A)** WB for RTP801, HSPC117, DDX1, CGI-99, and actin as loading control in HEK293 cells transfected with shRNA against RTP801. **(B-E)** Densitometric quantification of RTP801 **(B)**, HSPC117 **(C)**, DDX1 **(D)**, and CGI-99 **(E)** results. **(F)** WB for RTP801, HSPC117, DDX1, CGI-99, and actin as loading control in rat cortical neurons infected with shRNA against RTP801-containing lentiviruses. **(G-J)** Densitometric quantification of RTP801 **(G)**, HSPC117 **(H)**, DDX1 **(I)**, and CGI-99 **(J)** results. All data are analyzed with the unpaired two-tailed Student's t-test, and are represented as mean ± SEM. Values represent technical replicates of 3 independent experiments. **p < 0.01, and ***p < 0.001.

1.3. RTP801 does not affect the gene expression of DDX1 or RTCB

In parallel, we studied whether RTP801 could be affecting the gene expression of DDX1 and HSPC117. For this, we transfected HEK293 cells with shRTP801 and assessed the mRNA levels of *DDX1* and *RTCB* by RT-qPCR (**Figure 23**). First, we validated the correct silencing of *DDIT4* (RTP801 coding gene, **Figure 23A**) and observed a 25% downregulation, similar to the protein reduction results (**Figure 22B**). When we assessed the mRNA levels of *RTCB* and *DDX1* no significant changes were observed (**Figure 23B-C**), indicating that RTP801 is not regulating the gene expression of these factors either.

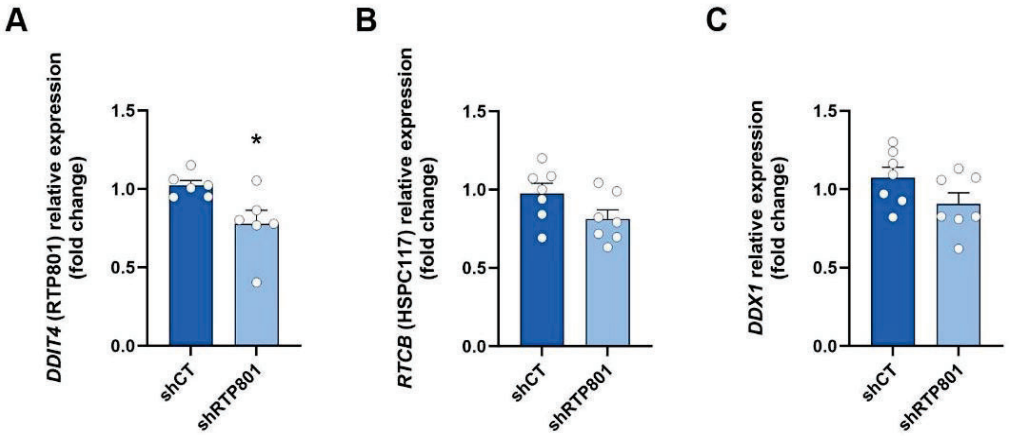

Figure 23. RTP801 does not affect the mRNA levels of *RTCB* or *DDX1*. HEK293 cells were transfected with shCT or shRTP801 and 3 days later, RNA was extracted, retrotranscribed and RT-qPCR was performed. Relative expression of *DDIT4* **(A)**, *RTCB* **(B)**, and *DDX1* **(C)**. *ACTB* (β-actin) was used to normalize the expression of all genes. All data are analyzed with the unpaired two-tailed Student's t-test, and are represented as mean ± SEM. Values represent technical replicates of 2 independent experiments. *p < 0.05.

1.4. HSPC117 and DDX1 modulate the protein stability of RTP801

Since RTP801 does not affect the protein stability of DDX1, HSPC117, nor CGI-99, we wondered whether the complex members could be regulating RTP801 protein stability. Note that RTP801 has a 2 to 5-minute half-life [91], [92] and is very sensitive to interactors and stressors. Therefore, we used shRNA to downregulate HSPC117 or DDX1 in HEK293 cells and analyzed the protein levels of the members of the complex by WB (**Figure 24A-E**). First, we validated the efficiency of shHSPC117 and shDDX1 (**Figure 24B-C**), and confirmed that the former caused a 30% reduction in its protein levels, whereas the latter led to a 45% decrease in DDX1 protein levels. Interestingly, the downregulation of HSPC117 significantly diminished DDX1 protein levels (**Figure 24C**). Regarding RTP801, both shHSPC117 and shDDX1 caused a significant reduction in its levels (**Figure 24D**), suggesting that both DDX1 and HSPC117 stabilize RTP801 protein. On the contrary, the levels of CGI-99 were unaffected by HSPC117 or DDX1 silencing (**Figure 24E**). Altogether, these results suggest that HSPC117 might be the master regulator of the complex since it modulates the protein levels of DDX1 and RTP801. In addition, DDX1 also appears to be important for the stability of RTP801.

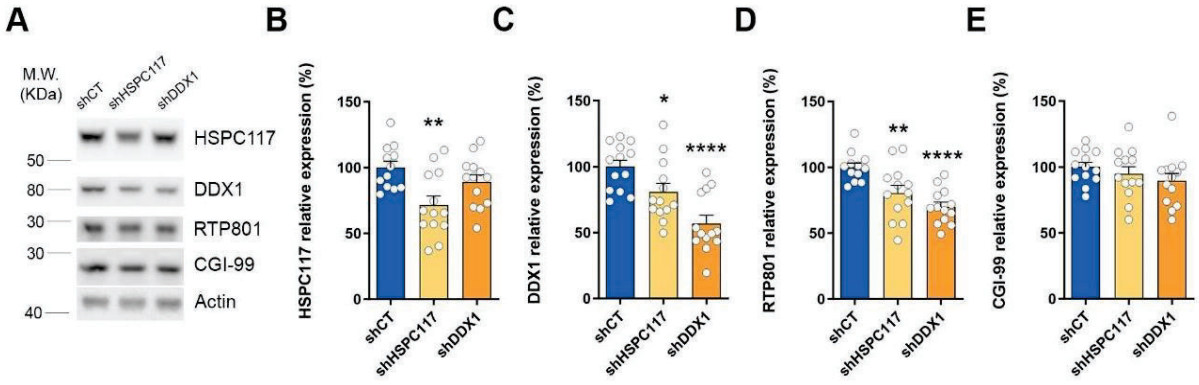

Figure 24. HSPC117 and DDX1 regulate the protein stability of RTP801. **(A)** WB for HSPC117, DDX1, RTP801, CGI-99, and actin as loading control in HEK293 cells transfected with shRNA against HSPC117 or against DDX1. **(B-E)** Densitometric quantification of HSPC117 **(B)**, DDX1 **(C)**, RTP801 **(D)**, and CGI-99 **(E)** results. All data are analyzed with the one-way ANOVA test and compared with Dunnett's multiple comparison test, and are represented as mean ± SEM. Values represent technical replicates of 3 independent experiments. *p < 0.05, **p < 0.01, and ***p < 0.0001.

1.5. HSPC117 and DDX1 do not affect the gene expression of *DDIT4*

To assess whether the regulation of HSPC117 and DDX1 over RTP801 protein levels is due to changes in *DDIT4* transcription, we knocked down HSPC117 or DDX1 and analyzed the mRNA levels of *DDIT4* by RT-qPCR (**Figure 25**). We first confirmed the correct knockdown of *RTCB*, which was a 30% (**Figure 25A**), and *DDX1*, which was a 40% (**Figure 25B**), as in **Figure 24**. Strikingly, HSPC117 downregulation caused a significant increase in the mRNA levels of *DDX1*. Regarding *DDIT4*, both shHSPC117 and shDDX1 tended to reduce its expression, but it did not reach significance (**Figure 25C**). Altogether, these results show that the regulation of HSPC117 and DDX1 over RTP801 is mostly at the protein levels (**Figure 24D**), rather than to gene expression (**Figure 25C**).

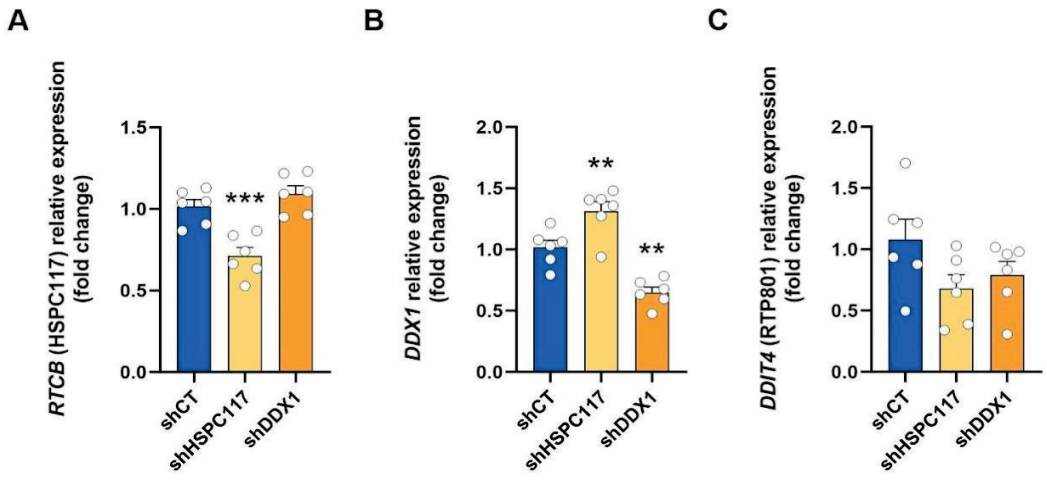

Figure 25. HSPC117 and DDX1 do not regulate the gene expression of *DDIT4*. HEK293 cells were transfected with shCT, shHSPC117, or shDDX1 and 3 days later, RNA was extracted, retrotranscribed and RT-qPCR was performed. Relative expression of *RTCB* **(A)**, *DDX1* **(B)**, and *DDIT4* **(C)**. *ACTB* (β-actin) was used to normalize the expression of all genes. All data are analyzed with the one-way ANOVA test and compared with Dunnett's multiple comparison test, and are represented as mean ± SEM. Values represent technical replicates of 2 independent experiments. **p < 0.01, and ***p < 0.001.

Overall, these data suggest that RTP801 does not regulate the mRNA or protein levels of the members of the complex, but rather, its own protein stability might depend on the protein levels of HSPC117 and DDX1.

2. Role of RTP801 in the mRNA ligase activity of the tRNA-LC

The tRNA-LC is a pentameric complex involved in the splicing of tRNAs [126], but also in the unconventional splicing of *XBP1* [191]. *XBP1* mRNA undergoes canonical splicing in the nucleus but retains a short, 26-nucleotide intron. This mRNA with intron (*XBP1u*, ***u**nspliced*) is translated, producing the protein XBP1u. However, the accumulation of unfolded or misfolded proteins in the ER activates the UPR, which leads to the cleavage of *XBP1u* mRNA in the cytoplasm by IRE1 and the subsequent ligation by the tRNA-LC. This mRNA (*XBP1s, **s**pliced*) is translated generating a transcription factor that helps to restore ER homeostasis. For instance, XBP1s promotes the transcription of chaperones, lipogenic enzymes, and *BDNF* [192], [199].

In the previous section of this thesis, we confirmed the interaction of RTP801 with 3 members of the tRNA-LC, and we found that RTP801 does not regulate their protein nor mRNA levels. Hence, in this section we aimed to investigate whether RTP801 interaction with the complex is translated to a modulation of its ligase activity, investigating first whether RTP801 could regulate the mRNA ligase activity of the tRNA-LC over *XBP1.*

2.1. RTP801 inhibits *XBP1* splicing *in vitro*

Since RTP801 interacts with DDX1, HSCP117, and CGI-99, but it does not regulate their mRNA or proteins levels, we hypothesized that it could be modulating their activity. To check whether RTP801 affected the mRNA ligase activity of the tRNA-LC we studied the splicing of *XBP1* when RTP801 was either downregulated or upregulated (**Figure 26**). Therefore, HEK293 cells were transfected either with shRTP801 (**Figure 26A-F**) or with a plasmid encoding for an eGFP-RTP801 fusion protein (**Figure 26G-L**). Strikingly, knocking down RTP801 by a 25 % (**Figure 26A**) caused a significant increase in *XBP1s* mRNA (**Figure 26B**) without altering the levels of *XBP1u* (**Figure 26C**), leading to an elevation of the *XBP1s/XBP1u* ratio (**Figure 26D**). Interestingly, we also observed a significant increase in *SEC24D* mRNA, a target gene of XBP1s as a transcription factor [224] (**Figure 26E**), but we found no changes in another target gene, *BDNF* [199] (**Figure 26F**). On the contrary, RTP801 overexpression (**Figure 26G**) resulted in a significant accumulation of *XBP1u* with no changes in *XBP1s*, which resulted in a reduced *XBP1s/XBP1u* ratio (**Figure 26H-J**). Regarding *SEC24D* and *BDNF*, no differences were observed when RTP801 was upregulated (**Figure 27K-L**). These results suggest that RTP801 inhibits the unconventional splicing of *XBP1*, since its levels inversely correlated with the *XBP1s/XBP1u* ratio.

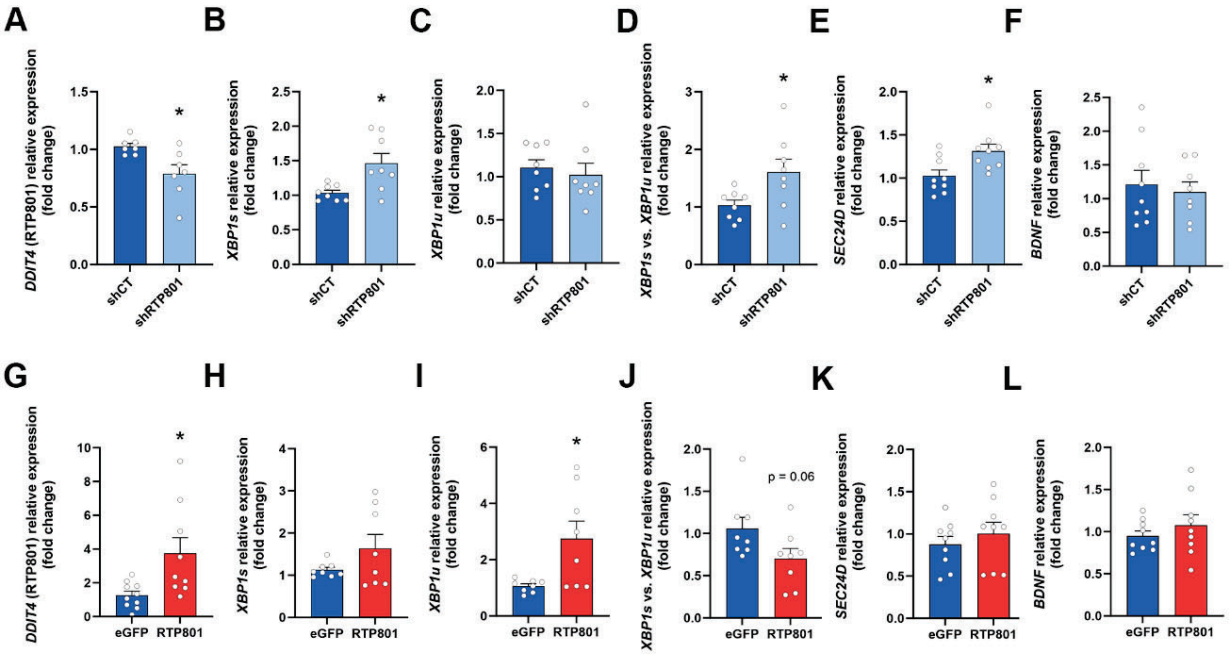

Figure 26. RTP801 inhibits the splicing of *XBP1 in vitro*. HEK293 cells were transfected with shCT, shRTP801, eGFP, or eGFP-RTP801. RNA was extracted, retrotranscribed and RT-qPCR was performed, 2 (for overexpressing vectors) or 3 (for silencing vectors) days later. **(A-F)** RT-qPCR results in HEK293 cells with downregulation of RTP801. Relative expression of *DDIT4* (RTP801 coding gene) **(A)**, *XBP1s* **(B)**, *XBP1u* **(C)**, *XBP1s/XBP1u* **(D)**, *SEC24D* **(E)**, and *BDNF* **(F)**. **(G-L)** RT-qPCR results in HEK293 cells with upregulation of RTP801. Relative expression of *DDIT4* **(G)**, *XBP1s* **(H)**, *XBP1u* **(I)**, *XBP1s/XBP1u* **(J)**, *SEC24D* **(K)**, and *BDNF* **(L)**. *ACTB* (β-actin) was used to normalize the expression of all genes. All data are analyzed with the unpaired two-tailed Student's t-test. Welch's correction was applied in panels **(A, B, D, G, H,** and **I)** because variances were unequal between the two conditions. All data are represented as mean ± SEM. Values represent technical replicates of 3 independent experiments. *p < 0.05.

2.2. HSPC117 silencing does not affect XBP1 splicing *in vitro*

Iwawaki *et al.* [225] and Jurkin *et al.* [191] found that HSPC117 silencing alone did not affect *XBP1* splicing *in vitro*, in contrast to what we found regarding RTP801 levels, which could, *per se*, affect the ligase activity of the complex. Hence, we wanted to confirm that, in our hands, HSPC117 silencing did not affect the unconventional splicing of *XBP1* either. Thus, HEK293 cells were transfected with shHSPC117 and the mRNA levels of *XBP1s* and *XBP1u* were assessed by RT-qPCR (**Figure 27**). The shRNA induced a 50% knockdown of *RTCB* expression (**Figure 27A**), but the mRNA levels of *XBP1s* and *XBP1u* were unaltered by HSPC117 silencing (**Figure 27B-C**). Consequently, the ratio between the levels of *XBP1s* and *XBP1u*, which is commonly used as a readout of splicing efficiency, was not significantly different between conditions (**Figure 27D**). Hence, we confirmed previous observations indicating that low levels of HSPC117 are sufficient to maintain *XBP1* splicing *in vitro*.

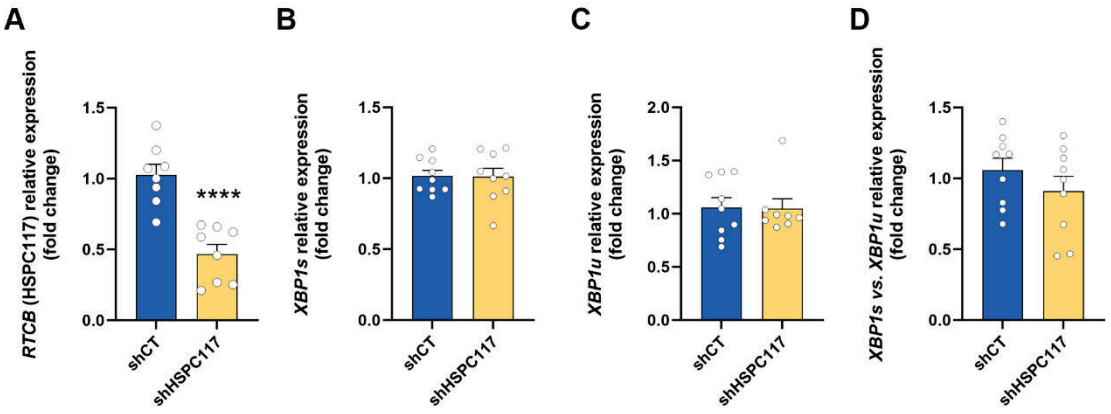

Figure 27. HSPC117 silencing does not affect *XBP1* splicing. HEK293 cells were transfected with shCT or shHSPC117 and 3 days later, RNA was extracted, retrotranscribed and RT-qPCR was performed. Relative expression of *RTCB* **(A)**, *XBP1s* **(B)**, and *XBP1u* **(C)** normalized to *ACTB* (β-actin). **(D)** Relative expression of *XBP1s* normalized to *XBP1u* as a readout of *XBP1* splicing. All data are analyzed with the unpaired two-tailed Student's t-test. Data in panel **(C)** were analyzed with Mann-Whitney U test because values did not pass the normality test. All data are represented as mean ± SEM. Values represent technical replicates of 3 independent experiments. ****p < 0.0001.

2.3. XBP1 splicing is impaired in the hippocampus of AD patients

Considering that RTP801 inhibits *XBP1* splicing *in vitro*, we explored whether this could occur in the context of the human pathology of AD, where RTP801 has been found upregulated both in hippocampal samples and lymphocytes [114], [121]. Since a long time between the patients' death and the obtention of tissue (known as postmortem delay) seriously affects the quality of the RNA samples (assessed by the RNA integrity number or RIN), we decided to evaluate XBP1 splicing by checking the protein levels of XBP1s and XBP1u (**Figure 28**), rather than the mRNA. Moreover, we also investigated the protein levels of effectors of the PERK branch of the UPR as an additional readout of ER stress (illustrated in **Figure 28A**).

First, we confirmed the elevation of RTP801 in hippocampal AD patients' samples compared to age-matched controls (CT) (**Figure 28B**), as we previously described [114]. In addition, we found no significant changes in HSPC117, DDX1, or CGI-99 protein levels (**Figure 28C-E**). Nonetheless, we found a drastic reduction in the protein levels of XBP1s with no changes in the levels of XBP1u, leading to a decreased XBP1s/XBP1u ratio in the hippocampus of AD patients (**Figure 28F-H**). Regarding the PERK branch of the UPR, we found significantly increased phosphorylation of eIF2α on serine 51 in the hippocampus of AD patients, whereas the levels of the transcription factor ATF4 were not altered (**Figure 28I-J**). Then, we studied whether any of the proteins with significantly different levels in the hippocampus of AD patients could be used as a classifier of

the presence or the absence of the disease. Thus, the protein levels of RTP801, XBP1s, and P-eIF2α Ser51 were used to plot ROC curves (**Figure 28K-M**), and they were found to be very good classifiers, as determined by the area under the curve (AUC), being RTP801 the best marker. Altogether, these results indicate that, although the protein levels of the members of the tRNA-LC are not altered in the hippocampus of AD patients, XBP1 splicing is dramatically reduced. In addition, the PERK branch of the UPR seems active in the hippocampus of AD patients, judged by the phosphorylation of its main effector eIF2α. Hence, these results suggest that elevated levels of RTP801 in the hippocampus of AD patients are specifically inhibiting the tRNA-LC activity over XBP1 splicing, without affecting the other branches of the UPR.

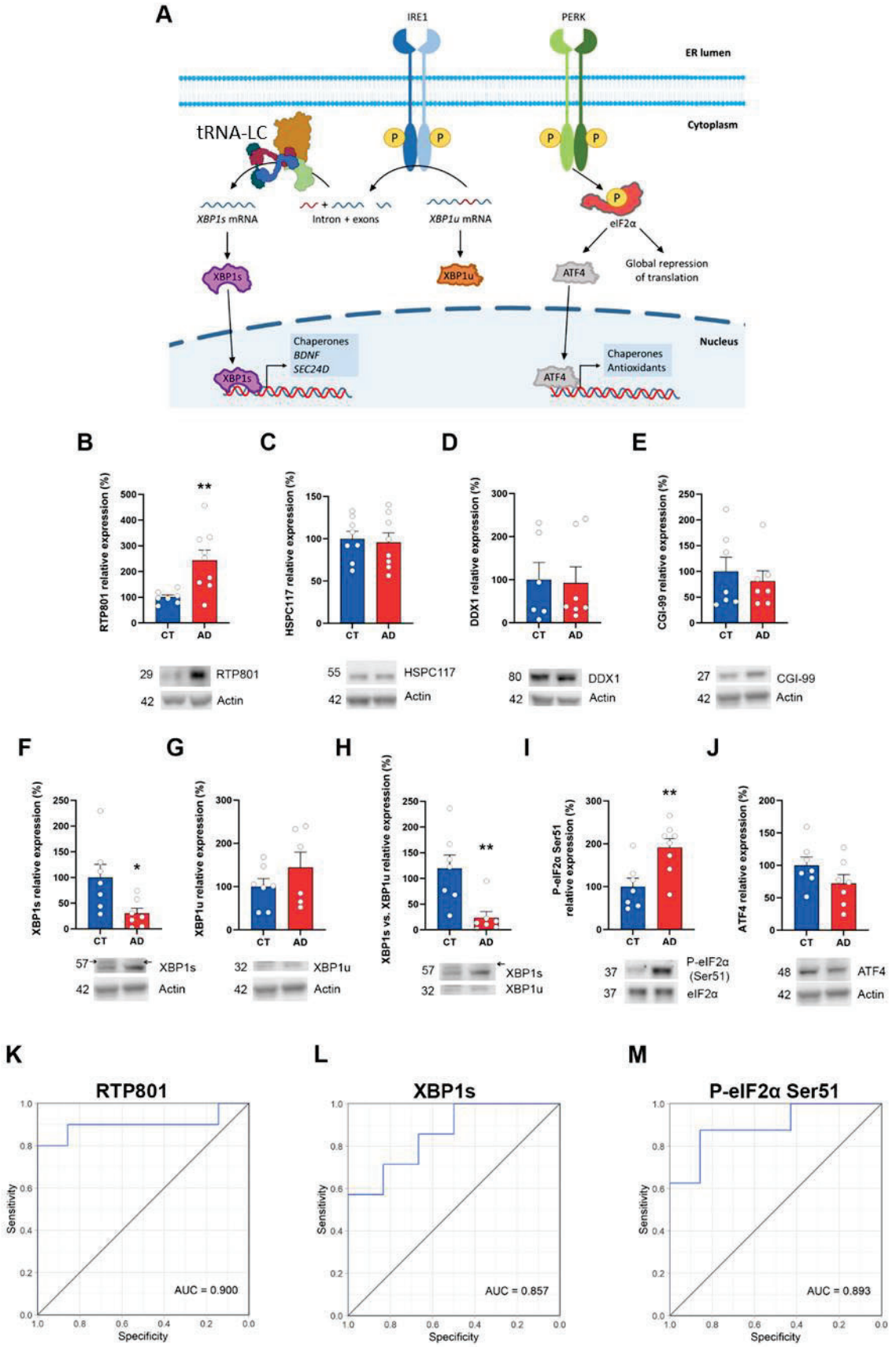
A
IRE1
PERK
ER lumen
Cytoplasm
tRNA-LC
P
XBP1s mRNA
Intron + exons
XBP1u mRNA
eIF2α
ATF4
Global repression of translation
XBP1s
XBP1u
Nucleus
Chaperones
BDNF
SEC24D
Chaperones
Antioxidants
B
C
D
E
RTP801 relative expression (%)
HSPC117 relative expression (%)
DDX1 relative expression (%)
CGI-99 relative expression (%)
CT
AD
29 RTP801
42 Actin
55 HSPC117
80 DDX1
27 CGI-99
F
G
H
I
J
XBP1s relative expression (%)
XBP1u relative expression (%)
XBP1s vs. XBP1u relative expression (%)
P-eIF2α Ser51 relative expression (%)
ATF4 relative expression (%)
57 XBP1s
32 XBP1u
37 P-eIF2α (Ser51)
37 eIF2α
48 ATF4
K
L
M
RTP801
XBP1s
P-eIF2α Ser51
Sensitivity
Specificity
AUC = 0.900
AUC = 0.857
AUC = 0.893

Figure 28. Reduced XBP1 splicing in the hippocampus of AD patients. (A) Graphical representation of the IRE1 and the PERK branches of the UPR. Accumulation of unfolded or misfolded proteins leads to the activation of the UPR. The effector of the IRE1 branch is XBP1s, a transcription factor whose mRNA requires the ligation by the tRNA-LC to be translated. The effector of the PERK branch is phosphorylated eIF2α, which promotes the translation of *ATF4*. **(B-J)** WB and densitometric quantification for RTP801 **(B)**, HSPC117 **(C)**, DDX1 **(D)**, CGI-99 **(E)**, XBP1s **(F)**, XBP1u **(G)**, XBP1s/XBP1u **(H)**, p-eIF2α Ser51 **(I)**, ATF4 **(J)**, and actin as loading control in human hippocampal samples. All data are analyzed with the unpaired two-tailed Student's t-test (except for panel **(D** and **H)**). The arrows in panels **(F** and **H)** indicate the specific band for XBP1s (≈ 57 kDa). Welch's correction was applied in panels **(B** and **F)** because variances were unequal between the two conditions. Data in panels **(D** and **H)** were analyzed with Mann-Whitney U test because values did not pass the normality test. All data are represented as mean ± SEM. *$p < 0.05$ and **$p < 0.01$. **(K-M)** ROC curves of RTP801 **(K)**, XBP1s **(L)**, and p-eIF2α Ser51 **(M)** obtained from the densitometric analyses of protein levels in **(B)**, **(F)**, and **(I)**, respectively.

2.4. Normalization of hippocampal RTP801 levels in the 5xFAD mouse model of AD promotes the splicing of *Xbp1*

Our results *in vitro* and in the hippocampus of AD patients suggested that RTP801 inhibited *XBP1* splicing, probably by means of its interaction with the tRNA-LC. Therefore, to confirm these data, we used the 5xFAD mouse model of AD, where we could modulate neuronal RTP801 levels and see the effect on *XBP1* splicing in *vivo*. Previously, we had already described that RTP801 silencing in the hippocampal neurons of 5xFAD and R6/1 mice (mouse models of AD and HD, respectively) prevented cognitive deficits, reduced gliosis, and decreased the protein levels of several inflammasome markers (summarized in **Figure 29A**) [114], [118]. Thus, we performed intra-hippocampal (CA1 and DG) injections of neuron-targeted AAVs containing GFP-tagged shCT or shRTP801 vectors (see Methodology section 3.6 for more information) in 6-month-old WT and 5xFAD mice. This approach generated four groups of mice namely: WT shCT, WT shRTP801, 5xFAD shCT, and 5xFAD shRTP801. One month after injection, the hippocampi were collected, and the RNA and the protein fractions were isolated, to perform biochemical and functionality experiments (**Figure 29B**). In this occasion, animals were not subjected to behavioral testing.

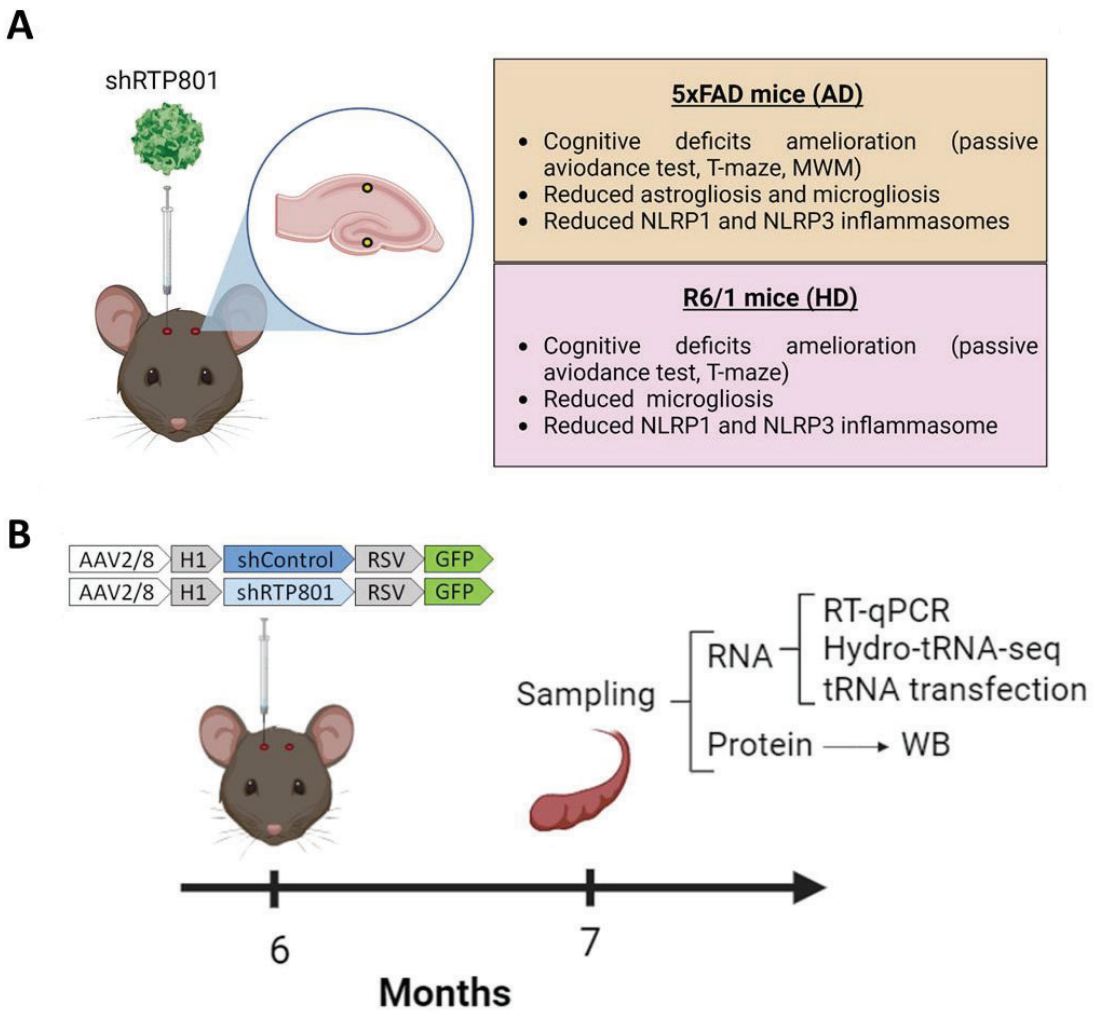

Figure 29. RTP801 silencing in 5xFAD mice. (A) Graphical representation of the effects of RTP801 genetic silencing in the dorsal hippocampus of 5xFAD and R6/1 mice [114], [118] RTP801 was downregulated using neuron-targeted AAVs containing shRTP801 bilaterally injected in the DG and the CA1 regions of the hippocampi. The effects of RTP801 in cognition and neuroinflammation for each mouse model are summarized in the color rectangles. **(B)** Timeline of mice surgery and sampling. WT and 5xFAD mice, at 6 months of age, were bilaterally injected in the dorsal hippocampus with neuron-directed AAVs containing shCT or shRTP801 and tagged with GFP. 4 weeks later, animals were euthanized, and the hippocampi were obtained for RT-qPCR, tRNA sequencing, tRNA transfection, and WB. Figure created with *Biorender.com*.

First, we assessed the magnitude of RTP801 silencing, by WB and RT-qPCR (**Figure 30**). By WB, we observed that the shRNA against RTP801 non-significantly reduced its protein levels (**Figure 30A-B**). Similarly, the expression of *Ddit4*, which was significantly augmented in 5xFAD mice compared to WT, also tended to decrease with the shRNA, assessed by RT-qPCR (**Figure 30C**).

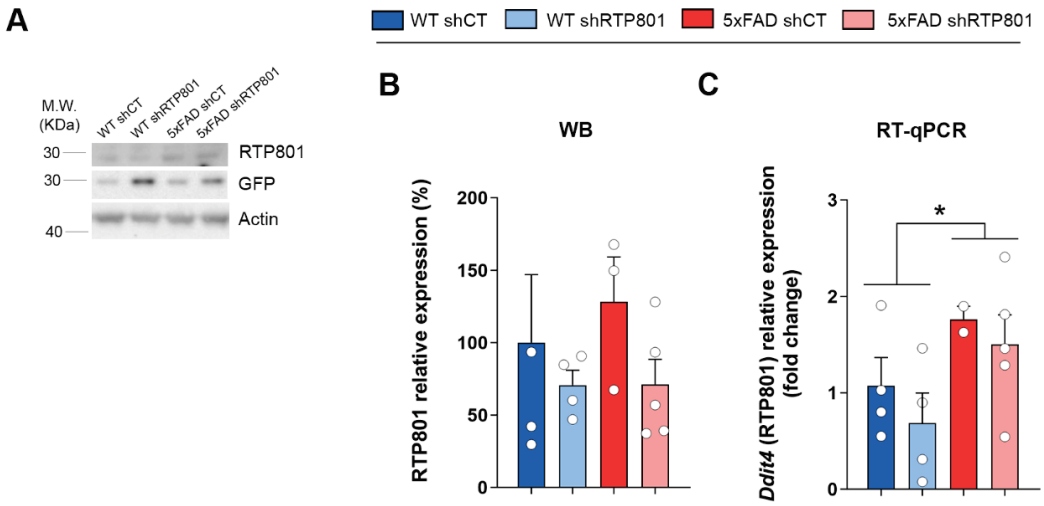

Figure 30. Genetic inhibition of RTP801 levels in the dorsal hippocampus of 5xFAD mice. (A) WB for RTP801 and GFP as loading control for transduced neurons in the dorsal hippocampus of 7-month-old WT shCT, WT shRTP801, 5xFAD shCT, and 5xFAD shRTP801 mice. **(B)** Densitometric quantification of RTP801 results. **(C)** RT-qPCR results for *Ddit4* in the dorsal hippocampus of WT shCT, WT shRTP801, 5xFAD shCT, and 5xFAD shRTP801 mice. *Hprt* was used to normalize the expression of *Ddit4*. Data are means ± SEM. In all comparisons two-way ANOVA with Tukey's post hoc test was performed. Each value represents one animal. *$p < 0.05$.

Since we obtained high quality RIN values of the total hippocampal RNA isolated from mice samples (**Table 7**), we assessed the splicing of *Xbp1* by RT-qPCR.

Condition	Sample	RIN	Condition	Sample	RIN
WT shCT	3	8.4	5xFAD shCT	1	8.1
	5	8.4		16	8.4
	6	8.5		18	8.3
	11	8.4	5xFAD shRTP801	2	8.2
	15	8.6		7	8.1
WT shRTP801	4	8.5		8	8.1
	10	8		12	8.5
	17	8.5		14	8.6
	21	8.9		19	8.3

Table 7. RNA integrity number (RIN) values of total RNA from the mouse hippocampal samples.

Thus, sncRNAs (17-200 nucleotides) and lRNAs (>200 nucleotides) were isolated from the total RNA with a commercial kit. The sncRNAs were posteriorly used for tRNA sequencing whereas the lRNAs were used for the assessment of *Xbp1* splicing by RT-qPCR (**Figure 31**). Regarding *Xbp1*

splicing, we found that the levels of *Xbp1s* mRNA are not altered in 5xFAD mice compared to WT animals (**Figure 31A**). However, *Xbp1u* tends to accumulate in 5xFAD mice, and, interestingly, RTP801 silencing significantly reduces the levels of the unspliced form of *Xbp1* (**Figure 31B**). As for the ratio between *Xbp1s* and *Xbp1u*, used as a readout of splicing efficiency, we observed that silencing RTP801 promotes *Xbp1* splicing (**Figure 31C**), which is in line with our *in vitro* results (see **Figure 27D**). In addition, when we monitored the expression of XBP1s transcriptional targets, we observed that RTP801 downregulation in 5xFAD mice increased the levels of *Bdnf* mRNA, a neurotrophin that plays an essential role in neuronal survival and growth, as well as in learning and memory [226] (**Figure 31D**). On the other hand, the mRNA levels of other XBP1s targets, such as *Sec24d* (**Figure 31E**) and *Kalirin-7* (**Figure 31F**) were invariable between experimental groups. Altogether, these results suggest that RTP801 impairs the activity of the tRNA-LC over *Xbp1* splicing in WT and 5xFAD mice. Indeed, the present data suggest that additional mechanisms may account for the induction of *Bdnf* detected in the 5xFAD mice with neuronal RTP801 silencing.

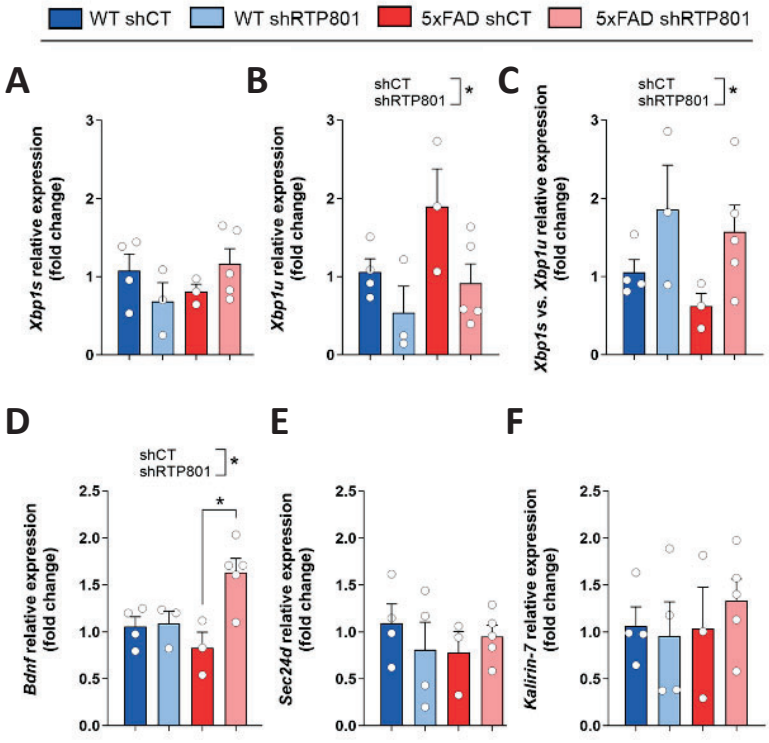

Figure 31. RTP801 downregulation in 5xFAD mice hippocampal neurons promotes *Xbp1* splicing. (A-F) RT-qPCR results relativized to *Hprt*. Relative expression of *Xbp1s* **(A)**, *Xbp1u* **(B)**, *Xbp1s/Xbp1u* **(C)**, *Bdnf* **(D)**, *Sec24d* **(E)**, and *Kalirin-7* **(F)**. Data are means ± SEM. Each value represents one animal. In all panels two-way ANOVA with Tukey's post hoc test was performed. *$p < 0.05$.

Overall, these data present RTP801 as a novel regulator of the mRNA ligase activity of the tRNA-LC over *XBP1* splicing, both *in vitro* and *in vivo*, and suggest that the abnormally high levels of RTP801 found in the hippocampus of AD patients might be also contributing to the impairment of this process.

3. Effect of RTP801 in the tRNA ligase activity of the tRNA-LC

tRNAs are transcribed as immature products containing 5' leader and 3' trailer sequences at their ends. Furthermore, around a 7% and a 5% of human and mouse pre-tRNAs present introns, respectively [141]. These introns must be spliced out during tRNA processing to obtain the mature tRNAs, which will participate in mRNA translation at the ribosomes. The splicing of introns requires their excision, which is performed by the TSEN complex [143], and the subsequent ligation. Nonetheless, the mammalian enzyme (or enzymes) that performs the ligation remained elusive until 2011, when Popow *et al.* [126] discovered the tRNA-LC using activity-guided chromatography followed by MS. They found that HSPC117 was the essential subunit of the complex and its depletion inhibited maturation of intron-containing pre-tRNAs both *in vitro* and in living cells. Interestingly, the individual depletion of any other member of the complex did not interfere with the tRNA ligase activity of the complex.

In the previous section of this thesis, we described that RTP801 inhibits the activity of the tRNA-LC over *XBP1* mRNA unconventional splicing, both *in vitro* and in a mouse model of AD. In this section, we aimed to study whether RTP801 could be also regulating the tRNA ligase activity of the complex.

3.1. tRNA isolation from total RNA

As mentioned in Results section 2.4, total RNA from mouse hippocampi was obtained, and after checking its quality (see **Table 7**), sncRNAs and lRNAs were isolated using a commercial kit. As expected, the amount of lRNA and sncRNA positively correlated with the amount of total RNA in the samples (**Figure 32A-B**, respectively). The lRNA represented the 86.37% of the total RNA, whereas the sncRNA represented only the 13.63% of all RNA amount. Importantly, no differences in these proportions were detected between experimental groups (**Figure 32C**). As aforementioned, the lRNA was used for RT-qPCR (see **Figure 31**) while the sncRNA was used for tRNA isolation. Briefly, sncRNA samples were resolved in a urea-polyacrylamide gel and, using UV shadowing, the 60-100 nt fractions (containing both pre-tRNAs and mature tRNAs, but tiny amounts of other sncRNAs such as rRNA or small nucleolar RNAs (snoRNAs)) were excised (more information in Methodology section 5.1). The tRNA-enriched fraction represented the 38.04% of the total amount of these sncRNAs (**Figure 32D**). Overall, this RNA characterization indicates that most of the RNA of the mouse hippocampus represents lRNA, and that approximately a third of the sncRNAs are precursor or mature tRNAs.

Then, part of the tRNA-enriched fraction was used to perform Hydro-tRNA-seq, a sequencing protocol specifically designed for pre-tRNA and mature tRNA detection and quantification [140]. This technique overcomes the high number of modifications found in tRNA by hydrolyzing it into more manageable fragments. Thus, during the sequencing process, the tRNA fractions were hydrolyzed, dephosphorylated, and rephosphorylated to be able to generate the cDNA library (see Methodology section 5.2 for more information). Analysis of the sequencing data was performed by the Bioinformatics Unit of the CRG, using the tRAX software, who sent us the curated data for further analyses.

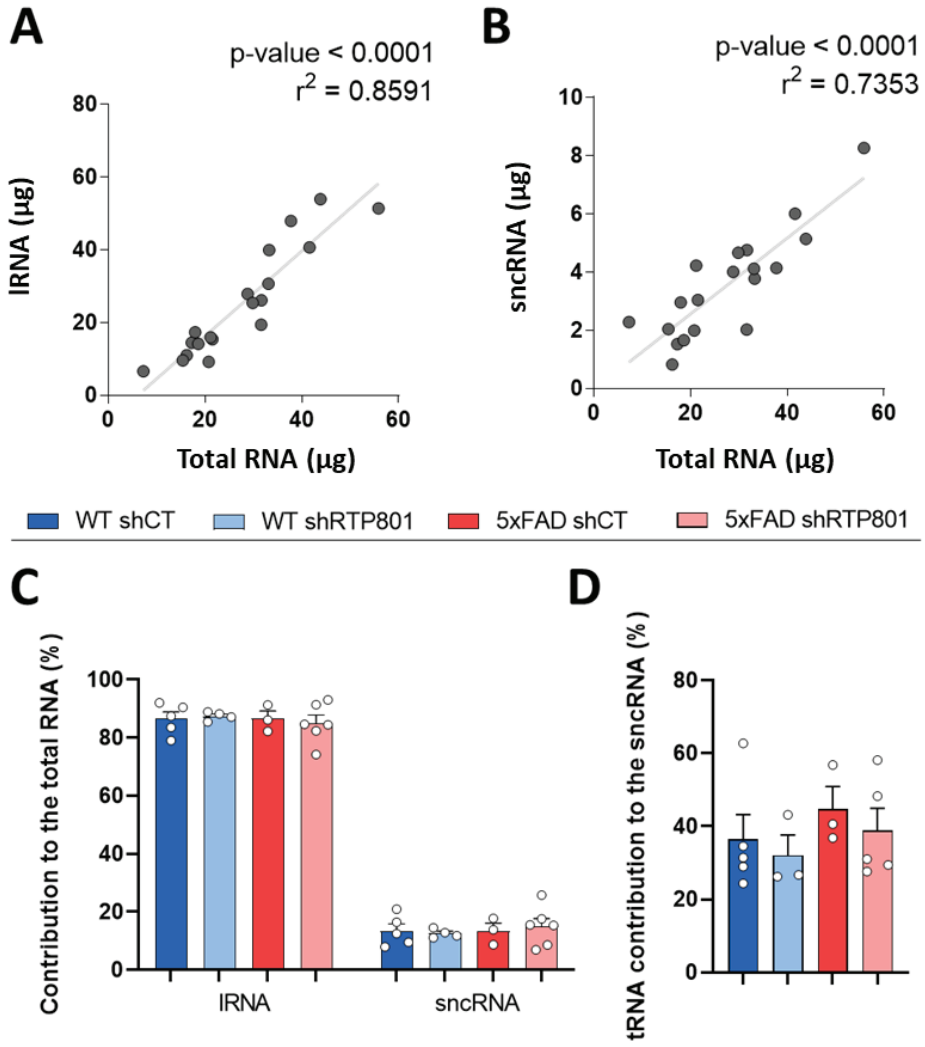

Figure 32. RNA characterization in the mouse hippocampus. (A-B) Pearson's correlation analyses comparing the initial amount of total RNA obtained from the mouse hippocampal samples with the amount of lRNA **(A)** or sncRNA **(B)** obtained after the usage of the commercial kit. **(C)** Contribution (in percentage) of the lRNA and the sncRNA to the total RNA. (**D)** Contribution (in percentage) of the tRNA to the sncRNA. Data are means ± SEM. Each value represents one animal. In panels **(C-D)** two-way ANOVA with Tukey's post hoc test was performed.

3.2. Characterization of the sequencing data

We first assessed the correct sequencing of our samples by characterizing the obtained reads. All samples passed the quality metrics generated by tRAX (**Table 8**), which demonstrates that the sequencing was successful.

Quality metric	Reference value	Obtained value (mean)
Sequencing read merging rate (%)	> 60	66.52
tRNA reads (%)	> 50	63.40
rRNA reads (%)	< 35	2.04
Reads mapping unannotated regions (%)	< 35	12.99
Read length average (nt)	< 40	39.78
Reads between 15 and 50 nt (%)	≥ 70	86.36
tRNAs with more than 20 reads (%)	≥ 50	97.7

Table 8. Quality assessment guidelines generated by tRAX.

Then, we characterized the types of sncRNAs present in our samples (**Figure 33**). We found that, on average, most of our merged reads mapped mature (51.8%) or precursor tRNAs (11.6%), in consonance with the bibliography [140]. Interestingly, mt-tRNAs represented an additional 15.3% of the reads. Other sncRNAs such as rRNAs or snoRNAs were also present but in a much lesser extent, as anticipated. No significant differences in the proportion of RNA types were found when animals were compared, either individually (**Figure 33A**) or grouped per condition (**Figure 33B**). These results indicate that the RNA fraction isolated from the urea-polyacrylamide gel was indeed enriched in tRNAs, either mature, precursor, or mitochondrial, and that it contained very low amounts of other undesired sncRNAs.

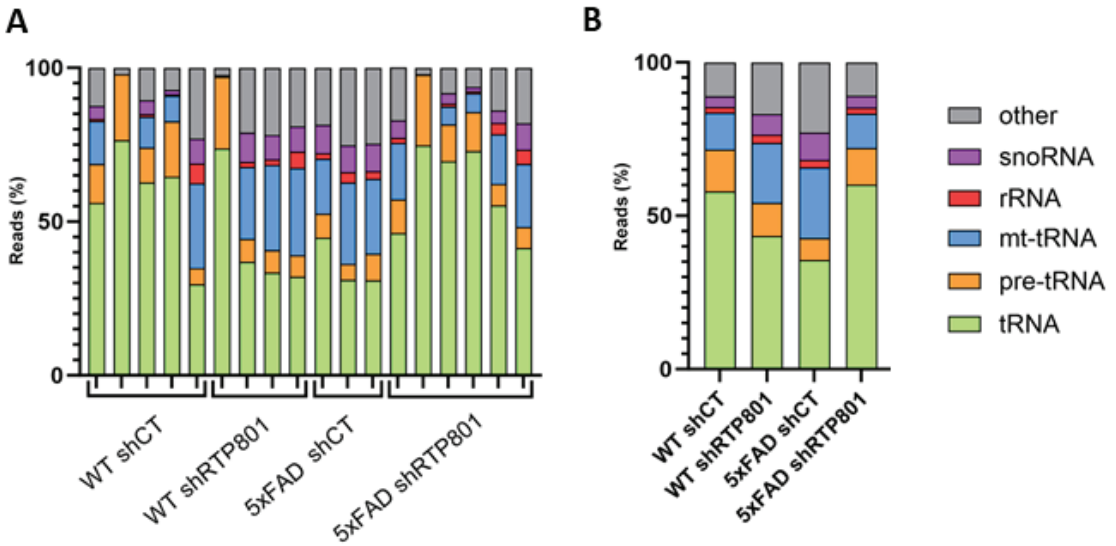

Figure 33. Characterization of Hydro-tRNA-seq merged reads. **(A-B)** Read distribution of the detected sncRNA types, individually **(A)** and grouped per condition **(B)**. Most of the reads corresponded to mature tRNAs, but pre-tRNAs and mt-tRNAs were also present. rRNAs and snoRNAs were detected in a much lesser extent, as expected. In panel **(A)** two-way ANOVA with Tukey's post hoc test was performed for each sncRNA type, but no significant differences were detected.

3.3. Specific accumulation of intron-containing pre-tRNAs in the hippocampus of 5xFAD mice

After confirming the favorable outcome of the sequencing, we compared the pool of precursor and mature tRNAs between WT shCT and 5xFAD shCT mice, classifying the tRNA species by their anticodon (**Figure 34**). Strikingly, all pre-tRNA isodecoders with intron-containing species (R/arginine-TCT, I/isoleucine-TAT, L/leucine-CAA, and Y/tyrosine-GTA) were significantly accumulated in 5xFAD mice (**Figure 34A**, indicated with a red square in the Y axis). This accumulation, however, was not observed as for the mature tRNAs (**Figure 34B**). Significant differences were also found in the levels of precursor tRNA-Ala-TGC, tRNA-Asp-GTC, and tRNA-Sec-TCA, as well as in mature tRNA-Asp-GTC, tRNA-Ile-AAT, and tRNA-Ser-CGA. Altogether, these results suggest that 5xFAD mice specifically accumulate intron-containing pre-tRNAs, which might be due to an impairment (or a slowdown) in tRNA splicing (either in the cleavage of the intron or in the tRNA halves ligation).

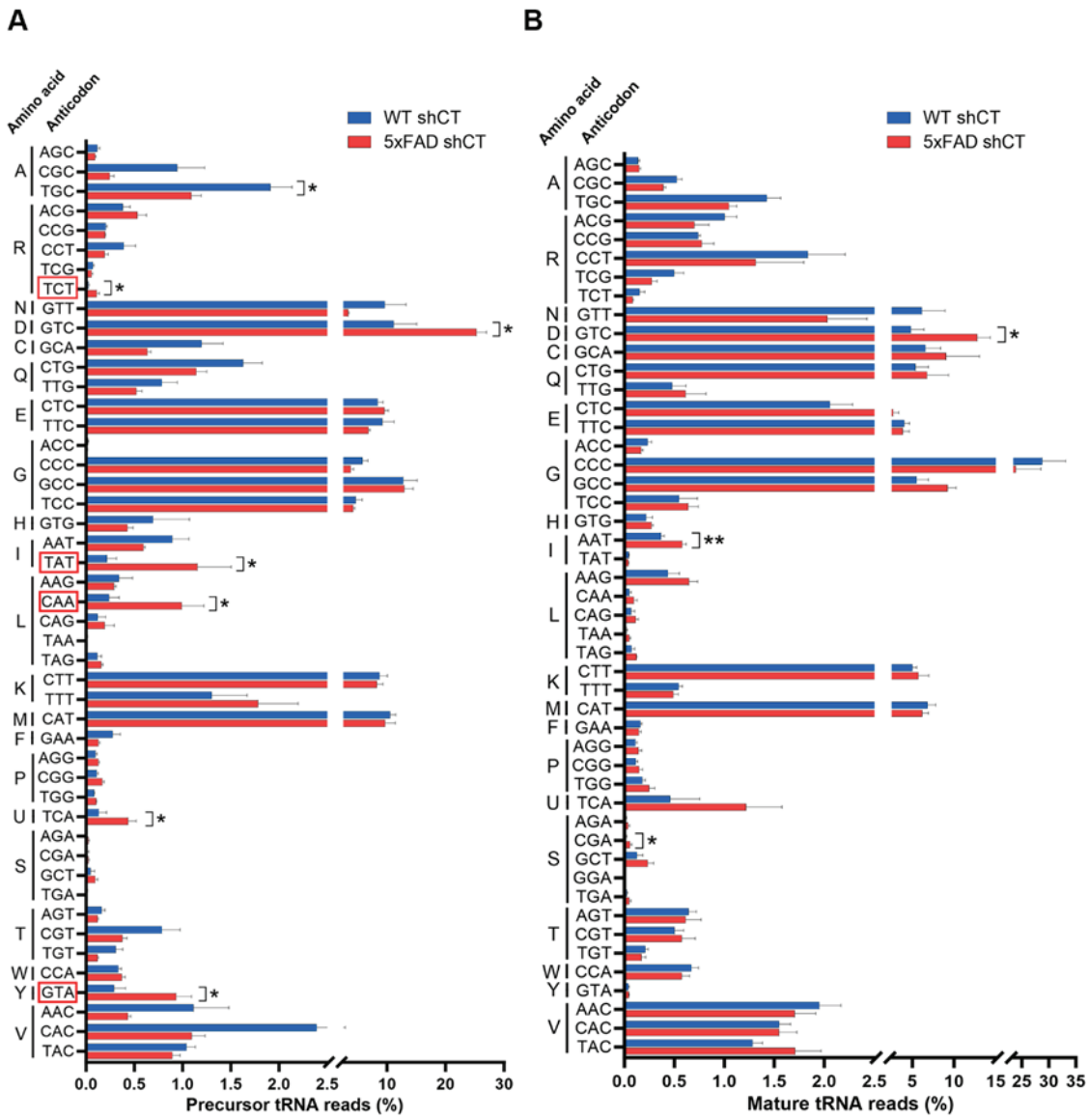

Figure 34. 5xFAD mice accumulate intron-containing pre-tRNAs. tRNAs were isolated from 7-month-old WT and 5xFAD mice and sequenced by Hydro-tRNA-seq. Reads mapping the 5' leader, the 3' trailer, or the intron were classified as pre-tRNA. The percentage of normalized counts for precursor **(A)** and mature **(B)** tRNA is depicted, classified by amino acid and anticodon. The red rectangles framing certain anticodons indicate that at least one of those pre-tRNA isodecoders has an intron. Data are means ± SEM. In all comparisons Student's t-test was performed. *p < 0.05 and **p < 0.01.

In accordance with the results obtained for the mature tRNAs, no differences were detected when we compared the abundance of the mt-tRNA species between WT shCT and 5xFAD shCT mice (**Figure 35**), suggesting that the alteration in the pool of tRNAs in 5xFAD mice might be limited to a very specific and well-defined subpopulation of tRNAs, namely those with intron.

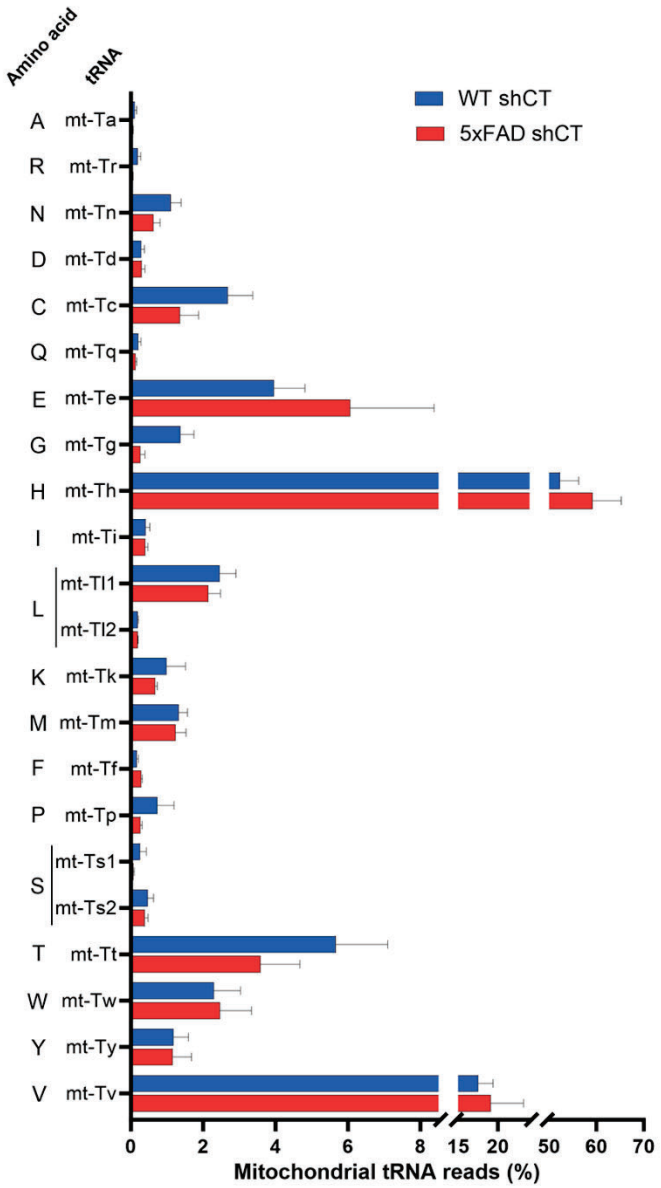

Figure 35. The pool of mt-tRNAs is not altered in the hippocampus of 5xFAD mice. tRNAs were isolated from 7-month-old WT and 5xFAD mice and sequenced by Hydro-tRNA-seq. The percentage of normalized counts for mt-tRNAs is depicted, classified by amino acid. Data are means ± SEM. In all comparisons Student's t-test was performed.

3.4. RTP801 silencing in hippocampal neurons prevents the accumulation of intron-containing pre-tRNAs in 5xFAD mice

So far, our results suggested that RTP801 could be inhibiting the ligase activity of the tRNA-LC. Hence, to test this observation *in vivo*, and having observed that 5xFAD mice have significantly higher levels of intron-containing pre-tRNA isodecoders in the hippocampus, we investigated whether the silencing of RTP801 could prevent this abnormal accumulation of pre-tRNAs. Thus, within the four isodecoder families that have pre-tRNAs with intron (R/arginine-TCT,

I/isoleucine-TAT, L/leucine-CAA, and Y/tyrosine-GTA), we compared the proportion of reads that mapped intron-containing pre-tRNA species between the four experimental groups (**Figure 36A-D**). We also assessed the abundance of other pre-tRNA species without intron (either isodecoders, isoacceptors, or related species) as negative controls (marked in red in the X axis). Additional information about the murine pre-tRNAs that contain intron can be found in **Table 9**. As observed in **Figure 35A**, virtually all intron-containing pre-tRNAs accumulate in 5xFAD mice. Remarkably, this accumulation is most of the times prevented when RTP801 is silenced in hippocampal neurons. For instance, both precursor tRNA-Arg-TCT-2-1 and tRNA-Leu-CAA-2-1 are significantly increased in 5xFAD animals and RTP801 downregulation prevents this aberrant accumulation. Notably, this pattern is not found in those pre-tRNAs without intron. Overall, these data show that the high levels of RTP801 found in 5xFAD mice could be involved in the specific accumulation of intron-containing pre-tRNAs, which is prevented by RTP801 neuronal silencing. Indeed, taking into consideration the previous results from this thesis, RTP801 seems to be inhibiting the activity of the tRNA-LC.

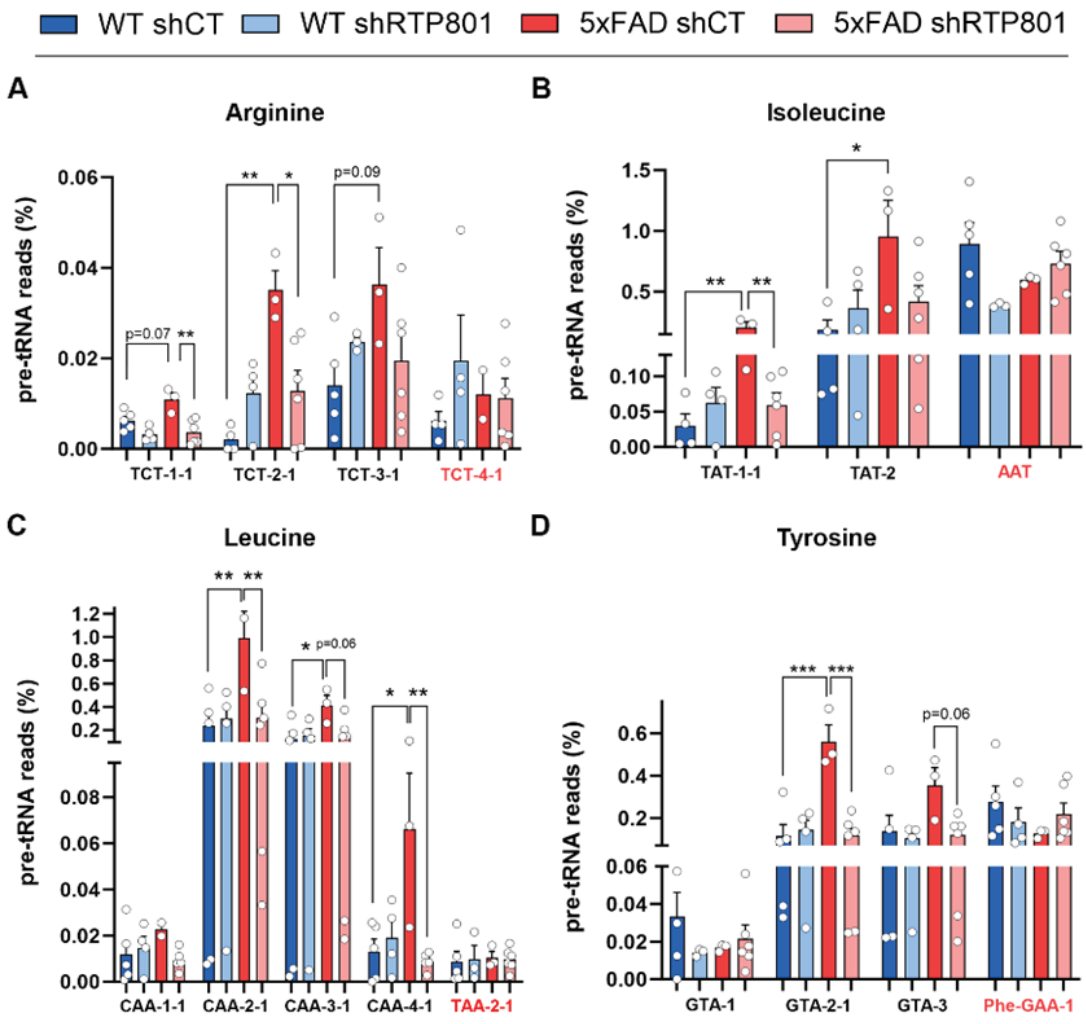

Figure 36. RTP801 downregulation in hippocampal neurons prevents the accumulation of intron-containing pre-tRNAs in 5xFAD mice. The percentage of normalized counts for pre-tRNA is depicted, classified by amino acid and anticodon. Different pre-tRNA species within an isodecoder family are represented. Pre-tRNA species in red do not have an intron and are included as a control. Since all tyrosine-accepting pre-tRNAs have intron, pre-tRNA-Phe-GAA-1 (also accepts an aromatic amino acid) was included as a control. In the cases where the number of reads was very scant, different tRNAs species were combined for the representation (for instance, pre-tRNA-Tyr-GTA-1-1/1-2/1-3/1-4/1-5 were grouped under the label Tyr-GTA-1). Relative expression of pre-tRNA-Arg-TCT **(A)**, pre-tRNA-Ile-TAT **(B)**, pre-tRNA-Leu-CAA **(C)**, and pre-tRNA-Tyr-GTA **(D)**. Data are means ± SEM. In all comparisons two-way ANOVA with Tukey's post hoc test was performed. Each value represents one animal. *p < 0.05, **p < 0.01, and ***p < 0.001.

tRNAs with intron	
Arg-TCT-1-1	Ile-TAT-2-3
Arg-TCT-2-1	Tyr-GTA-1-1
Arg-TCT-3-1	Tyr-GTA-1-2
Arg-TCT-5-1	Tyr-GTA-1-3
Leu-CAA-1-1	Tyr-GTA-1-4
Leu-CAA-2-1	Tyr-GTA-1-5
Leu-CAA-3-1	Tyr-GTA-2-1
Leu-CAA-4-1	Tyr-GTA-3-1
Ile-TAT-1-1	Tyr-GTA-3-2
Ile-TAT-2-1	Tyr-GTA-4-1
Ile-TAT-2-2	Tyr-GTA-5-1

Table 9. List of the 22 tRNAs with intron found in mice according to GtRNAdb. tRNAs in red were not detected by Hydro-tRNA-seq.

Considering that intron-containing pre-tRNAs accumulate in 5xFAD mice, we investigated whether this event was translated into a reduction of the levels of their mature forms. To check this, we performed the same analysis as in **Figure 36**, but on mature tRNAs (**Figure 37A-D**). Unexpectedly, we found no significant differences between conditions for any intron-containing tRNA.

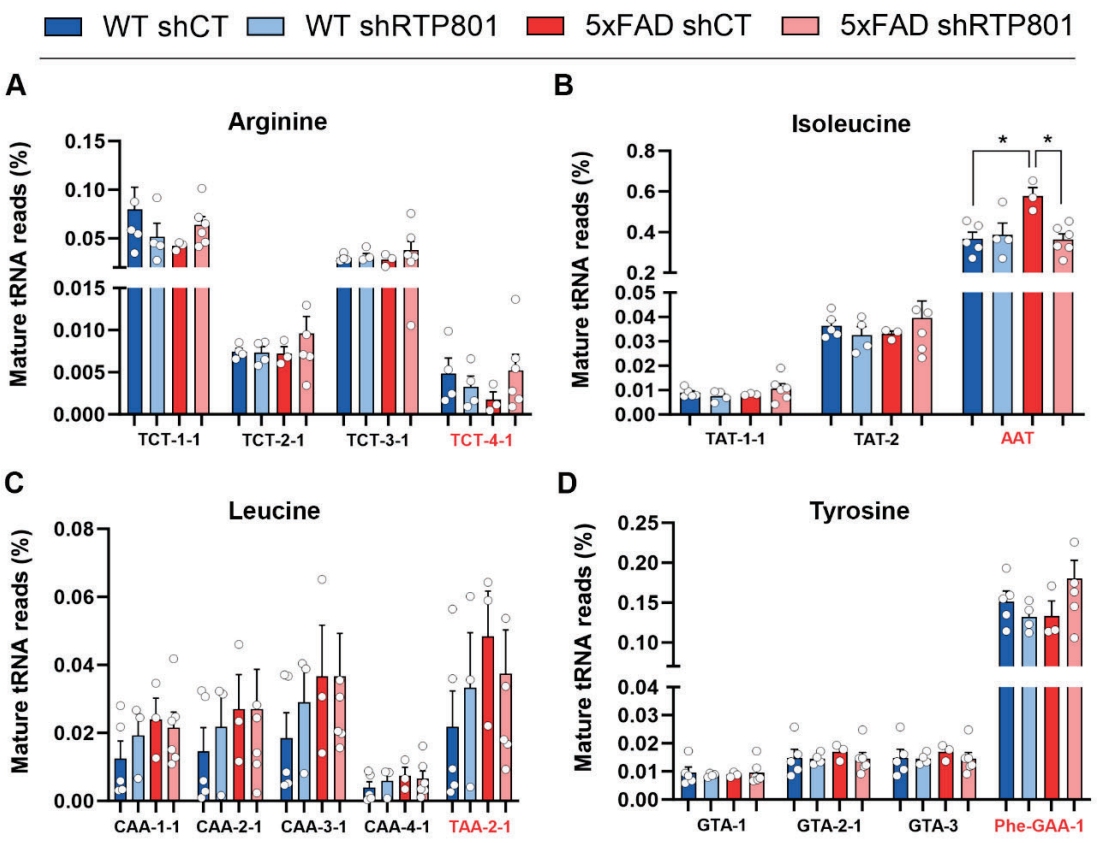

Figure 37. RTP801 downregulation in hippocampal neurons does not affect the pool of mature tRNAs in 5xFAD mice. The percentage of normalized counts for mature tRNA is depicted, classified by amino acid and anticodon. Different tRNA species within an isodecoder family are represented. tRNA species in red do not have an intron (on its immature form) and are included as a control. Since all tyrosine-accepting pre-tRNAs have intron, tRNA-Phe-GAA-1 (also accepts an aromatic amino acid) was included as a control. Relative expression of tRNA-Arg-TCT **(A)**, tRNA-Ile-TAT **(B)**, tRNA-Leu-CAA **(C)**, and tRNA-Tyr-GTA **(D)**. Data are means ± SEM. In all comparisons two-way ANOVA with Tukey's post hoc test was performed. Each value represents one animal. *p < 0.05.

Nonetheless, we observed increased levels of tRNA-Ile-AAT in 5xFAD shCT mice (as described in **Figure 34B**), which were prevented by RTP801 silencing. These results demonstrate that the abnormal pool of intron-containing pre-tRNAs found in 5xFAD mice does not lead to an altered pool of mature tRNAs.

3.5. The tRNA-enriched fraction derived from 5xFAD mice increases dendrite branching in hippocampal cultured neurons

In the 5xFAD mouse model, silencing RTP801 in hippocampal neurons prevents the appearance of the cognitive deficits and normalizes the inflammatory response [114]. However, nothing is known about how the accumulation of intron-containing pre-tRNAs can contribute to these

pathologic features observed in mice. To elucidate whether these pre-tRNAs contribute to neuron degeneration, we turned to *in vitro* models, assuming the limitations and the complexity of the approach. Hence, we used the 60-100 nucleotide-sized, tRNA-enriched fraction from each experimental group to treat mouse hippocampal neurons and assess toxicity and dendrite arborization (**Figure 38A-F**) (see Methodology section 5.1 and Results section 3.1 for more information about tRNA isolation; see **Figure 33** for more information about the RNA composition of the isolated fractions). As aforementioned, this fraction was enriched in tRNAs, containing an average of 51.8% of mature tRNA, 11.6% of pre-tRNA, and 15.3% of mt-tRNA. Since we did not find major differences in the pools of mature tRNA (**Figure 34B**) or mt-tRNA (**Figure 35**) between WT shCT and 5xFAD shCT mice, we assumed that any differential effect on neuronal cultures would be mostly due by the altered pre-tRNA pools.

Thus, mouse hippocampal cultured neurons were transfected with 100 ng of tRNA-enriched sncRNA for 30 h. Then, cultures were fixed and immunostained with antibodies against MAP2 and ClvCas3, and nuclei were stained with Hoechst 33342 (**Figure 38A**). Neuronal nuclei ($MAP2^+$) were classified into viable, condensed, or fragmented (**Figure 38B**) as previously described [86] using a machine learning pipeline that showed an accuracy of 97.62% (**Figure 38C**).

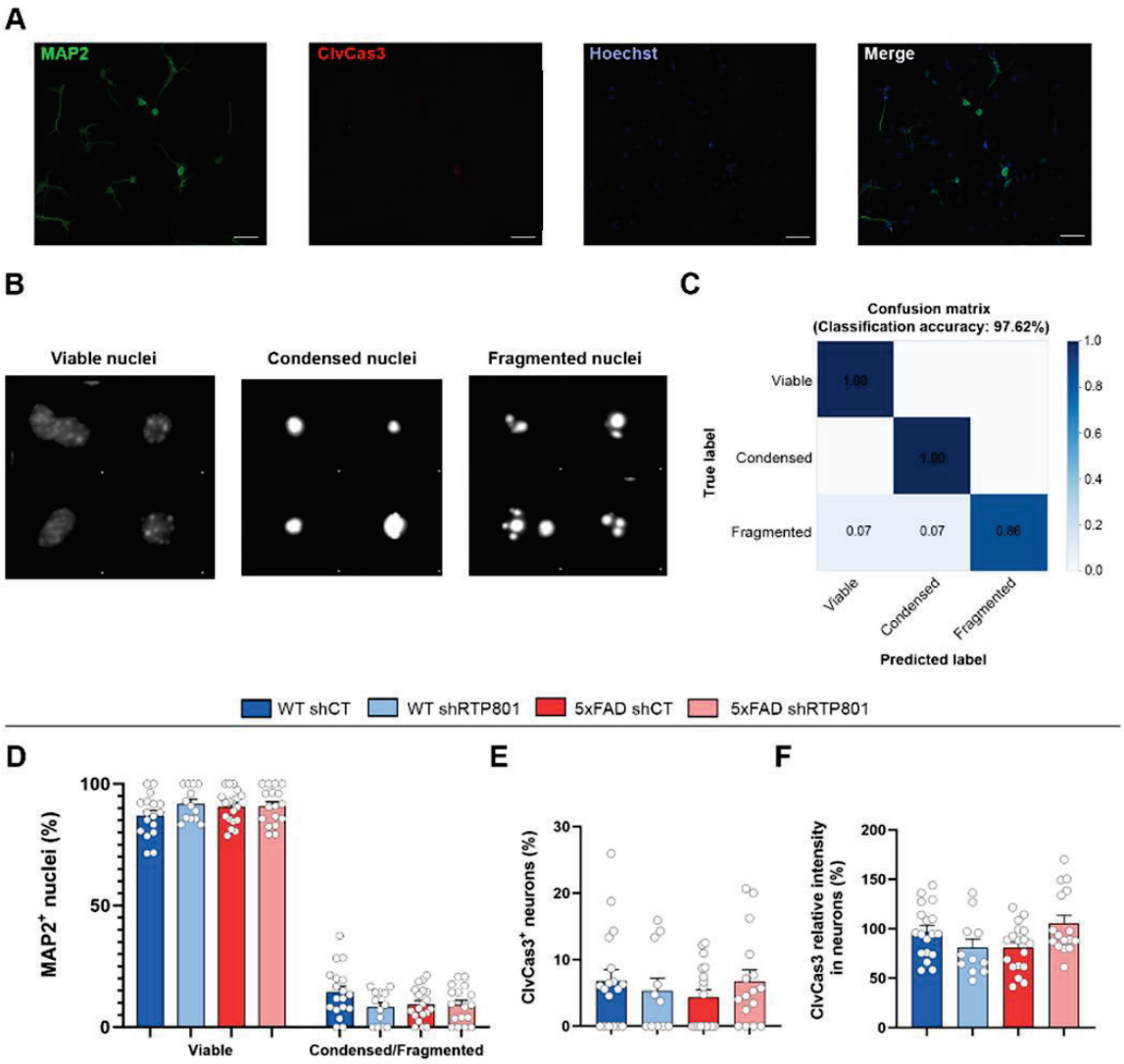

Figure 38. The tRNA-enriched fraction from 5xFAD mice is not toxic to cultured hippocampal neurons. **(A)** Representative images of tRNA-transfected mouse hippocampal neurons stained with MAP2, ClvCas3, and Hoechst 33342. **(B)** Classification of neuronal nuclei into viable, condensed, or fragmented with Cell Profiler Analyst. **(C)** Confusion matrix for the nuclei classification in **(B)**. **(D)** Proportion of viable and condensed/fragmented neuronal nuclei. **(E)** Percentage of ClvCas3$^+$ neurons. **(F)** ClvCas3 mean intensity in neurons. Scale bar = 50 µm. Data are means ± SEM. In all comparisons two-way ANOVA with Tukey's post hoc test was performed. Each value represents the mean of one microscope image, obtained from 2 independent experiments with technical replicates.

We found that any of the tRNA-enriched fractions affected neuron survival, assessed by the proportion of viable nuclei, which accounted for 90.03% of all neuronal nuclei (**Figure 38D**). Moreover, the proportion of ClvCas3$^+$ neurons (5.78% of them) was stable between conditions (**Figure 38E**) as well as the mean intensity of ClvCas3 immunostaining in neurons (**Figure 38F**).

Once observed that the tRNA-enriched fractions had no differential effect on neuron viability, we evaluated neuron arborization (**Figure 39A-F**). To do so, we obtained the neuron skeleton with Cell Profiler software (**Figure 39A**), and we quantified the primary dendrites, intermediate branches, endpoints, and the total tree length (**Figure 39B**), as previously described [215]. Regarding the number of primary dendrites (those that arise from the neuronal soma), we saw no differences between conditions, with an average of 8.18 branches per neuron (**Figure 39C**). However, we found that the tRNA-enriched fraction obtained from 5xFAD shCT mice significantly increased the number of intermediate branches compared to the WT shCT-derived sncRNA. Additionally, this increase in branching was not observed when neurons were treated with the tRNA fraction derived from 5xFAD mice with neuronal RTP801 silencing (**Figure 39D**). As for the number of endpoints, it tended to augment in 5xFAD shCT-treated neurons, and RTP801 silencing in the source neurons significantly reduced it (**Figure 39E**). Because of these results, the total tree length of the cultured neurons showed an identic pattern; it increased when neurons were treated with 5xFAD shCT-derived tRNAs and RTP801 silencing significantly decreased it (**Figure 39F**).

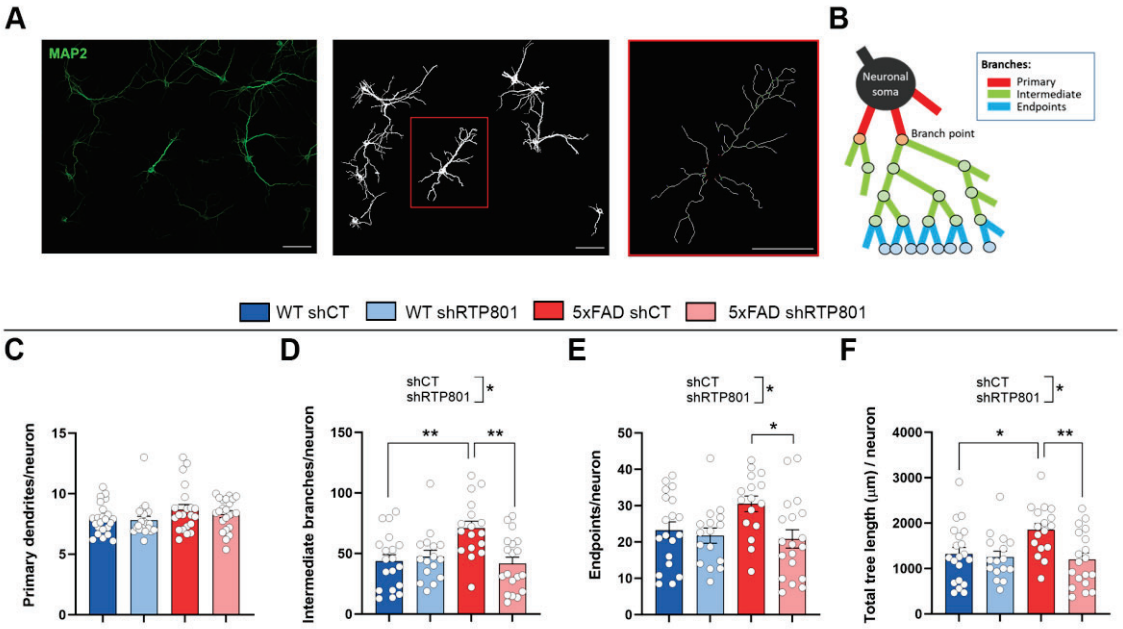

Figure 39. The tRNA-enriched fraction derived from 5xFAD shCT mice hippocampus increases cultured neuron arborization. (A) From MAP2 images, neurons not touching the borders of the image were identified as independent objects, and the neuron skeleton was obtained. **(B)** Schematic representation of the different types of branches found in a neuron (adapted from [215]). **(C-E)** Average number of primary dendrites **(C)**, intermediate branches **(D)**, and endpoints **(E)** per neuron. **(L)** Average total tree length (µm) per neuron. Scale bar = 50 µm. Data are means ± SEM. In all comparisons two-way ANOVA

with Tukey's post hoc test was performed. Each value represents the mean of one microscope image, obtained from 2 independent experiments with technical replicates. *$p < 0.05$ and **$p < 0.01$.

Overall, these data indicate that the 60-100 nt sncRNAs isolated from 5xFAD shCT (which are mainly constituted by mature and precursor tRNAs) induce changes in the branching of cultured hippocampal neurons, and this effect depends on the levels of RTP801. Considering that we found no major changes in the pools of mature and mitochondrial tRNAs between WT shCT and 5xFAD shCT hippocampus, this effect might be due to the differential pool of pre-tRNAs found in 5xFAD mice. However, experiments to elucidate the exact mechanisms for the abnormal effects of intron-containing pre-tRNAs and how this is translated to neurodegeneration are warranted.

DISCUSSION

As the global life expectancy increases, the prevalence of AD is continuously growing, and it is expected to be 2-4 times higher than now in 2050 [17]. The complex pathophysiology of AD complicates the development of disease-modifying therapies, and in fact, the only existing treatments are focused on alleviating the symptomatology. Thus, the comprehension of its pathophysiology is essential for the development of efficient curing therapies.

RTP801 is a stress-responsive protein whose levels are increased in the brains of patients with neurodegenerative diseases such as AD [114], HD [73], [118], or PD [71]. The main described function of RTP801 is to negatively regulate the mTOR/Akt pathway [71], [96], [97], but our group has recently described its involvement in transneuronal toxicity via EVs [86], and the modulation of neuroinflammation [114], [118]. In fact, silencing RTP801 in the hippocampus of 5xFAD [114] and R6/1 mice [118] prevents cognitive impairment and neuroinflammation. Hence, RTP801 seems a promising target for the treatment of neurodegenerative diseases.

Interestingly, preliminary MS results from our group [125] showed that RTP801 interacted with DDX1 and HSPC117, two members of the tRNA-LC [126]. This complex participates in tRNA splicing [126] and the unconventional splicing of *XBP1* mRNA [191], and thus, it is essential to regulate the cellular tRNA and mRNA pools [223]. Precisely, an appropriate composition of these pools is crucial for a correct protein synthesis. Considering that in recent years an altered translation has been proposed as a common pathological mechanism in many neurodegenerative diseases [227], the main objective of this thesis was to study the role of RTP801 over the tRNA-LC, in health and in the context of AD.

The present work shows that RTP801 interacts with three members of the tRNA-LC, specifically with HSPC117, DDX1, and CGI-99. However, it does not regulate their protein levels, neither in rat cortical neurons nor in HEK293 cells. Thus, RTP801 does not seem to play an important role in the architecture or the stability of the members of the complex, although it should be further investigated. We also found that RTP801 downregulation in HEK293 cells promoted the splicing of *XBP1* mRNA, while RTP801 overexpression inhibited it. Similarly, we found that XBP1 splicing is impaired in the hippocampus of AD patients, where RTP801 levels are elevated. Remarkably, *Xbp1* splicing is also modulated by RTP801 in the 5xFAD mice hippocampus, as well as the expression of *Bdnf*. These data suggest that RTP801 inhibits the splicing of *XBP1*, which is most probably due to its interaction with the tRNA-LC. Finally, we found that 5xFAD mice accumulate intron-containing pre-tRNAs in the hippocampus, and RTP801 genetic silencing in hippocampal neurons prevents this phenotype.

Overall, RTP801 seems to be a novel modulator of the activity of the tRNA-LC. In the context of AD, the high levels of RTP801 might be dysregulating the activity of the complex, leading to altered pre-tRNA and mRNA pools. The fact that RTP801 has also been described as a modulator of neuroinflammation [114], [118] and EVs toxicity [86] shows that it is a protein involved in several key cellular processes. Hence, RTP801 inhibition in hippocampal neurons might be an efficient therapeutic strategy to modulate different processes that are altered in AD.

1. RTP801 interacts with members of the tRNA-LC without affecting their protein levels

Until the discovery of the tRNA-LC in 2011 [126], it was not clear how the human 3'-phosphate ligation pathway worked. However, since then, several laboratories have studied both the architecture and the activity of the complex. Nonetheless, we are far from fully comprehending its regulation. Here, we confirmed preliminary results indicating that RTP801 interacted with members of the tRNA-LC. Moreover, we found that RTP801 protein levels did not affect the protein levels of DDX1, HSPC117, or CGI-99 nor their expression.

As aforementioned, in previous unpublished results from our group, endogenous RTP801 was immunoprecipitated in DSP-treated rat primary cortical neurons, and its interactors were studied by MS. Among the identified proteins were HSPC117 and DDX1, two members of the tRNA-LC. With this background, we first performed a GO biological process enrichment analysis of the interactors to check whether a particular process was shared between interactors. Interestingly, we found that 16 out of the 43 proteins were RNA binding proteins (including DDX1 and HSPC117), suggesting that RTP801 might be involved in RNA metabolism. Interestingly, Schwenzer *et al.* [161] described that oxidative stress triggered tRNA retrograde transport via the PERK-RTP801-mTOR axis, and Tajik *et al.* [228] recently reported that nuclear overexpression of RTP801 was associated with pancreatic tumor aggressiveness, but the exact mechanism by which this occurred (RTP801 binding to RNA, DNA, or transcription factors, among other potential mechanisms) was not described. However, to the best of our knowledge, any work has described a role of RTP801 in RNA metabolism to date.

To confirm the interaction of RTP801 with DDX1 and HSPC117, we immunoprecipitated endogenous RTP801 in DSP-treated HEK293 cells and detected them by WB. As expected, we were able to detect both. In addition, we detected CGI-99, another member of the complex. Unfortunately, we could not detect FAM98B (which is also part of the complex), meaning that the antibody was not as specific as expected or that the levels of this protein in HEK293 cells are under the limit of detection by WB. Since ASW is not necessary for the assembly of the complex [154], its presence in the immunoprecipitate was not assessed. Hence, our results point out that RTP801 interaction with the tRNA-LC is a conserved phenomenon between species and cell types, suggesting that it might have an essential function.

The tRNA-LC was described by Popow *et al.* in 2011 as a pentameric complex [126]. In their work, they detected by immunoaffinity chromatography a complex formed by HSPC117, DDX1, CGI-99, ASW, and FAM98B. Interestingly, these proteins were also detected when they performed

MS of a fraction enriched for 3'-phosphate RNA ligase activity, and when they studied HSPC117 interactors by MS. In recent years, new regulators of the activity of the complex (both competitors and cofactors) have been described (reviewed in [146]). For instance, in 2014, Popow *et al.* [147] identified that archease was required for full activity of the complex. Similarly, in 2021, the oxidoreductase PYROXD1 was found to interact with the complex and to protect HSPC117 against oxidation [149]. The fact that these proteins were not detected in the first MS experiments of Popow *et al.* [126] suggests that they form weak, transient, or context-dependent interactions with the complex. In line with this, we hypothesize that RTP801 must be an elusive interactor of the tRNA-LC, mostly due to its short half-life (2-5 minutes) [91], [92]. Indeed, this is corroborated by the fact that we were only able to detect RTP801 interacting with the complex when we treated our cell cultures with DSP, a chemical cross-linker.

Regarding the structure of the human complex, Kroupova *et al.* [154] presented a biochemical analysis of the inter-subunit interactions along with crystal structures of HSPC117 and the N-terminal domain of CGI-99. They found that the core of the complex is formed by HSPC117 and the C-terminal alpha-helical regions of DDX1, CGI-99, and FAM98B. While these four members were essential for the integrity of the complex, ASW was not. Therefore, RTP801 might be interacting with the core of the complex since we detected interaction with DDX1, HSPC117 and CGI-99. Conversely, RTP801 could, for instance, be interacting with the N-terminal region of DDX1, and not be in direct contact with HSPC117 or CGI-99. In that case, the detection of HSPC117 and CGI-99 in our immunoprecipitation experiments would have been an indirect finding, due to their interaction with DDX1. Thus, more biochemical and bioinformatic analyses are required to define the exact regions of interaction between these proteins.

In this thesis, we also studied the effect of RTP801 levels over the protein stability of DDX1, HSPC117, and CGI-99. We found that RTP801 downregulation did not affect their protein levels, neither in rat cortical neurons nor in HEK293 cells, the two cellular models where we had described their interaction. Similarly, when we silenced RTP801, we did not observe changes in the mRNA levels of *DDX1* or *RTCB*, which suggests that RTP801 does not regulate their transcription either. On the other way around, we explored whether HSPC117 and DDX1 could be modulating the protein levels of RTP801. We found that DDX1 downregulation induced a significant reduction in the protein levels of RTP801. In the same line, HSPC117 downregulation decreased the protein levels of both RTP801 and DDX1. As for the mRNA, DDX1 knockdown had no effect on the expression of *DDIT4* or *RTCB.* Surprisingly, HSPC117 downregulation induced a significant increase in the mRNA levels of *DDX1*. These results are summarized in **Table 10**.

			Downregulation		
			RTP801	HSPC117	DDX1
Levels	RTP801	mRNA	↓	=	=
		Protein	↓	↓	↓
	HSPC117	mRNA	=	↓	=
		Protein	=	↓	=
	DDX1	mRNA	=	↑	↓
		Protein	=	↓	↓
	CGI-99	mRNA	?	?	?
		Protein	=	=	=

Table 10. Summary of the effect of RTP801, HSPC117, and DDX1 downregulation in HEK293 cells on the mRNA and protein levels of the other members of the tRNA-LC. The red arrow indicates a reduction in the levels, the equal sign indicates no significant changes, the green arrow represents an increase, and the interrogation mark indicates that it has not been evaluated.

Hence, both DDX1 and HSPC117 knockdowns lead to a reduction in RTP801 protein levels without affecting its mRNA levels, which indicates that their regulation over RTP801 is proteostatic. In other words, DDX1 and HSPC117 might protect RTP801 protein from degradation, or less probably, increase the translation efficiency for *DDIT4* mRNA. Indeed, RTP801 can be degraded via the ubiquitin-proteasomal system [65], [94], and in the lysosomes [90]. Surprisingly, HSPC117 silencing caused an unexpected increase in the mRNA levels of *DDX1*. More experiments are required to fully understand the biological significance of this observation, but we hypothesize that *DDX1* expression might be increased to compensate the reduction in its protein levels, possibly via miRNAs. Indeed, the bacterial orthologue of HSPC117, called RtcB, has been described to mediate the ligation between a miRNA and its target mRNA *in vitro* [229]. Therefore, we can speculate that HSPC117 might mediate the ligation of an unidentified miRNA to *DDX1* mRNA.

Overall, the data summarized in **Table 10** suggest that RTP801 is not affecting the stability of the complex, although more experiments are needed to confirm it. For instance, RTP801 could be mediating the disassembly of the complex without altering the protein levels of its components. As for HSPC117, our results show that it is the main regulator of the protein stability of the members of the complex. The silencing of DDX1, despite affecting the protein levels of RTP801, did not alter the protein levels of HSPC117 or CGI-99. This is in accordance with the work of Popow *et al.* [126], who showed that depletion of HSPC117 causes a decrease in the protein levels of DDX1 and FAM98B, whereas DDX1 silencing only mildly affects the protein levels of FAM98B. They also showed that CGI-99 silencing causes a reduction in the protein levels of all

the members of the complex studied but HSPC117. The same outcome regarding CGI-99 silencing was described by Pérez-González *et al.* [230]. **Table 11** summarizes the results obtained by our group, by Popow *et al.* [126], and by Pérez-González *et al.* [230] respecting the inter-subunit protein regulation.

		Downregulation					
		RTP801	**HSPC117**	**DDX1**	**CGI-99**	**FAM98B**	**ASW**
Protein levels	**RTP801**	↓ (1)	↓ (1)	↓ (1)	?	?	?
	HSPC117	= (1)	↓ (1,2)	= (1,2)	= (2,3)	= (2)	= (2)
	DDX1	= (1)	↓ (1,2)	↓ (1,2)	↓ (2,3)	= (2)	= (2)
	CGI-99	= (1)	= (1)	= (1)	↓ (2,3)	?	?
	FAM98B	?	↓ (2)	= (2)	↓ (2,3)	↓ (2)	= (2)

Table 11. Summary of the effect of the downregulation of the members of the tRNA-LC on their protein levels. The red arrow indicates a reduction in the protein levels, the equal sign indicates no changes, and the interrogation mark indicates that it has not been evaluated. The number (1) means that the results have been obtained from this thesis, the number (2) shows the results obtained by Popow *et al.* [126], and the (3) indicates that the data was obtained from Pérez-González *et al.* [230] The data in (2) and (3) was not objectively quantified, and thus the signs in the table have been added subjectively, taking into consideration the WB images provided.

These results, illustrated in the form of a table, clearly suggest that HSPC117, followed by CGI-99 and DDX1, is the main regulator of the stability of the members of the complex. On the other hand, RTP801, FAM98B, and ASW do not seem to mediate the stability of their partners. As previously mentioned, the core of the tRNA-LC is composed by HSPC117 and the alpha-helical termini of DDX1, CGI-99, and FAM98B [154]. We hypothesize that the assembly of this complex might mask polyubiquitination sites or proteolytic cleavage sites found in the alpha-helical ends of DDX1 and FAM98B. Similarly, the interaction between the complex and RTP801 might protect the latter from lysosomal degradation or from being targeted to the proteasome by the three E3 ligases known to polyubiquitinate it: NEDD4, Parkin, and the CUL4-DDB1-ROC1-β-TrCP E3 ligase complex [90], [93], [95]. Thus, depletion of HSPC117 (and depletion of DDX1 and CGI-99 in a lesser extent) would render the complex members accessible for degradation. On the other hand, downregulation of RTP801 and ASW, which are not required for the integrity of the complex [126], [154], does not have any repercussion on the protein levels of the other members.

Overall, our results demonstrate that the stress-responsive protein RTP801 interacts with HSPC117, DDX1, and CGI-99, but does not affect their protein or mRNA levels. On the contrary,

HSPC117 appears as the master regulator of the stability of the complex. Our proposed model according to the results obtained in the Aim 1 of this thesis is illustrated in **Figure 40**.

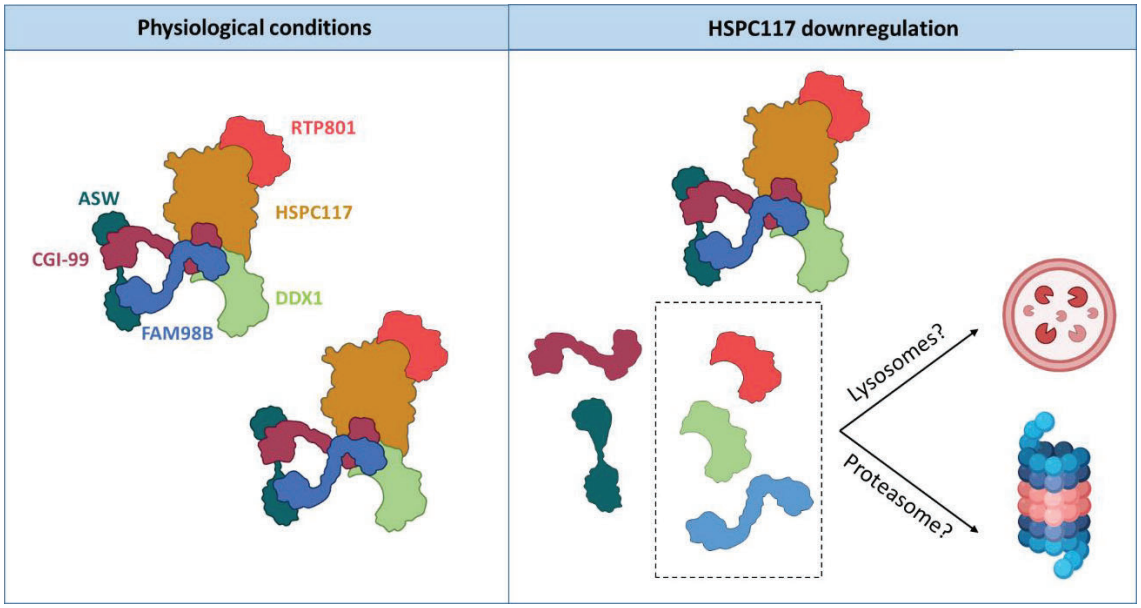

Figure 40. Proposed model for the tRNA-LC inter-subunit dynamics. According to the results obtained in the Aim 1 of this thesis, RTP801 co-immunoprecipitates with HSPC117, DDX1, and CGI-99, three members of the tRNA-LC. HSPC117 downregulation might cause the disassembly of the complex, which might lead to the protein degradation of RTP801 and DDX1 (and FAM98B). Figure created with *Biorender.com*.

2. RTP801 inhibits the splicing of *XBP1*

During the UPR, the ER-resident transmembrane protein IRE1 cleaves *XBP1u* mRNA, generating two exons and freeing a 26-nucleotide intron. This splicing event was first reported in yeast in 1997, [231] but the mammalian pathway was not described until 2001 [232] However, the mammalian ligase responsible for the ligation of *XBP1s* exons remained elusive until 2014, when three different groups simultaneously identified HSPC117/RtcB [191], [233], [234] (reviewed in [235]). The ligated *XBP1s* mRNA is translated, producing a transcription factor necessary for the restoration of ER homeostasis. Here, we found that RTP801 inhibits the splicing of *XBP1* both *in vitro* and *in vivo*. Moreover, we describe an impairment in XBP1 splicing in the hippocampus of AD patients, where RTP801 is upregulated.

First, we started by assessing the effect of HSPC117 downregulation over *XBP1* splicing. In HEK293 cells, we observed that a 50% knockdown of HPSC117 did not affect the mRNA levels of *XBP1s* nor *XBP1u*, resulting in an unaltered *XBP1s/XBP1u* ratio, which is commonly used as a splicing readout. These results agree with those of Iwawaki *et al.* [225], who used double-stranded RNA to knockdown HSPC117 in HeLa cells and saw no changes in the *XBP1s/XBP1u* ratio, assessed by qPCR. In line with this, Jurkin *et al.* [191] reported that depletion of HSPC117 alone in HeLa cells did not affect the splicing of *XBP1*. Similarly, depletion of its cofactor archease alone did not impair *XBP1* splicing either. Only when HSPC117 and archease were simultaneously knocked down, *XBP1* splicing was significantly decreased. Moreover, they found that a 50% reduction in the levels of HSPC117 in mouse plasma cells did not modify the splicing of *Xbp1*. Only when HSPC117 expression was fully abrogated, *Xbp1* splicing was significantly impaired. In the same line, Lu *et al.* [233]found that RtcB KO mouse embryonic stem cells showed a dramatic impairment in *Xbp1* splicing, and Kosmaczewski *et al.* [234] found that a total depletion of RtcB in *C. elegans* impaired xbp-1 splicing. All things considered, HSPC117 is necessary for *XBP1* ligation, and low levels of HSPC117 are sufficient to efficiently ligate *XBP1*, providing that archease is present to stimulate its enzymatic activity.

Then, we studied the influence of RTP801 on *XBP1* splicing *in vitro*, in HEK293 cells. We found that a 25% reduction in the levels of RTP801 was enough to increase the mRNA levels of *XBP1s* without affecting the levels of *XBP1u*, which led to an increased *XBP1s/XBP1u* ratio. In addition, RTP801 knockdown increased the mRNA levels of *SEC24D*, a target gene of XBP1s, but no changes were observed in the expression of *BDNF*, another transcriptional target. On the contrary, RTP801 overexpression had the opposite effect, inhibiting the splicing of *XBP1* mRNA, without having an impact on *SEC24D* or *BDNF* transcription. Overall, these findings present

RTP801 as an important inhibitor of *XBP1* splicing *in vitro*. Presumably, RTP801 inhibits *XBP1* splicing by interfering with the mRNA ligase activity of the tRNA-LC. However, our findings are not sufficient to undoubtedly make this statement. For instance, RTP801 could be inhibiting the cleavage of *XBP1u* instead of the ligation of *XBP1s* exons with identical outcome. Of course, the interaction of RTP801 with the ligase complex and the results that we obtained regarding tRNA splicing, clearly suggest that RTP801 is acting on the ligation step but more experiments are required to confirm it. One elegant way to solve this question would be to identify the region of RTP801 that interacts with the complex, mutate it, and check whether we obtain the same results.

Hence, here we present RTP801 as a competitor of the tRNA-LC. Another competitor of the complex is ANGEL2, as Pinto *et al.* reported in 2020 [152]. In their work, the *XBP1s/XBP1u* mRNA ratio was significantly increased in ANGEL2 KO cells compared to HEK293 cells. Conversely, overexpressing WT ANGEL2 in HEK293 cells decreased the *XBP1s/XBP1u* ratio. However, they nicely showed that overexpression of a mutant version of ANGEL2 had no effect on *XBP1* splicing. Similarly, Unlu *et al.* [150] presented CNP as an inhibitor of *XBP1* splicing in HEK293 cells. They described that shRNA-mediated CNP knockdown promoted *XBP1* splicing and the transcription of *SEC24D*, among other transcriptional targets. On the contrary, CNP upregulation inhibited *XBP1* splicing. Considering that we obtained almost identical results, RTP801 can be considered as a novel negative regulator of *XBP1* splicing, and a competitor of the tRNA-LC.

Interestingly, HSPC117 can be phosphorylated under stress conditions, which negatively affects *XBP1* mRNA splicing [236]. Specifically, HSPC117 is phosphorylated at Tyr306, which perturbs its interaction with IRE1, the enzyme that cleaves *XBP1u* mRNA, so that cleavage and ligation are uncoupled. As a result, *XBP1* splicing is diminished. On the contrary, protein tyrosine phosphatase 1B (PTP1B) dephosphorylates HSPC117, promoting *XBP1* splicing. Remarkably, RTP801 is a stress-induced protein that has not been associated to any enzymatic activity yet. Indeed, it is unknown the exact mechanism (or mechanisms) by which RTP801 mediates its biological functions, such as TSC1/2 activation, the mediation of the production and the cargo of EVs, or the modulation of neuroinflammation, among others. Regarding mTORC1 inactivation, Dennis *et al.* [108] reported that RTP801 KO cells had significantly higher levels of phosphorylated Akt at threonine 308 (p-Akt Thr308) than wild-type cells, and RTP801 overexpression decreased the levels of p-Akt Thr308. They also described that Akt co-immunoprecipitated with PP2A, a phosphatase that dephosphorylates Akt at Thr308, but this interaction was only observed in the presence of RTP801. Thus, they proposed that RTP801 interacted with PP2A and targeted it to Akt. Following this idea, we can hypothesize that RTP801

sequesters PTP1B and prevents the activating dephosphorylation of HSPC117. However, there are two arguments against this model. First, we did not detect PTP1B in our MS experiments (although it is true that we did not detect CGI-99 either, and we then found that co-immunoprecipitated with RTP801). Second, this model does not explain why RTP801 co-immunoprecipitates with HSPC117, DDX1, and CGI-99. A simple way to confirm or discard this hypothesis would be to evaluate whether p-HSPC117 Tyr306 is sensitive to RTP801 levels.

As aforementioned, we observed an increased transcription of *SEC24D* when RTP801 was downregulated in HEK293 cells, very similarly to the results found by Unlu *et al.* [150] when CNP was downregulated. Remarkably, SEC24D regulates the formation and the cargo of the vesicles in the secretory pathway [237]. Likewise, our group has recently described that RTP801 mediates the production and the content of EVs [86]. Vesicles from the secretory pathway can end up in multivesicular bodies [238], which fuse to the plasma membrane releasing EVs [239]. Hence, we speculate that RTP801 might indirectly mediate the cargo of EVs via SEC24D. In contrast, neither RTP801 downregulation nor overexpression affected the expression of *BDNF,* probably because HEK293 cells produce very low amounts of this neurotrophin.

An altered XBP1 pathway has been related with a variety of diseases, such as cardiovascular [62], [63], metabolic, and neurodegenerative diseases [64], as well as in cancer [65]. However, most of these findings were described in animal models, which do not perfectly reproduce the human pathophysiology. Therefore, here we explored the status of XBP1 splicing and the protein levels of the members of the tRNA-LC in human postmortem samples.

First, we confirmed the upregulation of RTP801 in the hippocampus of AD patients, a 2.5-fold increase in average, as we previously described [114]. The magnitude of RTP801 upregulation is higher than the one reported by Damjanac *et al.* [121] in lymphocytes, which suggests that RTP801 upregulation under stress conditions is more prominent in nervous system cells.

Then, we assessed the hippocampal protein levels of DDX1, HSPC117, and CGI-99, and found no significant differences between conditions. This is in line with the data of the Multi-'omics Atlas Project [240], an open resource with single-nuclei RNA-sequencing data from astrocyte and microglia nuclei isolated from non-affected individuals' and AD patients' brains. According to this database, the mean gene expression of *DDIT4* is increased in both the microglia and the astrocytes of AD patients, but the gene expression of *DDX1*, *RTCB* (coding gene for HSPC117), *RTRAF* (CGI-99), *FAM98B*, or *C2orf49* (ASW) does not appear to change between conditions. Nonetheless, increased levels of *RTCB* mRNA have been reported in the blood of AD patients [241]. Furthermore, Velásquez *et al.* [242] conducted proteomic analyses of AD patients' and

non-affected individuals' brains, and they found that DDX1 was significantly increased in AD. According to their proteomics data, no significant changes in the protein levels of HSPC117, FAM98B, or CGI-99 were detected. Unfortunately, neither ASW nor RTP801 were in the list of identified proteins. The results of Velásquez *et al.* [242] are in agreement with a bioinformatic analysis performed by Wang *et al.* [243] that predicted a key role of *DDX1* gene in the occurrence and development of AD. Surprisingly, a meta-analysis aimed to compare the genetic data from 32 gene expression datasets found that FAM98B was a differentially expressed gene in two of them, appearing in both as an upregulated transcript in AD [244]. Therefore, although we did not detect changes in the hippocampal protein levels of any of the members of the tRNA-LC between non-affected individuals and AD patients, increased levels of HSPC117, DDX1 and FAM98B might be observed in other brain regions or in other stages of the disease.

When we evaluated the status of XBP1 splicing, we found a drastic reduction in the protein levels of XBP1s in the hippocampus of AD patients, with no significant changes in the levels of XBP1u, which resulted in a significantly decreased XBP1s/XBP1u ratio. In line with our results, Reinhardt *et al.* [245] found a significant reduction in the splicing of *XBP1* in the frontal cortex of AD patients, and a tendency to decrease in the hippocampus that did not reach significance because of the very low sample size. Conversely, Hwan Lee *et al.* [246] described increased *XBP1* splicing in the temporal cortex of AD patients compared to age-matched controls. Indeed, it is speculated that XBP1 activation could happen at early time points in AD pathology followed by a reduction as the disease progresses (reviewed in Cissé *et al.* [247]).

In this work we also evaluated the PERK branch of the UPR, by studying the phosphorylation of eIF2α at serine 51 and the protein levels of ATF4. Interestingly, we found increased levels of p-eIF2α in AD patients' hippocampi, in accordance with previous results studying p-eIF2α in the cortex [248], [249], and hippocampus [250], [251] of AD patients (reviewed in Ohno *et al.* [252]). Nonetheless, we observed no differences in the protein levels of ATF4 between CT and AD patients. Considering that p-eIF2α promotes the translation of *ATF4* mRNA, we expected higher levels of ATF4 in AD patients' samples, as previously observed in their cortex [253]. However, despite not seeing differences in the protein levels of ATF4, its cellular sublocalization should be studied, since active ATF4 translocates to the nucleus [254]. Remarkably, ATF4 promotes the transcription of *DDIT4* [76], which might exacerbate ER stress via *XBP1s* inhibition, generating a positive feedback loop in the context of AD. Altogether, the observed increase in the levels of p-eIF2α suggests the presence of an active PERK branch in the hippocampus of AD patients, which contrasts with the impairment observed in XBP1 splicing. Thus, the drastic decrease in XBP1 splicing might be due to a localized defect in the splicing machinery rather than a general

deficiency of the UPR. We hypothesize that the upregulation of RTP801 in the hippocampus of AD patients might be specifically interfering with the activity of the tRNA-LC over *XBP1* splicing, which would contribute to the aggravation of AD pathology.

Interestingly, we also found that the protein levels of RTP801, XBP1s, and p-eIF2α Ser51 were very good predictors of the presence or absence of the disease, being RTP801 the best discriminator. Therefore, their levels in blood and cerebrospinal fluid must be further studied as potential biomarkers of AD. In fact, increased levels of *DDIT4* mRNA and RTP801 protein have already been described in blood cells of AD patients [121]. What is more, the blood mRNA levels of *DDIT4* were found to be significantly increased in AD patients, were good classifiers of the presence or absence of AD (AUC = 0.80), and negatively correlated with the score in a cognitive test commonly used to evaluate the possible presence of dementia [255].

Finally, to complement our results *in vitro* and in AD patients' hippocampus, we also investigated the splicing of *Xbp1* in a mouse model of the disease and whether it could be modulated by RTP801. Previous literature showed that overexpression of XBP1s in *Drosophila* [256] and *C. elegans* [257] protected against Aβ- and tau-mediated neurotoxicity, respectively. As for mice, virus-mediated delivery of XBP1s in the hippocampus restored cognitive function and synaptic plasticity in the 5xFAD [197] and 3xTg-AD [198] models of AD. On the other hand, LTP and spatial memory were impaired in mice lacking XBP1 in the nervous system, and XBP1s overexpression in neurons enhanced long-term memory [199]. In the same work, XBP1s was described to bind to the *Bdnf* promoter, and local expression of BDNF in the hippocampus of XBP1-deficient mice improved long-term memory. Altogether, they proposed that *Xbp1* splicing regulates cognition through the transcription of *Bdnf* and other memory-related genes, which hamper AD progression. Precisely, another transcriptional target of XBP1s is *Kalirin-7*, which controls synaptic plasticity. Cissé *et al.* [198] reported reduced levels of Kalirin-7 in primary neurons exposed to Aβ, in the brain of transgenic mouse models and in human AD brains. In addition, Kalirin-7 knockdown affected synaptic plasticity and memory formation in naïve mice, and reduction of endogenous Kalirin-7 in 3xTg-AD mice reverted the beneficial effects of XBP1s overexpression. Overall, BDNF and Kalirin-7 seem to mediate the beneficial effects of XBP1s in memory and cognition, as illustrated in **Figure 41**.

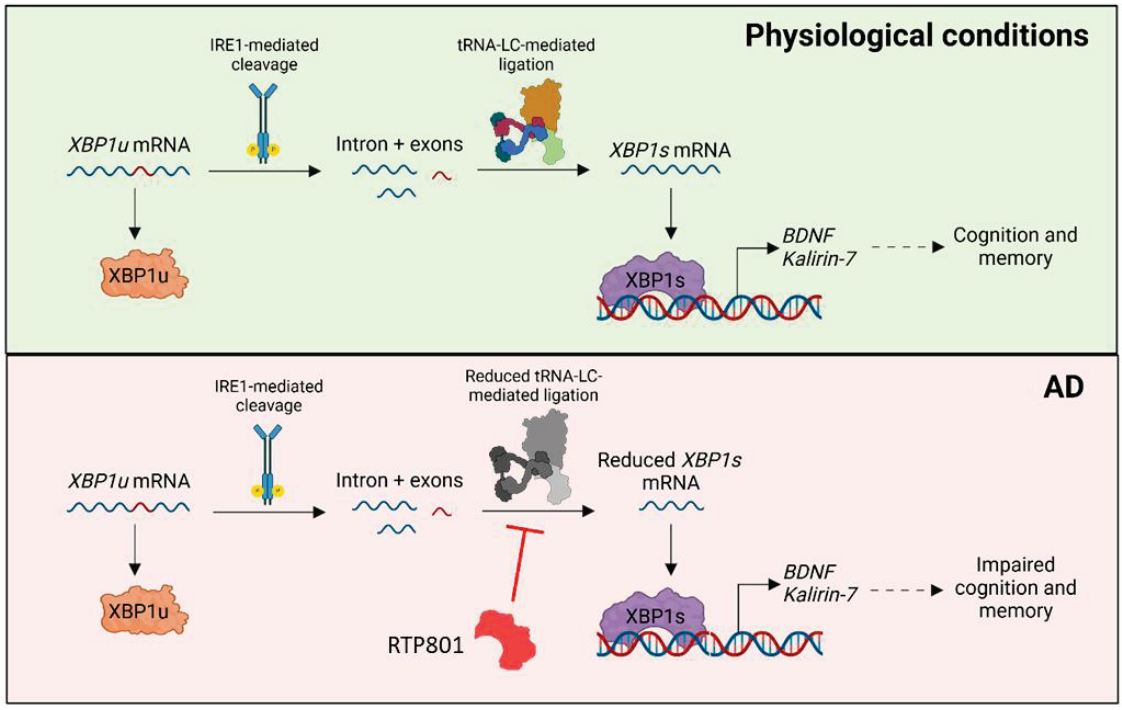

Figure 41. Proposed model for the beneficial effects of XBP1s, BDNF, and Kalirin-7 overexpression in the brain of mouse models of AD. In physiological conditions, *XBP1u* mRNA is translated generating XBP1u protein. When there is ER stress, the UPR is triggered and IRE1 cleaves *XBP1u* mRNA, freeing two exons that are ligated by the tRNA-LC. The resulting *XBP1s* mRNA is translated producing a transcription factor that promotes the expression of *BDNF* and *Kalirin-7*, which mediate cognition and memory. In AD, the ligation of XBP1s exons would be impaired by the action of RTP801, leading to reduced levels of *XBP1s* mRNA and protein. As a result, the protein levels of BDNF and Kalirin-7 would be reduced, resulting in impaired cognition and memory. In this pathological context, increased expression of XBP1s, BDNF, and/or Kalirin-7 reduces AD phenotype [197], [198], [199]. Figure created with *Biorender.com*.

In this work, we silenced RTP801 in hippocampal neurons of 6-month-old WT and 5xFAD mice and assessed *Xbp1* splicing by RT-qPCR. We observed no differences in the levels of *Xbp1s* between conditions. However, RTP801 knockdown significantly decreased *Xbp1u* levels, leading to an increase in *Xbp1s/Xbp1u* ratio. Interestingly, *Xbp1u* tended to accumulate (non-significantly) in 5xFAD shCT mice hippocampus, in a similar pattern to our results *in vitro*. When we assessed XBP1s transcriptional targets, we found no differences in the mRNA levels of *Sec24d* or *Kalirin-7* between conditions, but we observed that RTP801 silencing increased the mRNA levels of *Bdnf* in 5xFAD mice. We had previously described that RTP801 silencing in hippocampal neurons reduced neuroinflammation severity and prevented cognitive impairment in 5xFAD [114] and R6/1 [118] mice. Taking all this into consideration, RTP801 silencing might be beneficial by increasing *Xbp1* splicing and BDNF production, among other mechanisms.

Altogether, we can conclude that RTP801 inhibits *XBP1* splicing *in vitro* and *in vivo*, because its levels are always inversely correlated with the *XBP1s/XBP1u* ratio. And most likely, RTP801 effect is mediated by the interference with the ligase activity of the tRNA-LC, with which it interacts. However, there is still one question that remains unanswered: the fact that the levels of *XBP1s* and *XBP1u* do not follow the same pattern in all the experiments performed (**Table 12**). For instance, when we overexpress RTP801 in HEK293 cells we observe an accumulation of the unspliced form with no changes in the spliced. However, in AD patients' hippocampus (where RTP801 is upregulated) we find a decrease in the spliced form with no changes in the unspliced. The outcome is the same, a reduced *XBP1s/XBP1u* ratio, indicative of an inefficient *XBP1* splicing, but more experiments are needed to decipher the dynamics of *XBP1* splicing in the different models. For instance, RTP801 has a dual role depending on the cellular context, being anti-apoptotic in proliferating cells [64] and pro-apoptotic in differentiated cells [64], [71]. We speculate that this dual role could be extended to *XBP1* splicing inhibition, and thus, the exact mechanism of action might differ between HEK293 cells (human and proliferative) and 5xFAD hippocampal neurons (murine and predominantly differentiated).

HEK293	*XBP1s*	*XBP1u*	*XBP1s/XBP1u*
↓ RTP801	↑	=	↑
↑ RTP801	=	↑	↓
AD patients hippocampus	***XBP1s***	***XBP1u***	***XBP1s/XBP1u***
↑ RTP801	↓	=	↓
5xFAD mice hippocampus	***XBP1s***	***XBP1u***	***XBP1s/XBP1u***
↑ RTP801	=	↑	↓

Table 12. Summary of the levels of *XBP1s* and *XBP1u*, and their ratio in the experiments performed in the Aim 2 of this thesis. The red arrow indicates a reduction in the levels, the equal sign indicates no significant changes, and the green arrow represents an increase.

3. RTP801 inhibits the processing of intron-containing pre-tRNAs

tRNA genes are transcribed by RNA Pol III generating precursor molecules called pre-tRNAs. All human pre-tRNAs have 5' leader and 3' trailer sequences at their respective ends, but only around a 7% of them present an intron [141]. Introns are usually found one nucleotide after the anticodon, disrupting the anticodon stem-loop structure, and therefore, its splicing is required for tRNA maturation [142]. It is unclear which is the physiological function of introns, considering that they must be removed for tRNAs' function. However, there are some hypotheses regarding this aspect (reviewed in Yoshihisa *et al.* [142]). First, introns act as recognition motifs for tRNA-modifying enzymes [258]. Second, they mildly affect the expression of the tRNA genes containing them. Third, they might affect the formation and spacing of nucleosomes in the DNA [259]. Finally, the tRNA introns released during splicing can be circularized by HSPC117 (in collaboration with DDX1 and archease) generating tRNA intronic circular RNAs or (tric)RNAs [260], [261], whose physiological function remains elusive. Overall, tRNA splicing is essential for tRNA maturation and their canonical function in protein synthesis, and might be also important for other non-canonical functions performed by (tric)RNAs and tsRNAs.

In humans, intron cleavage is performed by the TSEN complex and Clp1 [143], whereas exon ligation is performed by the tRNA-LC [126], and specifically, by the ligase HSPC117. Here, we found that 7-month-old 5xFAD mice accumulate intron-containing pre-tRNAs in the hippocampus, and RTP801 silencing in hippocampal neurons prevents it. Moreover, we report that treatment of cultured neurons with the tRNA-enriched fraction from the hippocampus of 5xFAD shCT mice induces changes in neuron arborization without affecting neuron viability, a phenomenon that is not observed when cultures are treated with the hippocampal RNA from RTP801-silenced 5xFAD mice.

First, we obtained the 60-100 nt RNA fraction from the 4 experimental groups of mice (WT shCT, WT shRTP801, 5xFAD shCT, and 5xFAD shRTP801) and performed Hydro-tRNA-seq as described in [207]. When we analyzed the composition of our samples, classified by RNA type, we found that they were mainly composed of mature tRNA, followed by mt-tRNA, and pre-tRNA. Thus, our samples were highly enriched in different forms of tRNA. Similarly, Gogakos *et al.* [140], who developed Hydro-tRNA-seq, set up this sequencing technique in the 60-100 nt fraction of HEK293 cells and found that it was predominantly composed of mature tRNA, rRNA, and mt-tRNA. Surprisingly, only 1% of the reads mapped pre-tRNAs. We only come up with two possible explanations for this divergence: first, the pre-tRNA pool is less abundant (in proportion) in

human cells than in mouse tissue; second, when they did the RNA size selection, they accidentally left out the 88-100 fraction, which is enriched in pre-tRNAs [262].

Strikingly, we observed that the pre-tRNA isodecoder families with at least one intron-containing pre-tRNA species were significantly accumulated in 5xFAD shCT mice hippocampus. In other words, the following isodecoder families were increased: pre-tRNA-Arg-TCT, pre-tRNA-Ile-TAT, pre-tRNA-Leu-CAA, and pre-tRNA-Tyr-GTA. These four families include the 22 intron-containing pre-tRNA species found in the mouse genome. This specific accumulation of intron-containing pre-tRNAs suggests an impairment in tRNA splicing (either in tRNA cleavage or ligation) in 5xFAD mice hippocampus. To the best of our knowledge, the impact of AD in tRNA splicing has never been assessed, neither in patients' nor in mouse models' brains. However, tRNA modifications have been studied in the context of AD. For instance, Shafik *et al.* [263] reported hypomethylation of mitochondrial and cytosolic tRNAs in the cortex of 5xFAD mice. Similarly, tRNA hypomodification has been described in AD cellular models [264]. Furthermore, tRFs have also been investigated in AD, by Wu *et al.* [265]. They described increased levels of the ribonuclease ANG in the hippocampus of AD patients, as well as reduced levels of the methyltransferase Nsun2 (NOP2/Sun RNA methyltransferase 2), and they proposed that Nsun2-mediated tRNA methylation would make tRNAs less susceptible to ANG-mediated cleavage. Thus, Nsun2 and ANG dysregulation in AD would explain the altered pool of tRFs found in human AD hippocampi.

Unexpectedly, the accumulation of intro-containing pre-tRNAs in 5xFAD mice hippocampus did not cause a significant decrease in any of their mature forms. Nonetheless, Kosmaczewski *et al.* [234] described that RtcB null worms (RtcB is the orthologue of HSPC117 in *C. elegans*) presented higher levels of intron-containing pre-tRNAs, with no apparent variation in the levels of the trimmed, ligated form (mature). Interestingly, RtcB null worms were shorter and presented decreased lifespans. Likewise, Lu *et al.* [233] studied the effect of RtcB depletion in tRNA splicing using a conditional knockout. They found that 3 days after Cre induction, the levels of unspliced tyrosine pre-tRNA were significantly higher in RtcB KO cells, while the levels of spliced tyrosine tRNA did not vary. Furthermore, our results are in accordance with those obtained by Sekulovski *et al.* [266], who studied tRNA splicing in patients with pontocerebellar hypoplasia (PCH) due to mutations in the splicing machinery, and concretely in the TSEN complex. They found reduced splicing activity and accumulation of intron-containing pre-tRNAs in fibroblasts from PCH patients, analyzed by northern blot and by Hydro-tRNA-seq. Moreover, in their work, global levels of mature tRNAs also remained unaffected. Thus, an impairment in tRNA splicing (either in tRNA cleavage or ligation) affects the pool of intron-containing pre-tRNAs

without affecting the pool of mature tRNAs, and might contribute to neurodegeneration, as represented in **Figure 42**.

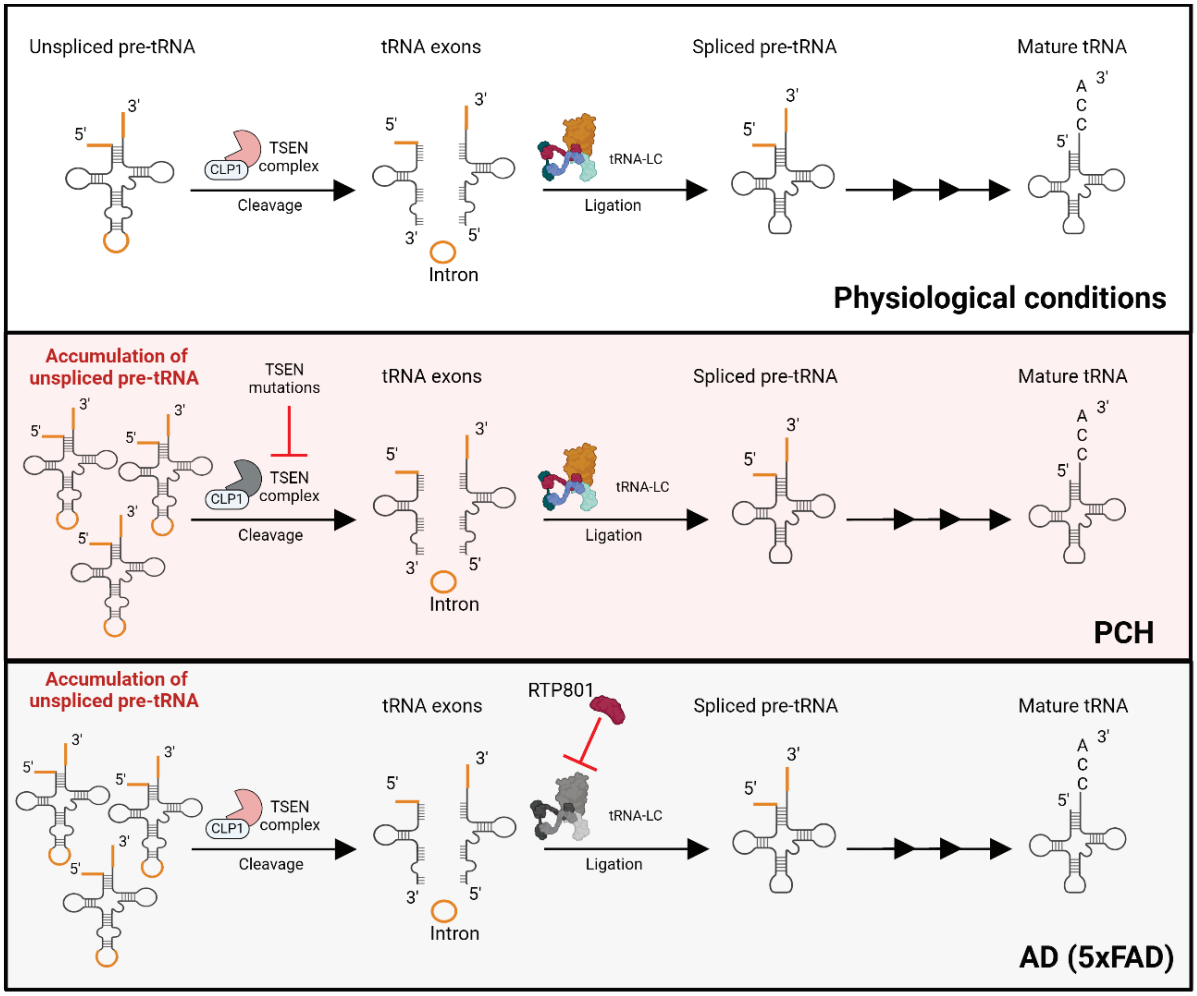

Figure 42. Proposed model of altered tRNA splicing in PCH and AD. In physiological conditions, the TSEN complex cleaves the pre-tRNA releasing two exons and an intron (it is unclear whether this happens before or after trailer and leader removal). Then the tRNA-LC ligates the tRNA exons, and the pre-tRNA undergoes other processing steps until becoming mature. Mutations in the TSEN complex result in accumulation of intron-containing pre-tRNAs with no changes in their mature levels [266]. Intron-containing pre-tRNAs are specifically accumulated in the hippocampus of 5xFAD mice, with no changes in their mature levels. An altered pool of intron-containing pre-tRNAs might contribute to neurodegeneration via unknown mechanisms, possibly by non-canonical functions of pre-tRNAs. Figure created with *Biorender.com*.

We also observed increased levels of pre-tRNA-Asp-GTC, and pre-tRNA-Sec-TCA, and decreased levels of pre-tRNA-Ala-TGC in 5xFAD shCT mice hippocampus compared to WT. Furthermore, the levels of mature tRNA-Asp-GTC, tRNA-Ile-AAT, and tRNA-Ser-CGA were significantly higher in 5xFAD mice hippocampus. Curiously, the only isodecoder family whose precursor and mature forms were both increased in 5xFAD mice hippocampus is Asp-GTC, suggesting an augmented transcription of the genes encoding these tRNA species. Interestingly, murine tRNA-Asp-GTC is

methylated by Nsun2 and TRDMT1 (tRNA aspartic acid methyltransferase 1, formerly named DNMT2 for DNA methyltransferase 2), which prevents its cleavage by ANG [267]. Since decreased protein levels of Nsun2 have been described in brains of AD patients [268], we would have expected reduced levels of mature tRNA-Asp-GTC in 5xFAD mice hippocampus instead.

In this thesis, we also explored the abundance of the different mt-tRNAs between WT shCT and 5xFAD shCT mice hippocampus and found no significant differences in any of them. Remarkably, mt-tRNAs are not processed the same way as the nuclear-encoded tRNAs. Indeed, mt-tRNA genes are transcribed as long polycistronic transcripts that contain multiple mt-tRNAs [136]. Moreover, mt-tRNAs do not present introns and thus, are not spliced (nor ligated by the tRNA-LC). Therefore, the fact that we did not observe any difference in the abundance of mt-tRNAs between WT and 5xFAD mice hippocampus suggests, once again, that only the processing of intron-containing tRNAs is altered in 5xFAD mice.

We then assessed whether RTP801 silencing in hippocampal neurons could affect tRNA splicing and noticed that it prevented the accumulation of intron-containing pre-tRNAs seen in 5xFAD mice. Indeed, for most of the pre-tRNA species evaluated, RTP801 knockdown caused a significant reduction in the pre-tRNA levels. Remarkably, this effect was not observed in those pre-tRNAs without intron. For instance, tRNA-Arg-TCT-2-1 and tRNA-Arg-TCT-4-1 have the same anticodon (and thus are charged with the same amino acid) and have a 75.7% sequence homology. The main difference between them is the presence of an intron in the former. Nevertheless, pre-tRNA-Arg-TCT-2-1 accumulates in 5xFAD shCT mice hippocampus, but pre-tRNA-Arg-TCT-4-1 does not. Moreover, RTP801 downregulation in 5xFAD mice hippocampus prevents the increase in pre-tRNA-Arg-TCT-2-1 levels. Once again, when we compared the mature levels of these tRNAs between the 4 groups of mice, no significant differences were detected (only for tRNA-Ile-AAT). Altogether, our results indicate that RTP801 regulates tRNA splicing and thus the pool of intron-containing pre-tRNAs, without affecting the pool of mature tRNAs in the hippocampus. Considering our results regarding *XBP1* splicing, RTP801 is in all probability regulating tRNA splicing by impairing the ligase activity of the tRNA-LC, either directly or indirectly. Nonetheless, we cannot discard that the effect of RTP801 over tRNA splicing is due to other mechanisms. For instance, Foretek *et al.* [182] reported that in yeast, 3' processing of pre-tRNAs is very fast under standard conditions, but slows down by an unknown mechanism under stress, resulting in the accumulation of pre-tRNAs such as pre-tRNA-Ile-TAT. If this mechanism was conserved across species, the high levels of the stress-responsive protein RTP801 in 5xFAD mice hippocampus could be slowing down pre-tRNA 3' processing, leading to an accumulation of pre-tRNAs. Nonetheless, there are two main drawbacks for this hypothesis.

First, although in their work Foretek *et al.* [182] only studied pre-tRNA processing in intron-containing pre-tRNAs, a slowdown in 3' processing should affect all pre-tRNAs, not only those with intron. Second, the co-immunoprecipitation of RTP801 with the members of the tRNA-LC would remain unanswered.

Finally, we investigated whether the 60-100 nt tRNA enriched fraction from the 4 groups of mice affected the viability and the arborization of mouse hippocampal cultured neurons. Neuron viability was evaluated by studying chromatin condensation, the amount of ClvCas3^{+} neurons, and its neuronal intensity. However, any of these analyses showed significant differences between the experimental conditions. This agrees with the work of Koltun *et al.* [212], who transfected mouse neuron-glia co-cultures with tRNAs and reported no affectation in neuron viability. Cao *et al.* [269] demonstrated that transfection of rat primary neuronal cultures with synthesized tRFs (14-30 nt long) induced neuron swelling and death. However, tRFs are not present in our working fraction, which comprises RNAs between 60-100 nt. Regarding neuron arborization, we found that the treatment of primary neurons with the tRNA-enriched sncRNA fraction from 5xFAD shCT mice hippocampus increased neuronal arborization. Specifically, we found an increase in the number of intermediate branches, which was accompanied by an augmented number of endpoints and increased tree length. Strikingly, these changes in neuron morphology were prevented when neurons were transfected with the tRNA-enriched fraction from RTP801-silenced 5xFAD mice hippocampus. Interestingly, increased spine density, branching, and dendrite length was described in organotypic hippocampal cultures after Aβ treatment [270]. Similarly, increased dendrite branching was found in the hippocampus of a mouse model of AD [271]. Indeed, it is speculated that excessive or aberrant synaptic plasticity might promote the development of AD [272]. Conversely, dendritic degeneration has also been reported in AD hippocampus [273], [274]. Altogether, our results show that the sncRNAs found in the 60-100 nt fraction (mainly mature tRNAs, mt-tRNAs, and pre-tRNAs, but also rRNAs and snoRNAs) derived from 5xFAD shCT mice hippocampus influence the branching of the receiving neurons, and this is somehow modulated by neuronal RTP801. This effect is probably due to the differential pool of intron-containing pre-tRNAs found in these mice, but we cannot discard the action of other sncRNAs, or even of abnormally modified mature tRNAs. Interestingly, Liu *et al.* [275] discovered that the 3' exon released during the unconventional splicing of *C. elegans xbp-1* mRNA was a biologically active non-coding RNA (ncRNA) essential for axon regeneration. Indeed, RtcB null worms presented higher levels of this ncRNA and augmented axon regeneration. Thus, if the production of this ncRNA were a conserved mechanism in mice, RTP801-mediated inhibition of the tRNA-LC would result in increased levels of *Xbp1* ncRNA in

5xFAD shCT mice hippocampus. Then, treatment of hippocampal cultured neurons with this ncRNA might result in an augmented neuron arborization. Nevertheless, the *xbp-1* fragment is 729 nt long in *C. elegans,* making quite unlikely that a potential murine *Xbp1* ncRNA were in our 60-100 nt fraction.

Here, we propose some theories to explain the potentially detrimental effect of the intron-containing pre-tRNAs accumulated in 5xFAD mice hippocampus. First, it has been demonstrated that human and murine pre-tRNA-Ile-TAT-2-3 can be transported into the cytoplasm to generate a miRNA called miR-1983 [276], which stimulates secretion of interferon-β [277], and targets insulin receptor β [278]. Precisely, pre-tRNA-Ile-TAT is increased in the hippocampus of our 5xFAD shCT mice. Second, by the generation of different types of tRF-1 (reviewed in Zhang *et al*. [279]). tRF-1 is generated from the 3' end of pre-tRNA and has diverse functions in cancer. Third, by the excessive production of (tric)RNAs [260], [261], which might have deleterious functions.

One puzzling aspect for us is the sequence of events during tRNA processing. In yeast, it is manifest that tRNA splicing occurs after 5' leader and 3' trailer removal, since these processes are distinctly compartmented. While trailer and leader removal take place in the nucleus, intron cleavage occurs in the outer surface of the mitochondria, and tRNA ligation is performed in the cytoplasm (reviewed in Hopper *et al.* [280]). However, in mammals both end trimming and tRNA splicing have been described in the nucleus (reviewed in Schaffer *et al.* [139]), complicating the deciphering of the exact chronology of the events. Theoretically, there are four possible options: 1) intron splicing precedes end trimming; 2) end trimming precedes intron splicing; 3) both processes occur simultaneously; 4) the order of the events depends on different features such as the tRNA specie, the cell type, the organism, etc. Supporting the last option is the work of Schneider *et al.* [281], who studied tyrosine tRNA processing in *Trypanosoma brucei*, a protist. They detected both unspliced/trimmed and spliced/untrimmed processing intermediates, suggesting that splicing and end processing occur independently. However, splicing tended to precede end processing. Indeed, there are works in animals endorsing that splicing occurs before end processing, since they only detected spliced/untrimmed intermediates [234], [282]. Taking all this into consideration, and keeping in mind our results, we speculate that tRNA splicing generally precedes 5' leader and 3' trailer removal, as depicted in **Figure 43**. If end trimming occurred first, the inhibition of the tRNA splicing ligase by RTP81 would primarily result in an increase of cleaved tRNAs (tRNA exons), which would have been classified as mature RNAs in our sequencing data. Conversely, if tRNA splicing happens before end processing, the inhibition of the ligation would result in an increase in tRNA halves carrying end extensions, which would

be classified as pre-tRNAs and would explain the accumulation of intron-containing pre-tRNAs observed in 5xFAD shCT mice hippocampus.

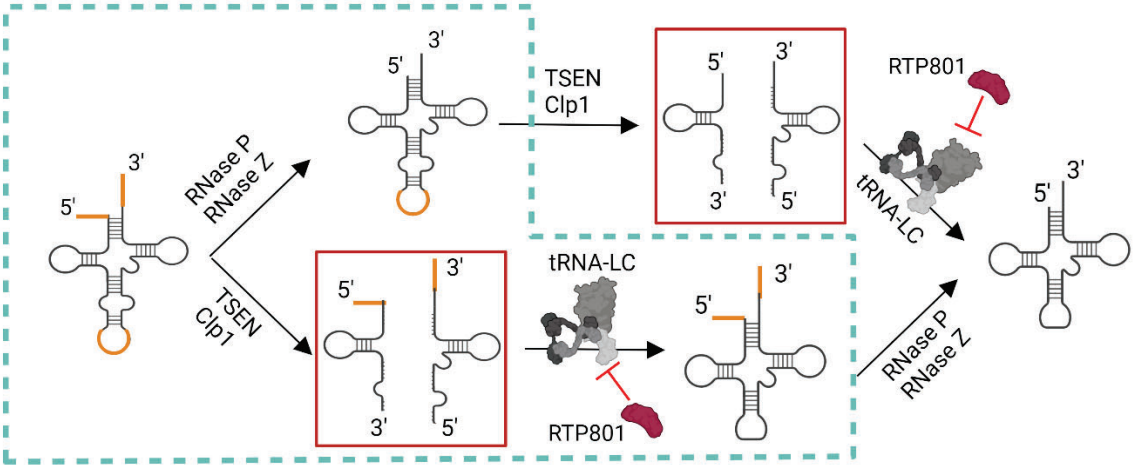

Figure 43. tRNA splicing seems to precede 5' leader and 3' trailer removal. Pre-tRNA processing assuming that end trimming precedes splicing (upper pathway) or vice versa (lower). In the upper possibility, pre-tRNA ends are first removed by RNAses P and Z, then cleavage is performed by the TSEN complex in collaboration with Clp1, and ligation is finally performed by the tRNA-LC. In the lower pathway, splicing takes place first, and then end trimming. The inhibition of the tRNA-LC by RTP801 would predominantly lead to the accumulation of the species framed by a red rectangle. The green dashed polygon surrounds all the tRNA species that would be classified as "pre-tRNA" in the sequencing analyses. Thus, in the upper pathway, RTP801-mediated inhibition of the ligation would mainly cause an increase in "mature tRNA", whereas in the lower pathway would result in an increase in "pre-tRNA", as observed in the 5xFAD shCT mice hippocampus. For simplicity, the hypothetical pathways where tRNA splicing and end trimming happen simultaneously, or their order depend on the cellular context, have not been depicted. Figure created with *Biorender.com*.

In this work, we have demonstrated that RTP801 co-immunoprecipitates with three members of the tRNA-LC, and that RTP801 inhibits the activity of the complex over *XBP1* and tRNA splicing. We had previously described that RTP801 silencing in hippocampal neurons of 5xFAD mice prevented cognitive impairment and reduced neuroinflammation [114], but we did not know by which mechanism. Here, we propose that RTP801 might do so by affecting the expression of *BDNF* and other XBP1s target genes, and by altering the pool of pre-tRNAs, which might have deleterious functions yet to discover. In addition, we speculate that RTP801 might affect other processes, such as NF-κB activation and the expression of the NLRP1 and NLRP3 inflammasomes. Furthermore, HSPC117, DDX1, CGI-99, and FAM98B are found in dendritic mRNA-containing cytoplasmic granules [283], and associate to form a complex that activates mRNA translation [284] and shuttles between the nucleus and the cytoplasm transporting RNAs [230]. Thus, high

levels of RTP801 might be also inhibiting these processes, leading to an altered proteostasis and contributing to neurodegeneration. And, as our group has previously described, RTP801 also mediates the intercellular transference of toxic species via EVs [86], being key for the spreading of pathological alterations across the brain.

In conclusion, in this thesis we present RTP801 as a novel interactor and regulator of the tRNA-LC both in the nucleus and the cytoplasm, and we propose that the stress-induced upregulation of RTP801 might contribute to AD pathology, by dysregulating XBP1s transcriptome and the cellular pre-tRNA pool (**Figure 44**), among other processes. Further experiments are needed to elucidate the exact region of RTP801 required for interaction and inhibition, as well as its exact mechanisms of action. But altogether, RTP801 appears to be a key protein that controls different cell processes, and thus, its inhibition could be an efficient therapeutic approach to simultaneously modulate many altered pathways in AD.

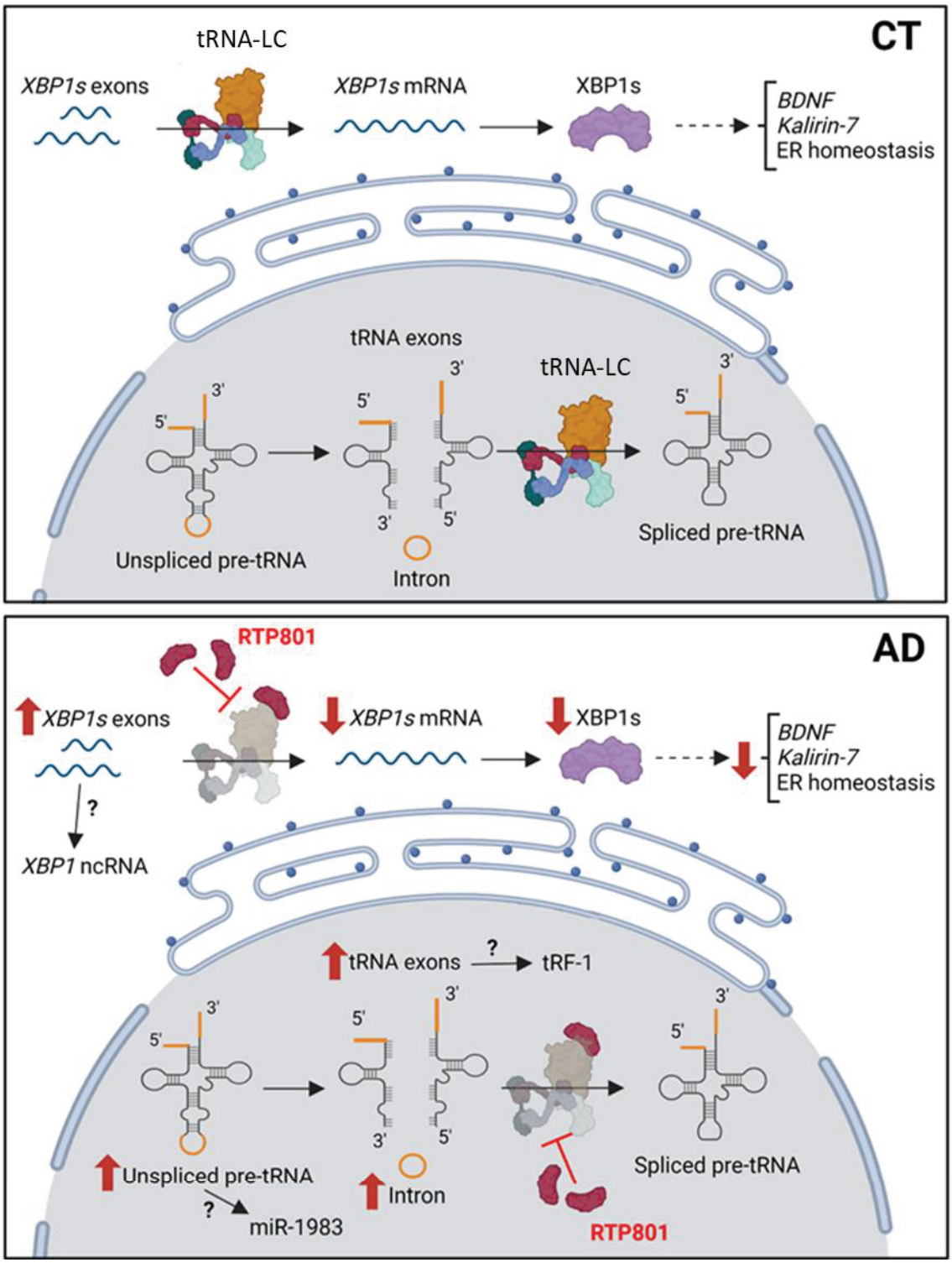

Figure 44. Proposed model for RTP801 inhibition over the tRNA-LC in the context of AD. In healthy individuals, RTP801 is expressed at low levels, and thus, the active tRNA-LC performs the ligation of tRNA exons and, under ER stress, the unconventional ligation of XBP1s exons. XBP1s protein transcribes *BDNF*, *Kalirin-7*, and other genes that promote ER homeostasis. In AD hippocampus, there is an upregulation of RTP801 that interferes with the activity of the tRNA-LC in the cytoplasm (outer surface of the ER) and in the nucleus. Consequently, the levels of XBP1s decrease, which might lead to decreased levels of its transcriptional targets. Conversely, the levels of intron-containing pre-tRNAs rise, which could result in an

increased production of tRF-1 and miR-1983. In AD panel, the tRNA-LC is depicted in gray to represent its inhibition by RTP801. The question marks indicate that it is unknown whether those events occur in AD brain. Figure created with *Biorender.com*

CONCLUSIONS

The main **conclusions** from this thesis can be summarized as follows:

1. RTP801 co-immunoprecipitates with DDX1 and HSPC117 in rat primary cortical neurons and in HEK293 cells. In addition, it co-immunoprecipitates with CGI-99 in HEK293 cells.

2. RTP801 does not regulate the protein levels of DDX1, HSPC117, or CGI-99 nor the gene expression of *DDX1* and *RTCB*.

3. HSPC117 and DDX1 modulate the protein levels of RTP801, but not its gene expression in HEK293 cells.

4. RTP801 silencing in HEK293 cells promotes *XBP1* splicing whereas RTP801 overexpression inhibits it.

5. The protein levels of XBP1s are drastically reduced in the hippocampus of AD patients.

6. The protein levels of RTP801, XBP1s, and p-eIF2α Ser51, are good classifiers of the presence or absence of AD.

7. RTP801 silencing in the hippocampal neurons of 6-month-old WT and 5xFAD mice promotes *Xbp1* splicing, and in the case of 5xFAD mice, *Bdnf* expression.

8. 7-month-old 5xFAD mice present an accumulation of intron-containing pre-tRNAs in the hippocampus, with no changes in the abundance of mt-tRNAs or mature tRNAs.

9. RTP801 silencing in the hippocampal neurons of 6-month-old 5xFAD mice prevents the accumulation of intron-containing pre-tRNAs.

10. Treatment of mouse hippocampal cultured neurons with the 60-100 nt tRNA-enriched fraction from the hippocampus of 5xFAD shCT mice increases neuron arborization without affecting viability, and this phenomenon is prevented when RTP801 is silenced in the source neurons.

REFERENCES

[1] D. M. Wilson, M. R. Cookson, L. Van Den Bosch, H. Zetterberg, D. M. Holtzman, and I. Dewachter, “Hallmarks of neurodegenerative diseases,” *Cell*, vol. 186, no. 4, pp. 693–714, Feb. 2023, doi: 10.1016/J.CELL.2022.12.032.

[2] R. N. L. Lamptey, B. Chaulagain, R. Trivedi, A. Gothwal, B. Layek, and J. Singh, “A Review of the Common Neurodegenerative Disorders: Current Therapeutic Approaches and the Potential Role of Nanotherapeutics,” *Int J Mol Sci*, vol. 23, no. 3, Feb. 2022, doi: 10.3390/IJMS23031851.

[3] M. F. Mendez and A. M. McMurtray, “Neurodegenerative Disorders,” *Encyclopedia of Stress*, pp. 840–844, 2007, doi: 10.1016/B978-012373947-6.00575-4.

[4] “2023 Alzheimer’s disease facts and figures,” *Alzheimer’s & Dementia*, vol. 19, no. 4, pp. 1598–1695, Apr. 2023, doi: 10.1002/ALZ.13016.

[5] R. A. Stelzmann, H. Norman Schnitzlein, and F. Reed Murtagh, “An english translation of alzheimer’s 1907 paper, ‘über eine eigenartige erkankung der hirnrinde,’” *Clinical Anatomy*, vol. 8, no. 6, pp. 429–431, Jan. 1995, doi: 10.1002/CA.980080612.

[6] H. Hippius and G. Neundörfer, “The discovery of Alzheimer’s disease,” *Dialogues Clin Neurosci*, vol. 5, no. 1, p. 101, 2003, doi: 10.31887/DCNS.2003.5.1/HHIPPIUS.

[7] G. G. Glenner and C. W. Wong, “Alzheimer’s disease: initial report of the purification and characterization of a novel cerebrovascular amyloid protein,” *Biochem Biophys Res Commun*, vol. 120, no. 3, pp. 885–890, May 1984, doi: 10.1016/S0006-291X(84)80190-4.

[8] J. G. Wood, S. S. Mirra, N. J. Pollock, and L. I. Binder, “Neurofibrillary tangles of Alzheimer disease share antigenic determinants with the axonal microtubule-associated protein tau (tau),” *Proceedings of the National Academy of Sciences*, vol. 83, no. 11, pp. 4040–4043, Jun. 1986, doi: 10.1073/PNAS.83.11.4040.

[9] I. Grundke-Iqbal, K. Iqbal, Y. C. Tung, M. Quinlan, H. M. Wisniewski, and L. I. Binder, “Abnormal phosphorylation of the microtubule-associated protein tau (tau) in Alzheimer cytoskeletal pathology.,” *Proceedings of the National Academy of Sciences*, vol. 83, no. 13, pp. 4913–4917, Jul. 1986, doi: 10.1073/PNAS.83.13.4913.

[10] K. S. Kosik, C. L. Joachim, and D. J. Selkoe, “Microtubule-associated protein tau (tau) is a major antigenic component of paired helical filaments in Alzheimer disease.,” *Proceedings of the National Academy of Sciences*, vol. 83, no. 11, pp. 4044–4048, Jun. 1986, doi: 10.1073/PNAS.83.11.4044.

[11] J. Kang *et al.*, “The precursor of Alzheimer’s disease amyloid A4 protein resembles a cell-surface receptor,” *Nature*, vol. 325, no. 6106, pp. 733–736, 1987, doi: 10.1038/325733A0.

[12] E. H. Corder *et al.*, “Gene dose of apolipoprotein E type 4 allele and the risk of Alzheimer’s disease in late onset families,” *Science*, vol. 261, no. 5123, pp. 921–923, Aug. 1993, doi: 10.1126/SCIENCE.8346443.

[13] A. M. Saunders *et al.*, “Association of apolipoprotein E allele epsilon 4 with late-onset familial and sporadic Alzheimer’s disease,” *Neurology*, vol. 43, no. 8, pp. 1467–1472, 1993, doi: 10.1212/WNL.43.8.1467.

[14] K. Hsiao, "Transgenic mice expressing Alzheimer amyloid precursor proteins," *Exp Gerontol*, vol. 33, no. 7–8, pp. 883–889, 1998, doi: 10.1016/S0531-5565(98)00045-X.

[15] W. E. Klunk *et al.*, "Imaging brain amyloid in Alzheimer's disease with Pittsburgh Compound-B," *Ann Neurol*, vol. 55, no. 3, pp. 306–319, 2004, doi: 10.1002/ANA.20009.

[16] "Alzheimer's & Brain Research Milestones | Alzheimer's Association." Accessed: Feb. 05, 2024. [Online]. Available: https://www.alz.org/alzheimers-dementia/research_progress/milestones

[17] R. Brookmeyer, E. Johnson, K. Ziegler-Graham, and H. M. Arrighi, "Forecasting the global burden of Alzheimer's disease," *Alzheimer's & Dementia*, vol. 3, no. 3, pp. 186–191, Jul. 2007, doi: 10.1016/J.JALZ.2007.04.381.

[18] H. Niu, I. Álvarez-Álvarez, F. Guillén-Grima, and I. Aguinaga-Ontoso, "Prevalence and incidence of Alzheimer's disease in Europe: A meta-analysis," *Neurología (English Edition)*, vol. 32, no. 8, pp. 523–532, Oct. 2017, doi: 10.1016/J.NRLENG.2016.02.009.

[19] M. F. Mendez, "Early-Onset Alzheimer's Disease," *Neurol Clin*, vol. 35, no. 2, p. 263, May 2017, doi: 10.1016/J.NCL.2017.01.005.

[20] J. M. Long and D. M. Holtzman, "Alzheimer Disease: An Update on Pathobiology and Treatment Strategies," *Cell*, vol. 179, no. 2, p. 312, Oct. 2019, doi: 10.1016/J.CELL.2019.09.001.

[21] A. T. Isik, "Late onset Alzheimer's disease in older people," *Clin Interv Aging*, vol. 5, p. 307, 2010, doi: 10.2147/CIA.S11718.

[22] S. E. Counts, M. D. Ikonomovic, N. Mercado, I. E. Vega, and E. J. Mufson, "Biomarkers for the Early Detection and Progression of Alzheimer's Disease," *Neurotherapeutics 2016 14:1*, vol. 14, no. 1, pp. 35–53, Oct. 2016, doi: 10.1007/S13311-016-0481-Z.

[23] R. A. Armstrong, "Risk factors for Alzheimer's disease," *Folia Neuropathol*, vol. 57, no. 2, pp. 87–105, 2019, doi: 10.5114/FN.2019.85929.

[24] C. Qiu, M. Kivipelto, and E. Von Strauss, "Epidemiology of Alzheimer's disease: occurrence, determinants, and strategies toward intervention," *Dialogues Clin Neurosci*, vol. 11, no. 2, p. 111, 2009, doi: 10.31887/DCNS.2009.11.2/CQIU.

[25] A. Heyman *et al.*, "Alzheimer's disease: genetic aspects and associated clinical disorders," *Ann Neurol*, vol. 14, no. 5, pp. 507–515, 1983, doi: 10.1002/ANA.410140503.

[26] C. Ballard, S. Gauthier, A. Corbett, C. Brayne, D. Aarsland, and E. Jones, "Alzheimer's disease," *Lancet*, vol. 377, no. 9770, pp. 1019–1031, 2011, doi: 10.1016/S0140-6736(10)61349-9.

[27] J. Hoogmartens, R. Cacace, and C. Van Broeckhoven, "Insight into the genetic etiology of Alzheimer's disease: A comprehensive review of the role of rare variants," *Alzheimer's & Dementia : Diagnosis, Assessment & Disease Monitoring*, vol. 13, no. 1, 2021, doi: 10.1002/DAD2.12155.

[28] C. Pottier *et al.*, "High frequency of potentially pathogenic SORL1 mutations in autosomal dominant early-onset Alzheimer disease," *Mol Psychiatry*, vol. 17, no. 9, pp. 875–879, Sep. 2012, doi: 10.1038/MP.2012.15.

[29] J. Verheijen *et al.*, "A comprehensive study of the genetic impact of rare variants in SORL1 in European early-onset Alzheimer's disease," *Acta Neuropathol*, vol. 132, no. 2, pp. 213–224, Aug. 2016, doi: 10.1007/S00401-016-1566-9.

[30] L. A. Farrer *et al.*, "Effects of Age, Sex, and Ethnicity on the Association Between Apolipoprotein E Genotype and Alzheimer Disease: A Meta-analysis," *JAMA*, vol. 278, no. 16, pp. 1349–1356, Oct. 1997, doi: 10.1001/JAMA.1997.03550160069041.

[31] E. Genin *et al.*, "APOE and Alzheimer disease: a major gene with semi-dominant inheritance," *Mol Psychiatry*, vol. 16, no. 9, pp. 903–907, Sep. 2011, doi: 10.1038/MP.2011.52.

[32] M. V. F. Silva, C. D. M. G. Loures, L. C. V. Alves, L. C. De Souza, K. B. G. Borges, and M. D. G. Carvalho, "Alzheimer's disease: risk factors and potentially protective measures," *Journal of Biomedical Science 2019 26:1*, vol. 26, no. 1, pp. 1–11, May 2019, doi: 10.1186/S12929-019-0524-Y.

[33] M. M. Mielke, J. E. Ransom, J. Mandrekar, P. Turcano, R. Savica, and A. W. Brown, "Traumatic Brain Injury and Risk of Alzheimer's Disease and Related Dementias in the Population," *J Alzheimers Dis*, vol. 88, no. 3, p. 1049, 2022, doi: 10.3233/JAD-220159.

[34] F. G. D. M. Coelho *et al.*, "Acute aerobic exercise increases brain-derived neurotrophic factor levels in elderly with Alzheimer's disease," *J Alzheimers Dis*, vol. 39, no. 2, pp. 401–408, 2014, doi: 10.3233/JAD-131073.

[35] W. G. Tharp and I. N. Sarkar, "Origins of amyloid-β," *BMC Genomics*, vol. 14, no. 1, Apr. 2013, doi: 10.1186/1471-2164-14-290.

[36] H. M. Brothers, M. L. Gosztyla, and S. R. Robinson, "The Physiological Roles of Amyloid-β Peptide Hint at New Ways to Treat Alzheimer's Disease," *Front Aging Neurosci*, vol. 10, no. APR, p. 118, Apr. 2018, doi: 10.3389/FNAGI.2018.00118.

[37] G. F. Chen *et al.*, "Amyloid beta: structure, biology and structure-based therapeutic development," *Acta Pharmacologica Sinica 2017 38:9*, vol. 38, no. 9, pp. 1205–1235, Jul. 2017, doi: 10.1038/aps.2017.28.

[38] G. R. Dawson *et al.*, "Age-related cognitive deficits, impaired long-term potentiation and reduction in synaptic marker density in mice lacking the beta-amyloid precursor protein," *Neuroscience*, vol. 90, no. 1, pp. 1–13, 1999, doi: 10.1016/S0306-4522(98)00410-2.

[39] A. F. Ikin, S. L. Sabo, L. M. Lanier, and J. D. Buxbaum, "A macromolecular complex involving the amyloid precursor protein (APP) and the cytosolic adapter FE65 is a negative regulator of axon branching," *Mol Cell Neurosci*, vol. 35, no. 1, pp. 57–63, May 2007, doi: 10.1016/J.MCN.2007.02.003.

[40] P. Soba *et al.*, "Homo- and heterodimerization of APP family members promotes intercellular adhesion," *EMBO J*, vol. 24, no. 20, pp. 3624–3634, Oct. 2005, doi: 10.1038/SJ.EMBOJ.7600824.

[41] H. Hampel *et al.*, "The Amyloid-β Pathway in Alzheimer's Disease," *Molecular Psychiatry 2021 26:10*, vol. 26, no. 10, pp. 5481–5503, Aug. 2021, doi: 10.1038/s41380-021-01249-0.

[42] G. F. Chen *et al.*, "Amyloid beta: Structure, biology and structure-based therapeutic development," *Acta Pharmacologica Sinica*, vol. 38, no. 9. Nature Publishing Group, pp. 1205–1235, Sep. 01, 2017. doi: 10.1038/aps.2017.28.

[43] M. Jouanne, S. Rault, and A. S. Voisin-Chiret, "Tau protein aggregation in Alzheimer's disease: An attractive target for the development of novel therapeutic agents," *Eur J Med Chem*, vol. 139, pp. 153–167, Oct. 2017, doi: 10.1016/J.EJMECH.2017.07.070.

[44] D. R. Thal, U. Rüb, M. Orantes, and H. Braak, "Phases of A beta-deposition in the human brain and its relevance for the development of AD," *Neurology*, vol. 58, no. 12, pp. 1791–1800, Jun. 2002, doi: 10.1212/WNL.58.12.1791.

[45] A. Serrano-Pozo, M. P. Frosch, E. Masliah, and B. T. Hyman, "Neuropathological Alterations in Alzheimer Disease," *Cold Spring Harb Perspect Med*, vol. 1, no. 1, Sep. 2011, doi: 10.1101/CSHPERSPECT.A006189.

[46] P. d'Errico and M. Meyer-Luehmann, "Mechanisms of Pathogenic Tau and Aβ Protein Spreading in Alzheimer's Disease," *Front Aging Neurosci*, vol. 12, p. 581817, Aug. 2020, doi: 10.3389/FNAGI.2020.00265/BIBTEX.

[47] S. Muralidar, S. V. Ambi, S. Sekaran, D. Thirumalai, and B. Palaniappan, "Role of tau protein in Alzheimer's disease: The prime pathological player," *Int J Biol Macromol*, vol. 163, pp. 1599–1617, Nov. 2020, doi: 10.1016/J.IJBIOMAC.2020.07.327.

[48] G. G. Kovacs, "Tauopathies," *Handb Clin Neurol*, vol. 145, pp. 355–368, 2017, doi: 10.1016/B978-0-12-802395-2.00025-0.

[49] H. Braak and E. Braak, "Neuropathological stageing of Alzheimer-related changes," *Acta Neuropathol*, vol. 82, no. 4, pp. 239–259, Sep. 1991, doi: 10.1007/BF00308809.

[50] S. Dujardin and B. T. Hyman, "Tau Prion-Like Propagation: State of the Art and Current Challenges," *Adv Exp Med Biol*, vol. 1184, pp. 305–325, 2019, doi: 10.1007/978-981-32-9358-8_23.

[51] J. Neddens *et al.*, "Phosphorylation of different tau sites during progression of Alzheimer's disease," *Acta Neuropathol Commun*, vol. 6, no. 1, p. 52, Jun. 2018, doi: 10.1186/S40478-018-0557-6/FIGURES/8.

[52] Z. R. Chen, J. B. Huang, S. L. Yang, and F. F. Hong, "Role of Cholinergic Signaling in Alzheimer's Disease," *Molecules*, vol. 27, no. 6, Mar. 2022, doi: 10.3390/MOLECULES27061816.

[53] A. V. Terry and J. J. Buccafusco, "The cholinergic hypothesis of age and Alzheimer's disease-related cognitive deficits: recent challenges and their implications for novel drug development," *J Pharmacol Exp Ther*, vol. 306, no. 3, pp. 821–827, Sep. 2003, doi: 10.1124/JPET.102.041616.

[54] K. Sharma, "Cholinesterase inhibitors as Alzheimer's therapeutics," *Mol Med Rep*, vol. 20, no. 2, p. 1479, 2019, doi: 10.3892/MMR.2019.10374.

[55] K. L. Lanctôt *et al.*, "Efficacy and safety of cholinesterase inhibitors in Alzheimer's disease: a meta-analysis," *CMAJ: Canadian Medical Association Journal*, vol. 169, no. 6, p. 557, Sep. 2003, doi: 10.1007/978-3-030-94960-0_53.

[56] K. X. Dou *et al.*, "Comparative safety and effectiveness of cholinesterase inhibitors and memantine for Alzheimer's disease: A network meta-analysis of 41 randomized controlled trials," *Alzheimers Res Ther*, vol. 10, no. 1, pp. 1–10, Dec. 2018, doi: 10.1186/S13195-018-0457-9/FIGURES/5.

[57] R. S. Petralia, "Distribution of Extrasynaptic NMDA Receptors on Neurons," *The Scientific World Journal*, vol. 2012, p. 11, 2012, doi: 10.1100/2012/267120.

[58] G. E. Hardingham and H. Bading, "Synaptic versus extrasynaptic NMDA receptor signalling: implications for neurodegenerative disorders," *Nature Reviews Neuroscience 2010 11:10*, vol. 11, no. 10, pp. 682–696, Sep. 2010, doi: 10.1038/nrn2911.

[59] J. Folch *et al.*, "Memantine for the Treatment of Dementia: A Review on its Current and Future Applications," *Journal of Alzheimer's Disease*, vol. 62, no. 3, p. 1223, 2018, doi: 10.3233/JAD-170672.

[60] R. R. Tampi and C. H. van Dyck, "Memantine: efficacy and safety in mild-to-severe Alzheimer's disease," *Neuropsychiatr Dis Treat*, vol. 3, no. 2, p. 245, 2007, doi: 10.2147/NEDT.2007.3.2.245.

[61] L. Söderberg *et al.*, "Lecanemab, Aducanumab, and Gantenerumab — Binding Profiles to Different Forms of Amyloid-Beta Might Explain Efficacy and Side Effects in Clinical Trials for Alzheimer's Disease," *Neurotherapeutics*, vol. 20, no. 1, p. 195, Jan. 2023, doi: 10.1007/S13311-022-01308-6.

[62] A. Rahman *et al.*, "Aducanumab for the treatment of Alzheimer's disease: a systematic review," *Psychogeriatrics*, vol. 23, no. 3, pp. 512–522, May 2023, doi: 10.1111/PSYG.12944.

[63] van D. CH *et al.*, "Lecanemab in Early Alzheimer's Disease," *N Engl J Med*, vol. 388, no. 1, pp. 142–143, 2023, doi: 10.1056/NEJMOA2212948.

[64] T. Shoshani *et al.*, "Identification of a novel hypoxia-inducible factor 1-responsive gene, RTP801, involved in apoptosis.," *Mol Cell Biol*, vol. 22, no. 7, pp. 2283–93, Apr. 2002, doi: 10.1128/mcb.22.7.2283-2293.2002.

[65] L. W. Ellisen *et al.*, "REDD1, a developmentally regulated transcriptional target of p63 and p53, links p63 to regulation of reactive oxygen species.," *Mol Cell*, vol. 10, no. 5, pp. 995–1005, Nov. 2002.

[66] Z. Wang, M. H. Malone, M. J. Thomenius, F. Zhong, F. Xu, and C. W. Distelhorst, "Dexamethasone-induced gene 2 (dig2) is a novel pro-survival stress gene induced rapidly by diverse apoptotic signals," *J Biol Chem*, vol. 278, no. 29, pp. 27053–27058, Jul. 2003, doi: 10.1074/JBC.M303723200.

[67] I. Tirado-Hurtado, W. Fajardo, and J. A. Pinto, "DNA damage inducible transcript 4 gene: The switch of the metabolism as potential target in cancer," *Front Oncol*, vol. 8, no. APR, p. 333124, Apr. 2018, doi: 10.3389/FONC.2018.00106/BIBTEX.

[68] M. N. Corradetti, K. Inoki, and K. L. Guan, "The stress-inducted proteins RTP801 and RTP801L are negative regulators of the mammalian target of rapamycin pathway," *J Biol Chem*, vol. 280, no. 11, pp. 9769–9772, Mar. 2005, doi: 10.1074/JBC.C400557200.

[69] H. O. Jin *et al.*, "Hypoxic condition- and high cell density-induced expression of Redd1 is regulated by activation of hypoxia-inducible factor-1alpha and Sp1 through the phosphatidylinositol 3-kinase/Akt signaling pathway," *Cell Signal*, vol. 19, no. 7, pp. 1393–1403, Jul. 2007, doi: 10.1016/J.CELLSIG.2006.12.014.

[70] J. Y. Kim, Y. G. Kwon, and Y. M. Kim, "The stress-responsive protein REDD1 and its pathophysiological functions," *Exp Mol Med*, vol. 55, no. 9, p. 1933, Sep. 2023, doi: 10.1038/S12276-023-01056-3.

[71] C. Malagelada, E. J. Ryu, S. C. Biswas, V. Jackson-Lewis, and L. A. Greene, "RTP801 Is Elevated in Parkinson Brain Substantia Nigral Neurons and Mediates Death in Cellular Models of Parkinson's Disease by a Mechanism Involving Mammalian Target of Rapamycin Inactivation," *Journal of Neuroscience*, vol. 26, no. 39, pp. 9996–10005, Sep. 2006, doi: 10.1523/JNEUROSCI.3292-06.2006.

[72] J. R. Kim *et al.*, "Identification of amyloid β-peptide responsive genes by cDNA microarray technology: Involvement of RTP801 in amyloid β-peptide toxicity," *Experimental & Molecular Medicine 2003 35:5*, vol. 35, no. 5, pp. 403–411, Oct. 2003, doi: 10.1038/emm.2003.53.

[73] N. Martín-Flores *et al.*, "RTP801 Is Involved in Mutant Huntingtin-Induced Cell Death," *Mol Neurobiol*, vol. 53, no. 5, pp. 2857–2868, Jul. 2016, doi: 10.1007/s12035-015-9166-6.

[74] L. Lin, T. M. Stringfield, X. Shi, and Y. Chen, "Arsenite induces a cell stress-response gene, RTP801, through reactive oxygen species and transcription factors Elk-1 and CCAAT/enhancer-binding protein," *Biochem J*, vol. 392, no. Pt 1, pp. 93–102, Nov. 2005, doi: 10.1042/BJ20050553.

[75] L. Lin, Y. Qian, X. Shi, and Y. Chen, "Induction of a cell stress response gene RTP801 by DNA damaging agent methyl methanesulfonate through CCAAT/Enhancer binding protein," *Biochemistry*, vol. 44, no. 10, pp. 3909–3914, Mar. 2005, doi: 10.1021/BI047574R/ASSET/IMAGES/MEDIUM/BI047574RN00001.GIF.

[76] H. O. Jin *et al.*, "Activating transcription factor 4 and CCAAT/enhancer-binding protein-beta negatively regulate the mammalian target of rapamycin via Redd1 expression in response to oxidative and endoplasmic reticulum stress," *Free Radic Biol Med*, vol. 46, no. 8, pp. 1158–1167, Apr. 2009, doi: 10.1016/J.FREERADBIOMED.2009.01.015.

[77] D. K. Lee *et al.*, "Lipopolysaccharide induction of REDD1 is mediated by two distinct CREB-dependent mechanisms in macrophages," *FEBS Lett*, vol. 589, no. 19 Pt B, pp. 2859–2865, Sep. 2015, doi: 10.1016/J.FEBSLET.2015.08.004.

[78] Y. Wu *et al.*, "REDD1 is a major target of testosterone action in preventing dexamethasone-induced muscle loss," *Endocrinology*, vol. 151, no. 3, pp. 1050–1059, Mar. 2010, doi: 10.1210/EN.2009-0530.

[79] B. S. Gordon, J. L. Steiner, D. L. Williamson, C. H. Lang, and S. R. Kimball, "Emerging role for regulated in development and DNA damage 1 (REDD1) in the regulation of skeletal muscle metabolism," *Am J Physiol Endocrinol Metab*, vol. 311, no. 1, pp. E157–E174, Jul. 2016, doi: 10.1152/AJPENDO.00059.2016/ASSET/IMAGES/LARGE/ZH10121675980004.JPEG.

[80] G. Michel *et al.*, "Plasma membrane translocation of REDD1 governed by GPCRs contributes to mTORC1 activation," *J Cell Sci*, vol. 127, no. Pt 4, pp. 773–787, Feb. 2014, doi: 10.1242/JCS.136432.

[81] S. S. Cho *et al.*, "Induction of REDD1 via AP-1 prevents oxidative stress-mediated injury in hepatocytes," *Free Radic Biol Med*, vol. 124, pp. 221–231, Aug. 2018, doi: 10.1016/J.FREERADBIOMED.2018.06.014.

[82] P. Horak *et al.*, "Negative feedback control of HIF-1 through REDD1-regulated ROS suppresses tumorigenesis," *Proc Natl Acad Sci U S A*, vol. 107, no. 10, pp. 4675–4680, Mar. 2010, doi: 10.1073/PNAS.0907705107/SUPPL_FILE/PNAS.200907705SI.PDF.

[83] S. Del Olmo-Aguado, C. Núñez-Álvarez, D. Ji, A. G. Manso, and N. N. Osborne, "RTP801 immunoreactivity in retinal ganglion cells and its down-regulation in cultured cells protect them from light and cobalt chloride," *Brain Res Bull*, vol. 98, pp. 132–144, Sep. 2013, doi: 10.1016/J.BRAINRESBULL.2013.08.002.

[84] M. P. Deyoung, P. Horak, A. Sofer, D. Sgroi, and L. W. Ellisen, "Hypoxia regulates TSC1/2-mTOR signaling and tumor suppression through REDD1-mediated 14-3-3 shuttling," *Genes Dev*, vol. 22, no. 2, pp. 239–251, 2008, doi: 10.1101/gad.1617608.

[85] N. Martín-Flores *et al.*, "Synaptic RTP801 contributes to motor-learning dysfunction in Huntington's disease," *Cell Death Dis*, vol. 11, no. 7, pp. 1–15, Jul. 2020, doi: 10.1038/s41419-020-02775-5.

[86] J. Solana-Balaguer *et al.*, "RTP801 mediates transneuronal toxicity in culture via extracellular vesicles," *J Extracell Vesicles*, vol. 12, no. 11, Nov. 2023, doi: 10.1002/JEV2.12378.

[87] S. Vega-Rubin-de-Celis, Z. Abdallah, L. Kinch, N. V. Grishin, J. Brugarolas, and X. Zhang, "Structural analysis and functional implications of the negative mTORC1 regulator REDD1," *Biochemistry*, vol. 49, no. 11, p. 2491, Mar. 2010, doi: 10.1021/BI902135E.

[88] D. K. Lee *et al.*, "REDD1 promotes obesity-induced metabolic dysfunction via atypical NF-κB activation," *Nat Commun*, vol. 13, no. 1, Dec. 2022, doi: 10.1038/S41467-022-34110-1.

[89] D. K. Lee *et al.*, "REDD-1 aggravates endotoxin-induced inflammation via atypical NF-κB activation," *FASEB J*, vol. 32, no. 8, pp. 4585–4599, Aug. 2018, doi: 10.1096/FJ.201701436R.

[90] M. Canal *et al.*, "Loss of NEDD4 contributes to RTP801 elevation and neuron toxicity: implications for Parkinson’s disease," *Oncotarget*, vol. 7, no. 37, pp. 58813–58831, Sep. 2016, doi: 10.18632/oncotarget.11020.

[91] S. R. Kimball, A. N. D. Do, L. Kutzler, D. R. Cavener, and L. S. Jefferson, "Rapid turnover of the mTOR complex 1 (mTORC1) repressor REDD1 and activation of mTORC1 signaling following inhibition of protein synthesis," *J Biol Chem*, vol. 283, no. 6, pp. 3465–3475, Feb. 2008, doi: 10.1074/JBC.M706643200.

[92] C. Malagelada, Z. H. Jin, V. Jackson-Lewis, S. Przedborski, and L. A. Greene, "Rapamycin protects against neuron death in in vitro and in vivo models of Parkinson's disease," *J*

Neurosci, vol. 30, no. 3, pp. 1166–1175, Jan. 2010, doi: 10.1523/JNEUROSCI.3944-09.2010.

[93] S. Katiyar *et al.*, "REDD1, an inhibitor of mTOR signalling, is regulated by the CUL4A–DDB1 ubiquitin ligase," *EMBO Rep*, vol. 10, no. 8, p. 866, 2009, doi: 10.1038/EMBOR.2009.93.

[94] C. Y. Tan and T. Hagen, "mTORC1 Dependent Regulation of REDD1 Protein Stability," *PLoS One*, vol. 8, no. 5, p. 63970, May 2013, doi: 10.1371/JOURNAL.PONE.0063970.

[95] J. Romaní-Aumedes *et al.*, "Parkin loss of function contributes to RTP801 elevation and neurodegeneration in Parkinson's disease," *Cell Death Dis*, vol. 5, no. 8, pp. e1364–e1364, Aug. 2014, doi: 10.1038/cddis.2014.333.

[96] J. Brugarolas *et al.*, "Regulation of mTOR function in response to hypoxia by REDD1 and the TSC1/TSC2 tumor suppressor complex.," *Genes Dev*, vol. 18, no. 23, pp. 2893–904, Dec. 2004, doi: 10.1101/gad.1256804.

[97] A. Sofer, K. Lei, C. M. Johannessen, and L. W. Ellisen, "Regulation of mTOR and cell growth in response to energy stress by REDD1," *Mol Cell Biol*, vol. 25, no. 14, pp. 5834–5845, Jul. 2005, doi: 10.1128/MCB.25.14.5834-5845.2005.

[98] A. Szwed, E. Kim, and E. Jacinto, "Regulation and metabolic functions of mTORC1 and mTORC2," *Physiol Rev*, vol. 101, no. 3, p. 1371, Jul. 2021, doi: 10.1152/PHYSREV.00026.2020.

[99] L. C. Kim, R. S. Cook, and J. Chen, "mTORC1 and mTORC2 in cancer and the tumor microenvironment," *Oncogene 2017 36:16*, vol. 36, no. 16, pp. 2191–2201, Oct. 2016, doi: 10.1038/onc.2016.363.

[100] M. Laplante and D. M. Sabatini, "mTOR Signaling in Growth Control and Disease," *Cell*, vol. 149, no. 2, pp. 274–293, Apr. 2012, doi: 10.1016/J.CELL.2012.03.017.

[101] L. Hou and E. Klann, "Activation of the phosphoinositide 3-kinase-Akt-mammalian target of rapamycin signaling pathway is required for metabotropic glutamate receptor-dependent long-term depression," *J Neurosci*, vol. 24, no. 28, pp. 6352–6361, Jul. 2004, doi: 10.1523/JNEUROSCI.0995-04.2004.

[102] M. Cammalleri *et al.*, "Time-restricted role for dendritic activation of the mTOR-p70S6K pathway in the induction of late-phase long-term potentiation in the CA1," *Proc Natl Acad Sci U S A*, vol. 100, no. 24, pp. 14368–14373, Nov. 2003, doi: 10.1073/PNAS.2336098100.

[103] N. Takei *et al.*, "Brain-Derived Neurotrophic Factor Induces Mammalian Target of Rapamycin-Dependent Local Activation of Translation Machinery and Protein Synthesis in Neuronal Dendrites," *Journal of Neuroscience*, vol. 24, no. 44, pp. 9760–9769, Nov. 2004, doi: 10.1523/JNEUROSCI.1427-04.2004.

[104] Y. Zhang, X. Gao, L. J. Saucedo, B. Ru, B. A. Edgar, and D. Pan, "Rheb is a direct target of the tuberous sclerosis tumour suppressor proteins," *Nat Cell Biol*, vol. 5, no. 6, pp. 578–581, Jun. 2003, doi: 10.1038/NCB999.

[105] S. L. Cai *et al.*, "Activity of TSC2 is inhibited by AKT-mediated phosphorylation and membrane partitioning," *J Cell Biol*, vol. 173, no. 2, pp. 279–289, Apr. 2006, doi: 10.1083/JCB.200507119.

[106] K. Inoki, Y. Li, T. Zhu, J. Wu, and K. L. Guan, "TSC2 is phosphorylated and inhibited by Akt and suppresses mTOR signalling," *Nat Cell Biol*, vol. 4, no. 9, pp. 648–657, Sep. 2002, doi: 10.1038/NCB839.

[107] J. H. Reiling and E. Hafen, "The hypoxia-induced paralogs Scylla and Charybdis inhibit growth by down-regulating S6K activity upstream of TSC in Drosophila," *Genes Dev*, vol. 18, no. 23, pp. 2879–2892, 2004, doi: 10.1101/gad.322704.

[108] M. D. Dennis, C. S. Coleman, A. Berg, L. S. Jefferson, and S. R. Kimball, "Erratum: REDD1 enhances protein phosphatase 2A-mediated dephosphorylation of Akt to repress mTORC1 signaling (Science Signaling 7:335 (ra68))," *Sci Signal*, vol. 8, no. 368, p. er4, 2015, doi: 10.1126/scisignal.aab1023.

[109] C. Malagelada, M. A. López-Toledano, R. T. Willett, Z. H. Jin, M. L. Shelanski, and L. A. Greene, "RTP801/REDD1 regulates the timing of cortical neurogenesis and neuron migration," *J Neurosci*, vol. 31, no. 9, pp. 3186–3196, Mar. 2011, doi: 10.1523/JNEUROSCI.4011-10.2011.

[110] L. Pérez-Sisqués *et al.*, "RTP801 regulates motor cortex synaptic transmission and learning," *Exp Neurol*, vol. 342, Aug. 2021, doi: 10.1016/J.EXPNEUROL.2021.113755.

[111] J. Su, H. Huang, S. Ju, and J. Shi, "Elevated RTP801 promotes cell proliferation in non-small cell lung cancer," *IUBMB Life*, vol. 70, no. 4, pp. 310–319, Apr. 2018, doi: 10.1002/IUB.1727.

[112] B. Chang *et al.*, "Overexpression of the recently identified oncogene REDD1 correlates with tumor progression and is an independent unfavorable prognostic factor for ovarian carcinoma," *Diagn Pathol*, vol. 13, no. 1, pp. 1–12, Nov. 2018, doi: 10.1186/S13000-018-0754-4/TABLES/8.

[113] Y. Feng *et al.*, "REDD1 overexpression in oral squamous cell carcinoma may predict poor prognosis and correlates with high microvessel density," *Oncol Lett*, vol. 19, no. 1, pp. 431–441, 2020, doi: 10.3892/OL.2019.11070.

[114] L. Pérez-Sisqués *et al.*, "RTP801/REDD1 contributes to neuroinflammation severity and memory impairments in Alzheimer's disease," *Cell Death Dis*, vol. 12, no. 6, Jun. 2021, doi: 10.1038/S41419-021-03899-Y.

[115] C. Malagelada, H. J. Zong, and L. A. Greene, "RTP801 is induced in Parkinson's disease and mediates neuron death by inhibiting Akt phosphorylation/activation," *J Neurosci*, vol. 28, no. 53, pp. 14363–14371, Dec. 2008, doi: 10.1523/JNEUROSCI.3928-08.2008.

[116] X. Sun *et al.*, "ATF4 protects against neuronal death in cellular Parkinson's disease models by maintaining levels of parkin," *J Neurosci*, vol. 33, no. 6, pp. 2398–2407, Feb. 2013, doi: 10.1523/JNEUROSCI.2292-12.2013.

[117] Z. Zhang *et al.*, "RTP801 is a critical factor in the neurodegeneration process of A53T α-synuclein in a mouse model of Parkinson's disease under chronic restraint stress," *Br J Pharmacol*, vol. 175, no. 4, pp. 590–605, Feb. 2018, doi: 10.1111/BPH.14091.

[118] L. Pérez-Sisqués *et al.*, "RTP801/REDD1 Is Involved in Neuroinflammation and Modulates Cognitive Dysfunction in Huntington's Disease.," *Biomolecules*, vol. 12, no. 1, Jan. 2021, doi: 10.3390/biom12010034.

[119] J. H. Yi *et al.*, "REDD1 Is Involved in Amyloid β-Induced Synaptic Dysfunction and Memory Impairment," *Int J Mol Sci*, vol. 21, no. 24, pp. 1–13, Dec. 2020, doi: 10.3390/IJMS21249482.

[120] J. Hugon, F. Mouton-Liger, J. Dumurgier, and C. Paquet, "PKR involvement in Alzheimer's disease," *Alzheimers Res Ther*, vol. 9, no. 1, Oct. 2017, doi: 10.1186/S13195-017-0308-0.

[121] M. Damjanac *et al.*, "PKR, a cognitive decline biomarker, can regulate translation via two consecutive molecular targets p53 and Redd1 in lymphocytes of AD patients," *J Cell Mol Med*, vol. 13, no. 8B, pp. 1823–1832, Aug. 2009, doi: 10.1111/J.1582-4934.2009.00688.X.

[122] M. Tible *et al.*, "PKR knockout in the 5xFAD model of Alzheimer's disease reveals beneficial effects on spatial memory and brain lesions," *Aging Cell*, vol. 18, no. 3, Jun. 2019, doi: 10.1111/ACEL.12887.

[123] S. G. Boaru, E. Borkham-Kamphorst, E. Van De Leur, E. Lehnen, C. Liedtke, and R. Weiskirchen, "NLRP3 inflammasome expression is driven by NF-κB in cultured hepatocytes," *Biochem Biophys Res Commun*, vol. 458, no. 3, pp. 700–706, Mar. 2015, doi: 10.1016/J.BBRC.2015.02.029.

[124] D. Y. W. Fann *et al.*, "Evidence that NF-κB and MAPK Signaling Promotes NLRP Inflammasome Activation in Neurons Following Ischemic Stroke," *Mol Neurobiol*, vol. 55, no. 2, pp. 1082–1096, Feb. 2018, doi: 10.1007/S12035-017-0394-9.

[125] M. Canal de la Iglesia, "Study of pro-apoptotic protein RTP801 homeostasis and its regulation by NEDD4 in Parkinson's disease," *TDX (Tesis Doctorals en Xarxa)*, Jun. 2016.

[126] J. Popow *et al.*, "HSPC117 Is the Essential Subunit of a Human tRNA Splicing Ligase Complex," *Science (1979)*, vol. 331, no. 6018, pp. 760–764, Feb. 2011, doi: 10.1126/science.1197847.

[127] J. Li and C. Liu, "Coding or Noncoding, the Converging Concepts of RNAs," *Front Genet*, vol. 10, no. MAY, 2019, doi: 10.3389/FGENE.2019.00496.

[128] L. Statello, C. J. Guo, L. L. Chen, and M. Huarte, "Gene regulation by long non-coding RNAs and its biological functions," *Nature Reviews Molecular Cell Biology 2020 22:2*, vol. 22, no. 2, pp. 96–118, Dec. 2020, doi: 10.1038/s41580-020-00315-9.

[129] B. Y. Lin, P. P. Chan, and T. M. Lowe, "tRNAviz: explore and visualize tRNA sequence features," *Nucleic Acids Res*, vol. 47, no. W1, p. W542, Jul. 2019, doi: 10.1093/NAR/GKZ438.

[130] F. CHAPEVILLE, F. LIPMANN, G. VON EHRENSTEIN, B. WEISBLUM, W. J. RAY, and S. BENZER, "On the role of soluble ribonucleic acid in coding for amino acids.," *Proc Natl Acad Sci U S A*, vol. 48, no. 6, pp. 1086–1092, Jun. 1962, doi: 10.1073/PNAS.48.6.1086/ASSET/41204ADF-737F-4CED-BF5A-84D27FC8F00C/ASSETS/PNAS.48.6.1086.FP.PNG.

[131] M. D. Berg and C. J. Brandl, "Transfer RNAs: diversity in form and function," *RNA Biol*, vol. 18, no. 3, p. 316, 2021, doi: 10.1080/15476286.2020.1809197.

[132] P. P. Chan, B. Y. Lin, A. J. Mak, and T. M. Lowe, "TRNAscan-SE 2.0: Improved detection and functional classification of transfer RNA genes," *Nucleic Acids Res*, vol. 49, no. 16, pp. 9077–9096, Sep. 2021, doi: 10.1093/NAR/GKAB688.

[133] L. A. Hughes *et al.*, "Copy number variation in tRNA isodecoder genes impairs mammalian development and balanced translation," *Nature Communications 2023 14:1*, vol. 14, no. 1, pp. 1–19, Apr. 2023, doi: 10.1038/s41467-023-37843-9.

[134] T. Pan, "Modifications and functional genomics of human transfer RNA," *Cell Research 2018 28:4*, vol. 28, no. 4, pp. 395–404, Feb. 2018, doi: 10.1038/s41422-018-0013-y.

[135] P. Loher, A. G. Telonis, and I. Rigoutsos, "MINTmap: fast and exhaustive profiling of nuclear and mitochondrial tRNA fragments from short RNA-seq data," *Scientific Reports 2017 7:1*, vol. 7, no. 1, pp. 1–20, Feb. 2017, doi: 10.1038/srep41184.

[136] D. Litonin *et al.*, "Human Mitochondrial Transcription Revisited: ONLY TFAM AND TFB2M ARE REQUIRED FOR TRANSCRIPTION OF THE MITOCHONDRIAL GENES IN VITRO*," *J Biol Chem*, vol. 285, no. 24, p. 18129, Jun. 2010, doi: 10.1074/JBC.C110.128918.

[137] T. Suzuki, A. Nagao, and T. Suzuki, "Human mitochondrial tRNAs: biogenesis, function, structural aspects, and diseases," *Annu Rev Genet*, vol. 45, pp. 299–329, 2011, doi: 10.1146/ANNUREV-GENET-110410-132531.

[138] A. R. D'Souza and M. Minczuk, "Mitochondrial transcription and translation: overview," *Essays Biochem*, vol. 62, no. 3, p. 309, Jul. 2018, doi: 10.1042/EBC20170102.

[139] A. E. Schaffer, O. Pinkard, and J. M. Coller, "tRNA Metabolism and Neurodevelopmental Disorders," *Annu Rev Genomics Hum Genet*, vol. 20, p. 359, Aug. 2019, doi: 10.1146/ANNUREV-GENOM-083118-015334.

[140] T. Gogakos, M. Brown, A. Garzia, C. Meyer, M. Hafner, and T. Tuschl, "Characterizing expression and processing of precursor and mature human tRNAs by hydro-tRNAseq and PAR-CLIP," *Cell Rep*, vol. 20, no. 6, p. 1463, Aug. 2017, doi: 10.1016/J.CELREP.2017.07.029.

[141] C. A. Schmidt and A. G. Matera, "tRNA introns: Presence, processing, and purpose," *Wiley Interdiscip Rev RNA*, vol. 11, no. 3, p. e1583, May 2020, doi: 10.1002/WRNA.1583.

[142] T. Yoshihisa, "Handling tRNA introns, archaeal way and eukaryotic way.," *Front Genet*, vol. 5, p. 213, 2014, doi: 10.3389/fgene.2014.00213.

[143] C. K. Hayne, C. A. Schmidt, M. I. Haque, A. Gregory Matera, and R. E. Stanley, "Reconstitution of the human tRNA splicing endonuclease complex: insight into the regulation of pre-tRNA cleavage," *Nucleic Acids Res*, vol. 48, no. 14, pp. 7609–7622, Aug. 2020, doi: 10.1093/NAR/GKAA438.

[144] S. Weitzer and J. Martinez, "The human RNA kinase hClp1 is active on 3' transfer RNA exons and short interfering RNAs," *Nature*, vol. 447, no. 7141, pp. 222–226, May 2007, doi: 10.1038/NATURE05777.

[145] J. Popow, A. Schleiffer, and J. Martinez, "Diversity and roles of (t)RNA ligases," *Cellular and Molecular Life Sciences*, vol. 69, no. 16, p. 2657, Aug. 2012, doi: 10.1007/S00018-012-0944-2.

[146] J. L. Gerber, S. Köhler, and J. Peschek, "Eukaryotic tRNA splicing-one goal, two strategies, many players," *Biol Chem*, vol. 403, no. 8–9, pp. 765–778, Jul. 2022, doi: 10.1515/HSZ-2021-0402/ASSET/GRAPHIC/J_HSZ-2021-0402_FIG_004.JPG.

[147] J. Popow, J. Jurkin, A. Schleiffer, and J. Martinez, "Analysis of orthologous groups reveals archease and DDX1 as tRNA splicing factors," *Nature*, vol. 511, no. 7507, pp. 104–107, Jul. 2014, doi: 10.1038/nature13284.

[148] K. K. Desai, C. L. Cheng, C. A. Bingman, G. N. Phillips, and R. T. Raines, "A tRNA splicing operon: Archease endows RtcB with dual GTP/ATP cofactor specificity and accelerates RNA ligation," *Nucleic Acids Res*, vol. 42, no. 6, pp. 3931–3942, Apr. 2014, doi: 10.1093/NAR/GKT1375.

[149] I. Asanović *et al.*, "The oxidoreductase PYROXD1 uses NAD(P)+ as an antioxidant to sustain tRNA ligase activity in pre-tRNA splicing and unfolded protein response," *Mol Cell*, vol. 81, no. 12, pp. 2520-2532.e16, Jun. 2021, doi: 10.1016/j.molcel.2021.04.007.

[150] I. Unlu, Y. Lu, and X. Wang, "The cyclic phosphodiesterase CNP and RNA cyclase RtcA fine-tune noncanonical XBP1 splicing during ER stress," *Journal of Biological Chemistry*, vol. 293, no. 50, pp. 19365–19376, Dec. 2018, doi: 10.1074/JBC.RA118.004872/ATTACHMENT/3E1FF6B0-02C6-453F-B0BF-8F3DD4B6AAC6/MMC1.DOCX.

[151] U. Das and S. Shuman, "2'-Phosphate cyclase activity of RtcA: a potential rationale for the operon organization of RtcA with an RNA repair ligase RtcB in Escherichia coli and other bacterial taxa," *RNA*, vol. 19, no. 10, pp. 1355–1362, Oct. 2013, doi: 10.1261/RNA.039917.113.

[152] P. H. Pinto *et al.*, "ANGEL2 is a member of the CCR4 family of deadenylases with 2',3'-cyclic phosphatase activity," *Science (1979)*, vol. 369, no. 6503, pp. 524–530, Jul. 2020, doi: 10.1126/SCIENCE.ABA9763.

[153] B. Schwer, A. Aronova, A. Ramirez, P. Braun, and S. Shuman, "Mammalian 2',3' cyclic nucleotide phosphodiesterase (CNP) can function as a tRNA splicing enzyme in vivo," *RNA*, vol. 14, no. 2, pp. 204–210, Feb. 2008, doi: 10.1261/RNA.858108.

[154] A. Kroupova *et al.*, "Molecular architecture of the human tRNA ligase complex," *Elife*, vol. 10, Dec. 2021, doi: 10.7554/ELIFE.71656.

[155] A. Slade, R. Kattini, C. Campbell, and M. Holcik, "Diseases Associated with Defects in tRNA CCA Addition," *Int J Mol Sci*, vol. 21, no. 11, Jun. 2020, doi: 10.3390/IJMS21113780.

[156] G. J. Arts, S. Kuersten, P. Romby, B. Ehresmann, and I. W. Mattaj, "The role of exportin-t in selective nuclear export of mature tRNAs," *EMBO J*, vol. 17, no. 24, pp. 7430–7441, Dec. 1998, doi: 10.1093/EMBOJ/17.24.7430.

[157] K. Chatterjee, R. T. Nostramo, Y. Wan, and A. K. Hopper, "tRNA dynamics between the nucleus, cytoplasm and mitochondrial surface: Location, location, location," *Biochim Biophys Acta*, vol. 1861, no. 4, p. 373, Apr. 2018, doi: 10.1016/J.BBAGRM.2017.11.007.

[158] G. Lipowsky *et al.*, "Coordination of tRNA nuclear export with processing of tRNA," *RNA*, vol. 5, no. 4, pp. 539–549, 1999, doi: 10.1017/S1355838299982134.

[159] H. H. Shaheen, R. L. Horetsky, S. R. Kimball, A. Murthi, L. S. Jefferson, and A. K. Hopper, "Retrograde nuclear accumulation of cytoplasmic tRNA in rat hepatoma cells in response to amino acid deprivation," *Proc Natl Acad Sci U S A*, vol. 104, no. 21, p. 8845, May 2007, doi: 10.1073/PNAS.0700765104.

[160] L. Zaitseva, R. Myers, and A. Fassati, "tRNAs promote nuclear import of HIV-1 intracellular reverse transcription complexes," *PLoS Biol*, vol. 4, no. 10, pp. 1689–1706, 2006, doi: 10.1371/JOURNAL.PBIO.0040332.

[161] H. Schwenzer *et al.*, "Oxidative Stress Triggers Selective tRNA Retrograde Transport in Human Cells during the Integrated Stress Response," *Cell Rep*, vol. 26, no. 12, pp. 3416-3428.e5, Mar. 2019, doi: 10.1016/J.CELREP.2019.02.077.

[162] S. Kirchner and Z. Ignatova, "Emerging roles of tRNA in adaptive translation, signalling dynamics and disease," *Nature Reviews Genetics 2014 16:2*, vol. 16, no. 2, pp. 98–112, Dec. 2014, doi: 10.1038/NRG3861.

[163] M. K. Mateyak and T. G. Kinzy, "eEF1A: Thinking Outside the Ribosome," *J Biol Chem*, vol. 285, no. 28, p. 21209, Jul. 2010, doi: 10.1074/JBC.R110.113795.

[164] I. Zivkovic, K. Ivkovic, N. Cvetesic, A. Marsavelski, and I. Gruic-Sovulj, "Negative catalysis by the editing domain of class I aminoacyl-tRNA synthetases," *Nucleic Acids Res*, vol. 50, no. 7, pp. 4029–4041, Apr. 2022, doi: 10.1093/NAR/GKAC207.

[165] C. Lorenz, C. E. Lünse, and M. Mörl, "tRNA Modifications: Impact on Structure and Thermal Adaptation," *Biomolecules*, vol. 7, no. 2, Jun. 2017, doi: 10.3390/BIOM7020035.

[166] M. Pereira, S. Francisco, A. S. Varanda, M. Santos, M. A. S. Santos, and A. R. Soares, "Impact of tRNA Modifications and tRNA-Modifying Enzymes on Proteostasis and Human Disease," *Int J Mol Sci*, vol. 19, no. 12, Dec. 2018, doi: 10.3390/IJMS19123738.

[167] S. Sekar *et al.*, "Alzheimer's disease is associated with altered expression of genes involved in immune response and mitochondrial processes in astrocytes," *Neurobiol Aging*, vol. 36, no. 2, pp. 583–591, Feb. 2015, doi: 10.1016/J.NEUROBIOLAGING.2014.09.027.

[168] J. E. Hoerter and S. R. Ellis, "Biochemistry, Protein Synthesis," *StatPearls*, Jul. 2023, Accessed: Jan. 22, 2024. [Online]. Available: https://www.ncbi.nlm.nih.gov/books/NBK545161/

[169] R. J. Jackson, C. U. T. Hellen, and T. V. Pestova, "The mechanism of eukaryotic translation initiation and principles of its regulation," *Nature Reviews Molecular Cell Biology 2010 11:2*, vol. 11, no. 2, pp. 113–127, Feb. 2010, doi: 10.1038/NRM2838.

[170] D. Wen *et al.*, "Discovery and investigation of misincorporation of serine at asparagine positions in recombinant proteins expressed in Chinese hamster ovary cells," *J Biol Chem*, vol. 284, no. 47, pp. 32686–32694, Nov. 2009, doi: 10.1074/JBC.M109.059360.

[171] N. Aharon-Hefetz, I. Frumkin, Y. Mayshar, O. Dahan, Y. Pilpel, and R. Rak, "Manipulation of the human tRNA pool reveals distinct tRNA sets that act in cellular proliferation or cell cycle arrest," *Elife*, vol. 9, pp. 1–28, Dec. 2020, doi: 10.7554/ELIFE.58461.

[172] H. Gingold *et al.*, "A dual program for translation regulation in cellular proliferation and differentiation," *Cell*, vol. 158, no. 6, pp. 1281–1292, 2014, doi: 10.1016/J.CELL.2014.08.011.

[173] F. Sarais, A. Perdomo-Sabogal, K. Wimmers, and S. Ponsuksili, "tiRNAs: Insights into Their Biogenesis, Functions, and Future Applications in Livestock Research," *Noncoding RNA*, vol. 8, no. 3, Jun. 2022, doi: 10.3390/NCRNA8030037.

[174] B. Liu, J. Cao, X. Wang, C. Guo, Y. Liu, and T. Wang, "Deciphering the tRNA-derived small RNAs: origin, development, and future," *Cell Death & Disease 2021 13:1*, vol. 13, no. 1, pp. 1–13, Dec. 2021, doi: 10.1038/s41419-021-04472-3.

[175] J. tao Wen, Z. hao Huang, Q. hui Li, X. Chen, H. lei Qin, and Y. Zhao, "Research progress on the tsRNA classification, function, and application in gynecological malignant tumors," *Cell Death Discovery 2021 7:1*, vol. 7, no. 1, pp. 1–9, Dec. 2021, doi: 10.1038/s41420-021-00789-2.

[176] A. Elkordy *et al.*, "Stress-induced tRNA cleavage and tiRNA generation in rat neuronal PC12 cells," *J Neurochem*, vol. 146, no. 5, pp. 560–569, Sep. 2018, doi: 10.1111/JNC.14321.

[177] Y. Xie, L. Yao, X. Yu, Y. Ruan, Z. Li, and J. Guo, "Action mechanisms and research methods of tRNA-derived small RNAs," *Signal Transduction and Targeted Therapy 2020 5:1*, vol. 5, no. 1, pp. 1–9, Jun. 2020, doi: 10.1038/s41392-020-00217-4.

[178] Z. Su, B. Wilson, P. Kumar, and A. Dutta, "Noncanonical Roles of tRNAs: tRNA Fragments and Beyond," *Annu Rev Genet*, vol. 54, pp. 47–69, Nov. 2020, doi: 10.1146/ANNUREV-GENET-022620-101840.

[179] M. Fu *et al.*, "Emerging roles of tRNA-derived fragments in cancer," *Mol Cancer*, vol. 22, no. 1, Dec. 2023, doi: 10.1186/S12943-023-01739-5.

[180] B. K. Choe and M. W. Taylor, "Kinetics of synthesis and characterization of transfer RNA precursors in mammalian cells," *Biochimica et Biophysica Acta (BBA) - Nucleic Acids and Protein Synthesis*, vol. 272, no. 2, pp. 275–287, Jun. 1972, doi: 10.1016/0005-2787(72)90251-1.

[181] A. Alexandrov *et al.*, "Rapid tRNA decay can result from lack of nonessential modifications," *Mol Cell*, vol. 21, no. 1, pp. 87–96, Jan. 2006, doi: 10.1016/J.MOLCEL.2005.10.036.

[182] D. Foretek, J. Wu, A. K. Hopper, and M. Boguta, "Control of Saccharomyces cerevisiae pre-tRNA processing by environmental conditions," *RNA*, vol. 22, no. 3, pp. 339–349, Mar. 2016, doi: 10.1261/RNA.054973.115.

[183] C. Megel, G. Morelle, S. Lalande, A. M. Duchêne, I. Small, and L. Maréchal-Drouard, "Surveillance and Cleavage of Eukaryotic tRNAs," *Int J Mol Sci*, vol. 16, no. 1, p. 1873, Jan. 2015, doi: 10.3390/IJMS16011873.

[184] A. Siwaszek, M. Ukleja, and A. Dziembowski, "Proteins involved in the degradation of cytoplasmic mRNA in the major eukaryotic model systems," *RNA Biol*, vol. 11, no. 9, pp. 1122–1136, Sep. 2014, doi: 10.4161/RNA.34406.

[185] E. Ruiz-Pesini *et al.*, "An enhanced MITOMAP with a global mtDNA mutational phylogeny," *Nucleic Acids Res*, vol. 35, no. Database issue, p. D823, Jan. 2007, doi: 10.1093/NAR/GKL927.

[186] E. A. Orellana, E. Siegal, and R. I. Gregory, "tRNA dysregulation and disease," *Nature Reviews Genetics 2022 23:11*, vol. 23, no. 11, pp. 651–664, Jun. 2022, doi: 10.1038/S41576-022-00501-9.

[187] J. A. Abbott, C. S. Francklyn, and S. M. Robey-Bond, "Transfer RNA and human disease," *Front Genet*, vol. 5, no. JUN, 2014, doi: 10.3389/FGENE.2014.00158.

[188] R. Ishimura *et al.*, "Ribosome stalling induced by mutation of a CNS-specific tRNA causes neurodegeneration," *Science (1979)*, vol. 345, no. 6195, pp. 455–459, Jul. 2014, doi: 10.1126/SCIENCE.1249749/SUPPL_FILE/1249749S1.MOV.

[189] T. Suzuki, "RNA Modifications in Health and Disease," *The FASEB Journal*, vol. 34, no. S1, pp. 1–1, Apr. 2020, doi: 10.1096/FASEBJ.2020.34.S1.00132.

[190] H. Fu, J. Hardy, and K. E. Duff, "Selective vulnerability in neurodegenerative diseases," *Nat Neurosci*, vol. 21, no. 10, pp. 1350–1358, Oct. 2018, doi: 10.1038/S41593-018-0221-2.

[191] J. Jurkin *et al.*, "The mammalian tRNA ligase complex mediates splicing of XBP1 mRNA and controls antibody secretion in plasma cells.," *EMBO J*, vol. 33, no. 24, pp. 2922–36, Dec. 2014, doi: 10.15252/embj.201490332.

[192] S. M. Park, T. Il Kang, and J. S. So, "Roles of XBP1s in Transcriptional Regulation of Target Genes," *Biomedicines*, vol. 9, no. 7, Jul. 2021, doi: 10.3390/BIOMEDICINES9070791.

[193] F. J. Guo, E. A. Lin, P. Liu, J. Lin, and C. Liu, "XBP1U inhibits the XBP1S-mediated upregulation of the iNOS gene expression in mammalian ER stress response," *Cell Signal*, vol. 22, no. 12, pp. 1818–1828, Dec. 2010, doi: 10.1016/J.CELLSIG.2010.07.006.

[194] F. Hinte, E. Van Anken, B. Tirosh, and W. Brune, "Repression of viral gene expression and replication by the unfolded protein response effector XBP1u," *Elife*, vol. 9, Feb. 2020, doi: 10.7554/ELIFE.51804.

[195] C. Chen *et al.*, " Signal peptide peptidase functions in ERAD to cleave the unfolded protein response regulator XBP 1u ," *EMBO J*, vol. 33, no. 21, pp. 2492–2506, Nov. 2014, doi: 10.15252/EMBJ.201488208/SUPPL_FILE/EMBJ201488208.REVIEWER_COMMENTS.PDF.

[196] S. Y. Liu *et al.*, "Polymorphism -116C/G of human X-box-binding protein 1 promoter is associated with risk of Alzheimer's disease," *CNS Neurosci Ther*, vol. 19, no. 4, pp. 229–234, Apr. 2013, doi: 10.1111/CNS.12064.

[197] C. Duran-Aniotz *et al.*, "The unfolded protein response transcription factor XBP1s ameliorates Alzheimer's disease by improving synaptic function and proteostasis," *Molecular Therapy*, vol. 31, no. 7, pp. 2240–2256, Jul. 2023, doi: 10.1016/j.ymthe.2023.03.028.

[198] M. Cissé *et al.*, "The transcription factor XBP1s restores hippocampal synaptic plasticity and memory by control of the Kalirin-7 pathway in Alzheimer model," *Mol Psychiatry*, vol. 22, no. 11, p. 1562, Nov. 2017, doi: 10.1038/MP.2016.152.

[199] G. Martínez *et al.*, "Regulation of Memory Formation by the Transcription Factor XBP1," *Cell Rep*, vol. 14, no. 6, pp. 1382–1394, Feb. 2016, doi: 10.1016/j.celrep.2016.01.028.

[200] T. Ximelis *et al.*, "Homozygous R136S mutation in PRNP gene causes inherited early onset prion disease," *Alzheimers Res Ther*, vol. 13, no. 1, Dec. 2021, doi: 10.1186/S13195-021-00912-6.

[201] H. Oakley *et al.*, "Intraneuronal beta-amyloid aggregates, neurodegeneration, and neuron loss in transgenic mice with five familial Alzheimer's disease mutations: potential factors in amyloid plaque formation," *J Neurosci*, vol. 26, no. 40, pp. 10129–10140, Oct. 2006, doi: 10.1523/JNEUROSCI.1202-06.2006.

[202] T. Kanno, A. Tsuchiya, and T. Nishizaki, "Hyperphosphorylation of Tau at Ser396 occurs in the much earlier stage than appearance of learning and memory disorders in 5XFAD mice," *Behavioural Brain Research*, vol. 274, pp. 302–306, 2014, doi: 10.1016/j.bbr.2014.08.034.

[203] L. Devi and M. Ohno, "Phospho-eIF2α level is important for determining abilities of BACE1 reduction to rescue cholinergic neurodegeneration and memory defects in 5XFAD mice," *PLoS One*, vol. 5, no. 9, 2010, doi: 10.1371/journal.pone.0012974.

[204] T. P. O'Leary, H. M. Mantolino, K. R. Stover, and R. E. Brown, "Age-related deterioration of motor function in male and female 5xFAD mice from 3 to 16 months of age," *Genes Brain Behav*, vol. 19, no. 3, pp. 1–11, 2020, doi: 10.1111/gbb.12538.

[205] W. A. Eimer and R. Vassar, "Neuron loss in the 5XFAD mouse model of Alzheimer's disease correlates with intraneuronal Aβ42 accumulation and Caspase-3 activation," *Mol Neurodegener*, vol. 8, no. 1, p. 1, 2013, doi: 10.1186/1750-1326-8-2.

[206] J. Szu, A. Jullienne, A. Obenaus, P. R. Territo, and M. Consortium, "Lifespan neuroimaging of the 5xFAD mouse model of Alzheimer's disease: Evolution of metabolic and vascular perturbations," *Alzheimer's & Dementia*, vol. 16, no. S4, pp. 4–5, 2020, doi: 10.1002/alz.040548.

[207] X. Hernandez-Alias, H. Benisty, M. H. Schaefer, and L. Serrano, "Translational efficiency across healthy and tumor tissues is proliferation-related," *Mol Syst Biol*, vol. 16, no. 3, p. 9275, Mar. 2020, doi: 10.15252/MSB.20199275/SUPPL_FILE/MSB199275-SUP-0013-SDATAFIG1.XLSX.

[208] A. D. Holmes, J. M. Howard, P. P. Chan, and T. M. Lowe, "tRNA Analysis of eXpression (tRAX): A tool for integrating analysis of tRNAs, tRNA-derived small RNAs, and tRNA modifications," *bioRxiv*, p. 2022.07.02.498565, Jul. 2022, doi: 10.1101/2022.07.02.498565.

[209] R. E. Mains, D. D. Kiraly, J. E. Eipper-Mains, X. M. Ma, and B. A. Eipper, "Kalrn promoter usage and isoform expression respond to chronic cocaine exposure," *BMC Neurosci*, vol. 12, p. 20, Feb. 2011, doi: 10.1186/1471-2202-12-20.

[210] L. Qin *et al.*, "EBV-LMP1 regulating AKT/mTOR signaling pathway and WWOX in nasopharyngeal carcinoma," *Int J Clin Exp Pathol*, vol. 10, no. 8, p. 8619, 2017, Accessed: Dec. 23, 2023. [Online]. Available: /pmc/articles/PMC6965410/

[211] J. Creus-Muncunill *et al.*, "Huntington's disease brain-derived small RNAs recapitulate associated neuropathology in mice," *Acta Neuropathol*, vol. 141, no. 4, pp. 565–584, Apr. 2021, doi: 10.1007/S00401-021-02272-9.

[212] B. Koltun *et al.*, "Measuring mRNA translation in neuronal processes and somata by tRNA-FRET," *Nucleic Acids Res*, vol. 48, no. 6, pp. E32–E32, Apr. 2020, doi: 10.1093/NAR/GKAA042.

[213] A. E. Carpenter *et al.*, "CellProfiler: image analysis software for identifying and quantifying cell phenotypes," *Genome Biol*, vol. 7, no. 10, Oct. 2006, doi: 10.1186/GB-2006-7-10-R100.

[214] D. R. Stirling, M. J. Swain-Bowden, A. M. Lucas, A. E. Carpenter, B. A. Cimini, and A. Goodman, "CellProfiler 4: improvements in speed, utility and usability," *BMC Bioinformatics*, vol. 22, no. 1, Dec. 2021, doi: 10.1186/S12859-021-04344-9.

[215] J. Solana-Balaguer *et al.*, "Neuron-derived extracellular vesicles contain synaptic proteins, promote spine formation, activate TrkB-mediated signalling and preserve neuronal complexity," *J Extracell Vesicles*, vol. 12, no. 9, p. 12355, Sep. 2023, doi: 10.1002/JEV2.12355.

[216] D. R. Stirling, A. E. Carpenter, and B. A. Cimini, "CellProfiler Analyst 3.0: accessible data exploration and machine learning for image analysis," *Bioinformatics*, vol. 37, no. 21, pp. 3992–3994, Nov. 2021, doi: 10.1093/BIOINFORMATICS/BTAB634.

[217] T. R. Jones *et al.*, "CellProfiler Analyst: data exploration and analysis software for complex image-based screens," *BMC Bioinformatics*, vol. 9, Nov. 2008, doi: 10.1186/1471-2105-9-482.

[218] X. Robin *et al.*, "pROC: An open-source package for R and S+ to analyze and compare ROC curves," *BMC Bioinformatics*, vol. 12, no. 1, pp. 1–8, Mar. 2011, doi: 10.1186/1471-2105-12-77/TABLES/3.

[219] H. Wickham, "ggpolt2 Elegant Graphics for Data Analysis," *Use R! series*, p. 211, 2016.

[220] M. V. Kuleshov *et al.*, "Enrichr: a comprehensive gene set enrichment analysis web server 2016 update," *Nucleic Acids Res*, vol. 44, no. 1, pp. W90–W97, 2016, doi: 10.1093/nar/gkw377.

[221] T. Tuller, "The effect of dysregulation of tRNA genes and translation efficiency mutations in cancer and neurodegeneration," *Front Genet*, vol. 3, no. OCT, p. 34818, Oct. 2012, doi: 10.3389/FGENE.2012.00201/BIBTEX.

[222] M. Torrent, G. Chalancon, N. S. De Groot, A. Wuster, and M. Madan Babu, "Cells alter their tRNA abundance to selectively regulate protein synthesis during stress conditions," *Sci Signal*, vol. 11, no. 546, Sep. 2018, doi: 10.1126/SCISIGNAL.AAT6409/SUPPL_FILE/AAT6409_SM.PDF.

[223] R. Rak *et al.*, "Dynamic changes in tRNA modifications and abundance during T cell activation," *Proc Natl Acad Sci U S A*, vol. 118, no. 42, Oct. 2021, doi: 10.1073/PNAS.2106556118/-/DCSUPPLEMENTAL.

[224] S. E. Bettigole *et al.*, "The transcription factor XBP1 is selectively required for eosinophil differentiation," *Nat Immunol*, vol. 16, no. 8, pp. 829–837, 2015, doi: 10.1038/ni.3225.

[225] T. Iwawaki and M. Tokuda, "Function of yeast and amphioxus tRNA ligase in IRE1alpha-dependent XBP1 mRNA splicing," *Biochem Biophys Res Commun*, vol. 413, no. 4, pp. 527–531, Oct. 2011, doi: 10.1016/J.BBRC.2011.08.129.

[226] S. Bathina and U. N. Das, "Brain-derived neurotrophic factor and its clinical Implications," *Archives of Medical Science*, vol. 11, no. 6, pp. 1164–1178, 2015, doi: 10.5114/aoms.2015.56342.

[227] S. Wang and S. Sun, “Translation dysregulation in neurodegenerative diseases: a focus on ALS,” *Mol Neurodegener*, vol. 18, no. 1, pp. 1–20, Dec. 2023, doi: 10.1186/S13024-023-00642-3/FIGURES/3.

[228] F. Tajik *et al.*, “Nuclear overexpression of DNA damage-inducible transcript 4 (DDIT4) is associated with aggressive tumor behavior in patients with pancreatic tumors,” *Sci Rep*, vol. 13, no. 1, Dec. 2023, doi: 10.1038/S41598-023-46484-3.

[229] C. Berk, Y. Wang, A. Laski, S. Tsagkris, and J. Hall, “Ligation of 2′, 3′-cyclic phosphate RNAs for the identification of microRNA binding sites,” *FEBS Lett*, vol. 595, no. 2, pp. 230–240, Jan. 2021, doi: 10.1002/1873-3468.13976.

[230] A. Pérez-González, A. Pazo, R. Navajas, S. Ciordia, A. Rodriguez-Frandsen, and A. Nieto, “hCLE/C14orf166 Associates with DDX1-HSPC117-FAM98B in a Novel Transcription-Dependent Shuttling RNA-Transporting Complex,” *PLoS One*, vol. 9, no. 3, Mar. 2014, doi: 10.1371/JOURNAL.PONE.0090957.

[231] C. Sidrauski and P. Walter, “The Transmembrane Kinase Ire1p Is a Site-Specific Endonuclease That Initiates mRNA Splicing in the Unfolded Protein Response,” *Cell*, vol. 90, no. 6, pp. 1031–1039, Sep. 1997, doi: 10.1016/S0092-8674(00)80369-4.

[232] H. Yoshida, T. Matsui, A. Yamamoto, T. Okada, and K. Mori, “XBP1 mRNA Is Induced by ATF6 and Spliced by IRE1 in Response to ER Stress to Produce a Highly Active Transcription Factor,” *Cell*, vol. 107, no. 7, pp. 881–891, Dec. 2001, doi: 10.1016/S0092-8674(01)00611-0.

[233] Y. Lu, F. X. Liang, and X. Wang, “A Synthetic Biology Approach Identifies the Mammalian UPR RNA Ligase RtcB,” *Mol Cell*, vol. 55, no. 5, pp. 758–770, Sep. 2014, doi: 10.1016/j.molcel.2014.06.032.

[234] S. G. Kosmaczewski *et al.*, “ The R tc B RNA ligase is an essential component of the metazoan unfolded protein response ,” *EMBO Rep*, vol. 15, no. 12, pp. 1278–1285, Dec. 2014, doi: 10.15252/EMBR.201439531/SUPPL_FILE/EMBR201439531.REVIEWER_COMMENTS.PDF .

[235] W. Filipowicz, “ Making ends meet: a role of RNA ligase RTCB in unfolded protein response ,” *EMBO J*, vol. 33, no. 24, pp. 2887–2889, Dec. 2014, doi: 10.15252/EMBJ.201490425/ASSET/F71FC9BC-7041-44CE-A7B3-455F192B2F3C/ASSETS/GRAPHIC/EMBJ201490425-FIG-0001-M.PNG.

[236] A. Papaioannou *et al.*, “Stress-induced tyrosine phosphorylation of RtcB modulates IRE1 activity and signaling outputs,” *Life Sci Alliance*, vol. 5, no. 5, May 2022, doi: 10.26508/LSA.202201379.

[237] S. Chatterjee, A. J. Choi, and G. Frankel, “A systematic review of Sec24 cargo interactome,” *Traffic*, vol. 22, no. 12, pp. 412–424, Dec. 2021, doi: 10.1111/TRA.12817.

[238] V. W. Hsu, S. Y. Lee, and J. S. Yang, “The evolving understanding of COPI vesicle formation,” *Nature Reviews Molecular Cell Biology 2009 10:5*, vol. 10, no. 5, pp. 360–364, Mar. 2009, doi: 10.1038/NRM2663.

[239] E. R. Abels and X. O. Breakefield, “Introduction to Extracellular Vesicles: Biogenesis, RNA Cargo Selection, Content, Release, and Uptake,” *Cell Mol Neurobiol*, vol. 36, no. 3, p. 301, Apr. 2016, doi: 10.1007/S10571-016-0366-Z.

[240] “A Multi-omics Atlas Project - Alzheimer’s Disease.” Accessed: Apr. 24, 2024. [Online]. Available: https://map-ad.org/

[241] A. Z. Samsudin *et al.*, “Differential gene expression of blood-based ABCA9, CNOT8, SESN1, UCP3, MAP2K1 and DDIT4 in Alzheimer’s disease,” *Neuroscience Research Notes*, vol. 6, no. 4, pp. 262.1-262.14, Dec. 2023, doi: 10.31117/NEUROSCIRN.V6I4.262.

[242] E. Velásquez *et al.*, “Topological Dissection of Proteomic Changes Linked to the Limbic Stage of Alzheimer’s Disease,” *Front Immunol*, vol. 12, p. 750665, Oct. 2021, doi: 10.3389/FIMMU.2021.750665/BIBTEX.

[243] Z. Wang, X. Yan, and C. Zhao, “Dynamical differential networks and modules inferring disrupted genes associated with the progression of Alzheimer’s disease,” *Exp Ther Med*, vol. 14, no. 4, p. 2969, Oct. 2017, doi: 10.3892/ETM.2017.4905.

[244] H. S. Gns, S. G. Rajalekshmi, and R. R. Burri, “Revelation of Pivotal Genes Pertinent to Alzheimer’s Pathogenesis: A Methodical Evaluation of 32 GEO Datasets,” *Journal of Molecular Neuroscience*, vol. 72, no. 2, p. 303, Feb. 2022, doi: 10.1007/S12031-021-01919-2.

[245] S. Reinhardt *et al.*, “Unfolded protein response signaling by transcription factor XBP-1 regulates ADAM10 and is affected in Alzheimer’s disease,” *FASEB Journal*, vol. 28, no. 2, pp. 978–997, 2014, doi: 10.1096/FJ.13-234864.

[246] J. H. Lee *et al.*, “Induction of the unfolded protein response and cell death pathway in Alzheimer’s disease, but not in aged Tg2576 mice,” *Exp Mol Med*, vol. 42, no. 5, p. 386, May 2010, doi: 10.3858/EMM.2010.42.5.040.

[247] M. Cissé, E. Duplan, and F. Checler, “The Transcription Factor XBP1 in Memory and Cognition: Implications in Alzheimer’s Disease,” *Molecular Medicine*, vol. 22, p. 905, Jan. 2016, doi: 10.2119/MOLMED.2016.00229.

[248] M. M. Oliveira *et al.*, “Correction of eIF2-dependent defects in brain protein synthesis, synaptic plasticity and memory in mouse models of Alzheimer’s disease,” *Sci Signal*, vol. 14, no. 668, Feb. 2021, doi: 10.1126/SCISIGNAL.ABC5429.

[249] T. O’Connor *et al.*, “Phosphorylation of the translation initiation factor eIF2alpha increases BACE1 levels and promotes amyloidogenesis,” *Neuron*, vol. 60, no. 6, pp. 988–1009, Dec. 2008, doi: 10.1016/J.NEURON.2008.10.047.

[250] C. RC, W. AK, N. HK, and H. J, “Phosphorylation of eukaryotic initiation factor-2alpha (eIF2alpha) is associated with neuronal degeneration in Alzheimer’s disease,” *Neuroreport*, vol. 13, no. 18, pp. 2429–2432, Dec. 2002, doi: 10.1097/00001756-200212200-00011.

[251] J. J. M. Hoozemans, E. S. Van Haastert, D. A. T. Nijholt, A. J. M. Rozemuller, P. Eikelenboom, and W. Scheper, “The unfolded protein response is activated in pretangle neurons in Alzheimer’s disease hippocampus,” *Am J Pathol*, vol. 174, no. 4, pp. 1241–1251, 2009, doi: 10.2353/AJPATH.2009.080814.

[252] M. Ohno, “Roles of eIF2α kinases in the pathogenesis of Alzheimer’s disease,” *Front Mol Neurosci*, vol. 7, no. 1 APR, Apr. 2014, doi: 10.3389/FNMOL.2014.00022.

[253] J. Lewerenz and P. Maher, “Basal levels of eIF2alpha phosphorylation determine cellular antioxidant status by regulating ATF4 and xCT expression,” *J Biol Chem*, vol. 284, no. 2, pp. 1106–1115, Jan. 2009, doi: 10.1074/JBC.M807325200.

[254] C. Zhang *et al.*, “ATF4 is directly recruited by TLR4 signaling and positively regulates TLR4-trigged cytokine production in human monocytes,” *Cell Mol Immunol*, vol. 10, no. 1, pp. 84–94, Jan. 2013, doi: 10.1038/cmi.2012.57.

[255] A. Z. Samsudin *et al.*, “Differential gene expression of blood-based ABCA9, CNOT8, SESN1, UCP3, MAP2K1 and DDIT4 in Alzheimer’s disease,” *Neuroscience Research Notes*, vol. 6, no. 4, pp. 262.1-262.14, Dec. 2023, doi: 10.31117/NEUROSCIRN.V6I4.262.

[256] S. Casas-Tinto, Y. Zhang, J. Sanchez-Garcia, M. Gomez-Velazquez, D. E. Rincon-Limas, and P. Fernandez-Funez, “The ER stress factor XBP1s prevents amyloid-β neurotoxicity,” *Hum Mol Genet*, vol. 20, no. 11, pp. 2144–2160, Jun. 2011, doi: 10.1093/HMG/DDR100.

[257] S. M. Waldherr, T. J. Strovas, T. A. Vadset, N. F. Liachko, and B. C. Kraemer, “Constitutive XBP-1s-mediated activation of the endoplasmic reticulum unfolded protein response protects against pathological tau,” *Nature Communications 2019 10:1*, vol. 10, no. 1, pp. 1–12, Sep. 2019, doi: 10.1038/S41467-019-12070-3.

[258] H. Grosjean, Z. Szweykowska-Kulinska, Y. Motorin, F. Fasiolo, and G. Simos, “Intron-dependent enzymatic formation of modified nucleosides in eukaryotic tRNAs: a review,” *Biochimie*, vol. 79, no. 5, pp. 293–302, 1997, doi: 10.1016/S0300-9084(97)83517-1.

[259] D. Donze and R. T. Kamakaka, “RNA polymerase III and RNA polymerase II promoter complexes are heterochromatin barriers in Saccharomyces cerevisiae,” *EMBO J*, vol. 20, no. 3, pp. 520–531, Feb. 2001, doi: 10.1093/EMBOJ/20.3.520.

[260] C. A. Schmidt, J. D. Giusto, A. Bao, A. K. Hopper, and A. Gregory Matera, “Molecular determinants of metazoan tricRNA biogenesis,” *Nucleic Acids Res*, vol. 47, no. 12, p. 6452, Jul. 2019, doi: 10.1093/NAR/GKZ311.

[261] Z. Lu *et al.*, “Metazoan tRNA introns generate stable circular RNAs in vivo,” *RNA*, vol. 21, no. 9, p. 1554, Sep. 2015, doi: 10.1261/RNA.052944.115.

[262] P. P. Chan and T. M. Lowe, “GtRNAdb 2.0: an expanded database of transfer RNA genes identified in complete and draft genomes,” *Nucleic Acids Res*, vol. 44, no. D1, pp. D184–D189, Jan. 2016, doi: 10.1093/NAR/GKV1309.

[263] A. M. Shafik, H. Zhou, J. Lim, B. Dickinson, and P. Jin, “Dysregulated mitochondrial and cytosolic tRNA m1A methylation in Alzheimer’s disease,” *Hum Mol Genet*, vol. 31, no. 10, p. 1673, May 2022, doi: 10.1093/HMG/DDAB357.

[264] M. Pereira *et al.*, “Amyloid pathology reduces ELP3 expression and tRNA modifications leading to impaired proteostasis,” *Biochim Biophys Acta Mol Basis Dis*, vol. 1870, no. 1, Jan. 2024, doi: 10.1016/J.BBADIS.2023.166857.

[265] W. Wu, I. Lee, H. Spratt, X. Fang, and X. Bao, “tRNA-Derived Fragments in Alzheimer’s Disease: Implications for New Disease Biomarkers and Neuropathological Mechanisms,” *J Alzheimers Dis*, vol. 79, no. 2, p. 793, 2021, doi: 10.3233/JAD-200917.

[266] S. Sekulovski *et al.*, "Assembly defects of human tRNA splicing endonuclease contribute to impaired pre-tRNA processing in pontocerebellar hypoplasia," *Nature Communications 2021 12:1*, vol. 12, no. 1, pp. 1–15, Sep. 2021, doi: 10.1038/s41467-021-25870-3.

[267] S. Blanco *et al.*, " Aberrant methylation of t RNA s links cellular stress to neuro-developmental disorders ," *EMBO J*, vol. 33, no. 18, pp. 2020–2039, Sep. 2014, doi: 10.15252/EMBJ.201489282/SUPPL_FILE/EMBJ201489282.REVIEWER_COMMENTS.PDF.

[268] Y. A. Kim *et al.*, "RNA methyltransferase NSun2 deficiency promotes neurodegeneration through epitranscriptomic regulation of tau phosphorylation," *Acta Neuropathol*, vol. 145, no. 1, pp. 29–48, Jan. 2023, doi: 10.1007/S00401-022-02511-7.

[269] Y. Cao, K. Liu, Y. Xiong, C. Zhao, and L. Liu, "Increased expression of fragmented tRNA promoted neuronal necrosis," *Cell Death & Disease 2021 12:9*, vol. 12, no. 9, pp. 1–15, Aug. 2021, doi: 10.1038/s41419-021-04108-6.

[270] C. Ortiz-Sanz *et al.*, "Early Effects of Aβ Oligomers on Dendritic Spine Dynamics and Arborization in Hippocampal Neurons," *Front Synaptic Neurosci*, vol. 12, p. 510901, Feb. 2020, doi: 10.3389/FNSYN.2020.00002/BIBTEX.

[271] B. A. Couch, G. J. Demarco, S. L. Gourley, and A. J. Koleske, "Increased Dendrite Branching in AβPP/PS1 Mice and Elongation of Dendrite Arbors by Fasudil Administration," *J Alzheimers Dis*, vol. 20, no. 4, p. 1003, 2010, doi: 10.3233/JAD-2010-091114.

[272] S. Kawabata, "Excessive/Aberrant and Maladaptive Synaptic Plasticity: A Hypothesis for the Pathogenesis of Alzheimer's Disease," *Front Aging Neurosci*, vol. 14, p. 913693, Jul. 2022, doi: 10.3389/FNAGI.2022.913693/BIBTEX.

[273] E. Falke, J. Nissanov, T. W. Mitchell, D. A. Bennett, J. Q. Trojanowski, and S. E. Arnold, "Subicular dendritic arborization in Alzheimer's disease correlates with neurofibrillary tangle density," *Am J Pathol*, vol. 163, no. 4, pp. 1615–1621, Oct. 2003, doi: 10.1016/S0002-9440(10)63518-3.

[274] N. Golovyashkina, L. Penazzi, C. Ballatore, A. B. Smith, L. Bakota, and R. Brandt, "Region-specific dendritic simplification induced by Aβ, mediated by tau via dysregulation of microtubule dynamics: A mechanistic distinct event from other neurodegenerative processes," *Mol Neurodegener*, vol. 10, no. 1, pp. 1–17, Nov. 2015, doi: 10.1186/S13024-015-0049-0/FIGURES/7.

[275] X. Liu *et al.*, "A functional non-coding RNA is produced from xbp-1 mRNA," *Neuron*, vol. 107, no. 5, p. 854, Sep. 2020, doi: 10.1016/J.NEURON.2020.06.015.

[276] D. Hasler *et al.*, "The Lupus Autoantigen La Prevents Mis-channeling of tRNA Fragments into the Human MicroRNA Pathway," *Mol Cell*, vol. 63, no. 1, pp. 110–124, Jul. 2016, doi: 10.1016/J.MOLCEL.2016.05.026.

[277] D. Shah *et al.*, "A novel miR1983-TLR7-IFNβ circuit licenses NK cells to kill glioma cells, and is under the control of galectin-1," *Oncoimmunology*, vol. 10, no. 1, 2021, doi: 10.1080/2162402X.2021.1939601.

[278] J. A. Chalmers *et al.*, “Hypothalamic miR-1983 Targets Insulin Receptor β and the Insulin-mediated miR-1983 Increase Is Blocked by Metformin,” *Endocrinology*, vol. 163, no. 1, pp. 1–14, Jan. 2022, doi: 10.1210/ENDOCR/BQAB241.

[279] Y. Zhang, H. Qian, J. He, and W. Gao, “Mechanisms of tRNA-derived fragments and tRNA halves in cancer treatment resistance,” *Biomark Res*, vol. 8, no. 1, Dec. 2020, doi: 10.1186/S40364-020-00233-0.

[280] A. K. Hopper, “Transfer RNA Post-Transcriptional Processing, Turnover, and Subcellular Dynamics in the Yeast Saccharomyces cerevisiae,” *Genetics*, vol. 194, no. 1, pp. 43–67, May 2013, doi: 10.1534/GENETICS.112.147470.

[281] K. Perry McNally, N. AgabianO, and S. Francisco, “THE JOURNAL OF BIOLOGICAL CHEMISTRY Splicing and 3’-Processing of the Tyrosine tRNA of Tkypanosoma brucei*,” vol. 268, no. 29, pp. 21868–21874, 1993, doi: 10.1016/S0021-9258(20)80621-8.

[282] N. H. Blewett, J. R. Iben, S. Gaidamakov, and R. J. Maraia, “La Deletion from Mouse Brain Alters Pre-tRNA Metabolism and Accumulation of Pre-5.8S rRNA, with Neuron Death and Reactive Astrocytosis,” *Mol Cell Biol*, vol. 37, no. 10, May 2017, doi: 10.1128/MCB.00588-16.

[283] Y. Kanai, N. Dohmae, and N. Hirokawa, “Kinesin transports RNA: Isolation and characterization of an RNA-transporting granule,” *Neuron*, vol. 43, no. 4, pp. 513–525, Aug. 2004, doi: 10.1016/j.neuron.2004.07.022.

[284] A. Pazo, A. Pérez-González, J. C. Oliveros, M. Huarte, J. P. Chavez, and A. Nieto, “hCLE/RTRAF-HSPC117-DDX1-FAM98B: A New Cap-Binding Complex That Activates mRNA Translation.,” *Front Physiol*, vol. 10, p. 92, 2019, doi: 10.3389/fphys.2019.00092.